Universiteit
Antwerpen

Faculteit Wetenschappen
Departement Fysica
Theorie van de Gecondenseerde Materie (TGM/CMT)

Spontane en geïnduceerde magnetisatie in twee- en driedimensionale Heisenberg ferromagneten

Een kwantummechanische behandeling

Spontaneous and induced magnetisation in two-dimensional and bulk Heisenberg ferromagnets

A quantum mechanical treatment

Proefschrift ingediend ter verkrijging van de graad van
doctor in de wetenschappen: fysica
aan de Universiteit Antwerpen, te verdedigen door

ir. Joren Vanherck

Promotoren
Prof. dr. Wim Magnus
Prof. dr. ir. Bart Sorée

Antwerpen, 2020

Jury

Prof. dr. Wim Magnus, Universiteit Antwerpen, België
Prof. dr. ir. Bart Sorée, Universiteit Antwerpen, België
Prof. dr. J. Verbeeck, Universiteit Antwerpen, België
Prof. dr. J. Hadermann, Universiteit Antwerpen, België
Prof. dr. M.V. Milošević, Universiteit Antwerpen, België
Prof. dr. B. Van Waeyenberge, Universiteit Gent, België
Prof. dr. E. Bousquet, Université de Liège, België

Contact
ir. Joren Vanherck

Universiteit Antwerpen
Faculteit Wetenschappen
Departement Fysica
Theorie van de Gecondenseerde Materie (TGM/CMT)
Groenenborgerlaan 171, 2020 Antwerpen, België
M: joren.vanherck@uantwerpen.be
T: +32 3 265 37 34

In samenwerking met **imec**
Datum publieke verdediging: 15/10/2020

Abstract

Two-dimensional (2D) materials have dominated the fields of solid-state physics and technology in recent years. With the experimental discovery of several atomically thin ferromagnets in 2017, magnetism has also properly entered this exciting domain. From a technological perspective, understanding the exact thin-film magnetisation behaviour is essential in the ever-continuing down-scaling of integrated circuit components, striving for cheaper, faster and more energy-efficient devices. While today predominantly present in memory devices, thin ferromagnets might also enter the realm of logic technologies, for example in the form of spin wave majority gates. From a scientific perspective, the origin of two-dimensional ferromagnetism is not well understood, as it seemingly contradicts the (in)famous Mermin-Wagner theorem—excluding the possibility of two-dimensional ferromagnetic ordering. To address this dissatisfying situation, we studied a quantum Heisenberg model with beyond-nearest-neighbour, anisotropic exchange interactions at non-zero temperatures. This model is believed to accurately describe some of the experimentally discovered 2D ferromagnets, such as CrI_3, $CrBr_3$ and $MnSe_2$. We obtained results using Zubarev's double-time temperature-dependent Green functions with Tyablikov's decoupling approximation, which are known to give meaningful results for the entire temperature range. We compared results for two- and three-dimensional materials, investigated the effect of an applied, homogeneous field in arbitrary direction and extended the methodology to properly account for magnetic dipolar interactions. This thesis reports on the calculated Curie temperatures, excitation spectra, and magnetisation magnitudes and angles.

We managed to reproduce the predictions of the Mermin-Wagner theorem and find that spontaneous magnetisation in 2D materials is still possible when an easy-axis exchange anisotropy is present. Combining our results with ab initio calculations allowed us to reproduce Curie temperatures in agreement with experiments. The behaviour of magnetism in easy-axis two-dimensional materials turns out to be similar to that of their bulk counterparts, while being distinct from easy-plane 2D materials. Overall, the magnetisation aligns mostly with the internal anisotropy at low temperatures and fields, while getting reoriented towards the homogeneous external field direction otherwise. Dipolar interactions might lead to an additional easy-plane anisotropy for thin films, but its corresponding long-range character might stabilise the magnetisation. In conclusion, we found an effective way to describe some recently discovered 2D ferromagnets, explaining their non-zero Curie temperatures by the presence of easy-axis anisotropy. In such materials,

our results allow predictions on the magnetisation at non-zero temperatures and applied fields at arbitrary angles. To stimulate further computational discoveries of monolayer ferromagnets, we made a computer program publicly available to calculate Curie temperatures based on our formalism. This application only requires ab initio calculated parameters as an input and can equally well be used to study effects of stress, strain or electrical fields on the transition temperature. Our methodology might further be extended to study multilayer materials, different magnetic interactions or even dynamical effects.

Samenvatting

De voorbije jaren waren tweedimensionale (2D) materialen niet weg te denken uit de vastestoffysica en -technologie. Pas sinds 2017 is ferromagnetisme ook experimenteel waargenomen in zulke materialen, die slechts één atoomlaag dik zijn. Vanuit een technologisch standpunt is het begrijpen van magnetisme in deze ultra-dunne limiet essentieel met het oog op de steeds verder doorgedreven verkleining van geïntegreerde elektronische componenten, waarbij er gestreefd wordt naar goedkopere, snellere en energiezuinigere apparaten. Hoewel dunne ferromagneten vandaag vooral gebruikt worden voor geheugenelementen, kunnen ze in de toekomst misschien ook een rol spelen bij de fabricatie van logische componenten, bijvoorbeeld in de vorm van spingolf-meerderheidspoorten. Vanuit een wetenschappelijk standpunt is het bestaan van tweedimensionale ferromagneten nog niet goed begrepen, aangezien het ogenschijnlijk in tegenspraak is met de bekende stelling van Mermin en Wagner—die onder bepaalde voorwaarden de ferromagnetische ordening in 2D materialen uitsluit. Om meer inzicht te krijgen in dit probleem, hebben we het kwantummechanische Heisenberg-model bestudeerd voor positieve temperaturen en met een uitwisselingsinteractie (exchange) die anisotroop is en tot voorbij de naaste buren reikt. Er wordt verwacht dat dit een goed model is voor enkele recentelijk ontdekte 2D ferromagneten zoals CrI_3, $CrBr_3$ en $MnSe_2$. We hebben numerieke resultaten verkregen door Zubarevs dubbeletijds- en temperatuursafhankelijke Greense functies met het Tyablikov ontkoppelingsschema te berekenen, waarvan bekend is dat het goede voorspellingen voor de magnetisatie oplevert over het volledige temperatuursinterval. De verkregen resultaten hebben we vergeleken voor twee- en driedimensionale materialen. Verder hebben we het effect onderzocht van een homogeen magneetveld dat in een willekeurige richting wordt aangelegd, en we hebben het formalisme uitgebreid om ook magnetische dipool-dipool-interacties mee in rekening te kunnen brengen. Dit proefschrift beschrijft de berekende Curie-temperaturen, excitatiespectra, evenals magnetisatiegroottes en -hoeken.

Met betrekking tot de voorspellingen van het Mermin-Wagner theorema hebben we aangetoond dat spontane magnetisatie bij positieve temperaturen nog steeds mogelijk is in 2D materialen die een easy-axis anisotropie vertonen. De combinatie van de verkregen resultaten met die van een aantal *ab initio* berekeningen stelde ons bovendien in staat om Curie-temperaturen te berekenen die overeenstemmen met experimentele waarnemingen. In 2D easy-axis materialen is het gedrag van de magnetisatie gelijklopend met dat van driedimensionale materialen, terwijl er een

groot verschil bestaat met 2D materialen met een easy-plane anisotropie. Over het algemeen is er een oplijning van de magnetisatie met de intrinsieke anisotropie bij lage temperaturen en kleine magnetische velden, terwijl deze zich heoriënteert in de richting van het aangelegde veld in de tegenovergestelde regimes. De dipool-dipool-interactie kan een extra bijdrage leveren tot de easy-plane anisotropie in dunne materialen, waarbij het bijbehorende langedrachtskarakter de magnetisatie wellicht stabiliseert. We besluiten dat we een effectieve manier hebben gevonden om enkele onlangs ontdekte 2D ferromagneten te beschrijven, waarbij de aanwezige easy-axis anisotropie kan verklaren dat de Curie-temperaturen positief zijn. Onze resultaten maken het mogelijk om de magnetisatie in 2D materialen te voorspellen bij eindige temperaturen en ook in de aanwezigheid van een magneetveld dat onder een willekeurige hoek kan worden aangelegd. Om verder computationeel onderzoek naar monolaagferromagneten te stimuleren stelden we een computerprogramma publiek beschikbaar om Curie-temperaturen te berekenen op basis van ons formalisme. Aangezien dit programma enkel afhangt van *ab initio* berekende parameters, kan het ook gebruikt worden om de effecten van druk- en trekspanning (strain) of elektrische velden op de overgangstemperatuur te onderzoeken. Op de lange termijn kan de beschreven methodologie uitgebreid worden naar materialen met meerdere lagen, andere magnetische interacties evenals dynamische effecten.

Dankwoord

Zoals bij elk groot project, is ook een doctoraat zeker niet enkel de verdienste van de auteur van het proefschrift.

Eerst en vooral wil ik uitdrukkelijk mijn promotoren en tevens dagelijkse begeleiders prof. dr. Wim Magnus en prof. dr. ir. Bart Sorée te bedanken. Terwijl ik verhalen hoor over verdwijntrucs die andere promotoren uithalen, om dan plots aan het einde van het doctoraat terug op te duiken, waren zij juist erg toegankelijk gedurende mijn hele doctoraat. Eender wanneer kon ik bij hen terecht met mijn vragen of om ideeën af te toetsen. Ik wil hen ook bedanken voor de vrijheid die ik kreeg om dingen die mij nuttig of interessant leken verder te onderzoeken. Naast hun wetenschappelijke ondersteuning, waren ze er ook steeds voor een leuke babbel over alles en niets, uiteraard met inbegrip van de nodige absurde fysica-humor. Ik wens ook prof. dr. Milorad V. Milošević en dr. Cihan Bacaksiz te bedanken voor de vlotte samenwerking en hun bijdragen aan dit werk. Verder bedank ik de leden van mijn doctoraatsjury voor hun interessante vragen en constructieve opmerkingen die verder hebben bijgedragen aan deze thesis in zijn uiteindelijke vorm. Daarnaast wil ik ook Imec bedanken om dit doctoraat financieel en praktisch mogelijk te maken en het Fonds Wetenschappelijk Onderzoek Vlaanderen (FWO) om enkele conferenties mee te financieren.

Naast deze directe bijdragers aan dit werk, zijn er uiteraard ook veel mensen die indirect hebben bijgedragen. Ik denk hierbij onder meer aan mijn bureaugenoten en (in)directe collega's Ahmed, Gautam, Rutger, Arnout, Sabyasachi, Dimitrios, Javier, Thomas, Frederic, Frederik en Olivier. Ook de vrienden en collega's die steeds voor aangename lunch- of koffiepauzes zorgden, zoals Nandi, Dieter, Eva, Stefanie, Johan, Elke, Timon, Nathan, Kalliopi, Bram en Ruhui, verdienen hier zeker een plek.

Tot slot wil ik uiteraard ook mijn partner Eline, ouders, zus, familie en vrienden bedanken om mij steeds te steunen in alles wat ik doe.

Contents

1 Introduction

1.1 Scientific motivation

Since *The rise of graphene* [1], the scientific interest in two-dimensional (2D) materials—especially layered van der Waals (vdW) compounds—has been ever-growing. These atomically thin substances are an ideal playground for new physical phenomena, while often having enhanced properties compared to their bulky counterparts, such as a higher electron mobility or an altered optical behaviour. While a two-dimensional ferromagnetic material was still missing, some of its properties, such as excitation spectra, could be probed through so-called semi-2D materials [2, 3]. These layered van der Waals compounds, with a weak interlayer coupling as compared to their intralayer interactions, are believed to have properties resembling those of two-dimensional magnets.

Finding a truly two-dimensional ferromagnetic substance was considered unlikely for a long time, because of the detrimental predictions of the Mermin-Wagner theorem [4]. This theorem excludes the possibility of ferromagnetic or antiferromagnetic ordering at non-zero temperatures in one- or two-dimensional isotropic materials in the absence of long-range magnetic interaction. The conditions to be fulfilled for the rigorous Mermin-Wagner theorem to hold are often not strictly valid in potential single-layered ferromagnets:

- The magnetic interaction P_{ij} between atoms (magnetic moments) i and j in the lattice should be of short range. Specifically, $\sum_j P_{ij} r_{ij}^2$ should be finite, where the sum is over all atoms in the lattice and r_{ij} is the distance between the atoms [5]. The magnetic dipole-dipole interaction is always present and has $P_{ij} \propto r_{ij}^{-3}$, such that the sum $\sum_j P_{ij} r_{ij}^2 \propto \int_0^\infty \mathrm{d}r \to \infty$ diverges.

- The continuous rotational SO(2) symmetry in the magnetisation direction should not be broken. This condition is typically violated in practice. A symmetry breaking can be induced through interfacial effects or by the presence of an intrinsic anisotropy in the 2D material, caused by, for example, spin-orbit coupling.

- The Mermin-Wagner theorem only holds in the limit of infinite lattices, and it is known that finite size effects can play an important role [6]. Excitations with the longest wave lengths—which are responsible for the absence of magnetisation—are suppressed in samples of finite size. This might have a stabilising effect for the magnetisation in thin ferromagnets [6]. However,

> atoms at the sides of such samples have fewer neighbours to interact with magnetically and might be more vulnerable for external disturbances [7]. These competing effects might tip the balance in either direction.

The Mermin-Wagner theorem is thus, in fact, inconclusive on the possibility of ferromagnetic ordering in two-dimensional materials. Note that other types of ordering, such as spin-spiral textures, are also not prohibited by the theorem.

In 2017, Huang et al. [8] and Gong et al. [9] reported [10] the experimental discovery of ferromagnetism in monolayers of chromium triiodide (CrI_3) and a bilayer chromium germanium telluride ($Cr_2Ge_2Te_6$), respectively. Both monolayers were obtained through mechanical exfoliation and placed on a SiO_2/Si substrate. A single layer of CrI_3 was found to be ferromagnetic up to the ferromagnetic transition (Curie) temperature $T_C = 45\,K$. For multilayered samples, the authors found that an even number of layers behaved antiferromagnetically, while an odd number of layers was ferromagnetic. Later it was found that even-layered samples can be switched from an antiferromagnetic to a ferromagnetic state by applying voltages [11–13]. Huang et al. explained their results through an Ising model (subsection 1.3.2) and antiferromagnetic coupling between different layers. $Cr_2Ge_2Te_6$, on the other hand, required a small external field of $0.075\,T$ to exhibit a ferromagnetic transition, which happens at a temperature that strongly depends on the precise applied field strength. Gong et al. showed that a nearly ideal two-dimensional isotropic Heisenberg ferromagnet (subsection 1.3.2), solved using renormalised spin wave theory, could explain some of their observations. However, they had to rescale their density functional theory (DFT) parameters to reproduce the correct transition temperature.

The first 2D ferromagnets boosted the scientific interest [13, 14], leading to more experimental discoveries. A non-zero Curie temperature was measured for monolayers of $CrBr_3$, another chromium trihalide, by Zhang et al. [15] and later by Kim et al. [16]. O'Hara et al. [17] found single-layer $MnSe_2$, grown on GaSe and $SnSe_2$ by molecular beam epitaxy, to exhibit room temperature spontaneous magnetisation. Also two-dimensional VSe_2 was found to have an in-plane spontaneous magnetisation at room temperature by Bonilla et al. [18]. This magnetisation is believed to be closely linked to charge density waves.

Theoretically, many fundamental questions remain unanswered, since the mechanism responsible for spontaneous magnetisation in two-dimensional ferromagnets is not well understood. It is unclear which of the conditions in the Mermin-Wagner theorem need to be violated and to which degree in order to get the observed ferromagnetic behaviour. This relates to the question of which parameters should be tweaked to effectively influence the magnetisation in thin films and how the Curie temperature of new materials can be predicted. In addition to these problems related to spontaneous magnetisation, it is also not clear how these single-layer

materials behave in external magnetic fields, possibly applied in an arbitrary direction. This understanding of basic properties is crucial to enable materials engineering and technological development.

1.2   Technological motivation

Magnetic materials and effects have always been ubiquitous in computer technologies, especially for memory applications. This is especially true since the onset of spintronics [19] in 1988 with the discovery of the giant magnetoresistance (GMR) effect by Albert Fert [20] and Peter Grünberg [21]. Magnetic and spintronic technologies (both using ferromagnets [19] and more recently also antiferromagnets [22–25]) are especially prosperous because of the plethora of possible effects to take advantage of: various spin Hall effects (SHE) [26], spin-orbit coupling (SOC) and spin-orbit torque (SOT), band spin splitting, spin transfer torque (STT) [27], the magnetoelectric effect (ME) [11, 12, 28, 29] and voltage control of magnetism [30, 31]... The emergence of two-dimensional magnetic materials in these technologies is unavoidable when devices are scaled down to limit costs. Moreover, new or enhanced effects exhibited by these thin magnetic compounds can open pathways to novel or improved devices [32]. For example, today, an active field of research is the engineering of magnetic tunnel junctions (MTJs) [33] for the use in spin transfer torque magnetic random access memories (STT-MRAM) [27]. These devices typically consist of a stack of many thin layers [13], one of which is a ferromagnet storing the state of the memory as its magnetisation direction. This direction, and thus the state of the memory, is switched by applying a spin-polarised current. A thinner ferromagnet would allow for lower critical currents. Moreover, MTJs that are entirely built from vdW materials could have a uniform barrier thickness, allowing for all-area tunnelling [32].

Traditionally, most logic devices are based on electronic transport. Recently, there have been a few proposals to use spin waves or magnetisation waves to perform logic operations [34–40]. Typically, these devices try to benefit from the inherent wave nature to calculate, for example, Fourier transforms in hardware. One of the most promising devices is the spin wave majority gate (SWMAG) [41, 42], which is schematically depicted in Figure 1.1. This device has multiple inputs and one output. The majority of the input states determines the output state, which can be used to create a reconfigurable AND/OR gate, for example. Internally, antennas or magnetoelectric cells create spin waves at the inputs [28]. These waves travel through thin ferromagnetic spin wave busses and generate the correct result at the output through wave interference. Benchmarks [43] show that this device can be two orders of magnitude more energy efficient than 10 nm CMOS technology, in which moving charges lead to Joule heating [34]. Through functional scaling, SWMAG circuits can decrease to less than half the size of their CMOS equivalent.
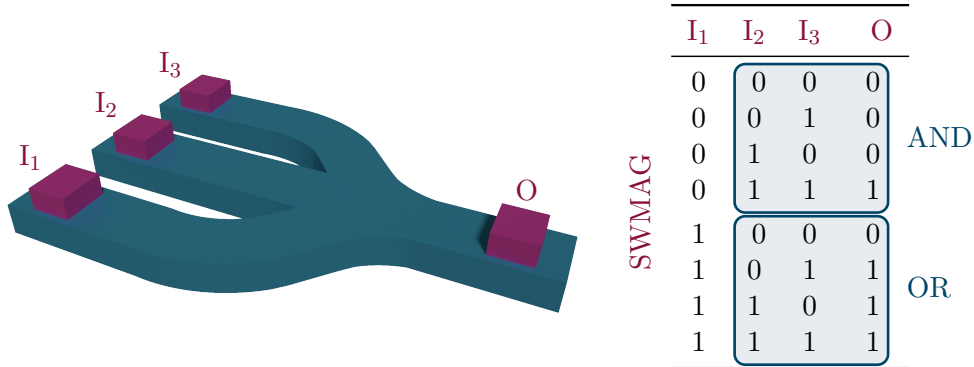
3

I_1	I_2	I_3	O	
0	0	0	0	
0	0	1	0	AND
0	1	0	0	
0	1	1	1	
1	0	0	0	
1	0	1	1	OR
1	1	0	1	
1	1	1	1	

Figure 1.1 Schematic representation of a spin wave majority gate with three inputs (I) and one output (O). Spin waves are generated below the inputs and travel through the ferromagnetic spin wave busses (blue) towards the crossing point. They interfere and travel to the output, where the state is detected. The truth table shows that switching I_1 makes the remainder of the device act as either an AND or an OR gate.

Since these devices will be slower compared to CMOS, they can be good candidates for Internet of Things (IoT) applications [39]. The working principle of the spin wave majority gate was demonstrated already in 2017 by Fischer et al. [44] with spin wave busses of 1.5 mm wide and 5.4 μm thick and progress has been going on to scale this device further down. The limit of this scaling endeavour will lead to ultra-thin ferromagnetic spin wave busses.

1.3 Magnetism and the Heisenberg model

In this thesis, we are interested in materials where the magnetisation originates from localised magnetic moments (spins). Their ferromagnetic interaction is well-described by Heisenberg-like spin lattice models, that we introduce rather extensively in this section. Note that these models are not a good fit for materials where magnetism originates from itinerant (free) electrons [45]. Moreover, they are also not well-suited to describe magnetisation domain dynamics, since they typically only describe the magnetisation behaviour in a single domain.

1.3.1 Origin of spin lattice models

An effective spin Hamiltonian can emerge from just Coulombic interactions and adherence to the Pauli exclusion principle. The di-hydrogen molecule H_2 is the most straightforward way to get some insight in the mechanisms at play. This molecule consists of two hydrogen atoms, labelled 1 and 2, with each an electron in its lowest energy orbital. These electrons are labelled A and B. Their momenta

and Coulombic interactions are described by the Hamiltonian

$$\hat{H} = \frac{\hat{\mathbf{p}}_A^2 + \hat{\mathbf{p}}_B^2}{2m_e} + \frac{e^2}{4\pi\epsilon_0} \left[\frac{1}{r_{AB}} - \frac{1}{r_{A1}} - \frac{1}{r_{A2}} - \frac{1}{r_{B1}} - \frac{1}{r_{B2}} \right], \tag{1.1}$$

where $r_{\alpha\beta}$ is the absolute distance between particles α and β, e is the electronic charge, m_e the electronic mass, $\hat{\mathbf{p}}_\alpha$ the momentum of electron α and ϵ_0 the permittivity of free space. The Hamiltonian is completely spin-independent and thus commutes with all spin operators.

We denote the total two-electron wave function of this system as $\Psi(\mathbf{r}_A\sigma_A, \mathbf{r}_B\sigma_B)$, where $\mathbf{r}_\alpha$ denotes the location of electron α and σ_α the projection of its spin along the **Z**-axis. Since the Hamiltonian commutes with any spin operator, the wave function can be safely factorised into a part ϕ that only has spatial dependence and a part χ that contains all the spin dependence. For the latter, a suitable basis can be found in the eigenfunctions of operators $\hat{\mathbf{S}}^2$ and $\hat{S}^Z$. The total wave function is thus

$$\Psi(\mathbf{r}_A\sigma_A, \mathbf{r}_B\sigma_B) = \phi(\mathbf{r}_A, \mathbf{r}_B)\chi(\sigma_A, \sigma_B). \tag{1.2}$$

Since the two electrons are identical fermions, they must obey the Pauli exclusion principle. This implies that their total wave function must be anti-symmetric when *exchanging* them, i.e. $\Psi(\mathbf{r}_A\sigma_A, \mathbf{r}_B\sigma_B) = -\Psi(\mathbf{r}_B\sigma_B, \mathbf{r}_A\sigma_A)$. The spin part of the wave function is anti-symmetric if it is in the spin singlet state

$$\chi_S(\sigma_A, \sigma_B) = \frac{1}{\sqrt{2}} \left(|\uparrow\downarrow\rangle - |\downarrow\uparrow\rangle \right) \tag{1.3a}$$

which has total spin $S = 0$. It is symmetric if it is in one of the three possible triplet states

$$\chi_T(\sigma_A, \sigma_B) = \begin{cases} |\uparrow\uparrow\rangle & S^Z = 1 \\ \frac{1}{\sqrt{2}} \left(|\uparrow\downarrow\rangle + |\downarrow\uparrow\rangle \right) & S^Z = 0 \\ |\downarrow\downarrow\rangle & S^Z = -1 \end{cases} \tag{1.3b}$$

which all have total spin $S = 1$, but different projections along the **Z**-axis. Since the total wave function must be anti-symmetric, the spatial part ϕ_S must be symmetric when the spins are in the singlet state. When the spins are in the triplet state, the spatial part ϕ_T must be anti-symmetric. Through this we see that, although ϕ is the solution to the Schrödinger equation with a spin-independent Hamiltonian $\hat{H}$, the spatial symmetry and total spin of the system are correlated as a result of the Pauli exclusion principle.

Since the Hamiltonian commutes with the spin-dependent part of the wave function, the energies of the singlet and triplet wave functions are

$$E_S(\mathbf{r}_{12}) = \iint d\mathbf{r}_A\, d\mathbf{r}_B\, \overline{\phi_S(\mathbf{r}_A, \mathbf{r}_B)} \hat{H} \phi_S(\mathbf{r}_A, \mathbf{r}_B) \tag{1.4a}$$

$$E_T(\mathbf{r}_{12}) = \iint d\mathbf{r}_A\, d\mathbf{r}_B\, \overline{\phi_T(\mathbf{r}_A, \mathbf{r}_B)} \hat{H} \phi_T(\mathbf{r}_A, \mathbf{r}_B). \tag{1.4b}$$

They can depend on the relative position $\mathbf{r}_{12}$ of the atomic nuclei. When the nuclei are far apart (and the electrons barely interacting), ϕ_S and ϕ_T can be well approximated by the (anti-)symmetric combination of unperturbed H atomic orbitals [46]. When the atoms are closer together, these atomic orbitals are perturbed and the Heitler-London approximation [47] can be used for a better description. While the details of those orbitals are not of interest here, we note that their electron density decays exponentially as function of the distance to the nucleus.

The spin value of each of the electron spins is $S_i = 1/2$, such that the expectation value of the squared spin operator is $\mathbf{S}_i^2 = S_i \cdot (S_i + 1) = 3/4$. Note that we use the convention $\hbar = 1$ here and in the remainder of this thesis. For the system's total spin expectation value, this means

$$\mathbf{S}^2 = (\mathbf{S}_A + \mathbf{S}_B)^2 = (\mathbf{S}_A^2 + \mathbf{S}_B^2 + 2\mathbf{S}_A \cdot \mathbf{S}_B) = \frac{3}{2} + 2\mathbf{S}_A \cdot \mathbf{S}_B, \tag{1.5}$$

while on the other hand $\mathbf{S}^2 = S \cdot (S + 1)$. From these two relations, one can easily determine that $\mathbf{S}_A \cdot \mathbf{S}_B = -3/4$ for the singlet state ($S = 0$), while $\mathbf{S}_A \cdot \mathbf{S}_B = 1/4$ for the triplet state ($S = 1$). For the system under consideration, the Hamiltonian

$$\hat{H} = \frac{1}{4} \left[E_S(\mathbf{r}_{12}) - 3E_T(\mathbf{r}_{12}) \right] - \left[E_S(\mathbf{r}_{12}) - E_T(\mathbf{r}_{12}) \right] \hat{\mathbf{S}}_A \cdot \hat{\mathbf{S}}_B \tag{1.6}$$

thus gives the same eigenvalues for Ψ_S and Ψ_T as the Hamiltonian with Coulombic interactions that we started from. Finally, with a shift in the zero-point energy the Hamiltonian can be written effectively as

$$\hat{H}_{ex} = -J(\mathbf{r}_{12}) \hat{\mathbf{S}}_A \cdot \hat{\mathbf{S}}_B. \tag{1.7}$$

This is called an exchange Hamiltonian, since the exchange of electrons in the Pauli principle leads to an effective energy, called the exchange energy or exchange strength $J(\mathbf{r}_{12})$. When the exchange Hamiltonian originates from the mechanisms described here, it is valid if the electrons are localised enough such that their orbitals are disturbed only slightly, but there is still some overlap between the orbitals as to yield a finite $J(\mathbf{r}_{12})$. Since the atomic orbitals fall off exponentially, $J(\mathbf{r}_{12})$ rapidly becomes very small as $\mathbf{r}_{12}$ grows. Other exchange mechanisms

may lead to exchange energies with a longer interaction range or other functional dependencies of the exchange Hamiltonian on the spin operators. Examples are super exchange, where an intermediate atom "carries" the exchange further; double exchange; the Hubbard model, where strong Coulombic screening allows electrons only to "hop" from one atom to another; or spin-orbit coupling in the starting Hamiltonian, which can lead to anisotropic exchange couplings.

By studying the simple H_2 molecule, we made it plausible that a magnetic material can be described by effective spins $\hat{\mathbf{S}}_i$ at the atom's lattice positions, which are indexed by i. Those spins interact through an exchange Hamiltonian

$$\hat{H}_{ex} = -\frac{1}{2} \sum_{i,j} J_{ij} \hat{\mathbf{S}}_i \cdot \hat{\mathbf{S}}_j, \tag{1.8}$$

with exchange strength $J_{ij} = J(\mathbf{r}_{ij})$ and a factor $1/2$ to correct for double-counting. It often suffices to consider only interactions between the nearest neighbours due to the exchange interaction's short-range nature. In practice, the exchange strength can be obtained either by comparing model predictions with experimental results or through DFT calculations.

It is only a small step to also add interactions with an externally applied magnetic flux density $\mathbf{B}$. The energy of a magnetic moment $\mathbf{m}$ in such a field is $-\mathbf{m} \cdot \mathbf{B}$, while the magnetic moment of a spin $\mathbf{S}$ is $\mathbf{m} = g_e \mu_B \mathbf{S}$, with g_e the landé g-factor and μ_B the Bohr magneton. The Hamiltonian describing the interaction of an external field $\mathbf{B}$ with a lattice of spins is thus

$$\hat{H}_B = -g_e \mu_B \mathbf{B} \cdot \sum_i \hat{\mathbf{S}}_i. \tag{1.9}$$

This Hamiltonian is typically referred to as the Zeeman Hamiltonian, after the energy splitting of spin-1/2 particles (electrons around a nucleus) in a magnetic field.

The combined Hamiltonian $\hat{H} = \hat{H}_{ex} + \hat{H}_B$ is typically referred to as the (quantum) Heisenberg model [45, 48–51]. While this model looks deceptively simple, it has only been solved exactly in one dimension by Bethe [52]. For all other situations one must either further simplify the Hamiltonian or fall back to approximative solution techniques.

1.3.2 Plethora of spin lattice models

Several variations on the quantum Heisenberg model are possible. They are introduced either because they are better solvable or because they describe the material more accurately. We give a brief overview of the most common ones.

One of the most straightforward simplifications is to treat the spins in the Hamiltonian as classical spins with fixed length:

$$\hat{H}_{\text{Heis,CL}} = -\frac{1}{2} \sum_{i,j} J_{ij} \mathbf{S}_i \cdot \mathbf{S}_j - g_e \mu_B B \cdot \sum_i \mathbf{S}_i. \tag{1.10}$$

This is typically referred to as the classical Heisenberg model or 3-vector model. It is easier to treat because one does not need to account for discrete quantum mechanical states or quantum statistics.

Similar to the 3-vector model, there is also a 1-vector model. It is one of the most studied systems in statistical mechanics and more commonly known as the Ising system:

$$\hat{H}_{\text{Ising}} = -\frac{1}{2} \sum_{i,j} J_{ij} S_i^Z S_j^Z - g_e \mu_B B \sum_i S_i^Z \tag{1.11a}$$

$$= -\frac{1}{2} S^2 \sum_{i,j} J_{ij} \sigma_i \sigma_j - g_e \mu_B S B \sum_i \sigma_i \tag{1.11b}$$

with $\sigma_i = \pm 1$. It only accounts for the Z-components of the spins, which have fixed length and can only take values ± 1. This Hamiltonian was proposed by Lenz [53] and first solved in one dimension by Ising [54], whose name was given to the model [55]. An extensive treatment of this model is given by Huang [56].

Apart from the description of ferromagnets, the Ising model can equally well be used to describe gasses, binary alloys or even neural networks [56, 57]. Gasses can sometimes be described by a lattice gas model, where atoms can move around on a lattice. Whether or not a site is occupied by an atom is then represented by σ_i being positive or negative [58]. Binary alloys are materials where atoms of two types can switch places. The interaction between atoms depends on whether they are of equal or different type. The occupation of a site by an atom of one type or the other can be associated with the sign of σ_i [59]. More recently, neural networks are being described by the Ising model. Each lattice site can represent a neuron, which either "fires" or not. The interactions J_{ij} then represent synapses that couple the neurons [60].

Next to its wide variety of application domains, the Ising model is popular because it can be solved exactly in some cases. The first solution in one dimension was by Ising [54] in 1925. In 1944, Onsager [61] found the first solution for a two-dimensional lattice of Ising spins. Although some progress has been made [62], an exact solution for the three-dimensional case is still not known to date. Nevertheless, such bulk systems have been studied extensively using Monte Carlo simulations, typically by employing the Metropolis-Hastings [63, 64] algorithm.

The classical Ising model can in turn be made slightly more complex by using quantum mechanical spins again:

$$\hat{H}_{\text{Ising,Q}} = -\frac{1}{2} \sum_{i,j} J_{ij} \hat{S}_i^Z \hat{S}_j^Z - g_e \mu_B B \sum_i \hat{S}_i^Z. \tag{1.12}$$

As far as the spin-1/2 system is concerned, the classical and quantum mechanical model are equivalent. For $S > 1/2$, each of the spins in the classical model can only take values $S_i^Z = \pm S$, while those in the quantum mechanical model can yield the $2S + 1$ distinct eigenstates $S_i^Z \in \{-S, -S + 1, \ldots + S\}$.

Next to the 1- and 3-vector model, there is of course also a 2-vector model

$$\hat{H}_{\text{XY}} = -\frac{1}{2} \sum_{i,j} J_{ij} \left(S_i^X S_j^X + S_i^Y S_j^Y \right) - g_e \mu_B B \cdot \sum_i S_i^Z, \tag{1.13}$$

which is often called the XY-model and has an obvious quantum mechanical extension. Here, it is customary to apply the magnetic field in the Z-direction. This model does not exhibit a conventional transition to long-range (ferromagnetic) order. Instead, its susceptibility diverges at temperatures below T_{KT}, known as the Berezinskii-Kosterlitz-Thouless [65, 66] temperature. It marks the onset topological order due to bound pairs of vortex and antivortex spin arrangements, leading to quasi-long range magnetic order [13].

Next to the simplifications and restrictions of the models above, the isotropic Heisenberg model is often further generalised to account for different anisotropies. One way to account for those is to consider an anisotropic exchange interaction

$$\hat{H}_{\text{ex}} = -\frac{1}{2} \sum_{i,j} \left[J_{ij}^X \hat{S}_i^X \hat{S}_j^X + J_{ij}^Y \hat{S}_i^Y \hat{S}_j^Y + J_{ij}^Z \hat{S}_i^Z \hat{S}_j^Z \right]. \tag{1.14}$$

This is called the XYZ-model when all exchange components are distinct $J^X \neq J^Y \neq J^Z$. When only two out of the three exchange components differ $J^X = J^Y \neq J^Z$, it is referred to as the XXZ-model. The latter is exactly solvable for $S = 1/2$ with nearest-neighbour interaction in one dimension using the Bethe Ansatz [52, 67]. As an alternative solution method, the spins can be mapped to fermions using the Jordan-Wigner transformation [68–70]. Some other physical phenomena, such as superfluidity in liquid Helium-II [71] and specific types of superconductivity [72], can also be mapped to—and thus understood in terms of—the XXZ-model. In chapter 3, we will have a closer look at the XXZ Heisenberg model.

Apart from adding anisotropy through the exchange interaction, one can also add it through a so-called single-ion anisotropy term

$$\hat{H}_{\text{single-ion}} = -\sum_i K_i \left(\hat{S}_i^Z \right)^2 \tag{1.15}$$

in the Hamiltonian. A term of this form can originate from spin-orbit coupling and gets its name from the fact that the spin operator in each term of the sum acts twice on the same lattice point. Typically, its effect on the system's behaviour is similar to that of the anisotropy in the XXZ Heisenberg model [73]. However, for $S = 1/2$ systems, the single-ion anisotropy merely shifts the zero-point energy, since $\left(S_i^Z\right)^2 = 1/4$. Another term that is always present whenever magnetic dipoles are involved is the dipolar interaction, which is long-range and anisotropic. It is often neglected because the energy associated with its interaction between two spins is typically a factor 10^{-2} smaller than that for exchange interactions. We will study its effects in more detail in chapter 4.

1.4 Common solution methods

In this section, we will give an overview of a few common solution methods to the introduced (quantum) models that are relevant for this work. In addition to these models, micromagnetic simulations [35, 40, 74, 75] are often necessary for the modelling of complex devices and their interaction with the environment. These simulations are based on the Landau–Lifshitz–Gilbert (LLG) equation [76], treating spins as classical moments and without reference to the discreteness of the atomic lattice. Most interactions are replaced by their phenomenological effects on the magnetisation.

1.4.1 Units and fields

We start with a brief overview of some of the conventions used in this thesis for the units in the field of magnetism. As discussed at the end of subsection 1.3.1, the energy E of a magnetic moment $\mathbf{m}$ in a magnetic field $\mathbf{B}$ is $E = -\mathbf{m} \cdot \mathbf{B}$. We will express energies E in units of milli-electronVolt [meV] and $\mathbf{B}$, also called the magnetic flux density, in units of Tesla [T]. As a result, the unit of the magnetic moment $\mathbf{m}$ is [meV/T]. The magnetic moment of a spin $\mathbf{S}$ is given by $\mathbf{m} = g_e \mu_B \mathbf{S}/\hbar$, where $\mathbf{S}$ has the units of the reduced Planck constant $\hbar = 6.58 \times 10^{-13}\,\text{meV s}$, the landé g-factor is dimensionless and approximately $g_e \approx 2$. The Bohr magneton is defined by $\mu_B = e\hbar/2m_e = 5.788 \times 10^{-2}\,\text{meV/T}$. As we did earlier, we will always express $\mathbf{S}$ in terms of the number of reduced Planck constants $\hbar$, i.e. $S = 1/2, 1 \ldots$ The magnetic moment of a spin $\mathbf{S}$ is thus $\mathbf{m} = g_e \mu_B \mathbf{S}$.

Typically, in electromagnetism [77], the B-field is expressed as $B = \mu_0 \left(\mathbf{H} + \mathbf{M}\right)$, where the $\mathbf{H}$-field is yet another magnetic field with units ampere per meter [A/m]. This means that the magnetisation $\mathbf{M}$ also has units [A/m]. The vacuum permeability is $\mu_0 = 1.257 \times 10^{-6}\,\text{T m/A}$. The magnetisation field $\mathbf{M}$ and $\mathbf{H}$-field are often related through $\mathbf{M} = \chi \mathbf{H}$, where χ is the volume magnetic susceptibility.

Since we will not deal with materials in the classical electromagnetic sense, but rather treat them as a collection of spins, we will use the following, slightly different conventions:

B External applied magnetic field, in units of Tesla [T];

M Magnetisation per spin in the lattice. This means that **M** is dimensionless with maximal magnitude $M_s = S$;

χ Magnetic susceptibility, defined through $\chi = \partial M / \partial B$ and consequently in units of inverse Tesla $[T^{-1}]$;

$\boldsymbol{\sigma}$ normalised magnetisation $\boldsymbol{\sigma} = \mathbf{M}/S = \mathbf{M}/M_s$.

1.4.2   Mean field theory

We will show the general scheme followed by mean field solutions. A good and more extended overview can be found in ref. [57]. We will derive a mean field solution for a general type of Heisenberg Hamiltonian

$$\hat{\mathrm{H}} = -\frac{1}{2} \sum_{i,j} J_{ij} \hat{\boldsymbol{S}}_i \cdot \hat{\boldsymbol{S}}_j - g_\mathrm{e} \mu_\mathrm{B} \mathbf{B} \cdot \sum_i \hat{\boldsymbol{S}}_i, \qquad (1.16)$$

where the spins $\hat{\boldsymbol{S}}_i$ can represent either quantum mechanical spin operators $\hat{\mathbf{S}}_i$, Ising spins $S_i^Z = S\sigma$ with $\sigma = \pm 1$, or classical spins $\mathbf{S}_i$. The exchange interaction is taken to be $J_{ij} = J$ when i and j are nearest neighbours, and $J_{ij} = 0$ otherwise. We want to find the homogeneous magnetisation $\mathbf{M} = \langle \hat{\boldsymbol{S}}_i \rangle$, where $\langle \cdots \rangle$ is the Canonical ensemble average. The magnetisation is assumed to be independent of the specific lattice point i in the homogeneous material.

The spins in the exchange term can be written as the sum of their average value and the fluctuations around this average $\hat{\boldsymbol{S}}_i = \mathbf{M} + (\hat{\boldsymbol{S}}_i - \mathbf{M})$, which leads to the identity

$$\hat{\boldsymbol{S}}_i \cdot \hat{\boldsymbol{S}}_j = \hat{\boldsymbol{S}}_i \cdot \mathbf{M} + \mathbf{M} \cdot \hat{\boldsymbol{S}}_j - M^2 + (\hat{\boldsymbol{S}}_i - \mathbf{M}) \cdot (\hat{\boldsymbol{S}}_j - \mathbf{M}) . \qquad (1.17)$$

One of the basic assumptions of the mean field theory is that the fluctuations $\hat{\boldsymbol{S}}_i - \mathbf{M}$ are small. They can thus be neglected when appearing in second order. The Hamiltonian is then

$$\hat{\mathrm{H}} \approx -\frac{1}{2} \mathbf{M} \cdot \sum_{i,j} J_{ij} (\hat{\boldsymbol{S}}_i + \hat{\boldsymbol{S}}_j) - g_\mathrm{e} \mu_\mathrm{B} \mathbf{B} \cdot \sum_i \hat{\boldsymbol{S}}_i, \qquad (1.18)$$

where the term contributing to an overall energy shift was left out, as it will not influence the final result. Relabelling the indices in the double sum and using

$J_{ji} = J_{ij}$ yields

$$\hat{H} \approx -\mathbf{M} \cdot \sum_{i,j} J_{ij}\hat{\boldsymbol{S}}_i - g_\mathrm{e}\mu_\mathrm{B}\mathbf{B} \cdot \sum_i \hat{\boldsymbol{S}}_i. \tag{1.19}$$

The mean-field Hamiltonian of a random spin $\hat{\boldsymbol{S}}_i$ is thus

$$\hat{H}^i_\mathrm{MF} = -g_\mathrm{e}\mu_\mathrm{B}\mathbf{B}_\mathrm{eff} \cdot \hat{\boldsymbol{S}}_i \tag{1.20}$$

where we introduced the effective field

$$\mathbf{B}_\mathrm{eff} = \frac{\mathbf{M}}{g_\mathrm{e}\mu_\mathrm{B}} J_\mathrm{tot} + \mathbf{B}, \ \text{with} \ J_\mathrm{tot} = \sum_j J_{ij} = zJ. \tag{1.21}$$

The coordination number z counts the number of nearest neighbours for a specific spin. The interaction of the spin at location i with all the other spins in the medium is thus represented by the interaction with the effective field they generate. The Hamiltonian $\hat{H}^i_\mathrm{MF}$ that is left, is the same as for a single spin $\hat{\boldsymbol{S}}_i$ in an external field $\mathbf{B}_\mathrm{eff}$. Such a representation is also often referred to as a molecular field theory, instead of mean field theory.

Since the exchange term in the original Hamiltonian is rotationally invariant, the spins (and thus the magnetisation) will naturally align with $\mathbf{B}$, which we will assume to be applied in the Z-direction. When the Z-projection of $\hat{\boldsymbol{S}}_i$ is $\mathcal{S}^Z$, its mean field energy is

$$E(\mathcal{S}^Z) = -g_\mathrm{e}\mu_\mathrm{B}\mathcal{S}^Z B_\mathrm{eff} \tag{1.22}$$

and its magnetisation $M = \mathcal{S}^Z$. The probability of the Z-projection of $\hat{\boldsymbol{S}}_i$ being $\mathcal{S}^Z$ is

$$p(\mathcal{S}^Z) = \frac{\mathrm{e}^{-\beta E(\mathcal{S}^Z)}}{\mathcal{Z}}, \ \text{with} \ \mathcal{Z} = \mathrm{Tr}\big[\mathrm{e}^{-\beta E(\mathcal{S}^Z)}\big] \tag{1.23}$$

the canonical partition function. In the latter, the trace represents the sum or integral over all possible discrete or continuous states $\mathcal{S}^Z$. We used the standard notation $\beta = k_\mathrm{B}T^{-1}$ for the inverse temperature. Since the spin at i was chosen arbitrarily, its average Z-projection equals the homogeneous magnetisation in the system and is given by

$$M = \langle \mathcal{S}^Z \rangle = \mathrm{Tr}[\mathcal{S}^Z p(\mathcal{S}^Z)] = \frac{\mathrm{Tr}\big[\mathcal{S}^Z \mathrm{e}^{-\beta E(\mathcal{S}^Z)}\big]}{\mathcal{Z}}. \tag{1.24}$$

For the different lattice models, different quantities need to be substituted. We introduce the variable $a = \beta S g_\mathrm{e}\mu_\mathrm{B}B_\mathrm{eff}$. For the classical Heisenberg model, which

has spins of fixed length S that can rotate, the Z-projection is $\mathcal{S}^Z = S\cos\theta$, with θ the angle of the spin relative to **Z**. The rotation of the spin is continuous, such that the traces denote an integration over all possible spin directions. The formula for the magnetisation is thus

$$M = \frac{\iint S\cos\theta \; \mathrm{e}^{a\cos\theta}\,\mathrm{d}\Omega}{\iint \mathrm{e}^{a\cos\theta}\,\mathrm{d}\Omega}, \tag{1.25}$$

with the solid angle differential $\mathrm{d}\Omega = \sin\theta\,\mathrm{d}\theta\,\mathrm{d}\phi$. For the Ising system, the spin of fixed length S can only point up or down. The Z-projection is $\mathcal{S}^Z = S\sigma$, with $\sigma = \pm 1$. The traces denote just the sum over these two possibilities, such that the magnetisation can be calculated as

$$M = \frac{S\mathrm{e}^{+a} - S\mathrm{e}^{-a}}{\mathrm{e}^{+a} + \mathrm{e}^{-a}}. \tag{1.26}$$

The quantum Heisenberg model is after the mean field approximation equivalent to the quantum Ising model: the X- and Y-components do not play a role and only the component in the direction of the applied field is accounted for. The Z-projection is $\mathcal{S}^Z = m_Z$, where m_Z can take the values $-S, -S+1, \ldots S$. As for the Ising model, the traces denote a sum over these $2S + 1$ possible states, leading to the magnetisation

$$M = \frac{\displaystyle\sum_{m_Z=-S}^{S} m_Z \,\mathrm{e}^{am_Z/S}}{\displaystyle\sum_{m_Z=-S}^{S} \mathrm{e}^{am_Z/S}}. \tag{1.27}$$

Working out the above formulas, leads for all three models to the solution

$$\frac{M}{S} = \mathcal{F}(a), \text{ with } a = \beta S g_{\mathrm{e}}\mu_{\mathrm{B}} B_{\mathrm{eff}} = \frac{1}{k_{\mathrm{B}}T}\left\{ S^2\frac{M}{S}J_{\mathrm{tot}} + S g_{\mathrm{e}}\mu_{\mathrm{B}}B \right\}, \tag{1.28}$$

which still needs to be solved for M/S. Only the function $\mathcal{F}(x)$ (see Figure 1.2) to substitute depends on the specific model:

$$\mathcal{F}(x) = \begin{cases} \tanh x & \text{Ising} \\ \mathcal{B}_S(x) & \text{quantum Ising/Heisenberg} \\ \mathcal{L}(x) & \text{classical Heisenberg,} \end{cases} \tag{1.29}$$

where the Langevin function $\mathcal{L}(x)$ and Brillouin function $\mathcal{B}_S(x)$ of order S are defined by

$$\mathcal{L}(x) = \coth x - \frac{1}{x} \tag{1.30a}$$

$$\mathcal{B}_S(x) = \frac{2S+1}{2S}\coth\left(\frac{2S+1}{2S}x\right) - \frac{1}{2S}\coth\left(\frac{x}{2S}\right). \tag{1.30b}$$
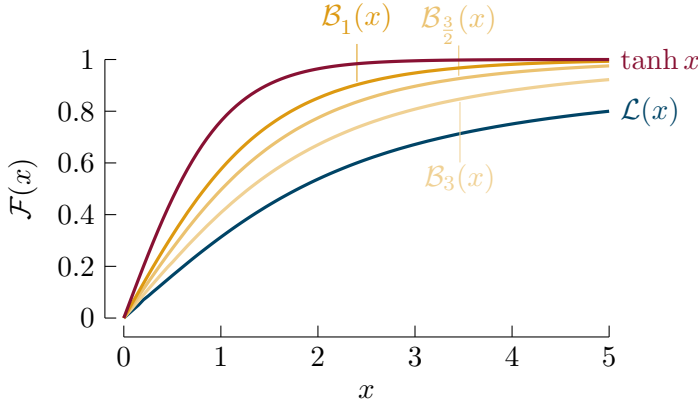
Figure 1.2 The behaviour of $\mathcal{F}(x)$ for the Ising model (red), the classical Heisenberg model (blue) and the quantum Ising/Heisenberg model with $S = 1, 3/2$ and 3 (yellow).

The functions $\mathcal{F}(x)$ all have a linear dependence on x for small x. At this point there are two important observations to make: (i) as required, the magnetisation in the quantum Heisenberg model reduces to that of the Ising model for $S = 1/2$ and to that of the classical Heisenberg model for $S \to \infty$, and (ii) the formulas do not depend on the specific lattice structure or its dimensionality. Only the number of nearest neighbours z plays a role. This is one of the problems of the mean field theory.

When considering non-interacting spins, i.e. $J_{\text{tot}} = 0$, our solution corresponds to Langevin's theory of paramagnetism. At room temperature, even for strong fields, the variable $a = \frac{g_e \mu_B}{k_B} S \frac{B}{T} \ll 1$ since $\frac{g_e \mu_B}{k_B} \approx 1.343 \, \text{K/T}$. The magnetisation thus increases linear in the field. The zero-field magnetic susceptibility is in this case

$$\chi = \lim_{B \to 0} \frac{\partial M}{\partial B} = \frac{C}{T}, \tag{1.31}$$

with C the Curie constant, given by

$$C = \begin{cases} S^2 \frac{g_e \mu_B}{k_B} & \text{Ising} \\ \frac{1}{3} S (S + 1) \frac{g_e \mu_B}{k_B} & \text{quantum Ising/Heisenberg} \\ \frac{1}{3} S^2 \frac{g_e \mu_B}{k_B} & \text{classical Heisenberg} \end{cases} . \tag{1.32}$$

This is Curie's law, which is typically observed in non-interacting, dilute collections of atoms such as paramagnetic salts. Only at very low temperatures, the limit $a \gg 1$ is reached and all the spins align approximately with the field, $M \approx 1$.

Now let us consider the case where the spins do interact, but there is no applied field $B \to 0$. The equation (1.28) then becomes

$$\frac{M}{S} = \mathcal{F}(a), \text{ with } a = \frac{S^2}{k_B T} J_{tot} \frac{M}{S} \tag{1.33}$$

and always has the solution $M = 0$. However, another solution is possible if the slope of $\mathcal{F}(a)$ exceeds 1 at $M = 0$, that is when

$$\left. \frac{d\mathcal{F}(a)}{dM} \right|_{B=0, M=0} > 1. \tag{1.34}$$

This condition is found to hold for temperatures below

$$T_C = \begin{cases} S^2 \frac{zJ}{k_B} & \text{Ising} \\ \frac{1}{3} S(S+1) \frac{zJ}{k_B} & \text{quantum Ising/Heisenberg} \\ \frac{1}{3} S^2 \frac{zJ}{k_B} & \text{classical Heisenberg} \end{cases}, \tag{1.35}$$

which we call the Curie temperature. This is the highest temperature below which the spontaneous magnetisation is found to be non-zero. The material is then in its ferromagnetic state. Three things should be noted about the mean field Curie temperatures:

- they are independent of the lattice structure or dimensionality of the system. For example, the mean field Curie temperature for the two-dimensional Heisenberg model is non-zero, while it should vanish according to the Mermin-Wagner theorem;

- the Ising and classical Heisenberg model scale with S as S^2. The quantum Ising and Heisenberg mode scale with S as $S(S+1)$, which is typical for quantum systems; and

- the Curie temperatures predicted through the mean field theory are typically too high compared to exact results or experiments. The overestimation is particularly large for systems with reduced dimensionality.

The first and third point are well illustrated by comparing with the exact result for the two-dimensional Ising model on a square ($z = 4$), hexagonal ($z = 6$) and honeycomb ($z = 3$) lattice:

$$T_C^{\text{Ising, exact}} = \begin{cases} \frac{2}{\ln(1+\sqrt{2})} S^2 \frac{J}{k_B} & \text{square [61]} \\ \frac{4}{\ln(3)} S^2 \frac{J}{k_B} & \text{hexagonal [78]} \\ \frac{2}{\ln(2+\sqrt{3})} S^2 \frac{J}{k_B} & \text{honeycomb [78]} \end{cases}. \tag{1.36}$$

Finally, we can also consider the situation where a small field is applied and internal interactions are present. The zero-field susceptibility can then be derived from

$$\chi = \lim_{B \to 0} \frac{\partial M}{\partial B} = \lim_{B \to 0} \frac{\partial M}{\partial B_{\text{eff}}} \frac{\partial B_{\text{eff}}}{\partial B} = \frac{C}{T} \left(1 + \frac{J_{\text{tot}}}{g_{\text{e}} \mu_{\text{B}}} \chi \right), \tag{1.37}$$

where we used the Curie law in the first factor and the expression for the effective field in the second. The zero-field susceptibility

$$\chi = \frac{C}{T - \Theta_{\text{C}}} \tag{1.38}$$

follows from solving this equation. This is the famous Curie-Weiss law with the Curie-Weiss temperature Θ_{C}, which is sometimes also referred to as the paramagnetic Curie temperature. For the mean field theory, the Curie-Weiss temperature equals the Curie temperature. Experimentally, however, the Curie-Weiss law is only found to be valid for large temperatures. At temperatures around the Curie temperature, the susceptibility typically behaves as $\chi^{-1} \propto |T - T_{\text{C}}|^{-\gamma}$ with $\gamma \approx 4/3$.

1.4.3 Spin wave theory

In this subsection, we derive some basic results of the linear spin wave theory. To keep the derivation clean and simple, we will derive results for a one-dimensional quantum Heisenberg chain in the absence of a magnetic field and at $T = 0$. This is sufficient to derive basic magnons and their dispersion relation. The results are then straightforward to extend to multiple dimensions and non-zero temperatures.

Consider

$$\hat{\text{H}} = -J \sum_{i=1}^{N} \hat{\mathbf{S}}_{i-1} \cdot \hat{\mathbf{S}}_i, \tag{1.39}$$

which is the isotropic Heisenberg Hamiltonian for N spins interacting ferromagnetically only with their nearest neighbours. We assume periodic boundary conditions with $i = N + 1 = 1$. By introducing the spin operators $\hat{\text{S}}_i^{\pm} = \hat{\text{S}}_i^x \pm i \hat{\text{S}}_i^y$ that obey the commutation relation $[\hat{\text{S}}_i^+, \hat{\text{S}}_j^-] = 2\hat{\text{S}}_i^z \delta_{ij}$ and using the cyclic boundary condition, the Hamiltonian can be written as

$$\hat{\text{H}} = -J \sum_{i=1}^{N} \left[\frac{1}{2} \left(\hat{\text{S}}_{i+1}^- \hat{\text{S}}_i^+ + \hat{\text{S}}_{i-1}^- \hat{\text{S}}_i^+ \right) + \hat{\text{S}}_{i-1}^z \hat{\text{S}}_i^z \right]. \tag{1.40}$$

When the spin at site i has z-component M, we write its state as $|M\rangle_i = |S, M\rangle_i$. The ground state for the total spin chain is

$$|0\rangle = \cdots |S\rangle_{i-1} |S\rangle_i |S\rangle_{i+1} \cdots \tag{1.41}$$

with all the spins aligned. The ground state with $M = S - 1$ at site i is written as

$$|\phi\rangle_i = \cdots |S\rangle_{i-1}|S-1\rangle_i|S\rangle_{i+1}\cdots. \tag{1.42}$$

For any site i, the relations $\hat{S}_i^+|0\rangle = 0$, $\hat{S}_i^-|0\rangle = \sqrt{2S}|\phi\rangle_i$ and $\hat{S}_i^z|0\rangle = S^2|0\rangle$ hold, such that $\hat{H}|0\rangle = -JNS^2|0\rangle$. The ground state $|0\rangle$ is thus indeed an eigenstate of the Hamiltonian, with associated ground state energy

$$E_0 = \langle 0 | \hat{H} | 0 \rangle = -JNS^2. \tag{1.43}$$

Thinking classically about this system, a state with a single spin's z-projection lowered by one, such as $|\phi\rangle_i$, would be assumed to be the lowest energy excitation. Using the relations

$$\hat{S}_{i\pm1}^-\hat{S}_i^+|\phi\rangle_j = \delta_{ij}\sqrt{2S}\hat{S}_{i\pm1}^-|0\rangle = 2S|\phi\rangle_{i\pm1} \tag{1.44a}$$

$$\hat{S}_{i-1}^z\hat{S}_i^z|\phi\rangle_j = S\left(S - \delta_{ij} - \delta_{i-1,j}\right)|\phi\rangle_j \tag{1.44b}$$

for this state, one finds that the Hamiltonian acts on it as

$$\hat{H}|\phi\rangle_j = -SJ\left[(|\phi\rangle_{j-1} - 2|\phi\rangle_j + |\phi\rangle_{j+1}) + NS|\phi\rangle_j\right]. \tag{1.45}$$

The first term indicates that the single-site spin reduction spreads out over time. The state with a localised spin lowering is not an eigenstate of the Hamiltonian!

The true lowest energy excitations are the so-called Bloch magnons [79] or spin waves

$$|\Phi(k)\rangle = \frac{1}{\sqrt{N}}\sum_{j=1}^{N}e^{ijk}|\phi\rangle_j, \tag{1.46}$$

which are collective excitations of the lattice. They spread the locally lowered spin-state over the entire lattice, each with a different phase factor. Such an excitation can exist with different wave vectors $k = 2\pi n/N$, where $n = -N/2 + 1, \ldots N/2$ and we assumed the lattice constant to be 1. Applying the Hamiltonian to the magnon state, confirms that it is an eigenstate of the system

$$\begin{aligned}
\hat{H}|\Phi(k)\rangle &= \frac{1}{\sqrt{N}}\sum_{j=1}^{N}e^{ijk}\hat{H}|\phi\rangle_j \\
&= -\frac{SJ}{\sqrt{N}}\sum_{j=1}^{N}e^{ijk}\left[(|\phi\rangle_{j-1} - 2|\phi\rangle_j + |\phi\rangle_{j+1}) + NS|\phi\rangle_j\right] \\
&= -\frac{SJ}{\sqrt{N}}\sum_{j=1}^{N}e^{ijk}\left[e^{ik} + e^{-ik} - 2 + NS\right]|\phi\rangle_j \\
&= -SJ\left[2\cos k - 2 + NS\right]|\Phi(k)\rangle,
\end{aligned} \tag{1.47}$$

with excitation energy

$$E_1 = \langle \Phi(k) | \hat{H} | \Phi(k) \rangle = \underbrace{S2J\left[1 - \cos k\right]}_{\omega(k)} \underbrace{-JNS^2}_{E_0}. \tag{1.48}$$

A single magnon thus adds an energy $\omega(k)$ to the system. A few important points need to be raised regarding these Bloch magnons:

- The spins in the system do not precess (which is anyway not possible in the classical sense), since $\langle \Phi(k) | \hat{S}_i^x | \Phi(k) \rangle = \langle \Phi(k) | \hat{S}_i^y | \Phi(k) \rangle = 0$. This is in contrast to the basic excitations in the classical Heisenberg model—which are confusingly also called spin waves. There, the spins precess around the z-direction with a time-dependent phase factor.

- The wave nature of the Bloch magnons is present in the phase factor e^{ijk} and becomes more apparent when considering the spin correlation function $\langle \Phi(k) | \hat{S}_j \cdot \hat{S}_l | \Phi(k) \rangle \propto \cos\left(k\left(j - l\right)\right)$.

- The magnon excitation energy $\omega(k)$ vanishes in the limit of small k. This means that very small excitations suffice for those long wave length magnons to be excited. In the limit $T \to 0$, the magnetisation dependence on temperature is $1 - M/S \propto T^{3/2}$ and is known as Bloch's $T^{3/2}$-law. This is in contrast to the results obtained from the mean field theory, for which the deviation from saturation magnetisation at low temperatures is exponentially small in T.

- A Bloch magnon is a boson, since it carries a unit spin. Bloch's non-interacting boson approximation is only valid at the lowest temperatures. Dyson took the calculations one step further,[80, 81] accounting for first-order interactions. His results are known as Dyson spin waves.

1.4.4   Holstein-Primakoff approximation

The last approximation that we want to discuss is the Holstein-Primakoff approximation [82], which is very popular in describing quantum spin systems [83–86]. Generally, it gives results of similar quality as Bloch or Dyson spin waves, but can be applied more systematically, with less cumbersome calculations for higher orders and for more general spin interactions.

The essential approximation made by Holstein and Primakoff was that the system is in *quasi-saturation*, meaning that $M \approx M_s$, or $\left(M_s - M\right)/M_s \ll 1$. This condition is always valid at temperatures far below the Curie temperature, with an increasing validity range for larger spin values S. In very strong magnetic fields, its usage may be valid throughout a large temperature range.

The basic procedure to follow for applying the Holstein-Primakoff approximation consists of four steps.

1. First one has to write the operators $\hat{S}_i^+$, $\hat{S}_i^-$ and $\hat{n}_i = S - \hat{S}_i^z$ in terms of bosonic creation and annihilation operators $\hat{a}_i^\dagger$ and $\hat{a}_i$ for magnon-like excitations, based on their effect on the total spin of the system:

$$\hat{S}_i^+ = \sqrt{2S}\left(1 - \hat{a}_i^\dagger\hat{a}_i/(2S)\right)^{1/2}\hat{a}_i \tag{1.49a}$$

$$\hat{S}_i^- = \sqrt{2S}\hat{a}_i^\dagger\left(1 - \hat{a}_i^\dagger\hat{a}_i/(2S)\right)^{1/2} \tag{1.49b}$$

$$\hat{n}_i = \hat{a}_i^\dagger\hat{a}_i. \tag{1.49c}$$

Each additionally created magnon-like excitation lowers the total spin value. This is typically referred to as the Holstein-Primakoff transformation.

2. The next step is to apply the condition of quasi-saturation, which can be translated into operator language as $\langle\hat{n}_i\rangle/(2S) = \langle\hat{a}_i^\dagger\hat{a}_i\rangle/(2S) \ll 1$. Generally, this boils down to replacing the terms $\left(1 - \hat{a}_i^\dagger\hat{a}_i/(2S)\right)^{1/2}$ by their approximate expectation value 1, in which case this approximation is also referred to as the linear spin wave approximation. Magnon interactions can be taken into account to higher order by keeping more terms in the Taylor expansion of this square root, to which one often refers as the renormalised spin wave approximation [87, 88]. Further, terms proportional to $\hat{n}_i\hat{n}_j$ may be neglected, as they have a small expectation value. Also terms containing a total of three creation or annihilation operators are to be neglected.

3. The third step is to transition to Fourier-transformed creation and annihilation operators. These allow to more naturally describe spin wave-like excitations. At this stage, the Hamiltonian is typically in diagonal form, such that the excitation eigenvalues can be extracted.

4. The final step is to calculate the partition function $\mathcal{Z}$, which allows to determine the magnetisation as

$$M = k_\mathrm{B}T\frac{\partial}{\partial B}\ln\mathcal{Z}. \tag{1.50}$$

In the proper regimes of validity, the Holstein-Primakoff approximation gives good results. However, it is clear from its basic premise that the derived theory is not valid up to, or even near, the ferromagnetic phase transition.

1.5 Outline

In the next chapter, we will introduce most of the necessary tools for the remainder of the thesis. Section 2.1 introduces the notation that we use for referring to

different lattice concepts. Next, in section 2.2, we extensively introduce our most important tool: Zubarev's double-time temperature-dependent Green functions. The following section is closely related and deals with the specificities of applying the Green function theory to ferromagnets.

We start chapter 3 with an extensive introduction of the main model in this thesis, which is a quantum Heisenberg model extended with anisotropic exchange interactions. This model is then transformed into a more generally useful form through a rotation into a magnetisation coordinate system. The obtained general equations are then partially solved in section 3.2, such that the obtained results can be re-used in chapter 4. In section 3.3, we continue the solution specifically for the extended Heisenberg model. The results comparing two- and three-dimensional cubic lattices are presented in section 3.4, followed by our calculations for honeycomb and hexagonal lattices (section 3.5). The latter two allow for comparison with experiments.

Chapter 4 introduces dipolar interactions into the Heisenberg model. After a coordinate rotation, the equations are brought into a similar form as before, such that the results obtained in section 3.2 can be applied. The final equations contain slowly converging lattice sums, which can be rewritten to converge faster by using the Ewald summation technique (section 4.2) and can be expanded to study their behaviour for low wave vectors (section 4.3).

In chapter 5, the main conclusions of this thesis are summarised, and we give some proposals for future work.

2 Formalism

2.1 Notation and lattice concepts

2.1.1 Direct and reciprocal lattice

Infinite and periodic crystals are conveniently described in two ways: through their direct lattice and through the spatial Fourier transformed reciprocal lattice.

The direct lattice is provided by its Bravais lattice, possibly complemented by a multiatomic basis (Figure 2.1). Given the crystal's primitive lattice vectors $\mathbf{a}_i$, any lattice position vector $\mathbf{r_l}$ on a d-dimensional Bravais lattice is uniquely determined by a d-tuple $\mathbf{l}$ through

$$\mathbf{r_l} = \sum_i^d l_i \mathbf{a}_i, \qquad l_i \in \mathbb{Z}. \tag{2.1}$$

The volume of the primitive cell is

$$v_a = \begin{cases} \|\mathbf{a}_1 \times \mathbf{a}_2\| & d = 2 \\ |\mathbf{a}_1 \cdot (\mathbf{a}_2 \times \mathbf{a}_3)| & d = 3 \end{cases} \tag{2.2}$$

and can be calculated as the volume of the entire crystal divided by the number of lattice sites for crystals with a monoatomic basis. Crystals that are not Bravais lattices can be described as a Bravais lattice with multiatomic basis. This basis is given by vectors $\mathbf{d}_\alpha$ that point from the Bravais lattice vectors $\mathbf{r_l}$ towards the atoms in the basis. The position of each atom in the crystal is then described uniquely by a position vector

$$\mathbf{r_{l\alpha}} = \mathbf{r_l} + \mathbf{d}_\alpha. \tag{2.3}$$

If the crystal is described by a Bravais lattice with a monoatomic basis, $\mathbf{d}_\alpha = \mathbf{0}$ is conventional and the index α of the position vector is dropped. The index is also dropped if the specific atom in the basis referred to is not of importance. This notation closely resembles that of Wallace [89].

The reciprocal lattice is given by the set of all vectors

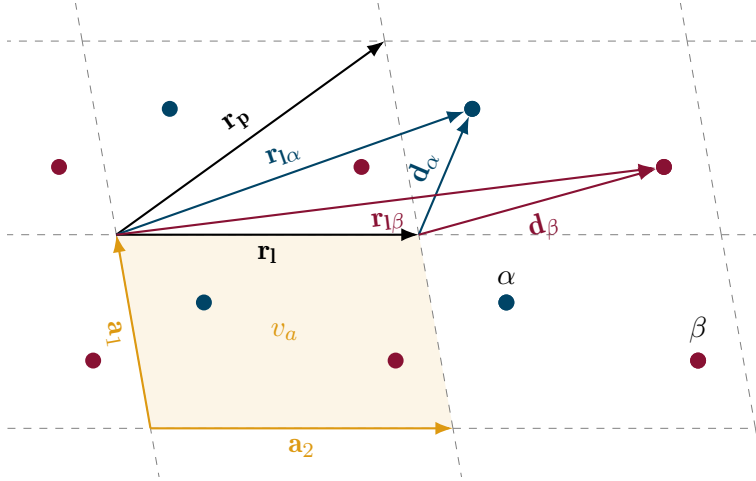$$\mathbf{G_m} = \sum_{i=1}^d m_i \mathbf{b}_i, \qquad m_i \in \mathbb{Z} \tag{2.4}$$

Figure 2.1 Direct lattice of a two-dimensional material with two atoms (α and β) in its basis. The primitive lattice vectors $\mathbf{a}_1$ and $\mathbf{a}_2$ span a yellow-shaded primitive cell with volume (area) v_a. Any Bravais lattice vector $\mathbf{r}_l$ or $\mathbf{r}_p$ can be constructed as an integer combination of the primitive lattice vectors. The Bravais lattice vector $\mathbf{r}_l$ together with an atomic basis vectors $\mathbf{d}_\alpha$ gives the position $\mathbf{r}_{l\alpha}$ of an atom in the α-sublattice.

that can be expressed in terms of primitive reciprocal vectors $\mathbf{b}_i$, defined in turn by

$$\mathbf{b}_i \cdot \mathbf{a}_j = 2\pi\delta_{ij}. \tag{2.5}$$

As a result, any reciprocal and direct lattice vector satisfy the relation

$$\mathbf{G_m} \cdot \mathbf{r_l} = 2\pi n, \qquad n \in \mathbb{Z}. \tag{2.6}$$

The reciprocal primitive cell—or first Brillouin zone (BZ)—has volume

$$v_b = \frac{(2\pi)^d}{v_a}. \tag{2.7}$$

2.1.2 Spatial Fourier transform

Consider a general function $f(\mathbf{r_{p\alpha}}, \mathbf{r_{l\beta}})$, which depends on the lattice vectors $\mathbf{r_{p\alpha}}$ and $\mathbf{r_{l\beta}}$ only through their difference $\mathbf{r_{p\alpha}} - \mathbf{r_{l\beta}}$ and on their places $\mathbf{d}_\alpha$ and $\mathbf{d}_\beta$ in the multiatomic basis. Such a function can be written as $f(\mathbf{r_{p\alpha}} - \mathbf{r_{l\beta}}, \mathbf{d}_\alpha, \mathbf{d}_\beta)$. Moreover, since the function has separate $\mathbf{d}_\alpha$ and $\mathbf{d}_\beta$ dependence, it can be rewritten such that its first argument is a Bravais lattice difference vector $\mathbf{r_{pl}} = \mathbf{r_{p\alpha}} - \mathbf{r_{l\alpha}} = \mathbf{r_p} - \mathbf{r_l}$. The function then becomes $f_{\mathbf{pl},\alpha\beta} = f(\mathbf{r_{pl}}, \mathbf{d}_\alpha, \mathbf{d}_\beta)$. When only a single first index is given, this means that $\mathbf{l} = \mathbf{0}$ was chosen as the origin, so $f_{\mathbf{p},\alpha\beta} = f(\mathbf{r_{p0}}, \mathbf{d}_\alpha, \mathbf{d}_\beta) = f(\mathbf{r_p}, \mathbf{d}_\alpha, \mathbf{d}_\beta)$. If f is furthermore not longer dependent on the sublattice α, we

drop this index and keep only the sublattice index to which the origin $\mathbf{l}$ belongs: $f_{\mathbf{p},\beta}$.

A function $f_{\mathbf{pl},\alpha\beta}$ can be expanded into its Fourier components $f_{\alpha\beta}(\mathbf{k})$ as

$$f_{\mathbf{pl},\alpha\beta} = \frac{1}{N} \sum_{\mathbf{k}\in\text{BZ}} e^{-i\mathbf{k}\cdot\mathbf{r}_{\mathbf{pl}}} f_{\alpha\beta}(\mathbf{k}) \tag{2.8}$$

to exploit the periodicity of the Bravais lattice. The sum is over the wave vectors $\mathbf{k} = (k^X, k^Y, k^Z)$ in the first Brillouin zone and N is the number of primitive cells in the Bravais lattice—also the number of wave vectors being summed over. This sum is well approximated by the integral

$$f_{\mathbf{pl},\alpha\beta} = \frac{1}{v_b} \int\limits_{\text{BZ}} e^{-i\mathbf{k}\cdot\mathbf{r}_{\mathbf{pl}}} f_{\alpha\beta}(\mathbf{k}) \, d\mathbf{k} \tag{2.9}$$

over the first Brillouin zone when the lattice is very large $(N \to \infty)$. The inverse Fourier transform is given by

$$f_{\alpha\beta}(\mathbf{k}) = \sum_{\mathbf{r}_{\mathbf{pl}}} e^{i\mathbf{k}\cdot\mathbf{r}_{\mathbf{pl}}} f_{\mathbf{pl},\alpha\beta} = \sum_{\mathbf{r}_{\mathbf{p}}} e^{i\mathbf{k}\cdot\mathbf{r}_{\mathbf{p}}} f_{\mathbf{p},\alpha\beta}, \tag{2.10}$$

where $\mathbf{r}_{\mathbf{p}}$ runs over all Bravais lattice vectors. An identity which often proves useful is the Fourier expansion of the spatial Kronecker delta function

$$\delta_{\mathbf{pl}} = \frac{1}{N} \sum_{\mathbf{k}\in\text{BZ}} e^{-i\mathbf{k}\cdot\mathbf{r}_{\mathbf{pl}}} = \frac{1}{N} \sum_{\mathbf{k}\in\text{BZ}} e^{-i\mathbf{k}\cdot\mathbf{r}_{\mathbf{lp}}}. \tag{2.11}$$

The notation with subindices both for the Bravais lattice position and the atomic basis position is rather heavy. Therefore, often only the Bravais lattice position will be written to indicate a lattice position. This can mean one of three things: (i) the lattice under consideration is monoatomic, (ii) the presented theory does not directly depend on the atomic basis position, or (iii) the atomic basis position is indicated in another manner. When the interpretation is not clear from notation alone, it will be clearly indicated.

2.1.3   Neighbour functions

We will often deal with interactions, such as the exchange interaction, that are isotropic with respect to the atoms spatial arrangement. Since these interactions depend only on the distance between lattice points, they can be expanded in terms of neighbour functions ζ_n which interact only with the n$^{\text{th}}$ nearest neighbours. Since these interactions are significant only over a limited distance, such an expansion

only needs to be carried out for one or at most a few nearest neighbours. There are z_n nearest neighbours that reside on lattice sites a distance a_n away. The first nearest-neighbour $z = z_1$ is called the coordination number. The neighbour functions are then

$$\zeta_{n,\mathbf{pl}} = \delta(\|\mathbf{r_{pl}}\| - a_n), \tag{2.12}$$

yielding non-zero values exactly for those atoms at $\mathbf{r_p}$ which are a distance a_n from $\mathbf{r_l}$. The Fourier transform of this function is

$$\zeta_n(\mathbf{k}) = \sum_{\mathbf{r_p}} e^{i\mathbf{k}\cdot\mathbf{r_p}} \zeta_{n,\mathbf{p}} = \sum_{\mathbf{p}\in\mathbb{N}_n} e^{i\mathbf{k}\cdot\mathbf{r_p}}, \tag{2.13}$$

where the set of nth nearest neighbours is denoted as

$$\mathbb{N}_n = \{\mathbf{p} \mid \|\mathbf{r_p}\| = a_n\}. \tag{2.14}$$

2.1.4 Lattice types

Standard books on solid state physics (e.g., Kittel [50] and Ashcroft and Mermin [45]) provide properties for the lattice types encountered in this thesis. The most important ones are summarised here, to avoid ambiguity in notation or definition. For every case, crystallographic unit vectors $(\mathbf{e}_1, \mathbf{e}_2, \mathbf{e}_3) = (\mathbf{X}, \mathbf{Y}, \mathbf{Z})$ will be used, with $\mathbf{Z}$ perpendicular to the plane of atoms for two-dimensional crystals. To keep the notation in this section compact, $\mathbf{X}, \mathbf{Y}$ and $\mathbf{Z}$ will sometimes be denoted as $\mathbf{e}_1, \mathbf{e}_2$ and $\mathbf{e}_3$, respectively. We will sometimes use the term *cubic* lattice to refer to the collection of the two-dimensional square and the three-dimensional simple cubic, face centred cubic and body centred cubic lattices.

Simple Cubic and Square

The simplest lattice structures are the three-dimensional ($d = 3$) Simple Cubic (SC) lattice, and its two-dimensional($d = 2$) variant, the SQuare (SQ) lattice. Their primitive lattice vectors are simply

$$\mathbf{a}_i = a\mathbf{e}_i, \tag{2.15}$$

where the lattice constant a equals the nearest-neighbour distance a_1. The Bravais lattice vectors are

$$\mathbf{r_l} = a\mathbf{l}, \text{ with } \mathbf{l} = \sum_{i=1}^{d} l_i \mathbf{e}_i, \tag{2.16}$$

spanning a primitive cell volume $v_a = a^d$. The primitive reciprocal vectors

$$\mathbf{b}_i = \frac{2\pi}{a}\mathbf{e}_i, \tag{2.17}$$

lead to the reciprocal lattice vectors

$$\mathbf{G_m} = \frac{2\pi}{a}\mathbf{m}, \text{ with } \mathbf{m} = \sum_{i=1}^{d} m_i \mathbf{e}_i. \tag{2.18}$$

The first Brillouin zone is defined by the inequalities $|k^X|, |k^Y|, |k^Z| \leqslant \pi/a$. The $z = 2 \times d$ nearest neighbours are

$$\mathbb{N}_1^{\text{SC}} = \{(\pm a, 0, 0), (0, \pm a, 0), (0, 0, \pm a)\} \tag{2.19a}$$

$$\mathbb{N}_1^{\text{SQ}} = \{(\pm a, 0), (0, \pm a)\}, \tag{2.19b}$$

leading to Fourier transformed neighbour functions

$$\zeta_1^{\text{SC}}(\mathbf{k}) = 2\left[\cos ak^X + \cos ak^Y + \cos ak^Z\right] \tag{2.20a}$$

$$\zeta_1^{\text{SQ}}(\mathbf{k}) = 2\left[\cos ak^X + \cos ak^Y\right]. \tag{2.20b}$$

Body Centred Cubic

The Body Centred Cubic (BCC) lattice with lattice constant a has primitive lattice vectors

$$\mathbf{a}_i = \frac{a}{2}\sum_{j=1}^{3}(-1)^{\delta_{ij}}\,\mathbf{e}_j. \tag{2.21}$$

The Bravais lattice vectors are then

$$\mathbf{r_l} = \frac{a}{2}\sum_{i=1}^{3}\sum_{j=1}^{3}(-1)^{\delta_{ij}}\,l_i\mathbf{e}_j, \tag{2.22}$$

spanning a primitive cell volume $v_a = a^3/2$ with nearest-neighbour distance $a_1 = \frac{\sqrt{3}a}{2}$. The primitive reciprocal vectors are

$$\mathbf{b}_i = \frac{2\pi}{a}\sum_{j=1}^{3}(1 - \delta_{ij})\,\mathbf{e}_j, \tag{2.23}$$

leading to reciprocal lattice vectors

$$\mathbf{G_m} = \frac{2\pi}{a}\sum_{i=1}^{3}\sum_{j=1}^{3}(1 - \delta_{ij})\,m_i\mathbf{e}_j. \tag{2.24}$$

A wave vector $\mathbf{k}$ belongs to the first Brillouin zone when it satisfies $|k^i| + |k^j| \leqslant 2\pi/a$ for each combination of components $i, j \in \{X, Y, Z\}$. With the $z = 8$ nearest neighbours

$$\mathbb{N}_1^{\mathrm{BCC}} = \left\{ \left(\pm\frac{a}{2}, \pm\frac{a}{2}, \pm\frac{a}{2} \right) \right\} \tag{2.25}$$

the Fourier transformed neighbour function becomes

$$\zeta_1^{\mathrm{BCC}}(\mathbf{k}) = 8 \cos\left(\frac{a}{2}k^X\right) \cos\left(\frac{a}{2}k^Y\right) \cos\left(\frac{a}{2}k^Z\right). \tag{2.26}$$

Face Centred Cubic

The Face Centred Cubic (FCC) lattice is basically the same as the BCC lattice in reciprocal space and vice versa. With a lattice constant a, its primitive lattice vectors are

$$\mathbf{a}_i = \frac{a}{2} \sum_{j=1}^{3} (1 - \delta_{ij}) \, \mathbf{e}_j. \tag{2.27}$$

The Bravais lattice vectors are

$$\mathbf{r_l} = \frac{a}{2} \sum_{i=1}^{3} \sum_{j=1}^{3} (1 - \delta_{ij}) \, l_i \mathbf{e}_j. \tag{2.28}$$

spanning a primitive cell volume $v_a = a^3/4$ with nearest-neighbour distance $a_1 = \frac{a}{\sqrt{2}}$. This leads to primitive reciprocal vectors

$$\mathbf{b}_i = \frac{2\pi}{a} \sum_{j=1}^{3} (-1)^{\delta_{ij}} \, \mathbf{e}_j, \tag{2.29}$$

and reciprocal lattice vectors

$$\mathbf{G_m} = \frac{2\pi}{a} \sum_{i=1}^{3} \sum_{j=1}^{3} (-1)^{\delta_{ij}} \, m_i \mathbf{e}_j, \tag{2.30}$$

The first Brillouin zone reduces to the region $|k^X|, |k^Y|, |k^Z| \leqslant 2\pi/a$ with the additional restriction $|k^X| + |k^Y| + |k^Z| \leqslant 3\pi/(2a)$. The coordination number for the FCC lattice is $z = 12$. These nearest neighbours are located at the positions

$$\mathbb{N}_1^{\mathrm{FCC}} = \left\{ \left(\pm\frac{a}{2}, \pm\frac{a}{2}, 0 \right), \left(\pm\frac{a}{2}, 0, \pm\frac{a}{2} \right), \left(0, \pm\frac{a}{2}, \pm\frac{a}{2} \right) \right\}, \tag{2.31}$$

leading to the Fourier transformed neighbour function

$$\begin{aligned} \zeta_1^{\mathrm{FCC}}(\mathbf{k}) = 4 \Big[&\cos\left(\frac{a}{2}k^X\right) \cos\left(\frac{a}{2}k^Y\right) + \cos\left(\frac{a}{2}k^X\right) \cos\left(\frac{a}{2}k^Z\right) \\ &+ \cos\left(\frac{a}{2}k^Y\right) \cos\left(\frac{a}{2}k^Z\right) \Big]. \end{aligned} \tag{2.32}$$

Hexagonal

In two-dimensional crystals with a HEXagonal (HEX)—also called triangular—Bravais lattice, each atom has $z_1 = 6$ nearest neighbours at a distance $a_1 = a$, with a the lattice constant. The primitive lattice vectors

$$\mathbf{a}_1 = \frac{\sqrt{3}}{2}a\mathbf{X} + \frac{1}{2}a\mathbf{Y} \text{ and } \mathbf{a}_2 = \frac{\sqrt{3}}{2}a\mathbf{X} - \frac{1}{2}a\mathbf{Y} \tag{2.33}$$

have length $\|\mathbf{a}_i\| = a$ and define the Bravais lattice

$$\mathbf{r_l} = \frac{a}{2}\left[\sqrt{3}\left(l_1 + l_2\right)\mathbf{X} + \left(l_1 - l_2\right)\mathbf{Y}\right] \tag{2.34}$$

with primitive cell volume $v_a = \sqrt{3}a^2/2$. Turning to momentum space, the primitive reciprocal vectors are

$$\mathbf{b}_1 = \frac{2\pi}{a}\left(\frac{1}{\sqrt{3}}\mathbf{X} + \mathbf{Y}\right) \text{ and } \mathbf{b}_2 = \frac{2\pi}{a}\left(\frac{1}{\sqrt{3}}\mathbf{X} - \mathbf{Y}\right) \tag{2.35}$$

and have length $\|\mathbf{b}_i\| = 4\pi/(\sqrt{3}a)$. The reciprocal lattice vectors are

$$\mathbf{G_m} = \frac{2\pi}{a}\left[\frac{1}{\sqrt{3}}\left(m_1 + m_2\right)\mathbf{X} + \left(m_1 - m_2\right)\mathbf{Y}\right]. \tag{2.36}$$

Just as the primitive cell, the first Brillouin zone is hexagonal with boundaries

$$|k^X| \leqslant \frac{2\pi}{\sqrt{3}a} \text{ and } \frac{1}{\sqrt{3}}|k^X| + |k^Y| \leqslant \frac{4\pi}{3a}. \tag{2.37}$$

The nearest-neighbour locations are

$$\mathbb{N}_1^{\text{HEX}} = \{\pm\mathbf{a}_1, \pm\mathbf{a}_2, \pm\left(\mathbf{a}_1 - \mathbf{a}_2\right)\}, \tag{2.38}$$

yielding the Fourier transformed neighbour function

$$\zeta_1^{\text{HEX}}(\mathbf{k}) = 4\cos\left(\frac{\sqrt{3}}{2}ak^X\right)\cos\left(\frac{a}{2}k^Y\right) + 2\cos ak^Y. \tag{2.39}$$

Honeycomb

The HONeycomb (HON) lattice (Figure 2.3) is a hexagonal Bravais lattice with two atoms in its basis. This means that each of these two atomic basis positions form a sublattice—which themselves are hexagonal Bravais lattices—that will be denoted by A and B. The honeycomb lattice is thus described by the hexagonal primitive lattice vectors, Bravais lattice vectors and primitive cell volume, supplemented with the two atomic basis vectors

$$\mathbf{d}_{\text{A}} = \mathbf{0} \text{ and } \mathbf{d}_{\text{B}} = \frac{a}{\sqrt{3}}\mathbf{X}, \tag{2.40}$$
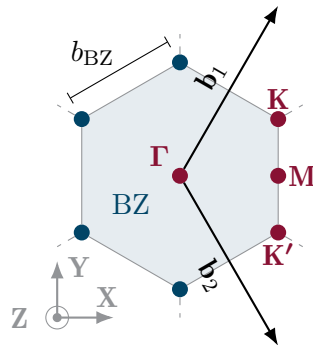
Figure 2.2 Sketch of the reciprocal space, the primitive reciprocal vectors $\mathbf{b}_1$ and $\mathbf{b}_2$ that span this space, and first Brillouin zone (shaded region) of the hexagonal and honeycomb lattice types. The red points highlight the symmetry points $\mathbf{\Gamma}$, $\mathbf{M}$, $\mathbf{K}$ and $\mathbf{K'}$ and b_{BZ} indicates the Brillouin zones side length.
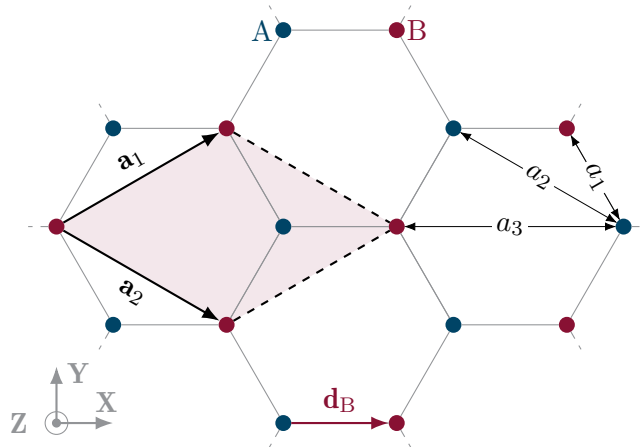
Figure 2.3 Sketch of the honeycomb lattice. The two sublattices—A (blue) and B (red)—each form a hexagonal lattice with primitive lattice vectors $\mathbf{a}_1$ and $\mathbf{a}_2$, which determine the primitive unit cell (shaded red). The atomic basis vector $\mathbf{d}_{\mathrm{B}}$ points from the A towards the B sublattice. The nth neighbour distances a_n are also shown.

which point from the Bravais lattice to either the atom on the A or B sublattice. The identical Bravais lattice ensures identical reciprocal lattice properties. In materials with a honeycomb lattice structure, not only interactions with the $z_1 = 3$ first nearest neighbours, but also those with the $z_2 = 6$ second and $z_3 = 3$ third nearest neighbours are often important. The positions of the n$^{\text{th}}$ nearest neighbours depends on the sublattice of the reference atom. The first nearest neighbours of an atom at sublattice A/B are located at positions

$$\mathbb{N}_{1,\text{A/B}}^{\text{HON}} = \{\pm\mathbf{d}_\text{B}, \pm\left(\mathbf{d}_\text{B} - \mathbf{a}_1\right), \pm\left(\mathbf{d}_\text{B} - \mathbf{a}_2\right)\}, \tag{2.41}$$

such that the Fourier transformed neighbour function is

$$\begin{aligned} \zeta_{1,\text{A/B}}^{\text{HON}}(\mathbf{k}) = \; &\cos\left(\frac{a}{\sqrt{3}}k^X\right) + 2\cos\left(\frac{a}{2\sqrt{3}}k^X\right)\cos\left(\frac{a}{2}k^Y\right) \\ &\pm \text{i}\left[\sin\left(\frac{a}{\sqrt{3}}k^X\right) - 2\sin\left(\frac{a}{2\sqrt{3}}k^X\right)\cos\left(\frac{a}{2}k^Y\right)\right]. \end{aligned} \tag{2.42}$$

The second nearest neighbours lie on the same sublattice as the reference atom. Since each sublattice itself forms a hexagonal Bravais lattice, the second nearest neighbours and their corresponding Fourier transformed neighbour function are equivalent to that for the first nearest neighbours of the hexagonal lattice:

$$\mathbb{N}_{2,\text{A/B}}^{\text{HON}} = \mathbb{N}_1^{\text{HEX}} \text{ and } \zeta_{2,\text{A/B}}^{\text{HON}}(\mathbf{k}) = \zeta_1^{\text{HEX}}(\mathbf{k}), \tag{2.43}$$

independent of the reference lattice. Finally, the third nearest neighbours

$$\mathbb{N}_{1,\text{A/B}}^{\text{HON}} = \{\pm\left(\mathbf{d}_\text{B} - \mathbf{a}_1 - \mathbf{a}_2\right), \pm\left(\mathbf{d}_\text{B} - \mathbf{a}_1 + \mathbf{a}_2\right), \pm\left(\mathbf{d}_\text{B} + \mathbf{a}_1 - \mathbf{a}_2\right)\}, \tag{2.44}$$

are similar to the first nearest neighbours, but mirrored over $\mathbf{Y}$ and elongated by a factor 2. The corresponding Fourier transformed neighbour function is

$$\begin{aligned} \zeta_{3,\text{A/B}}^{\text{HON}}(\mathbf{k}) = \; &\cos\left(\frac{2a}{\sqrt{3}}k^X\right) + 2\cos\left(\frac{a}{\sqrt{3}}k^X\right)\cos ak^Y \\ &\pm \text{i}\left[-\sin\left(\frac{2a}{\sqrt{3}}k^X\right) + 2\sin\left(\frac{a}{\sqrt{3}}k^X\right)\cos ak^Y\right]. \end{aligned} \tag{2.45}$$

2.2 Double-time temperature-dependent Green functions

In this section, the general solution framework will be introduced. This heavily relies on double-time temperature-dependent Green functions, which we will introduce extensively, together with some of their relevant properties. We closely follow a combination of the approaches given by Zubarev [90] and Callen [91] and important remarks of Stevens and Toombs [92] that were further detailed by Ramos and Gomes [93] and others [94–99].

2.2.1   Time correlation functions

Many observable quantities can be expressed as a time correlation function

$$C_{\hat{B}\hat{A}}(t,t') = \langle \hat{B}(t')\hat{A}(t) \rangle, \tag{2.46}$$

which is the canonical ensemble average of the product of operators $\hat{A}(t)$ and $\hat{B}(t')$ in the Heisenberg representation evaluated at times t and t'. A Heisenberg operator can be expressed in terms of a Schrödinger-type operator $\hat{A} = \hat{A}(0)$ as

$$\hat{A}(t) = e^{i\hat{H}t}\hat{A}e^{-i\hat{H}t} \tag{2.47}$$

and evolves according to the Heisenberg equation of motion

$$i\frac{d\hat{A}(t)}{dt} = [\hat{A}(t),\,\hat{H}(t)] = \hat{A}(t)\hat{H}(t) - \hat{H}(t)\hat{A}(t). \tag{2.48}$$

The canonical ensemble average itself is

$$\langle\ldots\rangle = \mathcal{Z}^{-1}\,\mathrm{Tr}\big(e^{-\beta\hat{H}}\ldots\big), \text{ where } \mathcal{Z} = \mathrm{Tr}\big(e^{-\beta\hat{H}}\big). \tag{2.49}$$

In the above, we use units with $\hbar = 1$ and introduce the systems Hamiltonian $\hat{H}$ and inverse temperature $\beta = 1/k_{\mathrm{B}}T$, with k_{B} the Boltzmann constant.

The correlation functions of a system in statistical equilibrium depend only on the time difference $t - t'$:

$$C_{\hat{B}\hat{A}}(t - t') = \langle \hat{B}(0)\hat{A}(t - t') \rangle. \tag{2.50}$$

At equal times $t = t'$, these time correlation functions give the average values of products of operators, i.e.

$$C_{\hat{B}\hat{A}}(0) = \langle \hat{B}(0)\hat{A}(0) \rangle = \langle \hat{B}\hat{A} \rangle. \tag{2.51}$$

It is often useful to consider the spectral density

$$\mathcal{S}(\omega) = \frac{1}{2\pi}\int\limits_{-\infty}^{\infty} C_{\hat{B}\hat{A}}(t)e^{i\omega t}\,dt \tag{2.52}$$

which is the Fourier transform of the time correlation function $C_{\hat{B}\hat{A}}(t)$. The correlation function can in turn be expressed in terms of this spectral density through the inverse Fourier transform

$$C_{\hat{B}\hat{A}}(t) = \langle \hat{B}\hat{A}(t) \rangle = \int\limits_{-\infty}^{\infty} \mathcal{S}(\omega)e^{-i\omega t}\,d\omega\,. \tag{2.53a}$$

Now, by substituting $t \to t + \mathrm{i}\beta$ and noting that $\langle \hat{\mathrm{B}}\hat{\mathrm{A}}(t + \mathrm{i}\beta) \rangle = \langle \hat{\mathrm{A}}(t)\hat{\mathrm{B}} \rangle$, also the correlation function of the commuted operators can be expressed through the same spectral density as

$$\langle \hat{\mathrm{A}}(t)\hat{\mathrm{B}} \rangle = \int\limits_{-\infty}^{\infty} \mathcal{S}(\omega) \mathrm{e}^{\beta\omega} \mathrm{e}^{-\mathrm{i}\omega t} \, \mathrm{d}\omega \,. \tag{2.53b}$$

The final goal of this all, is to calculate quantities related to the time correlation functions. Using the Heisenberg equation of motion (2.48), we find the corresponding identity

$$\mathrm{i}\frac{\mathrm{d}C_{\hat{\mathrm{B}}\hat{\mathrm{A}}}(t)}{\mathrm{d}t} = \langle \hat{\mathrm{B}}[\hat{\mathrm{A}}(t),\, \hat{\mathrm{H}}(t)] \rangle = \langle \hat{\mathrm{B}} \{\hat{\mathrm{A}}(t)\hat{\mathrm{H}}(t) - \hat{\mathrm{H}}(t)\hat{\mathrm{A}}(t)\} \rangle, \tag{2.54}$$

from which the time correlation functions can in principle be obtained by direct integration when supplemented with adequate boundary conditions. In practice, these calculations are hard to perform. That is why we will introduce in the remainder of this section a more indirect method for evaluating the time correlation functions. That method, based on Green functions and their equation of motion, has the advantage of making it easier to satisfy the boundary conditions using spectral theorems.

2.2.2 Definition and properties

Zubarev's [90] double-time temperature-dependent retarded and advanced Green functions, involving two operators $\hat{\mathrm{A}}$ and $\hat{\mathrm{B}}$, are defined as

$$G_\eta^{\mathrm{r}}(t, t') = \langle\!\langle \hat{\mathrm{A}}(t);\, \hat{\mathrm{B}}(t') \rangle\!\rangle_\eta^{\mathrm{r}} = -\mathrm{i}\theta(t - t')\langle [\hat{\mathrm{A}}(t),\, \hat{\mathrm{B}}(t')]_\eta \rangle \tag{2.55a}$$

$$G_\eta^{\mathrm{a}}(t, t') = \langle\!\langle \hat{\mathrm{A}}(t);\, \hat{\mathrm{B}}(t') \rangle\!\rangle_\eta^{\mathrm{a}} = \mathrm{i}\theta(t' - t)\langle [\hat{\mathrm{A}}(t),\, \hat{\mathrm{B}}(t')]_\eta \rangle \tag{2.55b}$$

Both types come in two flavours: the commutator ($\eta = -1$) and anti-commutator ($\eta = +1$) Green functions. The square brackets with subscript $\eta = \mp$ indeed denote either a commutator or anti-commutator $[\hat{\mathrm{A}},\, \hat{\mathrm{B}}]_\eta = \hat{\mathrm{A}}\hat{\mathrm{B}} + \eta\hat{\mathrm{B}}\hat{\mathrm{A}}$. When no such subscript is present, we are always referring to the commutator ($\eta = -$). In the definition of the Green function, the Heaviside or step function

$$\theta(t) = \begin{cases} 1, & t \geqslant 0 \\ 0, & t < 0 \end{cases} \tag{2.56}$$

makes the retarded Green function vanish for times $t < t'$ and the advanced Green function when $t > t'$. Note that the Green functions take the averages over the canonical ensemble and not just over the ground state of the system. As such, they do not only depend on time, but also on temperature.

Referring to thermal equilibrium, the Green functions only depend on the times t and t' through their difference $t - t'$, such that they can be written as $G_\eta^{\mathrm{r}}(t - t')$ and $G_\eta^{\mathrm{a}}(t - t')$. This is an immediate consequence of the analogous property of time correlation functions and the fact that the discontinuous factor $\theta(t - t')$ only depends on this difference.

The Fourier transform and its inverse of the retarded Green function are

$$G_\eta^{\mathrm{r}}(E) = \frac{1}{2\pi} \int\limits_{-\infty}^{\infty} G_\eta^{\mathrm{r}}(t) \mathrm{e}^{\mathrm{i}Et}\, \mathrm{d}t \tag{2.57a}$$

$$G_\eta^{\mathrm{r}}(t) = \int\limits_{-\infty}^{\infty} G_\eta^{\mathrm{r}}(E) \mathrm{e}^{-\mathrm{i}Et}\, \mathrm{d}E\,. \tag{2.57b}$$

The Fourier component $G_\eta^{\mathrm{r}}(E)$ can be written more explicitly as

$$G_\eta^{\mathrm{r}}(E) = \frac{1}{2\pi\mathrm{i}} \int\limits_{-\infty}^{\infty} \mathrm{e}^{\mathrm{i}Et} \theta(t) \left\{ \langle \hat{A}(t)\hat{B} \rangle + \eta \langle \hat{B}\hat{A}(t) \rangle \right\} \mathrm{d}t \tag{2.58}$$

using the definition of $G_\eta^{\mathrm{r}}(t)$ and the previously introduced time correlation functions. Using the latter's spectral representation (2.53), this becomes

$$G_\eta^{\mathrm{r}}(E) = \int\limits_{-\infty}^{\infty} \mathrm{d}\omega\, \mathcal{S}(\omega)\, (\mathrm{e}^{\beta\omega} + \eta)\, \frac{1}{2\pi\mathrm{i}} \int\limits_{-\infty}^{\infty} \mathrm{d}t\, \mathrm{e}^{\mathrm{i}(E-\omega)t} \theta(t). \tag{2.59}$$

The integral representations of the step function and Dirac delta

$$\theta(t) = \lim_{\epsilon \to 0^+} \frac{-1}{2\pi\mathrm{i}} \int\limits_{-\infty}^{\infty} \frac{\mathrm{e}^{-\mathrm{i}xt}}{x + \mathrm{i}\epsilon}\, \mathrm{d}x \ \text{ and } \ \delta(t) = \frac{1}{2\pi} \int\limits_{-\infty}^{\infty} \mathrm{e}^{-\mathrm{i}xt}\, \mathrm{d}x \tag{2.60}$$

allow to write the retarded Green function's Fourier components in the form

$$G_\eta^{\mathrm{r}}(E) = \frac{1}{2\pi} \lim_{\epsilon \to 0^+} \int\limits_{-\infty}^{\infty} \mathrm{d}\omega\, \mathcal{S}(\omega)\, (\mathrm{e}^{\beta\omega} + \eta)\, \frac{1}{E - \omega + \mathrm{i}\epsilon}. \tag{2.61}$$

A similar calculation for the advanced Green function yields

$$G_\eta^{\mathrm{a}}(E) = \frac{1}{2\pi} \lim_{\epsilon \to 0^+} \int\limits_{-\infty}^{\infty} \mathrm{d}\omega\, \mathcal{S}(\omega)\, (\mathrm{e}^{\beta\omega} + \eta)\, \frac{1}{E - \omega - \mathrm{i}\epsilon}. \tag{2.62}$$

Up to this point, we have considered E to be real. Removing this restriction, the advanced and retarded Fourier transformed Green functions can be continued analytically [90] in the complex plane. These two functions can be combined to form

$$G_\eta(E) = \frac{1}{2\pi} \int\limits_{-\infty}^{\infty} \mathrm{d}\omega \, \mathcal{S}(\omega) \, (\mathrm{e}^{\beta\omega} + \eta) \, \frac{1}{E - \omega} = \begin{cases} G_\eta^{\mathrm{r}}(E) & \mathrm{Im}(E) > 0 \\ G_\eta^{\mathrm{a}}(E) & \mathrm{Im}(E) < 0 \end{cases}, \qquad (2.63)$$

representing a single analytical function in the complex plane with a singularity at $E = \omega$ on the real axis. We now continue to work with this Green function.

2.2.3   Equation of motion

Up to now, there is still no feasible way to calculate the Green functions. Direct calculation from their definition (2.55) is difficult, since it requires calculating ensemble averages. As discussed before, this is typically impossible as the exact eigenstates of the Hamiltonian $\hat{H}$ are generally unknown. The Green function equation of motion, which we derive here, provides an alternative.

The derivative of the Green functions (2.55) with respect to time t is

$$\mathrm{i}\frac{\mathrm{d}G_\eta(t)}{\mathrm{d}t} = \frac{\mathrm{d}\theta(t)}{\mathrm{d}t}\langle[\hat{A}(t), \, \hat{B}]_\eta\rangle + \left\langle\!\!\left\langle \mathrm{i}\frac{\mathrm{d}\hat{A}(t)}{\mathrm{d}t}; \, \hat{B} \right\rangle\!\!\right\rangle_\eta. \qquad (2.64)$$

Because the Heaviside function has the property $\mathrm{d}\theta(-t)\,/\mathrm{d}t = -\mathrm{d}\theta(t)\,/\mathrm{d}t$, this expression is the same for both the retarded and advanced Green function. As a consequence, we can just as well use the analytically continued Green function. The Heaviside function is related to the Dirac delta function through

$$\theta(t) = \int\limits_{-\infty}^{t} \delta(x)\,\mathrm{d}x\,. \qquad (2.65)$$

Together with the Heisenberg equation of motion (2.48), this leads to the Green function equation of motion

$$\mathrm{i}\frac{\mathrm{d}G_\eta(t)}{\mathrm{d}t} = \delta(t)\langle[\hat{A}(t), \, \hat{B}]_\eta\rangle + \left\langle\!\!\left\langle [\hat{A}(t), \, \hat{H}(t)]; \, \hat{B} \right\rangle\!\!\right\rangle_\eta. \qquad (2.66)$$

This equation of motion is similar to that for the time correlation functions (2.54), except for the first singular term containing $\delta(t)$ and originating from the discontinuous term in the Green function definition. Most often, the equation of motion is converted from a differential equation into an algebraic equation by Fourier transforming both the Green functions (2.57) and the Dirac delta (2.60).

By equating each Fourier component, the algebraic equation of motion in frequency domain becomes

$$\omega G_\eta(\omega) = \frac{1}{2\pi} \langle [\hat{A},\, \hat{B}]_\eta \rangle + \langle\!\langle [\hat{A},\, \hat{H}];\, \hat{B} \rangle\!\rangle_{\eta,\omega}. \qquad (2.67)$$

The Green function in the last term typically contains a product of more operators than the original Green function, which is then called a higher order Green function. These higher order Green functions have their own equation of motion, which, in turn, contain even higher order Green functions. In this way, a chain of coupled equations for the Green functions can be constructed. Together with appropriate boundary conditions—which are facilitated by spectral theorems that we discuss in the next section—such a chain of equations represents an exact solution for the original Green function $G_\eta(t)$. Because this exact solution is in general extremely complicated, an approximation is needed in order to decouple this chain of equations. By this, we mean that the approximation allows to reduce the infinite chain into a finite set of equations, which can then be solved. When more equations of the chain are taken into account, the approximate solution is expected to get closer to the exact result.

2.2.4   Spectral theorem

We want to be able to express time correlation functions in terms of Green functions, which we can calculate through their equations of motion. The tools that enable us to do so, are spectral theorems. We will derive the spectral representations for the time correlation functions and the Green functions separately, combining them to get the desired result.

Spectral representation of time correlation functions

Consider a Hamiltonian $\hat{H}$ that has eigenstates $|n\rangle$ and eigenvalues E_n, that is $\hat{H}|n\rangle = E_n|n\rangle$, such that the set of eigenstates $\{|n\rangle\}$ forms a basis for the complete Hilbert space under consideration. The statistical averaging operation appearing (2.49) in the definition of the time correlation function (2.46) can then be written explicitly as

$$C_{\hat{B}\hat{A}}(t) = \langle \hat{B}(0)\hat{A}(t) \rangle = \mathcal{Z}^{-1} \sum_n \langle n\,|\,\hat{B}(0)\hat{A}(t)\,|\,n\rangle \mathrm{e}^{-\beta E_n}. \qquad (2.68)$$

To obtain this expression, we used the cyclic permutation properties of the trace together with the matrix property that if $M = UDU^{-1}$ with D a diagonal matrix, then $\mathrm{e}^M = U\mathrm{e}^D U^{-1}$. The time correlation function can now further be expanded

in the complete set of eigenstates $\{|n\rangle\}$ to find

$$
\begin{aligned}
\langle\hat{B}(0)\hat{A}(t)\rangle &= \mathcal{Z}^{-1}\sum_{n,m}\langle n\,|\,\hat{B}(0)\,|\,m\rangle\langle m\,|\,\hat{A}(t)\,|\,n\rangle\mathrm{e}^{-\beta E_n} \\
&= \mathcal{Z}^{-1}\sum_{n,m}\langle n\,|\,\hat{B}\,|\,m\rangle\langle m\,|\,\hat{A}\,|\,n\rangle\mathrm{e}^{-\beta E_n}\mathrm{e}^{-\mathrm{i}(E_n-E_m)t},
\end{aligned}
\tag{2.69}
$$

where the second equality employs the Heisenberg representation of the operators and the actions

$$
\mathrm{e}^{-\mathrm{i}\hat{H}t}|n\rangle = \mathrm{e}^{-\mathrm{i}E_n t}|n\rangle \text{ and } \langle m|\mathrm{e}^{\mathrm{i}\hat{H}t} = \langle m|\mathrm{e}^{\mathrm{i}E_m t}
\tag{2.70}
$$

of the Hamiltonian on the eigenstates. Similarly, the time correlation function for the commuted operators is

$$
\langle\hat{A}(t)\hat{B}(0)\rangle = \mathcal{Z}^{-1}\sum_{n,m}\langle n\,|\,\hat{B}\,|\,m\rangle\langle m\,|\,\hat{A}\,|\,n\rangle\mathrm{e}^{-\beta E_m}\mathrm{e}^{-\mathrm{i}(E_n-E_m)t}.
\tag{2.71}
$$

The spectral density $\mathcal{S}(\omega)$ of $C_{\hat{B}\hat{A}}(t)$ can be written as

$$
\mathcal{S}(\omega) = \mathcal{Z}^{-1}\sum_{n,m}\langle n\,|\,\hat{B}\,|\,m\rangle\langle m\,|\,\hat{A}\,|\,n\rangle\mathrm{e}^{-\beta E_n}\delta(\omega - E_n + E_m)
\tag{2.72}
$$

by using the above time correlation function in its definition (2.52). This expression for the spectral representation using the eigenstates of the Hamiltonian will prove to be useful for the discussion of some subtle points that are often forgotten [92, 93] when applying the Green function method. For those Green functions, it is important to calculate the (anti-)commutator averages

$$
\langle[\hat{A}(t),\,\hat{B}]_-\rangle = \mathcal{Z}^{-1}\sum_{\substack{n,m\\E_n\neq E_m}}\langle n\,|\,\hat{B}\,|\,m\rangle\langle m\,|\,\hat{A}\,|\,n\rangle\left(\mathrm{e}^{-\beta E_m} - \mathrm{e}^{-\beta E_n}\right)\mathrm{e}^{-\mathrm{i}(E_n-E_m)t}
\tag{2.73a}
$$

$$
\langle[\hat{A}(t),\,\hat{B}]_+\rangle = \mathcal{Z}^{-1}\sum_{n,m}\langle n\,|\,\hat{B}\,|\,m\rangle\langle m\,|\,\hat{A}\,|\,n\rangle\left(\mathrm{e}^{-\beta E_m} + \mathrm{e}^{-\beta E_n}\right)\mathrm{e}^{-\mathrm{i}(E_n-E_m)t}.
\tag{2.73b}
$$

All the diagonal ($E_n = E_m$) contributions in the commutator expectation value are cancelled out by the difference of exponentials, even in the case of degenerate energy levels. To the contrary, these diagonal contribution are included in the anti-commutator expectation value. This will have important implications for the spectral representation of the Green functions.

Spectral representation of Green functions

Using the Green function in terms of the corresponding spectral density (2.63), we can use the spectral representation of that spectral density (2.72) to find

$$G_\eta(E) = \frac{1}{2\pi\mathcal{Z}} \int\limits_{-\infty}^{\infty} \mathrm{d}\omega \sum_{n,m} \langle n\,|\,\hat{\mathrm{B}}\,|\,m\rangle\langle m\,|\,\hat{\mathrm{A}}\,|\,n\rangle \mathrm{e}^{-\beta E_n} \left(\mathrm{e}^{\beta\omega} + \eta\right) \frac{\delta(\omega - E_n + E_m)}{E - \omega}. \tag{2.74}$$

Performing the integral gives

$$G_-(E) = \frac{1}{2\pi\mathcal{Z}} \sum_{\substack{n,m \\ E_n \neq E_m}} \langle n\,|\,\hat{\mathrm{B}}\,|\,m\rangle\langle m\,|\,\hat{\mathrm{A}}\,|\,n\rangle \left(\mathrm{e}^{-\beta E_m} - \mathrm{e}^{-\beta E_n}\right) \frac{1}{E + E_m - E_n} \tag{2.75a}$$

$$G_+(E) = \frac{1}{2\pi\mathcal{Z}} \sum_{n,m} \langle n\,|\,\hat{\mathrm{B}}\,|\,m\rangle\langle m\,|\,\hat{\mathrm{A}}\,|\,n\rangle \left(\mathrm{e}^{-\beta E_m} + \mathrm{e}^{-\beta E_n}\right) \frac{1}{E + E_m - E_n}. \tag{2.75b}$$

The same overall structure as in the spectral representation of the time correlation function of the (anti-)commutator (2.73)—which appear in the definition of the Green functions—can be identified. Also here, the diagonal terms do not contribute in the commutator case. As such, only off-diagonal ($E_n \neq E_m$) matrix elements of the operators $\hat{\mathrm{A}}$ and $\hat{\mathrm{B}}$ are involved for the commutator Green function, while all matrix elements are present in the anti-commutator Green function.

In these explicit forms, the Green functions $G_\eta(E)$ can again be seen to be analytic functions for $\mathrm{Im}(E) \neq 0$, with singularities on the real axis, corresponding to the excitations of the system. From the explicit expression for the commutator Green function, one can see that the limit for $E \to 0$ (in the complex plane) exists. This limit,

$$\lim_{E \to 0} G_-(E) = \frac{1}{2\pi\mathcal{Z}} \sum_{\substack{n,m \\ E_n \neq E_m}} \langle n\,|\,\hat{\mathrm{B}}\,|\,m\rangle\langle m\,|\,\hat{\mathrm{A}}\,|\,n\rangle \left(\mathrm{e}^{-\beta E_m} - \mathrm{e}^{-\beta E_n}\right) \frac{1}{E_m - E_n}, \tag{2.76}$$

which is well-defined, can be used as the value for $G_-(0)$. We can write this regularity at the origin of the commutator Green function also as

$$\lim_{E \to 0} \{EG_-(E)\} = 0. \tag{2.77}$$

Due to the presence of diagonal terms, the corresponding result for anti-commutator Green functions is

$$\lim_{E \to 0} \{EG_+(E)\} = \frac{K}{\pi} \quad \text{with} \quad K = \frac{1}{\mathcal{Z}} \sum_{\substack{n,m \\ E_n = E_m}} \langle n\,|\,\hat{\mathrm{B}}\,|\,m\rangle\langle m\,|\,\hat{\mathrm{A}}\,|\,n\rangle \mathrm{e}^{-\beta E_n}. \tag{2.78}$$

This means that if, and only if, the anti-commutator Green function $G_+(E)$ has a pole at the origin, this pole has corresponding residue K/π, with K non-zero. This different behaviour of the commutator and anti-commutator Green function can be of fundamental importance when determining correlation functions based on the Green function. For example, in a two-spin $S = 1/2$ system, incorrect results are obtained for the longitudinal correlation function $\langle \hat{S}_1^Z \hat{S}_2^Z \rangle$ when K is not accounted for [93, 100, 101]. This fact is often overlooked, and was first discussed by Stevens and Toombs [92] and further detailed by Ramos and Gomes [93].

Time correlation functions in terms of Green functions

Now it is time to combine the spectral representations of time correlation functions with those of Green functions, as to express the former in terms of the latter.

By direct comparison of K, Eq. (2.78), with the spectral density $\mathcal{S}(\omega)$, Eq. (2.72), the latter can be split in two parts as

$$\mathcal{S}(\omega) = \mathcal{S}_0(\omega) + \mathcal{S}'(\omega). \tag{2.79}$$

The first term is defined by

$$\mathcal{S}_0(\omega) = K\delta(\omega) \tag{2.80}$$

and corresponds to the excitations that do not require any energy. The second term is the remaining part of the spectral density, namely

$$\mathcal{S}'(\omega) = \mathcal{Z}^{-1} \sum_{\substack{n,m \\ E_n \neq E_m}} \langle n \,|\, \hat{B} \,|\, m \rangle \langle m \,|\, \hat{A} \,|\, n \rangle \mathrm{e}^{-\beta E_n} \delta(\omega - E_n + E_m). \tag{2.81}$$

Its definition implies that $\mathcal{S}'(0) = 0$, meaning that $\mathcal{S}'(\omega)$ represents only the excitation spectrum. Substituting the split spectral density (2.79) in the time correlation functions (2.53) gives

$$\langle \hat{B}\hat{A}(t) \rangle = K + \int\limits_{-\infty}^{\infty} \mathcal{S}'(\omega)\mathrm{e}^{-\mathrm{i}\omega t} \,\mathrm{d}\omega \tag{2.82a}$$

$$\langle \hat{A}(t)\hat{B} \rangle = K + \int\limits_{-\infty}^{\infty} \mathcal{S}'(\omega)\mathrm{e}^{\beta\omega}\mathrm{e}^{-\mathrm{i}\omega t} \,\mathrm{d}\omega \,. \tag{2.82b}$$

Similarly, substituting the split spectral density (2.79) in the Green function definition (2.63) yields

$$G_-(E) = \frac{1}{2\pi} \int\limits_{-\infty}^{\infty} d\omega \, \mathcal{S}'(\omega) \, (e^{\beta\omega} - 1) \, \frac{1}{E - \omega} \qquad (2.83a)$$

$$G_+(E) = \frac{1}{2\pi} \int\limits_{-\infty}^{\infty} d\omega \, \mathcal{S}(\omega) \, (e^{\beta\omega} + 1) \, \frac{1}{E - \omega}. \qquad (2.83b)$$

The first term of the split spectral density is not present anymore in the commutator Green function, as the term in brackets vanishes at $\omega = 0$. Another way to understand this, is that the diagonal terms are not present in the expectation value of the commutator $\langle [\hat{A}(t), \hat{B}]_- \rangle$, Eq. (2.73). On the other hand, the anti-commutator Green function contains the entire spectral density.

The just derived Green function representations allow us to write the spectral densities $\mathcal{S}'(\omega)$ and $\mathcal{S}(\omega)$ as

$$\mathcal{S}'(\omega) = \frac{1}{e^{\beta\omega} - 1} i \lim_{\epsilon \to 0^+} \left\{ G_-(\omega + i\epsilon) - G_-(\omega - i\epsilon) \right\} \qquad (2.84a)$$

$$\mathcal{S}(\omega) = \frac{1}{e^{\beta\omega} + 1} i \lim_{\epsilon \to 0^+} \left\{ G_+(\omega + i\epsilon) - G_+(\omega - i\epsilon) \right\}, \qquad (2.84b)$$

which can be verified by direct substitution of the Green functions together with the Dirac delta identity

$$\delta(x) = \frac{1}{2\pi i} \lim_{\epsilon \to 0^+} \left\{ \frac{1}{x - i\epsilon} - \frac{1}{x + i\epsilon} \right\}. \qquad (2.85)$$

This expression for $\mathcal{S}'(\omega)$ puts restrictions on the decoupling schemes to break the infinite chain of equations (2.67) when determining commutator Green functions. Acceptable decoupling schemes ensure that $G_-(E)$ has no pole at $E = 0$ and that $\mathcal{S}'(0) = 0$. If this is not verified, calculations based on the commutator Green functions might be entirely misleading. Substituting $\mathcal{S}'(\omega)$ in the above equation for $\langle \hat{B}\hat{A}(t) \rangle$, finally gives

$$\langle \hat{B}\hat{A}(t) \rangle = K + \lim_{\epsilon \to 0^+} i \int\limits_{-\infty}^{\infty} \frac{G_-(\omega + i\epsilon) - G_-(\omega - i\epsilon)}{e^{\beta\omega} - 1} e^{-i\omega t} \, d\omega. \qquad (2.86)$$

Since the integrand is just $\mathcal{S}'(\omega)e^{-i\omega t}$, with $\mathcal{S}'(\omega)$ defined such that $\mathcal{S}'(0) = 0$ always holds, we are assured that it is well-defined at $\omega = 0$.

Apart from a useful expression, the spectral theorem (2.86), this section shows that the commutator Green function should be treated with care. While the commutator

Green function only relates to the off-diagonal matrix elements ($E_n \neq E_m$) of operators $\hat{A}$ and $\hat{B}$, the time correlation function itself also involves the diagonal ones. The constant K in the spectral theorem accounts for this missing part, assuring the correct long-time value of the correlation function $\langle \hat{B}\hat{A}(t \to \infty) \rangle$ [94]. But how do we know the value of K? In general, its definition (2.78) does not help, since the exact eigenstates are not known. A strategy that does work is the following: The physical considerations behind the decoupling procedure that is being followed, does not depend on the Green functions being of commutator or anti-commutator type. We can thus determine the anti-commutator Green function from the equation of motion (2.67) with the same decoupling procedure. If this anti-commutator Green function has a pole at $E = 0$, the constant K is given by π times the residue at this pole, see Eq. (2.78). If there is no pole at the origin, the constant K is zero.

2.2.5 Generic calculation method

The goal, of calculating the time correlation functions in a different way then directly integrating their equation of motion (2.54), is now achieved. Since it took quite some effort to derive this calculation method, we summarise it here.

First, write down the Green function equation of motion (2.67) in frequency domain

$$\omega G_\eta(\omega) = \frac{1}{2\pi}\langle [\hat{A},\ \hat{B}]_\eta \rangle + \langle\langle [\hat{A},\ \hat{H}];\ \hat{B} \rangle\rangle_{\eta,\omega}. \qquad (2.87)$$

The last term is in general a higher order Green function, for which again an equation of motion can be written down. Repeating this procedure results in an infinite chain of coupled equations. In order to find a solution, this chain should be decoupled in one way or the other. Typically, some of the higher order Green functions are approximated by the lower order ones. Often, this decoupling approximation happens already in the first iteration. The decoupled equations of motion yield a solution for the Green function G_η.

Subsequently, the obtained Green function can be used in the spectral theorem, resulting in the time correlation function

$$\langle \hat{B}\hat{A}(t) \rangle = K + \lim_{\epsilon \to 0^+} i \int\limits_{-\infty}^{\infty} \frac{G_-(\omega + i\epsilon) - G_-(\omega - i\epsilon)}{e^{\beta\omega} - 1} e^{-i\omega t}\, d\omega, \qquad (2.88)$$

which is then usually evaluated at $t = 0$ to extract an expectation value. We typically use the commutator Green functions, to ease calculations with spin operators. To find the constant K, we need to look back at the equation of motion for anti-commutator Green functions. If that equation does not admit a pole at

$E = 0$, the constant K vanishes. Otherwise, it can be calculated as

$$K = \pi \lim_{E \to 0} \left\{ E G_+(E) \right\} \tag{2.89}$$

and one must check the regularity condition

$$\lim_{E \to 0} \left\{ E G_-(E) \right\} = 0 \tag{2.90}$$

for the decoupling approximation of the commutator Green function to be valid.

2.3   Magnetisation calculations

In this section, we will study in more detail the equations that typically appear when calculating magnetisation vectors in anisotropic Heisenberg magnetic spin systems. It will turn out that some specific difficulties are intrinsic to these systems. A general, analytical framework will be useful in understanding those difficulties. Analyzing them in their generality will ease the solution for specific systems in the following chapters. Some of the notation and parts of the general technique in this section are based on papers by Fröbrich and Knutz. A good overview of those papers is given in their review [102].

2.3.1   Single Green functions in spin lattice systems

In a Heisenberg magnetic spin system, the Green function

$$G_{\eta;\mathbf{p},\mathbf{j}}(\omega) = \langle\!\langle \hat{A}_{\mathbf{p}}; \hat{B}_{\mathbf{j}} \rangle\!\rangle_{\eta,\omega} \tag{2.91}$$

is typically used, where the operators $\hat{A}_{\mathbf{p}}$ and $\hat{B}_{\mathbf{j}}$ are combinations of components of spin-operators $\hat{\mathbf{S}}_{\mathbf{p}}$ and $\hat{\mathbf{S}}_{\mathbf{j}}$ acting at lattice positions $\mathbf{r}_{\mathbf{p}}$ and $\mathbf{r}_{\mathbf{j}}$. For simplicity, the multiatomic basis index is dropped here, but the complete derivation is straightforward to generalise. This Green function has equation of motion (2.67)

$$\omega G_{\eta;\mathbf{p},\mathbf{j}}(\omega) = \frac{1}{2\pi} \langle [\hat{A}_{\mathbf{p}}, \hat{B}_{\mathbf{j}}]_\eta \rangle + \langle\!\langle [\hat{A}_{\mathbf{p}}, \hat{H}]; \hat{B}_{\mathbf{j}} \rangle\!\rangle_{\eta,\omega}. \tag{2.92}$$

In the simplest case, the higher order Green function can be approximated as being proportional to a combination of Green functions $G_{\eta;\mathbf{l},\mathbf{j}}(\omega)$ that are of the same form as the original one, but possibly acting at a different lattice site $\mathbf{l}$ instead of $\mathbf{p}$. Such a decoupling approximation would have the form

$$\langle\!\langle [\hat{A}_{\mathbf{p}}, \hat{H}]; \hat{B}_{\mathbf{j}} \rangle\!\rangle_{\eta,\omega} \to \sum_{\mathbf{l}} \Gamma_{\mathbf{pl}} G_{\eta;\mathbf{l},\mathbf{j}}(\omega) = \sum_{\mathbf{l}} \Gamma_{\mathbf{pl}} \langle\!\langle \hat{A}_{\mathbf{l}}; \hat{B}_{\mathbf{j}} \rangle\!\rangle_{\eta,\omega}, \tag{2.93}$$

such that the equation of motion becomes

$$\sum_{\mathbf{l}} \left(\omega \delta_{\mathbf{pl}} - \Gamma_{\mathbf{pl}} \right) G_{\eta;\mathbf{l},\mathbf{j}}(\omega) = \frac{1}{2\pi} \langle [\hat{A}_{\mathbf{p}}, \hat{B}_{\mathbf{j}}]_{\eta} \rangle. \tag{2.94}$$

We will refer to the term on the right-hand side as the inhomogeneous term. Since the spin operators—and by extension the Green functions—are tied to a periodic lattice, the lattices translational symmetry should be exploited by Fourier transforming the equation of motion into reciprocal space. We do so by expanding the Green function and the inhomogeneous term in Fourier components (2.8) and then recognising the part in parentheses as a Fourier component (2.10) itself. The equality that results should hold for every wave vector $\mathbf{k}$ separately, such that the equation of motion becomes

$$\left(\omega - \Gamma(\mathbf{k}) \right) G_{\eta}(\omega, \mathbf{k}) = \frac{1}{2\pi} \langle [\hat{A}, \hat{B}]_{\eta}(\mathbf{k}) \rangle. \tag{2.95}$$

This time- and space-Fourier transformed equation leads directly to the Green function

$$G_{\eta}(\omega, \mathbf{k}) = \frac{1}{2\pi} \frac{\langle [\hat{A}, \hat{B}]_{\eta}(\mathbf{k}) \rangle}{\omega - \Gamma(\mathbf{k})}, \tag{2.96}$$

which can in turn be used in the spectral theorem (2.86) to find the desired expectation value. For now, we assume that the approximation was not trivial, in the sense that $\Gamma(\mathbf{k}) = 0$ only for a finite number of wave vectors. The corresponding expectation value with $t = 0$ (e.g., the magnetisation) is then

$$\langle \hat{B}\hat{A} \rangle(\mathbf{k}) = \int_{-\infty}^{\infty} \frac{\delta\left(\omega - \Gamma(\mathbf{k}) \right) \langle [\hat{A}, \hat{B}]_{\eta}(\mathbf{k}) \rangle}{e^{\beta\omega} + \eta} \, \mathrm{d}\omega = \frac{\langle [\hat{A}, \hat{B}]_{\eta}(\mathbf{k}) \rangle}{e^{\beta\Gamma(\mathbf{k})} + \eta}, \tag{2.97}$$

where the first equality uses the Dirac delta representation (2.85). Finally, we will be mainly concerned with average local properties, such as the magnetisation, in a translational invariant system. These properties are calculated as an expectation value of operators acting on a single lattice point, which can be achieved by summing all Fourier components in reciprocal space. In translational invariant systems, the explicit lattice point dependence can be removed. In the result

$$\langle \hat{B}\hat{A} \rangle = \langle \hat{B}_{\mathbf{j}}\hat{A}_{\mathbf{j}} \rangle = \frac{1}{N} \sum_{\mathbf{k} \in \mathrm{BZ}} \langle \hat{B}\hat{A} \rangle(\mathbf{k}) = \frac{1}{N} \sum_{\mathbf{k} \in \mathrm{BZ}} \frac{\langle [\hat{A}, \hat{B}]_{\eta}(\mathbf{k}) \rangle}{e^{\beta\Gamma(\mathbf{k})} + \eta}, \tag{2.98}$$

the sum over all wave vectors can be replaced by the integral (2.9)

$$\langle \hat{B}\hat{A} \rangle = \frac{1}{v_b} \int_{\mathrm{BZ}} \frac{\langle [\hat{A}, \hat{B}]_{\eta}(\mathbf{k}) \rangle}{e^{\beta\Gamma(\mathbf{k})} + \eta} \, \mathrm{d}\mathbf{k} \tag{2.99}$$

over the first Brillouin zone for large enough systems.

2.3.2   Multiple Green functions in spin lattice systems

The theory given in the previous subsection only works in the simplest cases. There are two reasons calling for more than one type of Green function. The first being that the desired properties require different operators $\hat{A}_\mathbf{p}$ and $\hat{B}_\mathbf{j}$ in the expectation value, and as a consequence also different Green functions. The second reason is that the simple decoupling approximation (2.93) is insufficient to capture the physics of the system. In that case, the higher order Green functions can be decoupled as a combination of lower order ones, but possibly of different type than the original Green function. Subsequently, one also needs to solve the equation of motion for those Green functions of different types. While this might seem rather abstract at this point, it will become more clear in the specific problem that we deal with in later chapters.

We will now formalise the solution method when multiple Green functions are involved. In analogy to the time- and space-Fourier transformed equation of motion (2.95) when only a single type of Green function is evolved, the equation of motion when $\mathcal{N}$ Green functions are involved is (we drop the explicit frequency dependence to keep the notation readable)

$$(\omega \mathbb{1} - \boldsymbol{\Gamma}(\mathbf{k})) \cdot \mathbf{G}_\eta(\mathbf{k}) = \frac{1}{2\pi} \boldsymbol{\Psi}_\eta(\mathbf{k}). \tag{2.100}$$

Here, $\mathbf{G}_\eta(\mathbf{k})$ denotes a column vector of dimensions $\mathcal{N} \times 1$, in which each element G_η^τ is a single type of Fourier-transformed Green function $\langle\!\langle \hat{A}; \hat{B} \rangle\!\rangle_\eta (\mathbf{k})$. Likewise, the inhomogeneity term is the $\mathcal{N} \times 1$ column vector $\boldsymbol{\Psi}_\eta(\mathbf{k})$, where the elements $\Psi_\eta^\tau(\mathbf{k})$ are the corresponding expectation values $\langle [\hat{A}, \hat{B}]_\eta(\mathbf{k}) \rangle$. The $\mathcal{N} \times \mathcal{N}$ matrix $\boldsymbol{\Gamma}(\mathbf{k})$ contains the space-Fourier transformed coefficients

$$\Gamma^{\tau\lambda}(\mathbf{k}) = \sum_{\mathbf{r_{pl}}} e^{i\mathbf{k} \cdot \mathbf{r_{pl}}} \Gamma_\mathbf{pl}^{\tau\lambda} \tag{2.101}$$

of the generalised decoupling approximations

$$\langle\!\langle [\hat{A}_\mathbf{p}, \hat{H}]; \hat{B}_\mathbf{j} \rangle\!\rangle_\eta \rightarrow \sum_\lambda \sum_\mathbf{l} \Gamma_\mathbf{pl}^{\tau\lambda} G_{\eta;\mathbf{l},\mathbf{j}}^\lambda. \tag{2.102}$$

Each row τ in the matrix equation of motion (2.100) corresponds to the equation of motion of a single Green function $\langle\!\langle \hat{A}_\mathbf{p}(t); \hat{B}_\mathbf{j}(0) \rangle\!\rangle_\eta$ that can be used to calculate the time correlation function $C_{\hat{B}_\mathbf{j}\hat{A}_\mathbf{p}}(t) = \langle \hat{B}_\mathbf{j}(0)\hat{A}_\mathbf{p}(t) \rangle$. The time- and space-Fourier transforms of each of these time correlation functions can be seen as the τth component of a time correlation vector $\mathbf{C}(\mathbf{k})$. Typically, only the expectation values

$$c_{\hat{B}_\mathbf{j}\hat{A}_\mathbf{p}} = \frac{1}{v_b} \int\limits_{\text{BZ}} C_{\hat{B}_\mathbf{j}\hat{A}_\mathbf{p}}(\mathbf{k}) \, d\mathbf{k} \tag{2.103}$$

will be of interest, which are the components of the expectation value vector

$$\mathbf{c} = \frac{1}{v_b} \int\limits_{\text{BZ}} C(\mathbf{k}) \, \mathrm{d}\mathbf{k} \, . \tag{2.104}$$

The goal of this subsection is now to solve the matrix equation of motion (2.100) in order to calculate some components of this expectation value vector **c** and solve problems that might arise while doing so.

An important part in the analysis of this problem will be the wave vector **k** dependence of some of the elements. This dependence is present in the decoupling coefficient matrix $\boldsymbol{\Gamma}(\mathbf{k})$ and the vector $\mathbf{G}_\eta(\mathbf{k})$. The commutator inhomogeneity vector $\boldsymbol{\Psi}_-(\mathbf{k})$ is **k**-independent because the commutator of spin operators is local in the lattice site indices—spin operators are of Bose-type on different lattice sites. This means that $\boldsymbol{\Psi}_-(\mathbf{k}) = \boldsymbol{\Psi}_-$. On the other hand, the anti-commutator inhomogeneity vector $\boldsymbol{\Psi}_+(\mathbf{k})$ does in general depend on the momentum **k**. It can be related to the commutator inhomogeneity by $\boldsymbol{\Psi}_+(\mathbf{k}) = \boldsymbol{\Psi}_- + 2\mathbf{C}(\mathbf{k})$.

A final thing to note before we continue, is that $\boldsymbol{\Gamma}(\mathbf{k})$ and $\boldsymbol{\Psi}_-$ depend in a numerical calculation on (a previous estimate of) **c**, while $\boldsymbol{\Psi}_+(\mathbf{k})$ depends also on $\mathbf{C}(\mathbf{k})$. But, knowledge of $G_\eta(\mathbf{k})$ allows for the calculation of $\mathbf{C}(\mathbf{k})$.

Solving the equation of motion

To solve the matrix equation of motion (2.100), we perform the transformation

$$\mathbf{L}(\mathbf{k})\boldsymbol{\Gamma}(\mathbf{k})\mathbf{R}(\mathbf{k}) = \boldsymbol{\Omega}(\mathbf{k}) \tag{2.105}$$

to the basis of eigenvectors of $\boldsymbol{\Gamma}(\mathbf{k})$, in the assumption that it is diagonalisable. The matrix $\mathbf{L}(\mathbf{k})$ ($\mathbf{R}(\mathbf{k})$) contains in its rows (columns) the left (right) eigenvectors of $\boldsymbol{\Gamma}(\mathbf{k})$. The matrix $\boldsymbol{\Omega}(\mathbf{k})$ is diagonal with as elements the eigenvalues $\omega^\tau(\mathbf{k})$ corresponding to the left and right eigenvectors $\mathbf{L}^\tau(\mathbf{k})$ and $\mathbf{R}^\tau(\mathbf{k})$. We assume that $\Omega(\mathbf{k})$ is a $\mathcal{N} \times \mathcal{N}$ matrix, which has $\mathcal{N}_0$ eigenvalues with $\omega^\tau = 0$. The other $\mathcal{N} - \mathcal{N}_0$ eigenvalues are assumed to be distinct.

We multiply the equation of motion (2.100) from the left by $\mathbf{L}(\mathbf{k})$ and insert $\mathbf{R}(\mathbf{k}) \cdot \mathbf{L}(\mathbf{k}) = \mathbb{1}$, such that it becomes

$$\mathbf{L}(\mathbf{k}) \left(\omega \mathbb{1} - \boldsymbol{\Gamma}(\mathbf{k}) \right) \mathbf{R}(\mathbf{k})\mathbf{L}(\mathbf{k})\mathbf{G}_\eta(\mathbf{k}) = \frac{1}{2\pi}\mathbf{L}(\mathbf{k})\boldsymbol{\Psi}_\eta(\mathbf{k}) \tag{2.106a}$$

$$\left(\omega \mathbb{1} - \boldsymbol{\Omega}(\mathbf{k}) \right) \boldsymbol{\mathcal{G}}_\eta(\mathbf{k}) = \frac{1}{2\pi}\boldsymbol{\Psi}_\eta(\mathbf{k}) \tag{2.106b}$$

with the transformed quantities

$$\boldsymbol{\mathcal{G}}_\eta(\mathbf{k}) = \mathbf{L}(\mathbf{k})\mathbf{G}_\eta(\mathbf{k}) \tag{2.107a}$$

$$\boldsymbol{\Psi}_\eta(\mathbf{k}) = \mathbf{L}(\mathbf{k})\boldsymbol{\Psi}_\eta(\mathbf{k}) \tag{2.107b}$$

$$\boldsymbol{\mathcal{C}}(\mathbf{k}) = \mathbf{L}(\mathbf{k})\mathbf{C}(\mathbf{k}). \tag{2.107c}$$

This new set of equations of motion for the transformed Green functions is now decoupled, making it easy to solve. The τth of $\mathcal{N}$ Green functions is given by

$$\mathcal{G}_\eta^\tau(\mathbf{k}) = \frac{1}{2\pi} \frac{\Psi_\eta^\tau(\mathbf{k})}{\omega - \omega^\tau}. \tag{2.108}$$

Applying spectral theorem

To obtain the time correlation function, we apply the spectral theorem (2.86). First, we do this separately for the Green functions corresponding to non-zero and zero eigenvalues in the diagonalised decoupling matrix. Afterwards we combine the results

For those eigenvalues where $\omega^\tau \neq 0$, it suffices to use the commutator Green functions and the simple form of the spectral theorem:

$$\forall \tau : \omega^\tau(\mathbf{k}) \neq 0 \rightarrow \mathcal{C}^\tau(\mathbf{k}) = \frac{\Psi_-^\tau(\mathbf{k})}{e^{\beta\omega^\tau(\mathbf{k})} - 1} = \nu^\tau(\mathbf{k})\Psi_-^\tau(\mathbf{k}), \tag{2.109}$$

where we wrote the Bose occupation number as

$$\nu^\tau(\mathbf{k}) = \frac{1}{e^{\beta\omega^\tau(\mathbf{k})} - 1}. \tag{2.110}$$

These results for the non-null space can be grouped again using vector notation. The vectors belonging to the non-null space will be denoted with a superscript $\mathbb{1}$. The solution is then

$$\boldsymbol{\mathcal{C}}^{\mathbb{1}}(\mathbf{k}) = \boldsymbol{\mathcal{E}}^{\mathbb{1}}(\mathbf{k})\boldsymbol{\Psi}_-^{\mathbb{1}}(\mathbf{k}), \tag{2.111}$$

where $\boldsymbol{\mathcal{E}}^{\mathbb{1}}(\mathbf{k})$ is a diagonal matrix containing the Bose occupation factors

$$\mathcal{E}^{\mathbb{1},\lambda\tau}(\mathbf{k}) = \nu^\tau(\mathbf{k})\delta_{\lambda\tau}. \tag{2.112}$$

In case of vanishing eigenvalues, $\omega^\tau = 0$, we need to use (initially) the anti-commutator Green function and its spectral theorem:

$$\forall \tau : \omega^\tau(\mathbf{k}) = 0 \rightarrow \mathcal{C}^\tau(\mathbf{k}) = \frac{\Psi_+^\tau(\mathbf{k})}{e^{\beta\omega^\tau(\mathbf{k})} + 1}\bigg|_{\omega^\tau=0} = \frac{1}{2}\Psi_+^\tau(\mathbf{k}). \tag{2.113}$$

The regularity condition for the commutator Green function dictates that

$$\lim_{\omega \to 0} \left\{ \omega \mathcal{G}_-^\tau(\mathbf{k}) \right\} = 0 \tag{2.114}$$

must hold, where we also know that

$$\mathcal{G}_-^\tau(\mathbf{k}) = \frac{1}{2\pi} \frac{\Psi_-^\tau(\mathbf{k})}{\omega - \omega^\tau}. \tag{2.115}$$

Since we are considering the null space, we know $\omega^\tau = 0$, such that the regularity condition becomes

$$\lim_{\omega \to 0} \left\{ \frac{1}{2\pi} \frac{\omega}{\omega - 0} \Psi_-^\tau(\mathbf{k}) \right\} = \frac{1}{2\pi} \Psi_-^\tau(\mathbf{k}) = \frac{1}{2\pi} \mathbf{L}^\tau(\mathbf{k}) \mathbf{\Psi}_- = 0. \tag{2.116}$$

As noted before, the commutator and anti-commutator inhomogeneity vectors are related as $\mathbf{\Psi}_+(\mathbf{k}) = \mathbf{\Psi}_- + 2\mathbf{C}(\mathbf{k})$, such that the transformed anti-commutator inhomogeneity vector is

$$\Psi_+^\tau(\mathbf{k}) = \mathbf{L}^\tau(\mathbf{k}) \mathbf{\Psi}_+(\mathbf{k}) = \mathbf{L}^\tau(\mathbf{k}) \left(\mathbf{\Psi}_- + 2\mathbf{C}(\mathbf{k}) \right). \tag{2.117}$$

The regularity condition can thus equivalently be expressed as

$$\Psi_+^\tau(\mathbf{k}) = 2\mathbf{L}^\tau(\mathbf{k}) \mathbf{C}(\mathbf{k}) \tag{2.118}$$

such that the expression for the correlation function becomes

$$\forall \tau : \omega^\tau(\mathbf{k}) = 0 \to \mathcal{C}^\tau(\mathbf{k}) = \mathbf{L}^\tau(\mathbf{k}) \mathbf{C}(\mathbf{k}). \tag{2.119}$$

Note that this identity is just the defining equation of $\boldsymbol{C}(\mathbf{k})$ for every component τ. As a result, the equations of motion belonging to the null space do not contribute any new information that helps in solving the problem. Any information contained in them, is also present in the corresponding regularity condition. For formal reasons, the results for the null space can still be grouped using vector notation, denoting them with a superscript $\mathbb{0}$:

$$\boldsymbol{\mathcal{C}}^{\mathbb{0}}(\mathbf{k}) = \mathbf{L}^{\mathbb{0}}(\mathbf{k}) \mathbf{C}(\mathbf{k}). \tag{2.120}$$

The results for the null and non-null space can be combined by grouping the vectors and matrices belonging to both spaces. The general rule is that the components belonging to the null space are written last in all vectors or matrices. This is possible by choosing the order of the eigenvectors in the transformation matrices

$$\mathbf{L}(\mathbf{k}) = \begin{bmatrix} \mathbf{L}^{\mathbb{1}}(\mathbf{k}) \\ \mathbf{L}^{\mathbb{0}}(\mathbf{k}) \end{bmatrix} \text{ and } \mathbf{R}(\mathbf{k}) = \begin{bmatrix} \mathbf{R}^{\mathbb{1}}(\mathbf{k}) & \mathbf{R}^{\mathbb{0}}(\mathbf{k}) \end{bmatrix} \tag{2.121}$$

appropriately. The transformed correlation and commutator inhomogeneous vectors are then

$$\mathcal{C}(\mathbf{k}) = \begin{bmatrix} \mathcal{C}^{\mathbb{1}}(\mathbf{k}) \\ \mathcal{C}^{\mathbb{0}}(\mathbf{k}) \end{bmatrix} \text{ and } \boldsymbol{\Psi}_-(\mathbf{k}) = \begin{bmatrix} \Psi_-^{\mathbb{1}}(\mathbf{k}) \\ \Psi_-^{\mathbb{0}} \end{bmatrix} = \begin{bmatrix} \Psi_-^{\mathbb{1}}(\mathbf{k}) \\ 0 \end{bmatrix}. \tag{2.122}$$

We also define the $\mathcal{N} \times \mathcal{N}$ matrix

$$\boldsymbol{\mathcal{E}}(\mathbf{k}) = \begin{bmatrix} \boldsymbol{\mathcal{E}}^{\mathbb{1}}(\mathbf{k}) & 0 \\ 0 & 0 \end{bmatrix}, \tag{2.123}$$

with $\boldsymbol{\mathcal{E}}^{\mathbb{1}}(\mathbf{k})$ the $(\mathcal{N} - \mathcal{N}_{\mathbb{0}}) \times (\mathcal{N} - \mathcal{N}_{\mathbb{0}})$ sub-matrix containing Bose factors on the diagonal. The full transformed time correlation function is then

$$\mathcal{C}(\mathbf{k}) = \boldsymbol{\mathcal{E}}(\mathbf{k}) \cdot \boldsymbol{\Psi}_-(\mathbf{k}) + \begin{bmatrix} \mathbf{0} \\ \mathcal{C}^{\mathbb{0}}(\mathbf{k}) \end{bmatrix}. \tag{2.124}$$

Transforming back to original variables

The above correlation function in untransformed variables is

$$\mathbf{L}(\mathbf{k})\mathbf{C}(\mathbf{k}) = \begin{bmatrix} \boldsymbol{\mathcal{E}}^{\mathbb{1}}(\mathbf{k}) & 0 \\ \mathbf{0} & \mathbf{0} \end{bmatrix} \cdot \begin{bmatrix} \mathbf{L}^{\mathbb{1}}(\mathbf{k}) \\ \mathbf{0} \end{bmatrix} \cdot \boldsymbol{\Psi}_-(\mathbf{k}) + \begin{bmatrix} \mathbf{0} \\ \mathbf{L}^{\mathbb{0}}(\mathbf{k}) \end{bmatrix} \cdot \mathbf{C}(\mathbf{k}). \tag{2.125}$$

Multiplying from the left by $\mathbf{R}(\mathbf{k})$ gives

$$\underbrace{\mathbf{R}(\mathbf{k})\mathbf{L}(\mathbf{k})}_{\mathbb{1}} \mathbf{C}(\mathbf{k}) = \begin{bmatrix} \mathbf{R}^{\mathbb{1}}(\mathbf{k}) \cdot \boldsymbol{\mathcal{E}}^{\mathbb{1}}(\mathbf{k}) \cdot \mathbf{L}^{\mathbb{1}}(\mathbf{k}) \\ \mathbf{0} \end{bmatrix} \cdot \boldsymbol{\Psi}_-(\mathbf{k}) + \begin{bmatrix} \mathbf{0} \\ \mathbf{R}^{\mathbb{0}}(\mathbf{k}) \cdot \mathbf{L}^{\mathbb{0}}(\mathbf{k}) \end{bmatrix} \cdot \mathbf{C}(\mathbf{k})$$

$$\tag{2.126}$$

and rearranging terms leads to

$$\underbrace{\begin{bmatrix} \mathbf{R}^{\mathbb{1}}(\mathbf{k}) \cdot \mathbf{L}^{\mathbb{1}}(\mathbf{k}) \\ \mathbf{0} \end{bmatrix}}_{\mathbf{P}^{\mathbb{1}}(\mathbf{k})} \cdot \mathbf{C}(\mathbf{k}) = \begin{bmatrix} \mathbf{R}^{\mathbb{1}}(\mathbf{k}) \cdot \boldsymbol{\mathcal{E}}^{\mathbb{1}}(\mathbf{k}) \cdot \mathbf{L}^{\mathbb{1}}(\mathbf{k}) \\ \mathbf{0} \end{bmatrix} \cdot \boldsymbol{\Psi}_-(\mathbf{k}). \tag{2.127}$$

the projector onto the non-null space, $\mathbf{P}^{\mathbb{1}}(\mathbf{k})$, is singular whenever the null space has a dimension different from zero, i.e. whenever $\exists \tau : \omega^{\tau} = 0$.

Problem in obtaining solution

As indicated before, we are interested in calculating (some components of) $\mathbf{c} = \frac{1}{v_b} \int_{\text{BZ}} \mathbf{C}(\mathbf{k}) \, d\mathbf{k}$. However, we can not just calculate

$$\mathbf{C}(\mathbf{k}) = (\mathbf{P}^{\mathbb{1}}(\mathbf{k}))^{-1} \mathbf{R}^{\mathbb{1}}(\mathbf{k}) \boldsymbol{\mathcal{E}}^{\mathbb{1}}(\mathbf{k}) \mathbf{L}^{\mathbb{1}}(\mathbf{k}) \boldsymbol{\Psi}_-(\mathbf{k}) \tag{2.128}$$

and integrate over the first Brillouin zone, since the projector $\mathbf{P}^\mathbb{1}(\mathbf{k})$ is singular in general (as we will see in the next chapters). This problem can be overcome in most cases however. Note that if the projector $\mathbf{P}^\mathbb{1}(\mathbf{k}) = \mathbf{P}^\mathbb{1}$ is independent of $\mathbf{k}$, it can be pulled out of the integral, such that

$$
\int\limits_{\text{BZ}} \mathbf{P}^\mathbb{1}\mathbf{C}(\mathbf{k})\,\mathrm{d}\mathbf{k} = \mathbf{P}^\mathbb{1} \int\limits_{\text{BZ}} \mathbf{C}(\mathbf{k})\,\mathrm{d}\mathbf{k} = v_b \mathbf{P}^\mathbb{1}\mathbf{c} = \mathbf{P}^\mathbb{1} \int\limits_{\text{BZ}} \mathbf{R}^\mathbb{1}(\mathbf{k})\boldsymbol{\mathcal{E}}^\mathbb{1}(\mathbf{k})\mathbf{L}^\mathbb{1}(\mathbf{k})\boldsymbol{\Psi}_-(\mathbf{k})\,\mathrm{d}\mathbf{k}\,.
$$

$$(2.129)$$

In this way, one can calculate $\mathcal{N} - \mathcal{N}_\mathbb{0}$ components of $\mathbf{c}$ by inverting the non-singular part of $\mathbf{P}^\mathbb{1}$. The remaining components can then be found from the $\mathcal{N}_\mathbb{0}$ regularity conditions

$$
\mathbf{L}^\mathbb{0}(\mathbf{k})\boldsymbol{\Psi}_- = 0. \tag{2.130}
$$

As an extension, Fröbrich and Knutz [102] developed a technique for which it is sufficient if one of the eigenvectors is $\mathbf{k}$-independent. Another possibility that is often exploited, is to choose the Green functions or expectation values to calculate in advance, in such a way that there is no null space. In terms of magnetisation calculations, this typically means choosing a fixed direction of magnetisation in advance, even though it is not known in advance that this is right direction. In this work, we will employ a combination of this last approach with the technique developed by Fröbrich and Knutz and we will see that this will allow calculations in some cases, even when none of the eigenvectors is $\mathbf{k}$-independent.

2.3.3   Simple example

To make the theory presented in the previous subsections more tangible, we will here demonstrate the use of single Green functions on spin lattice systems. This will help to see the main steps of the solution, and is a good reference to make comparisons with more advanced results later on. Specifically, we will study a spin lattice model on a cubic lattice with spins $S = 1/2$ in a magnetic field applied along the Z-direction with only nearest-neighbour exchange interaction.

In the Heisenberg model [45, 48–51], the Hamiltonian describing a ferromagnetic crystal is

$$
\hat{\mathrm{H}} = -g_\mathrm{e}\mu_\mathrm{B} B \sum_{\mathbf{d}} \hat{\mathrm{S}}_\mathbf{d}^Z - \frac{1}{2} \sum_{\mathbf{d},\mathbf{l}} J_{\mathbf{l}\mathbf{d}}\hat{\mathbf{S}}_\mathbf{d} \cdot \hat{\mathbf{S}}_\mathbf{l}. \tag{2.131}
$$

The vector operator $\hat{\mathbf{S}}_\mathbf{d}$ acts on the atomic spin at lattice site $\mathbf{r}_\mathbf{d}$ and has crystallographic components $(\hat{\mathrm{S}}_\mathbf{d}^X, \hat{\mathrm{S}}_\mathbf{d}^Y, \hat{\mathrm{S}}_\mathbf{d}^Z)$. The external magnetic field B is applied parallel to the Z-axis. The second term represents the exchange interaction between

the lattice spins. The positive exchange interaction $J_{\mathbf{ld}} = J\zeta_{1,\mathbf{ld}}$ represents the interaction between neighbouring spins and has strength J. An additional factor $1/2$ arises from the double-counting of lattice sites $\mathbf{d}$ and $\mathbf{l}$.

For easier comparison with the following chapters we introduce a magnetisation coordinate system $\{\mathbf{x}, \mathbf{y}, \mathbf{z}\}$ where the z-direction is defined to be in the average spin direction. The expectation value for the spin component in that direction $\langle \hat{\mathbf{S}}_{\mathbf{d}}^z \rangle$ is what we will call the magnetisation of the system M. Since the system is homogeneous, the magnetisation does not depend on the lattice site. The expectation values of the spin components transverse to the magnetisation direction vanish $\langle \hat{\mathbf{S}}_{\mathbf{d}}^x \rangle = \langle \hat{\mathbf{S}}_{\mathbf{d}}^y \rangle = 0$ because of the specific choice of $\mathbf{z}$. From the Hamiltonian itself, it is already clear that the spins will preferentially align in the Z-direction. The magnetisation coordinate system is thus the same as the crystallographic coordinate system. The spin components can thus be written as $(\hat{\mathbf{S}}_{\mathbf{d}}^x, \hat{\mathbf{S}}_{\mathbf{d}}^y, \hat{\mathbf{S}}_{\mathbf{d}}^z)$ and can be combined to form the operators $\hat{\mathbf{S}}_{\mathbf{d}}^{\pm} = \hat{\mathbf{S}}_{\mathbf{d}}^x \pm \mathrm{i}\hat{\mathbf{S}}_{\mathbf{d}}^y$. Using the spin commutation relations for $S = 1/2$, the magnetisation can be expressed as

$$M = \langle \hat{\mathbf{S}}_{\mathbf{d}}^z \rangle = \frac{1}{2} - \langle \hat{\mathbf{S}}_{\mathbf{d}}^- \hat{\mathbf{S}}_{\mathbf{d}}^+ \rangle, \tag{2.132}$$

where the operator combination $\hat{\mathbf{S}}_{\mathbf{d}}^- \hat{\mathbf{S}}_{\mathbf{d}}^+$ counts the number of down spins at lattice site $\mathbf{r_d}$. This means that it returns 0 if the state is spin-up and 1 if it is spin-down.

An important observation is that the average z-component of the spin (and as a consequence also the magnetisation) does not evolve in time,

$$\left\langle \frac{\mathrm{d}\hat{\mathbf{S}}_{\mathbf{d}}^z}{\mathrm{d}t} \right\rangle = \frac{\mathrm{d}\langle \hat{\mathbf{S}}^z \rangle}{\mathrm{d}t} = 0. \tag{2.133}$$

This stationarity arises because the same Hamiltonian $\hat{\mathrm{H}}$ that appears in the average expectation value $\langle \ldots \rangle$ of Eq. (2.49) is the same as the one appearing in the time-evolution (2.48) of the operator $\hat{\mathbf{S}}_{\mathbf{d}}^z(t)$. In the calculation of the time-evolution of the average, this makes it possible to use the identity $\hat{\mathrm{H}}\mathrm{e}^{c\hat{\mathrm{H}}} = \mathrm{e}^{c\hat{\mathrm{H}}}\hat{\mathrm{H}}$, where c is a complex number An identical reasoning shows that any observable $\hat{\mathrm{A}}(t)$ under these conditions has to be stationary.

To calculate an expectation value $\langle \hat{\mathbf{S}}_{\mathbf{j}}^- \hat{\mathbf{S}}_{\mathbf{p}}^+ \rangle$ with the Green function formalism that we presented, we first need to determine the Green function

$$G_{-;\mathbf{p},\mathbf{j}}^+ = \langle\!\langle \hat{\mathbf{S}}_{\mathbf{p}}^+; \hat{\mathbf{S}}_{\mathbf{j}}^- \rangle\!\rangle_- \tag{2.134}$$

from its equation of motion

$$\omega G_{-;\mathbf{p},\mathbf{j}}^+ = \frac{1}{2\pi} \langle [\hat{\mathbf{S}}_{\mathbf{p}}^+, \hat{\mathbf{S}}_{\mathbf{j}}^-] \rangle + \langle\!\langle [\hat{\mathbf{S}}_{\mathbf{p}}^+, \hat{\mathrm{H}}]; \hat{\mathbf{S}}_{\mathbf{j}}^- \rangle\!\rangle_- . \tag{2.135}$$

For the particular system under consideration, Bloomfield and Nafari [94] showed that the commutator Green functions are sufficient and well-defined. The commutators in the equation of motion are

$$[\hat{S}_{\mathbf{p}}^+, \, \hat{S}_{\mathbf{j}}^-] = 2\hat{S}_{\mathbf{p}}^z \delta_{\mathbf{pj}} \tag{2.136}$$

$$[\hat{S}_{\mathbf{p}}^+, \, \hat{H}] = g_e \mu_B B \hat{S}_{\mathbf{p}}^+ - J \sum_{\mathbf{l}} \zeta_{1,\mathbf{lp}} \left(\hat{S}_{\mathbf{l}}^+ \hat{S}_{\mathbf{p}}^z - \hat{S}_{\mathbf{p}}^+ \hat{S}_{\mathbf{l}}^z \right), \tag{2.137}$$

where we made use of basic spin commutation relations. The above equation of motion is thus equivalent to

$$\omega G_{-;\mathbf{p,j}}^+ = \frac{2M}{2\pi} \delta_{\mathbf{pj}} + g_e \mu_B B G_{-;\mathbf{p,j}}^+ - J \sum_{\mathbf{l}} \zeta_{1,\mathbf{lp}} \left(G_{-;\mathbf{lp,j}}^{+z} - G_{-;\mathbf{pl,j}}^{+z} \right), \tag{2.138}$$

where the higher order Green functions are written as

$$G_{-;\mathbf{lp,j}}^{+z} = \langle\!\langle \hat{S}_{\mathbf{l}}^+ \hat{S}_{\mathbf{p}}^z; \, \hat{S}_{\mathbf{j}}^- \rangle\!\rangle_- . \tag{2.139}$$

To solve the equation of motion, these higher order Green functions need to be decoupled.

The most straightforward and most commonly used lowest order decoupling scheme was independently proposed by Tyablikov [103, 104] and Englert [105]. This scheme—commonly known as the Tyablikov decoupling or random phase approximation (RPA) [106]—is given by

$$G_{-;\mathbf{lp,j}}^{+z} \to \langle \hat{S}_{\mathbf{l}}^+ \rangle G_{-;\mathbf{p,j}}^z + \langle \hat{S}_{\mathbf{p}}^z \rangle G_{-;\mathbf{l,j}}^+ = M G_{-;\mathbf{l,j}}^+ \tag{2.140}$$

and corresponds to neglecting part of the correlation between spins at different lattice sites. The expectation value in the first term vanishes because the magnetisation is in the z-direction. This decoupling reduces the equation of motion to

$$\sum_{\mathbf{l}} \left(\omega \delta_{\mathbf{pl}} - \Gamma_{\mathbf{pl}} \right) G_{-;\mathbf{l,j}}^+ = \frac{1}{2\pi} 2M \delta_{\mathbf{pj}} \tag{2.141a}$$

with

$$\Gamma_{\mathbf{pl}} = \left(g_e \mu_B B + M J \zeta_1(0) \right) \delta_{\mathbf{pl}} - M J \zeta_{1,\mathbf{lp}}. \tag{2.141b}$$

This equation of motion can now be Fourier transformed into reciprocal space, such that it is cast in a form similar to Eq. (2.95):

$$\left(\omega - \Gamma(\mathbf{k}) \right) G_-^+(\mathbf{k}) = \frac{1}{2\pi} 2M \tag{2.142a}$$

with the Fourier-transformed decoupling matrix elements

$$\Gamma(\mathbf{k}) = g_{\mathrm{e}}\mu_{\mathrm{B}}B + MJ\left(\zeta_1(0) - \zeta_1(\mathbf{k})\right). \tag{2.142b}$$

These decoupling matrix elements correspond to the characteristic excitation energies (or energy spectrum) $\omega(\mathbf{k})$ of the elementary excitations in the system. In contrast to the usual linear spin wave theory, the elementary excitations (spin waves) depend on the temperature through the magnetisation M. In higher order approximations, the pole of the equation disappears and there is damping of the spin waves. The solution for the Green function

$$G_-^+(\mathbf{k}) = \frac{1}{2\pi}\frac{2M}{\omega - \Gamma(\mathbf{k})} \tag{2.143}$$

can be read off immediately from the algebraic equation of motion, which leads to the expectation value

$$\langle \hat{\mathrm{S}}^- \hat{\mathrm{S}}^+ \rangle(\mathbf{k}) = \frac{2M}{\mathrm{e}^{\beta\Gamma(\mathbf{k})} - 1}. \tag{2.144}$$

Transforming back to real space and evaluating both operators in the expectation value at the same lattice point yields

$$\langle \hat{\mathrm{S}}_{\mathbf{d}}^- \hat{\mathrm{S}}_{\mathbf{d}}^+ \rangle = \frac{1}{v_b}\int\limits_{\mathrm{BZ}} \frac{2M}{\mathrm{e}^{\beta\Gamma(\mathbf{k})} - 1}\,\mathrm{d}\mathbf{k} = \frac{1}{2} - M. \tag{2.145}$$

Finally, using the identity $\int_{\mathrm{BZ}} 1\,\mathrm{d}\mathbf{k} = v_b$ and the relation $\coth(x/2) = 1 + 2/(\mathrm{e}^x - 1)$, the magnetisation in the Heisenberg spin system is given by

$$M^{-1} = \frac{2}{v_b}\int\limits_{\mathrm{BZ}} \coth\left(\frac{1}{2}\beta\Gamma(\mathbf{k})\right)\mathrm{d}\mathbf{k}. \tag{2.146}$$

Due to the smart factoring out of lattice-structure dependent terms in the neighbour functions, the above result holds for any two- or three-dimensional lattice with single atomic basis. Notice that this relation still needs to be solved self-consistently, since the magnetisation also appears in the system's excitation energy $\Gamma(\mathbf{k})$.

Depending on the specific form of $\Gamma(\mathbf{k})$, the integration can be challenging and requires specific numerical integration techniques to be computed efficiently. Typically, the integrand will have a singularity or near-singularity at the origin. Through symmetry properties, such an integrand can be transformed to have the singularity at one of the end-points of the integration domain. These integrands can be handled using Gauss-Legendere quadrature, which does not sample points at the boundary of the integration domains, but convergence will generally be

slow. To overcome such problems, we resorted to the little-known tanh-sinh—or double exponential (DE)—quadrature [107–111]. This quadrature is known to be particularly fast at handling integrands with end-point singularities. We wrote a manuscript [112] on the best-practices for implementing this quadrature in a limited-precision floating point environment and on its performance for multiple integration, as little information was available on those topics. The content of this manuscript is reproduced (except for the layout) in appendix A.

3 Anisotropy in ferromagnets

3.1 Extended Heisenberg model

As was the case for the simple model, the extended Heisenberg Hamiltonian

$$\hat{H} = \hat{H}_B + \hat{H}_{ex} \tag{3.1}$$

has two contributing terms, the exchange term $\hat{H}_{ex}$ and the Zeeman term $\hat{H}_B$. It differs in four ways from the simple model: (i) the exchange interaction is anisotropic, (ii) the crystal can have a multiatomic basis, (iii) general spins $S \geqslant 1/2$ are allowed, and (iv) the magnetic field can be applied in an arbitrary direction. We will describe these differences in more detail now, adding a few further restrictions along the way to get specific results.

The exchange interaction

$$\hat{H}_{ex} = -\frac{1}{2} \sum_{\mathbf{d},\mathbf{l}} J_{\mathbf{ld}} \left[(1 - \Delta_{\mathbf{ld}}) \, (\hat{S}_{\mathbf{d}}^X \hat{S}_{\mathbf{l}}^X + \hat{S}_{\mathbf{d}}^Y \hat{S}_{\mathbf{l}}^Y) + (1 + \Delta_{\mathbf{ld}}) \, \hat{S}_{\mathbf{d}}^Z \hat{S}_{\mathbf{l}}^Z \right] \tag{3.2}$$

is now anisotropic in spin space, meaning that it has a different strength between different spin components. The exchange interaction takes the form of a diagonal tensor. It differentiates between the in-plane spin components, interacting with strengths $J_{\mathbf{ld}}^X = J_{\mathbf{ld}}^Y = J_{\mathbf{ld}} \, (1 - \Delta_{\mathbf{ld}})$, and the out-of-plane spin component, interacting with strength $J_{\mathbf{ld}}^Z = J_{\mathbf{ld}} \, (1 + \Delta_{\mathbf{ld}})$. The minus sign in the definition ensures that ferromagnetic interaction corresponds to a positive exchange strength $J_{\mathbf{ld}} > 0$ and the factor $1/2$ corrects for double-counting of interactions. The anisotropy parameter $\Delta_{\mathbf{ld}}$ can vary from -1 over 0 to 1, corresponding to respectively the XY-model, isotropic Heisenberg model and quantum Ising model and everything in between (see subsection 1.3.2 and Figure 3.1). The sum should be interpreted as being over all lattice points in a possibly multiatomic crystal. We will only start writing the atomic basis index when the distinction of sublattices becomes important.

The Zeeman term

$$\hat{H}_B = -g_e \mu_B \mathbf{B} \cdot \sum_{\mathbf{d}} \hat{\mathbf{S}}_{\mathbf{d}} \tag{3.3}$$

describes the interactions of all the spins on the lattice with the externally applied magnetic flux density $\mathbf{B}$, which is now allowed to be in any direction. Since
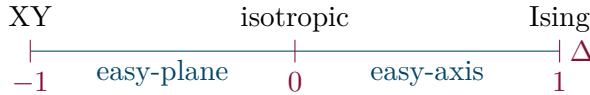
Figure 3.1 At the anisotropy minimum, the Hamiltonian is equivalent to the XY-model, with only in-plane spin components interacting. Increasing the anisotropy from there, the interaction becomes easy-plane anisotropic. At $\Delta_{\mathbf{ld}} = 0$, isotropic exchange is recovered. Further increasing the anisotropy leads to an effective easy-axis exchange. At its maximum, the interaction corresponds to an Ising model. Notice, however, that the classical Ising model corresponds to $S = 1/2$ (or classically scaled version thereof), while our model employs quantum spins $S \geqslant 1/2$.
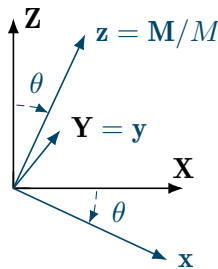

Figure 3.2 Rotation from the crystallographic coordinate system $\{\mathbf{X}, \mathbf{Y}, \mathbf{Z}\}$ (black) towards the magnetisation coordinate system $\{\mathbf{x}, \mathbf{y}, \mathbf{z}\}$ (blue) by rotating over an angle θ in counter-clockwise direction around the $\mathbf{Y}$-axis.

$\hat{H}_{ex}$ is invariant in spin space under rotation in the XY-plane and reflection over the XY-plane, it is sufficiently general to consider $\mathbf{B} = B^X \mathbf{X} + B^Z \mathbf{Z}$ with $B^X = B \sin \theta_B$ and $B^Z = B \cos \theta_B$. The angle θ_B of the applied field with respect to the out-of-plane direction $\mathbf{Z}$ can moreover be restricted to $0 \leqslant \theta_B \leqslant \pi/2$.

Before we start applying the general scheme as set out in Sec. 2.3, we will perform a rotation of the reference coordinate system, from the crystallographic $\{\mathbf{X}, \mathbf{Y}, \mathbf{Z}\}$ to the so-called magnetisation coordinate system $\{\mathbf{x}, \mathbf{y}, \mathbf{z}\}$, where $\mathbf{z}$ is chosen along the magnetisation direction. While the latter is still unknown, this choice of coordinate system ensures that the magnetisation will only have a z-component. The impact of this will become more apparent during the calculations. Several authors [102, 113–115] pointed out that performing such a rotation before any decoupling approximations are made, is also beneficial for the quality of those decoupling schemes. The system's symmetry ensures that its magnetisation lies in the XZ-plane. This means that the magnetisation coordinate system can be obtained from the crystallographic coordinate system by counter-clockwise rotating over an angle θ around $\mathbf{Y} = \mathbf{y}$ (Fig. 3.2). Such a rotation is mathematically

described by

$$\begin{bmatrix} \mathbf{x} \\ \mathbf{y} \\ \mathbf{z} \end{bmatrix} = \mathbf{R_Y}(\theta) \cdot \begin{bmatrix} \mathbf{X} \\ \mathbf{Y} \\ \mathbf{Z} \end{bmatrix} \quad \text{with } \mathbf{R_Y}(\theta) = \begin{bmatrix} \cos\theta & 0 & -\sin\theta \\ 0 & 1 & 0 \\ \sin\theta & 0 & \cos\theta \end{bmatrix}. \quad (3.4)$$

By introducing a single magnetisation angle θ—which is independent of the referenced lattice point—we assume that the magnetisation is homogeneous, taking equal values on arbitrary (sub)lattice points. This is a reasonable assumption when the described material is homogeneous itself. It is in contrast with anti-ferromagnets or multilayer materials, where different canting angles on different sublattices or layers are very common [115–117]. In those cases, the magnetisation angle and magnitude must be allowed to depend on the sublattice or layer.

Using the above rotation matrix, the extended Heisenberg Hamiltonian can be expressed in the magnetisation coordinate system. The Zeeman term retains its previous form, as it is a scalar product, invariant under rotation. Both $\hat{\mathbf{S}}$ and

$$\mathbf{B} = B^x \mathbf{x} + B^z \mathbf{z}, \text{ with } B^x = B\sin(\theta_B - \theta) \text{ and } B^z = B\cos(\theta_B - \theta), \quad (3.5)$$

are now written in the new coordinate system. The exchange term changes more drastically to

$$\hat{H}_{ex} = -\frac{1}{2} \sum_{\mathbf{d},\mathbf{l}} \left[J^{xx}_{\mathbf{ld}} \hat{S}^x_{\mathbf{d}} \hat{S}^x_{\mathbf{l}} + J^{yy}_{\mathbf{ld}} \hat{S}^y_{\mathbf{d}} \hat{S}^y_{\mathbf{l}} + J^{zz}_{\mathbf{ld}} \hat{S}^z_{\mathbf{d}} \hat{S}^z_{\mathbf{l}} + J^{zx}_{\mathbf{ld}} \hat{S}^z_{\mathbf{d}} \hat{S}^x_{\mathbf{l}} + J^{xz}_{\mathbf{ld}} \hat{S}^x_{\mathbf{d}} \hat{S}^z_{\mathbf{l}} \right], \quad (3.6a)$$

where the exchange interaction tensor gained symmetric off-diagonal components

$$\begin{aligned} J^{xx}_{\mathbf{ld}} &= J_{\mathbf{ld}} \left[1 - \Delta_{\mathbf{ld}} \cos 2\theta \right] \\ J^{yy}_{\mathbf{ld}} &= J_{\mathbf{ld}} \left(1 - \Delta_{\mathbf{ld}} \right) \\ J^{zz}_{\mathbf{ld}} &= J_{\mathbf{ld}} \left[1 + \Delta_{\mathbf{ld}} \cos 2\theta \right] \\ J^{xz}_{\mathbf{ld}} = J^{zx}_{\mathbf{ld}} &= -J_{\mathbf{ld}} \Delta_{\mathbf{ld}} \sin 2\theta. \end{aligned} \quad (3.6b)$$

3.2   General results

For further calculations, it will be more convenient to work with the spin operators $\hat{S}^\pm = \hat{S}^x \pm i\hat{S}^y$. In terms of those operators, the Zeeman Hamiltonian is

$$\hat{H}_B = -g_e \mu_B \sum_{\mathbf{d}} \left[B^+ \hat{S}^+_{\mathbf{d}} + B^- \hat{S}^-_{\mathbf{d}} + B^z \hat{S}^z_{\mathbf{d}} \right], \text{ with } B^+ = B^- = \frac{B^x}{2} \quad (3.7)$$

and the exchange Hamiltonian becomes

$$\hat{H}_{ex} = -\frac{1}{2} \sum_{\mathbf{d},\mathbf{l}} \left[J_{\mathbf{ld}}^{++} \hat{S}_{\mathbf{d}}^{+} \hat{S}_{\mathbf{l}}^{+} + J_{\mathbf{ld}}^{--} \hat{S}_{\mathbf{d}}^{-} \hat{S}_{\mathbf{l}}^{-} + J_{\mathbf{ld}}^{zz} \hat{S}_{\mathbf{d}}^{z} \hat{S}_{\mathbf{l}}^{z} \right.$$
$$\left. + J_{\mathbf{ld}}^{+z} \hat{S}_{\mathbf{d}}^{+} \hat{S}_{\mathbf{l}}^{z} + J_{\mathbf{ld}}^{-z} \hat{S}_{\mathbf{d}}^{-} \hat{S}_{\mathbf{l}}^{z} + J_{\mathbf{ld}}^{+-} \hat{S}_{\mathbf{d}}^{+} \hat{S}_{\mathbf{l}}^{-} \right] , \tag{3.8a}$$

with exchange tensor components

$$J_{\mathbf{ld}}^{++} = J_{\mathbf{ld}}^{--} = \frac{1}{2} J_{\mathbf{ld}} \Delta_{\mathbf{ld}} \sin^2 \theta$$
$$J_{\mathbf{ld}}^{zz} = J_{\mathbf{ld}} \left[1 + \Delta_{\mathbf{ld}} \cos 2\theta \right]$$
$$J_{\mathbf{ld}}^{+-} = J_{\mathbf{ld}} - J_{\mathbf{ld}} \Delta_{\mathbf{ld}} \cos^2 \theta \tag{3.8b}$$
$$J_{\mathbf{ld}}^{+z} = J_{\mathbf{ld}}^{-z} = -J_{\mathbf{ld}} \Delta_{\mathbf{ld}} \sin 2\theta.$$

To obtain the latter, we relabelled some lattice position indices, used the bosonic commutator relation for spins at different lattice sites, and used the property that exchange interactions are typically symmetric, such that $J_{\mathbf{ld}} = J_{\mathbf{dl}}$ and $\Delta_{\mathbf{ld}} = \Delta_{\mathbf{dl}}$. The calculations in this section will be performed for the general Hamiltonians $\hat{H}_B$ and $\hat{H}_{ex}$, as given in equations (3.7) and (3.8a). Since we will not make any reference to exchange-specific properties of $J_{\mathbf{ld}}^{\tau v}$ or magnetic field-specific properties of B^{τ}, we will be able to reuse the derived results when treating the dipolar interaction in the next chapter.

3.2.1 Green functions and their equation of motion

We will now apply the Green function theory as outlined in Sec. 2.3, supplemented with the technique of Callen [91] to account for $S \geqslant \frac{1}{2}$. The Green functions of interest are the commutator Green functions

$$G_{\mathbf{p},\mathbf{j}}^{\alpha,\tau}(\omega, \lambda) = \langle\!\langle \hat{S}_{\mathbf{p}}^{\tau}; e^{\lambda \hat{S}_{\mathbf{j}}^{z}} \hat{S}_{\mathbf{j}}^{-} \rangle\!\rangle , \text{ with } \tau \in \{+, -, z\} \text{ and } \mathbf{p} \in \alpha. \tag{3.9}$$

Here and in the future, the comma-separated subscripts (in this case $\mathbf{p}$ and $\mathbf{j}$) always indicate the lattice position indices of the first, respectively second operator in the Green function. The superscripts are always related to the first operator: the first, if present, indicates the sublattice of the multiatomic basis to which the first operator belongs (i.e. $\mathbf{p} \in \alpha$ in this case), while the last indicates the vector component of the first operator (which can be any of the components $\tau \in \{+, -, z\}$). The real-valued parameter λ is necessary to treat higher spin values $S > 1/2$ and its usefulness will become apparent in subsection 3.2.4. We will not continue to write the frequency dependence ω. The Green function obeys the equation of motion

$$\omega G_{\mathbf{p},\mathbf{j}}^{\alpha,\tau}(\lambda) = \frac{1}{2\pi} \langle [\hat{S}_{\mathbf{p}}^{\tau}, e^{\lambda \hat{S}_{\mathbf{j}}^{z}} \hat{S}_{\mathbf{j}}^{-}] \rangle \delta_{\mathbf{pj}} + \langle\!\langle [\hat{S}_{\mathbf{p}}^{\tau}, \hat{H}]; e^{\lambda \hat{S}_{\mathbf{j}}^{z}} \hat{S}_{\mathbf{j}}^{-} \rangle\!\rangle , \quad \mathbf{p} \in \alpha. \tag{3.10}$$

We write the inhomogeneous term as

$$\Psi^{\alpha,\tau}(\lambda) = \langle [\hat{S}_{\mathbf{p}}^{\tau},\, e^{\lambda \hat{S}_{\mathbf{p}}^{z}} \hat{S}_{\mathbf{p}}^{-}] \rangle, \quad \mathbf{p} \in \alpha. \tag{3.11}$$

The commutators $[\hat{S}_{\mathbf{p}}^{\tau},\, \hat{H}]$ require some work, but are further easily calculated using standard spin-commutator relations. They are

$$
\begin{aligned}
[\hat{S}_{\mathbf{p}}^{\pm},\, \hat{H}] = {}&\pm g_{\mathrm{e}}\mu_{\mathrm{B}}\left[B^{z}\hat{S}_{\mathbf{p}}^{\pm} - 2B^{\mp}\hat{S}_{\mathbf{p}}^{z} \right] \\
&\pm \frac{1}{2}\sum_{\mathbf{l}}\left\{ -4J_{\mathbf{lp}}^{\mp\mp}\hat{S}_{\mathbf{p}}^{z}\hat{S}_{\mathbf{l}}^{\mp} + 2J_{\mathbf{lp}}^{zz}\hat{S}_{\mathbf{p}}^{\pm}\hat{S}_{\mathbf{l}}^{z} - 2J_{\mathbf{lp}}^{+-}\hat{S}_{\mathbf{p}}^{z}\hat{S}_{\mathbf{l}}^{\pm} \right. \\
&\qquad\qquad \left. -2J_{\mathbf{lp}}^{\mp z}\hat{S}_{\mathbf{p}}^{z}\hat{S}_{\mathbf{l}}^{z} + J_{\mathbf{lp}}^{\pm z}\hat{S}_{\mathbf{p}}^{\pm}\hat{S}_{\mathbf{l}}^{\pm} + J_{\mathbf{lp}}^{\mp z}\hat{S}_{\mathbf{p}}^{\pm}\hat{S}_{\mathbf{l}}^{\mp} \right\}
\end{aligned}
\tag{3.12a}
$$

and

$$
\begin{aligned}
[\hat{S}_{\mathbf{p}}^{z},\, \hat{H}] = {}&-g_{\mathrm{e}}\mu_{\mathrm{B}}\left[B^{+}\hat{S}_{\mathbf{p}}^{+} - B^{-}\hat{S}_{\mathbf{p}}^{-} \right] \\
&-\frac{1}{2}\sum_{\mathbf{l}}\left\{ +2J_{\mathbf{lp}}^{++}\hat{S}_{\mathbf{p}}^{+}\hat{S}_{\mathbf{l}}^{+} - 2J_{\mathbf{lp}}^{--}\hat{S}_{\mathbf{p}}^{-}\hat{S}_{\mathbf{l}}^{-} + J_{\mathbf{lp}}^{+-}\hat{S}_{\mathbf{p}}^{+}\hat{S}_{\mathbf{l}}^{-} \right. \\
&\qquad\qquad \left. -J_{\mathbf{lp}}^{+-}\hat{S}_{\mathbf{p}}^{-}\hat{S}_{\mathbf{l}}^{+} + J_{\mathbf{lp}}^{+z}\hat{S}_{\mathbf{p}}^{+}\hat{S}_{\mathbf{l}}^{z} - J_{\mathbf{lp}}^{-z}\hat{S}_{\mathbf{p}}^{-}\hat{S}_{\mathbf{l}}^{z} \right\}.
\end{aligned}
\tag{3.12b}
$$

3.2.2 Decoupling higher order Green functions

Substituting these commutators in the equation of motion, they introduce higher order Green functions $\langle\langle \hat{S}_{\mathbf{p}}^{\tau}\hat{S}_{\mathbf{l}}^{v};\, e^{\lambda \hat{S}_{\mathbf{j}}^{z}}\hat{S}_{\mathbf{j}}^{-} \rangle\rangle$ with $\mathbf{p}$ belonging to sublattice α and $\mathbf{l}$ to a possibly different sublattice β. The two spin operators in the first argument never act on the exact same lattice point, i.e. the same Bravais lattice point and sublattice. As in subsection 2.3.3, the higher order Green functions can be decoupled in terms of lower order Green functions by neglecting a part of the correlation between spins at different lattice sites. This Tyablikov decoupling [103–105] now comes down to

$$\langle\langle \hat{S}_{\mathbf{p}}^{\tau}\hat{S}_{\mathbf{l}}^{v};\, e^{\lambda \hat{S}_{\mathbf{j}}^{z}}\hat{S}_{\mathbf{j}}^{-} \rangle\rangle \;\to\; \langle \hat{S}_{\mathbf{p}}^{\tau}\rangle G_{\mathbf{l},\mathbf{j}}^{\beta,v}(\lambda) + \langle \hat{S}_{\mathbf{l}}^{v}\rangle G_{\mathbf{p},\mathbf{j}}^{\alpha,\tau}(\lambda), \quad \mathbf{p}\in\alpha, \mathbf{l}\in\beta. \tag{3.13}$$

Performing the decoupling in the magnetisation coordinate system gives higher quality results and more straightforward calculations [102, 113–115]. This can be understood by looking at the expectation values for the different spin components. In the magnetisation coordinate system, the expectation values of the x- and y-components vanish, implying that

$$\langle \hat{S}_{\mathbf{j}}^{+}\rangle = \langle \hat{S}_{\mathbf{j}}^{-}\rangle = 0. \tag{3.14}$$

Moreover, it is defined such that the magnetisation is completely in the z-direction. The homogeneous magnetisation M^{α} on sublattice α is thus $M^{\alpha} = \langle \hat{S}_{\mathbf{j}}^{z}\rangle$ with $\mathbf{j}\in\alpha$. While it is possible to continue working with distinct magnetisation magnitudes on the different sublattices, we already assumed during the coordinate transformation

that the magnetisation direction θ is the same for each lattice point. Immediately assuming equal magnetisation magnitudes $M^\alpha = M^\beta$ on each sublattice is thus reasonable at this point. We define the homogeneous magnetisation magnitude

$$M = \langle \hat{S}^z_{\mathbf{j}} \rangle, \tag{3.15}$$

which ranges from 0 to its saturation value $M_{\mathrm{s}} = S$. A normalised magnetisation can be defined as $\sigma = M/M_{\mathrm{s}}$. Similar to the magnetisation and its angle, we also assume the inhomogeneity term $\Psi^\tau(\lambda) = \Psi^{\alpha,\tau}(\lambda)$ to be sublattice-independent.

Utilising all of the above—the notation for the inhomogeneous term, the commutator relations of spin components with the Hamiltonian, the Tyablikov decoupling approximation and the spin component expectation values—the Green function equation of motion becomes

$$\omega G^{\alpha,\pm}_{\mathbf{p,j}} = \frac{1}{2\pi}\Psi^\pm(\lambda)\delta_{\mathbf{pj}} + \left[\pm g_{\mathrm{e}}\mu_{\mathrm{B}}B^z \pm M\sum_{\mathbf{l}} J^{zz}_{\mathbf{lp}} \right] G^{\alpha,\pm}_{\mathbf{p,j}}$$

$$+ \left[\mp g_{\mathrm{e}}\mu_{\mathrm{B}}2B^\mp \mp M\sum_{\mathbf{l}} J^{\mp z}_{\mathbf{lp}} \right] G^{\alpha,z}_{\mathbf{p,j}}$$

$$+ \left[\mp 2M\sum_{\mathbf{l}} J^{\mp\mp}_{\mathbf{lp}} G^{\beta,\mp}_{\mathbf{l,j}} \right] + \left[\mp M\sum_{\mathbf{l}} J^{+-}_{\mathbf{lp}} G^{\beta,\pm}_{\mathbf{l,j}} \right] \tag{3.16a}$$

$$+ \left[\mp M\sum_{\mathbf{l}} J^{\mp z}_{\mathbf{lp}} G^{\beta,z}_{\mathbf{l,j}} \right], \quad \mathbf{p} \in \alpha, \mathbf{l} \in \beta$$

$$\omega G^{\alpha,z}_{\mathbf{p,j}} = \frac{1}{2\pi}\Psi^z(\lambda)\delta_{\mathbf{pj}} - \left[g_{\mathrm{e}}\mu_{\mathrm{B}}B^+ + \frac{1}{2}M\sum_{\mathbf{l}} J^{+z}_{\mathbf{lp}} \right] G^{\alpha,+}_{\mathbf{p,j}}$$

$$+ \left[g_{\mathrm{e}}\mu_{\mathrm{B}}B^- + \frac{1}{2}M\sum_{\mathbf{l}} J^{-z}_{\mathbf{lp}} \right] G^{\alpha,-}_{\mathbf{p,j}}, \quad \mathbf{p} \in \alpha, \mathbf{l} \in \beta \tag{3.16b}$$

where $\mathbf{l}$ sums over all lattice points. In each term of the sum, β is the specific sublattice to which $\mathbf{l}$ belongs. Due to the different commutator relations $[\hat{S}^\tau_{\mathbf{p}}, \hat{H}]$ for the different spin components τ, there are now 3 equations of motion for each sublattice α. Continuing to follow the steps set out in Section 2.3, we perform a spatial Fourier transform (2.8) to exploit the lattice translational symmetry. The Green functions can be expanded into their Fourier components as

$$G^{\alpha,\tau}_{\mathbf{p,j}} = \frac{1}{N}\sum_{\mathbf{k}\in\mathrm{BZ}} \mathrm{e}^{-\mathrm{i}\mathbf{k}\cdot\mathbf{r}_{\mathbf{jp}}} G^{\alpha,\tau}(\mathbf{k}), \tag{3.17}$$

while the Fourier transformed exchange tensor components are

$$J^{\tau\upsilon}_{\beta\alpha}(\mathbf{k}) = \sum_{\mathbf{r_l}} \mathrm{e}^{\mathrm{i}\mathbf{k}\cdot\mathbf{r}_{\mathbf{lp}}} J^{\tau\upsilon}_{\mathbf{lp}}, \quad \mathbf{p} \in \alpha, \mathbf{l} \in \beta \text{ and } \tau, \upsilon \in \{+, -, z\}, \tag{3.18}$$

where the sum is over the Bravais lattice points, not over the sublattices. Additionally, we define

$$J_\alpha^{\tau\upsilon}(0) = \sum_\beta J_{\beta\alpha}^{\tau\upsilon}(0), \tag{3.19}$$

where we sum over all sublattices. The equations of motion now become

$$
\begin{aligned}
\omega G^{\alpha,\pm}(\mathbf{k}) = {} & \frac{1}{2\pi}\Psi^\pm(\lambda) + \left[\pm g_\mathrm{e}\mu_\mathrm{B}B^z \pm MJ_\alpha^{zz}(0)\right]G^{\alpha,\pm}(\mathbf{k}) \\
& + \left[\mp g_\mathrm{e}\mu_\mathrm{B}2B^\mp \mp MJ_\alpha^{\mp z}(0)\right]G^{\alpha,z}(\mathbf{k}) \\
& \mp 2M\sum_\beta J_{\beta\alpha}^{\mp\mp}(\mathbf{k})G^{\beta,\mp}(\mathbf{k}) \mp M\sum_\beta J_{\beta\alpha}^{+-}(\mathbf{k})G^{\beta,\pm}(\mathbf{k}) \\
& \mp M\sum_\beta J_{\beta\alpha}^{\mp z}(\mathbf{k})G^{\beta,z}(\mathbf{k})
\end{aligned}
\tag{3.20a}
$$

$$
\begin{aligned}
\omega G^{\alpha,z}(\mathbf{k}) = {} & \frac{1}{2\pi}\Psi^z(\lambda) - \left[g_\mathrm{e}\mu_\mathrm{B}B^+ + \frac{1}{2}MJ_\alpha^{+z}(0)\right]G^{\alpha,+}(\mathbf{k}) \\
& + \left[g_\mathrm{e}\mu_\mathrm{B}B^- + \frac{1}{2}MJ_\alpha^{-z}(0)\right]G^{\alpha,-}(\mathbf{k}).
\end{aligned}
\tag{3.20b}
$$

The equations of motion for Green functions related to different sublattices are coupled through the inter-lattice exchange interactions.

Te inhomogeneity term $\Psi^\tau(\lambda)$ can be split in two terms as

$$\Psi^\tau(\lambda) = \langle[\hat{S}_\mathbf{p}^\tau, \mathrm{e}^{\lambda\hat{S}_\mathbf{p}^z}]\hat{S}_\mathbf{p}^- + \mathrm{e}^{\lambda\hat{S}_\mathbf{p}^z}[\hat{S}_\mathbf{p}^\tau, \hat{S}_\mathbf{p}^-]\rangle, \tag{3.21}$$

by using the general commutator relation $[\hat{A}, \hat{B}\hat{C}] = [\hat{A}, \hat{B}]\hat{C} + \hat{B}[\hat{A}, \hat{C}]$. Further, we use the spin commutators

$$[\hat{S}_\mathbf{p}^\pm, \mathrm{e}^{\lambda\hat{S}_\mathbf{p}^z}] = (\mathrm{e}^{\mp\lambda} - 1)\,\mathrm{e}^{\lambda\hat{S}_\mathbf{p}^z}\hat{S}_\mathbf{p}^\pm \tag{3.22}$$

that were also used by Callen [91], and some more generally known spin relations. The different inhomogeneity terms can then be written as

$$
\begin{aligned}
\Psi^+(\lambda) &= \langle[\hat{S}_\mathbf{p}^+, \mathrm{e}^{\lambda\hat{S}_\mathbf{p}^z}]\hat{S}_\mathbf{p}^- + \mathrm{e}^{\lambda\hat{S}_\mathbf{p}^z}[\hat{S}_\mathbf{p}^+, \hat{S}_\mathbf{p}^-]\rangle \\
&= \langle(\mathrm{e}^{-\lambda} - 1)\,\mathrm{e}^{\lambda\hat{S}_\mathbf{p}^z}\hat{S}_\mathbf{p}^+\hat{S}_\mathbf{p}^- + 2\mathrm{e}^{\lambda\hat{S}_\mathbf{p}^z}\hat{S}_\mathbf{p}^z\rangle \\
&= \langle(\mathrm{e}^{-\lambda} - 1)\,\mathrm{e}^{\lambda\hat{S}_\mathbf{p}^z}\left(S(S+1) + \hat{S}_\mathbf{p}^z - (\hat{S}_\mathbf{p}^z)^2\right) + 2\mathrm{e}^{\lambda\hat{S}_\mathbf{p}^z}\hat{S}_\mathbf{p}^z\rangle \\
&= S(S+1)(\mathrm{e}^{-\lambda} - 1)\langle\mathrm{e}^{\lambda\hat{S}_\mathbf{p}^z}\rangle + (\mathrm{e}^{-\lambda} + 1)\langle\mathrm{e}^{\lambda\hat{S}_\mathbf{p}^z}\hat{S}_\mathbf{p}^z\rangle \\
&\quad - (\mathrm{e}^{-\lambda} - 1)\langle\mathrm{e}^{\lambda\hat{S}_\mathbf{p}^z}(\hat{S}_\mathbf{p}^z)^2\rangle
\end{aligned}
\tag{3.23a}
$$

$$\Psi^-(\lambda) = \langle[\hat{S}_\mathbf{p}^-, \mathrm{e}^{\lambda\hat{S}_\mathbf{p}^z}]\hat{S}_\mathbf{p}^-\rangle = (\mathrm{e}^{+\lambda} - 1)\langle\mathrm{e}^{\lambda\hat{S}_\mathbf{p}^z}\hat{S}_\mathbf{p}^-\hat{S}_\mathbf{p}^-\rangle = 0 \tag{3.23b}$$

$$\Psi^z(\lambda) = \langle\mathrm{e}^{\lambda\hat{S}_\mathbf{p}^z}[\hat{S}_\mathbf{p}^z, \hat{S}_\mathbf{p}^-]\rangle = -\langle\mathrm{e}^{\lambda\hat{S}_\mathbf{p}^z}\hat{S}_\mathbf{p}^-\rangle = 0, \tag{3.23c}$$

where the expectation values of the operator combinations in last two quantities vanish. These operator combinations alter the **z** spin component, such that their expectation values are bound to vanish.

3.2.3 Vectorised equation of motion

The equations of motion can be cast in the vector form of Eq. (2.100),

$$(\omega\mathbb{1} - \boldsymbol{\Gamma}(\mathbf{k})) \cdot \mathbf{G}(\mathbf{k}) = \frac{1}{2\pi}\boldsymbol{\Psi}(\mathbf{k}), \tag{3.24}$$

where the Green function vector $\mathbf{G}(\mathbf{k})$ and the inhomogeneity vector $\boldsymbol{\Psi}(\mathbf{k})$,

$$\mathbf{G}(\mathbf{k}) = \begin{bmatrix} \mathbf{G}^\alpha(\mathbf{k}) \\ \mathbf{G}^\beta(\mathbf{k}) \\ \vdots \end{bmatrix} \text{ and } \boldsymbol{\Psi}(\mathbf{k}) = \begin{bmatrix} \boldsymbol{\Psi}^\alpha(\lambda) \\ \boldsymbol{\Psi}^\alpha(\lambda) \\ \vdots \end{bmatrix}, \tag{3.25}$$

are composed of the sublattice-specific component vectors

$$\mathbf{G}^\alpha(\mathbf{k}) = \begin{bmatrix} G^{\alpha,+}(\mathbf{k}) \\ G^{\alpha,-}(\mathbf{k}) \\ G^{\alpha,z}(\mathbf{k}) \end{bmatrix} \text{ and } \boldsymbol{\Psi}^\alpha(\mathbf{k}) = \begin{bmatrix} \Psi^+(\lambda) \\ \Psi^-(\lambda) \\ \Psi^z(\lambda) \end{bmatrix} = \begin{bmatrix} \Psi^+(\lambda) \\ 0 \\ 0 \end{bmatrix}. \tag{3.26}$$

These different Green functions are coupled through the matrix

$$\boldsymbol{\Gamma}(\mathbf{k}) = \begin{bmatrix} \boldsymbol{\Gamma}^{\alpha\alpha}(\mathbf{k}) & \boldsymbol{\Gamma}^{\alpha\beta}(\mathbf{k}) & \cdots \\ \boldsymbol{\Gamma}^{\beta\alpha}(\mathbf{k}) & \boldsymbol{\Gamma}^{\beta\beta}(\mathbf{k}) & \cdots \\ \vdots & \vdots & \ddots \end{bmatrix} \tag{3.27}$$

with block matrices

$$\boldsymbol{\Gamma}^{\alpha\beta}(\mathbf{k}) = \begin{bmatrix} \Gamma^{\alpha\beta,++}(\mathbf{k}) & \Gamma^{\alpha\beta,+-}(\mathbf{k}) & \Gamma^{\alpha\beta,+z}(\mathbf{k}) \\ \Gamma^{\alpha\beta,-+}(\mathbf{k}) & \Gamma^{\alpha\beta,--}(\mathbf{k}) & \Gamma^{\alpha\beta,-z}(\mathbf{k}) \\ \Gamma^{\alpha\beta,z+}(\mathbf{k}) & \Gamma^{\alpha\beta,z-}(\mathbf{k}) & \Gamma^{\alpha\beta,zz}(\mathbf{k}) \end{bmatrix}, \tag{3.28}$$

containing the elements

$$\Gamma^{\alpha\beta,++}(\mathbf{k}) = \left[+g_{\mathrm{e}}\mu_{\mathrm{B}}B^z + MJ^{zz}_\alpha(0) \right]\delta_{\alpha\beta} - MJ^{+-}_{\beta\alpha}(\mathbf{k}) \tag{3.29a}$$

$$\Gamma^{\alpha\beta,+-}(\mathbf{k}) = -2MJ^{--}_{\beta\alpha}(\mathbf{k}) \tag{3.29b}$$

$$\Gamma^{\alpha\beta,+z}(\mathbf{k}) = \left[-2g_{\mathrm{e}}\mu_{\mathrm{B}}B^- - MJ^{-z}_\alpha(0) \right]\delta_{\alpha\beta} - MJ^{-z}_{\beta\alpha}(\mathbf{k}) \tag{3.29c}$$

$$\Gamma^{\alpha\beta,-+}(\mathbf{k}) = +2MJ^{++}_{\beta\alpha}(\mathbf{k}) \tag{3.29d}$$

$$\Gamma^{\alpha\beta,--}(\mathbf{k}) = \left[-g_{\mathrm{e}}\mu_{\mathrm{B}}B^z - MJ^{zz}_\alpha(0) \right]\delta_{\alpha\beta} + MJ^{+-}_{\beta\alpha}(\mathbf{k}) \tag{3.29e}$$

$$\Gamma^{\alpha\beta,-z}(\mathbf{k}) = \left[+2g_{\mathrm{e}}\mu_{\mathrm{B}}B^+ + MJ^{+z}_\alpha(0) \right]\delta_{\alpha\beta} + MJ^{+z}_{\beta\alpha}(\mathbf{k}) \tag{3.29f}$$

$$\Gamma^{\alpha\beta,z+}(\mathbf{k}) = -\left[g_{\mathrm{e}}\mu_{\mathrm{B}}B^+ + MJ^{+z}_\alpha(0)/2 \right]\delta_{\alpha\beta} \tag{3.29g}$$

$$\Gamma^{\alpha\beta,z-}(\mathbf{k}) = \left[g_{\mathrm{e}}\mu_{\mathrm{B}}B^- + MJ^{-z}_\alpha(0)/2 \right]\delta_{\alpha\beta} \tag{3.29h}$$

$$\Gamma^{\alpha\beta,zz}(\mathbf{k}) = 0. \tag{3.29i}$$

If $J_{\mathbf{ld}} = J_{\mathbf{dl}}$ and $\Delta_{\mathbf{ld}} = \Delta_{\mathbf{dl}}$ for the diagonal submatrices $\boldsymbol{\Gamma}^{\alpha\alpha}(\mathbf{k})$ (coupling the Green function components of a given sublattice, $\beta = \alpha$), these components are all real-valued because the sum in the Fourier transform of $J_{\beta\alpha}^{\tau\upsilon}(\mathbf{k})$ is over all lattice points in the same Bravais lattice as the reference point. The off-diagonal submatrix $\boldsymbol{\Gamma}^{\alpha\beta}(\mathbf{k})$ (coupling Green functions related to different sublattices, $\beta \neq \alpha$) elements typically have both a real and complex component. We will reuse the general result above, later when dealing with the dipolar interactions.

3.2.4   Larger spin values

Before we continue the calculation of Green functions from the vector equation of motion, we will disclose why we are specifically interested in the Green function $G_{\mathbf{p},\mathbf{j}}^{\alpha,+}(\lambda) = \langle\!\langle \hat{\mathrm{S}}_{\mathbf{p}}^+ ; \mathrm{e}^{\lambda \hat{\mathrm{S}}_{\mathbf{j}}^z} \hat{\mathrm{S}}_{\mathbf{j}}^- \rangle\!\rangle$, as we defined it. This Green function can be used to find the expectation value $c^+(\lambda) = \langle \mathrm{e}^{\lambda \hat{\mathrm{S}}_{\mathbf{p}}^z} \hat{\mathrm{S}}_{\mathbf{p}}^- \hat{\mathrm{S}}_{\mathbf{p}}^+ \rangle$ by using the spectral theorem. Since we are calculating homogeneous quantities, the expectation value must be independent of the sublattice. Since it does not play any important role in this subsection (and the calculation holds for each sublattice separately), we will not write any sublattice indices anymore. Notice that for $S = 1/2$, the expectation value evaluated at $\lambda = 0$ is $c^+(0) = \langle \hat{\mathrm{S}}_{\mathbf{p}}^- \hat{\mathrm{S}}_{\mathbf{p}}^+ \rangle = 1/2 - \langle \hat{\mathrm{S}}_{\mathbf{p}}^z \rangle$, immediately giving access to the magnetisation, as we showed in subsection 2.3.3. For higher spins,

$$\hat{\mathrm{S}}_{\mathbf{p}}^- \hat{\mathrm{S}}_{\mathbf{p}}^+ = S\,(S+1) - \hat{\mathrm{S}}_{\mathbf{p}}^z - (\hat{\mathrm{S}}_{\mathbf{p}}^z)^2 \tag{3.30}$$

contains a term quadratic in $\hat{\mathrm{S}}_{\mathbf{p}}^z$, which is also unknown, rendering a direct determination of the magnetisation from $c^+(0)$ impossible. To be able to calculation the magnetisation for larger spin values $S \geqslant 1/2$, the factor containing λ was added to the Green functions. In this subsection, we will see how it helps to pin down the magnetisation This method was pioneered by Callen [91]. In his paper, he combines it with a decoupling scheme different from the Tyablikov decoupling, making it sometimes unclear which steps are a consequence of treating higher spin values and which steps originate from the different decoupling scheme. To make this distinction more clear, we will provide a full derivation of the necessary framework here. Alternatively, Tahir-Kheli and ter Haar [118] proposed to use Green functions of the form $\langle\!\langle \hat{\mathrm{S}}_{\mathbf{p}}^+ ; (\hat{\mathrm{S}}_{\mathbf{j}}^-)^n (\hat{\mathrm{S}}_{\mathbf{j}}^+)^{n-1} \rangle\!\rangle$, which can also be used to do the calculations for higher S. While the final results are identical, the method of Tahir-Kheli and ter Haar requires to solve a non-trivial set of $2S + 1$ equations for each distinct value of S, whereas Callen's method will give us a direct expression for arbitrary S. Both methods are discussed in the excellent book on quantum theory of ferromagnetism by Nolting and Ramakanth [119].

Using the spin relation (3.30), the expectation value definition is

$$\begin{aligned} c^+(\lambda) = \langle \mathrm{e}^{\lambda \hat{\mathrm{S}}_{\mathbf{p}}^z} \hat{\mathrm{S}}_{\mathbf{p}}^- \hat{\mathrm{S}}_{\mathbf{p}}^+ \rangle &= S\,(S+1)\,\langle \mathrm{e}^{\lambda \hat{\mathrm{S}}_{\mathbf{p}}^z} \rangle - \langle \mathrm{e}^{\lambda \hat{\mathrm{S}}_{\mathbf{p}}^z} \hat{\mathrm{S}}_{\mathbf{p}}^z \rangle - \langle \mathrm{e}^{\lambda \hat{\mathrm{S}}_{\mathbf{p}}^z} (\hat{\mathrm{S}}_{\mathbf{p}}^z)^2 \rangle \\ &= S\,(S+1)\,\Omega(\lambda) - \Omega'(\lambda) - \Omega''(\lambda), \end{aligned} \tag{3.31}$$

where we introduced the function

$$\Omega(\lambda) = \langle \mathrm{e}^{\lambda \hat{S}_{\mathbf{p}}^z} \rangle \tag{3.32}$$

with its first and second derivatives $\Omega'(\lambda)$ and $\Omega''(\lambda)$ with respect to λ. The first derivative evaluated at $\lambda = 0$,

$$\frac{\mathrm{d}\Omega(\lambda)}{\mathrm{d}\lambda}\bigg|_{\lambda=0} = \langle \hat{S}_{\mathbf{p}}^z \rangle = M \tag{3.33}$$

is the magnetisation and thus the quantity that we try to determine. Later on, we will see that the solution for the expectation value $c^+(\lambda)$ from the Green function equation of motion and the spectral theorem can be written in the form

$$c^+(\lambda) = \Phi \cdot \Psi^+(\lambda), \tag{3.34}$$

where Φ depends among others on the magnetisation and temperature, but not on λ. The inhomogeneity term (3.23) can further be written as

$$\Psi^+(\lambda) = S\,(S+1)\,(\mathrm{e}^{-\lambda} - 1)\,\Omega(\lambda) + (\mathrm{e}^{-\lambda} + 1)\,\Omega'(\lambda) - (\mathrm{e}^{-\lambda} - 1)\,\Omega''(\lambda) \tag{3.35}$$

by using the notation with $\Omega(\lambda)$. Combining the above expressions for the expectation value $c^+(\lambda)$ and rearranging terms, we find the differential equation

$$\Omega''(\lambda) + \frac{(1+\Phi)\,\mathrm{e}^{\lambda} + \Phi}{(1+\Phi)\,\mathrm{e}^{\lambda} - \Phi}\Omega'(\lambda) - S\,(S+1)\,\Omega(\lambda) = 0 \tag{3.36}$$

To solve this differential equation, the boundary conditions

$$\Omega(0) = 1 \tag{3.37a}$$

$$\prod_{r=-S}^{+S}\left(\frac{\mathrm{d}}{\mathrm{d}\lambda} - r\right)\Omega(\lambda)\bigg|_{\lambda=0} = 0 \tag{3.37b}$$

should be used. The first immediately follows from the definition of $\Omega(\lambda)$. The second is obtained by taking the average of the operator identity

$$\prod_{r=-S}^{+S}(\hat{S}_{\mathbf{p}}^z - r) = 0, \tag{3.38}$$

where r can take on integer or half-integer values depending on S.

A step-by-step solution of the differential equation with its boundary conditions is given in appendix B and results through relation (3.33) in the expression [91]

$$M = \frac{(S - \Phi)\,(1+\Phi)^{2S+1} + (S + \Phi + 1)\,\Phi^{2S+1}}{(1+\Phi)^{2S+1} - \Phi^{2S+1}} \tag{3.39}$$

for the magnetisation in a system with spin $S \geqslant 1/2$. We now still need to find the factor Φ, which we will do by determining $c^+(\lambda)$ from its corresponding Green function.

3.3   Results for extended Heisenberg model

From here on, the calculations are not valid for arbitrary interactions anymore. They are specific for the extended Heisenberg model as specified in Sec. 3.1. We can now continue the calculation of the Green functions from the vector equation of motion. For our purposes here, only having an applied field and an anisotropic exchange interaction, we may simplify these results. Because the applied field will always be in the xz-plane, we can use $B^\pm = B^x/2$. Moreover, we already know from Eq. (3.8b) that the exchange tensor components $J_{\mathbf{ld}}^{++} = J_{\mathbf{ld}}^{--}$ and $J_{\mathbf{ld}}^{+z} = J_{\mathbf{ld}}^{-z}$ are equal, and so are their Fourier transforms. The block matrices then become

$$\mathbf{\Gamma}^{\alpha\beta}(\mathbf{k}) = \begin{bmatrix} \Gamma^{\alpha\beta,++}(\mathbf{k}) & -\Gamma^{\alpha\beta,-+}(\mathbf{k}) & \Gamma^{\alpha\beta,+z}(\mathbf{k}) \\ \Gamma^{\alpha\beta,-+}(\mathbf{k}) & -\Gamma^{\alpha\beta,++}(\mathbf{k}) & -\Gamma^{\alpha\beta,+z}(\mathbf{k}) \\ \Gamma^{\alpha\beta,z+} & -\Gamma^{\alpha\beta,z+} & 0 \end{bmatrix}. \tag{3.40}$$

with components

$$\Gamma^{\alpha\beta,++}(\mathbf{k}) = -\Gamma^{\alpha\beta,--}(\mathbf{k}) = \left[g_e \mu_B B^z + M J_\alpha^{zz}(0) \right] \delta_{\alpha\beta} - M J_{\beta\alpha}^{+-}(\mathbf{k}) \tag{3.41a}$$

$$\Gamma^{\alpha\beta,-+}(\mathbf{k}) = -\Gamma^{\alpha\beta,+-}(\mathbf{k}) = 2 M J_{\beta\alpha}^{++}(\mathbf{k}) \tag{3.41b}$$

$$\Gamma^{\alpha\beta,+z}(\mathbf{k}) = -\Gamma^{\alpha\beta,-z}(\mathbf{k}) = -\left[g_e \mu_B B^x + M J_\alpha^{+z}(0) \right] \delta_{\alpha\beta} - M J_{\beta\alpha}^{+z}(\mathbf{k}) \tag{3.41c}$$

$$\Gamma^{\alpha\beta,z+} = -\Gamma^{\alpha\beta,z-} = -\left[g_e \mu_B B^x + M J_\alpha^{+z}(0) \right] \delta_{\alpha\beta}/2 \tag{3.41d}$$

$$\Gamma^{\alpha\beta,zz}(\mathbf{k}) = 0. \tag{3.41e}$$

With this simplification, one can directly check that for each sublattice α, there is a vanishing eigenvalue with corresponding left eigenvector

$$\mathbf{L}_{\mathbb{0}}^\alpha = \begin{bmatrix} \cdots & \mathbf{L}_{\mathbb{0}}^{\alpha\beta} & \mathbf{L}_{\mathbb{0}}^{\alpha\alpha} & \mathbf{L}_{\mathbb{0}}^{\alpha\gamma} & \cdots \end{bmatrix} \tag{3.42a}$$

which is built from the sub-blocks

$$\mathbf{L}_{\mathbb{0}}^{\alpha\beta} = \begin{bmatrix} -\Gamma^{\alpha\beta,z+}, & -\Gamma^{\alpha\beta,z+}, & \Gamma^{\alpha\beta,++}(\mathbf{k}) + \Gamma^{\alpha\beta,-+}(\mathbf{k}) \end{bmatrix}. \tag{3.42b}$$

Since the equation of motion's coefficient matrix has a null-space of size equal to the number of sublattices, there are as many regularity conditions (2.130) that need to be satisfied. For each sublattice α, the corresponding zero left eigenvector $\mathbf{L}_{\mathbb{0}}^\alpha$ and the inhomogeneity vector $\mathbf{\Psi}$, cf. Eq. (3.25), yield

$$\begin{aligned} 0 &= \mathbf{L}_{\mathbb{0}}^\alpha(\mathbf{k}) \cdot \mathbf{\Psi} \\ &= -\sum_\beta \Gamma^{\alpha\beta,z+} \Psi^+(\lambda) \\ &= -\Gamma^{\alpha\alpha,z+} \Psi^+(\lambda) \end{aligned} \tag{3.43}$$

in the equation of the regularity condition. Since the inhomogeneity term $\Psi^+(\lambda)$ is not identical zero, the above condition becomes $\Gamma^{\alpha\alpha,z+} = 0$, which is more explicitly

$$g_{\mathrm{e}}\mu_{\mathrm{B}}B^x = -MJ_\alpha^{+z}(0) = M\sin 2\theta \sum_{\mathbf{l}} J_{\mathbf{lp}}\Delta_{\mathbf{lp}}, \quad \mathbf{p} \in \alpha. \qquad (3.44)$$

The sum is over all atoms in every sublattice.

The regularity condition relates the magnetisation angle θ with the magnetisation magnitude M (which is determined by Eq. (3.39)) for given applied fields, exchange interactions and lattice structures. That is why we call it the angular condition. We will discuss the specific relationship later on. Here, one should note that the regularity conditions originating from the different sublattices only differ through the reference point of the summation. This summation itself does not depend on M nor θ. The regularity conditions can thus only be satisfied consistently if the atomic lattice and the exchange interaction between the atoms have sufficient symmetries, such that the sum is independent of the reference point's sublattice. This will most often be the case. If not sufficient symmetry is present in the problem, the magnetisation magnitude and angle will not be the same on each sublattice. In that case, the regularity conditions would relate those sublattice-dependent magnitudes and angles.

If the regularity condition is satisfied, the third row in $\mathbf{\Gamma}^{\alpha\beta}(\mathbf{k})$ consists of all-zeroes. Consequently, every third row in the overall coefficient matrix $\mathbf{\Gamma}(\mathbf{k})$ only contains zeroes. This renders it particular straightforward to find the solution $G^{\alpha,z}(\mathbf{k}) = 0$ for the z-component of every sublattice α to the equation of motion (3.24). Since those components vanish identically, we can eliminate every third row and column of $\mathbf{\Gamma}(\mathbf{k})$, $\mathbf{G}(\mathbf{k})$ and $\mathbf{\Psi}(\mathbf{k})$ in the vector equation of motion (3.24). The block matrices forming $\mathbf{\Gamma}(\mathbf{k})$ are then

$$\mathbf{\Gamma}^{\alpha\beta}(\mathbf{k}) = \begin{bmatrix} \Gamma^{\alpha\beta,++}(\mathbf{k}) & -\Gamma^{\alpha\beta,-+}(\mathbf{k}) \\ \Gamma^{\alpha\beta,-+}(\mathbf{k}) & -\Gamma^{\alpha\beta,++}(\mathbf{k}) \end{bmatrix}. \qquad (3.45)$$

To make further progress, we limit the calculations further to having only two atomic sublattices, A and B. It is certainly possible to repeat a similar calculation for crystals with more atoms in the atomic basis. Further, we make a few reasonable assumptions on the form of the exchange interaction:

- We assume that the exchange strength $J_{\mathbf{lp}} = J_{\mathbf{pl}}$ and anisotropy $\Delta_{\mathbf{lp}} = \Delta_{\mathbf{pl}}$ are symmetric. This is a natural consequence of the exchange interaction being an interaction between two atoms, without preferential reference to one or the other.

- We assume that the exchange strength $J_{\mathbf{lp}}$ and anisotropy $\Delta_{\mathbf{lp}}$ with $\mathbf{l}, \mathbf{p} \in A$ are equal to those with $\mathbf{l}, \mathbf{p} \in B$. This assumption holds in general, because the exchange interaction typically only depends on the distance between the lattice points under consideration.

Under these assumptions, one can check from Eq. (3.18) that $J_{\beta\alpha}^{\tau\upsilon}(\mathbf{k}) = \overline{J_{\alpha\beta}^{\tau\upsilon}}(\mathbf{k})$ and $J_{\mathrm{AA}}^{\tau\upsilon}(\mathbf{k}) = J_{\mathrm{BB}}^{\tau\upsilon}(\mathbf{k})$. This also guarantees a single solution of θ for a given M from the regularity condition.

With only two sublattices and these assumptions, the coefficient matrix $\boldsymbol{\Gamma}$ reduces to having the form

$$\boldsymbol{\Gamma} = MJ_{\mathrm{tot}} \begin{bmatrix} a & -h & f & -g \\ h & -a & g & -f \\ \overline{f} & -\overline{g} & a & -h \\ \overline{g} & -\overline{f} & h & -a \end{bmatrix} \tag{3.46a}$$

with the shorthands

$$a = \Gamma^{\mathrm{AA},++}(\mathbf{k})/(MJ_{\mathrm{tot}}) \tag{3.46b}$$

$$h = \Gamma^{\mathrm{AA},-+}(\mathbf{k})/(MJ_{\mathrm{tot}}) \tag{3.46c}$$

$$f = \Gamma^{\mathrm{AB},++}(\mathbf{k})/(MJ_{\mathrm{tot}}) = f_{\mathrm{R}} + \mathrm{i}f_{\mathrm{I}} \tag{3.46d}$$

$$g = \Gamma^{\mathrm{AB},-+}(\mathbf{k})/(MJ_{\mathrm{tot}}) = g_{\mathrm{R}} + \mathrm{i}g_{\mathrm{I}}, \tag{3.46e}$$

where $a, h, f_{\mathrm{R}}, f_{\mathrm{I}}, g_{\mathrm{R}}$ and g_{I} are all real values. The quantity $J_{\mathrm{tot}} = \sum_n z_n J_n$ is introduced as a measure for the total exchange strength. The four eigenvalues of the coefficient matrix $\boldsymbol{\Gamma}$ are

$$\omega_{\oplus\pm} = \oplus MJ_{\mathrm{tot}} \sqrt{a^2 + f_{\mathrm{R}}^2 + f_{\mathrm{I}}^2 - (h^2 + g_{\mathrm{R}}^2 + g_{\mathrm{I}}^2) \pm 2\sqrt{F}} \tag{3.47}$$

with

$$F = a^2 \left(f_{\mathrm{R}}^2 + f_{\mathrm{I}}^2\right) - 2ah\left(f_{\mathrm{R}}g_{\mathrm{R}} + f_{\mathrm{I}}g_{\mathrm{I}}\right) + h^2\left(g_{\mathrm{R}}^2 + g_{\mathrm{I}}^2\right) - \left(f_{\mathrm{R}}g_{\mathrm{I}} - f_{\mathrm{I}}g_{\mathrm{R}}\right)^2. \tag{3.48}$$

The circled $\oplus$ sign has the same meaning as a normal $\pm$ sign. Since the $\oplus$- and $\pm$-signs also function to label the four distinct eigenvalues, the circle was added to know which sign comes where in the equation. When the labelling itself is unimportant, we will often use the simpler notation $\omega_{\pm} = \oplus\omega_{\oplus\pm}$. For each eigenvalue, there is a corresponding left and right eigenvector

$$\mathbf{L}_{\oplus\pm} = \begin{bmatrix} L_{\oplus\pm}^{(1)}, & L_{\oplus\pm}^{(2)}, & L_{\oplus\pm}^{(3)}, & L_{\oplus\pm}^{(4)} \end{bmatrix} \text{ and } \mathbf{R}_{\oplus\pm} = \begin{bmatrix} R_{\oplus\pm}^{(1)} \\ R_{\oplus\pm}^{(2)} \\ R_{\oplus\pm}^{(3)} \\ R_{\oplus\pm}^{(4)} \end{bmatrix}, \tag{3.49}$$

which we choose such that the matrices

$$\mathbf{L} = \begin{bmatrix} \mathbf{L}_{\ominus-} \\ \mathbf{L}_{\oplus-} \\ \mathbf{L}_{\ominus+} \\ \mathbf{L}_{\oplus+} \end{bmatrix} \text{ and } \mathbf{R} = \begin{bmatrix} \mathbf{R}_{\ominus-}, & \mathbf{R}_{\oplus-}, & \mathbf{R}_{\ominus+}, & \mathbf{R}_{\oplus+} \end{bmatrix} \tag{3.50}$$

are orthonormal, $\mathbf{L} \cdot \mathbf{R} = \mathbf{R} \cdot \mathbf{L} = \mathbb{1}$, while they obviously transform the transformation matrix into its diagonal form through

$$\mathbf{L} \cdot \mathbf{\Gamma} \cdot \mathbf{R} = \Omega = \begin{bmatrix} \omega_{\ominus-} & 0 & 0 & 0 \\ 0 & \omega_{\oplus-} & 0 & 0 \\ 0 & 0 & \omega_{\ominus+} & 0 \\ 0 & 0 & 0 & \omega_{\oplus+} \end{bmatrix}. \tag{3.51}$$

Finally, we also define the vectors

$$\mathbf{L}^{(n)} = \begin{bmatrix} L_{\ominus-}^{(n)} \\ L_{\oplus-}^{(n)} \\ L_{\ominus+}^{(n)} \\ L_{\oplus+}^{(n)} \end{bmatrix} \text{ and } \mathbf{R}^{(n)} = \begin{bmatrix} R_{\ominus-}^{(n)}, & R_{\oplus-}^{(n)}, & R_{\ominus+}^{(n)}, & R_{\oplus+}^{(n)} \end{bmatrix} \tag{3.52}$$

containing the nth component of the eigenvectors. For the calculations later on, we only need to know the components

$$L_{\oplus\pm}^{(1)} = a\left(f_{\mathrm{R}}^2 + f_{\mathrm{I}}^2\right) - h\left(f_{\mathrm{R}}g_{\mathrm{R}} + f_{\mathrm{I}}g_{\mathrm{I}}\right) \pm \left(a + \frac{\omega_{\oplus\pm}}{MJ_{\text{tot}}}\right)\sqrt{F} \tag{3.53}$$

$$L_{\oplus\pm}^{(3)} = -\left(a + \frac{\omega_{\oplus\pm}}{MJ_{\text{tot}}}\right)(af_{\mathrm{R}} - hg_{\mathrm{R}}) \mp f_{\mathrm{R}}\sqrt{F} + g_{\mathrm{I}}\left(f_{\mathrm{R}}g_{\mathrm{I}} - f_{\mathrm{I}}g_{\mathrm{R}}\right) \tag{3.54}$$

$$+ \mathrm{i}\left\{-\left(a + \frac{\omega_{\oplus\pm}}{MJ_{\text{tot}}}\right)(af_{\mathrm{I}} - hg_{\mathrm{I}}) \mp f_{\mathrm{I}}\sqrt{F} - g_{\mathrm{R}}\left(f_{\mathrm{R}}g_{\mathrm{I}} - f_{\mathrm{I}}g_{\mathrm{R}}\right)\right\}$$

of the left eigenvectors. The corresponding components of the right eigenvectors turn out to be related as

$$R_{\oplus\pm}^{(n)} = \frac{MJ_{\text{tot}}\kappa_{\oplus\pm}\overline{L_{\oplus\pm}^{(n)}}}{\pm 4\sqrt{F}\omega_{\oplus\pm}}, \text{ where } \kappa_{\oplus\pm}^{-1} = L_{\oplus\pm}^{(1)}. \tag{3.55}$$

This immediately implies that $\kappa_{\oplus\pm}L_{\oplus\pm}^{(1)} = \kappa_{\oplus\pm}\overline{L_{\oplus\pm}^{(1)}} = 1$.

Using these eigenvectors, the Green function equation of motion transforms into

$$(\omega\mathbb{1} - \mathbf{\Omega})\,\boldsymbol{\mathcal{G}} = \frac{1}{2\pi}\mathbf{L}\boldsymbol{\Psi} \tag{3.56}$$

with $\boldsymbol{\mathcal{G}} = \mathbf{L} \cdot \mathbf{G}$, as we anticipated in Eq. (2.106b). We do not write any $\mathbf{k}$ dependence for conciseness. Since we eliminated the null-space of $\boldsymbol{\Gamma}$ beforehand, the solution of the equation of motion for the transformed Green functions is

$$
\boldsymbol{\mathcal{G}} = \begin{bmatrix} \mathcal{G}_{\ominus-} \\ \mathcal{G}_{\oplus-} \\ \mathcal{G}_{\ominus+} \\ \mathcal{G}_{\oplus+} \end{bmatrix} , \text{ with } \mathcal{G}_{\oplus\pm} = \frac{1}{2\pi} \frac{\mathbf{L}_{\oplus\pm} \cdot \boldsymbol{\Psi}}{\omega - \omega_{\oplus\pm}}.
\tag{3.57}
$$

With the appropriate spectral theorem, the corresponding transformed expectation values become

$$
\boldsymbol{\mathcal{C}} = \begin{bmatrix} \mathcal{C}^{\ominus-} \\ \mathcal{C}^{\oplus-} \\ \mathcal{C}^{\ominus+} \\ \mathcal{C}^{\oplus+} \end{bmatrix} , \text{ where } \mathcal{C}^{\oplus\pm} = \mathbf{L}_{\oplus\pm} \cdot \mathbf{C} = \nu_{\oplus\pm} \mathbf{L}_{\oplus\pm} \cdot \boldsymbol{\Psi}
\tag{3.58}
$$

with the Bose occupation numbers

$$
\nu_{\oplus\pm} = \frac{1}{e^{\beta\omega_{\oplus\pm}} - 1}.
\tag{3.59}
$$

The spatial Fourier transforms $\mathbf{C}$ of the original expectation values

$$
\mathbf{C_{pj}} = \begin{bmatrix} C_{\mathbf{pj}}^{\mathrm{A},+} \\ C_{\mathbf{pj}}^{\mathrm{A},-} \\ C_{\mathbf{pj}}^{\mathrm{B},+} \\ C_{\mathbf{pj}}^{\mathrm{B},-} \end{bmatrix} \text{ with } C_{\mathbf{pj}}^{\alpha,\tau} = \langle e^{\lambda \hat{\mathrm{S}}_{\mathbf{j}}^z} \hat{\mathrm{S}}_{\mathbf{j}}^- \hat{\mathrm{S}}_{\mathbf{p}}^\tau \rangle, \mathbf{p} \in \alpha
\tag{3.60}
$$

can be obtained as $\mathbf{C} = \mathbf{R}\boldsymbol{\mathcal{C}}$. We are particularly interested in the components $C^{\mathrm{A},+}$ or $C^{\mathrm{B},+}$ as these will lead us to finding the magnetisation.

Combining the chain of expressions above, we find (with $C^{\mathrm{A},+} = C^1$ and $C^{\mathrm{B},+} = C^3$)

$$
\begin{aligned}
C^n &= \mathbf{R}^{(n)}\boldsymbol{\mathcal{C}}, \qquad \text{n=1,3} \\
&= R_{\ominus-}^{(n)}\mathcal{C}^{\ominus-} + R_{\oplus-}^{(n)}\mathcal{C}^{\oplus-} + R_{\ominus+}^{(n)}\mathcal{C}^{\ominus+} + R_{\oplus+}^{(n)}\mathcal{C}^{\oplus+} \\
&= \big[R_{\ominus-}^{(n)}\nu_{\ominus-}\mathbf{L}_{\ominus-} + R_{\oplus-}^{(n)}\nu_{\oplus-}\mathbf{L}_{\oplus-} \\
&\quad + R_{\ominus+}^{(n)}\nu_{\ominus+}\mathbf{L}_{\ominus+} + R_{\oplus+}^{(n)}\nu_{\oplus+}\mathbf{L}_{\oplus+} \big] \cdot \boldsymbol{\Psi} \\
&= \big[R_{\ominus-}^{(n)}\nu_{\ominus-} (L_{\ominus-}^{(1)} + L_{\ominus-}^{(3)}) + R_{\oplus-}^{(n)}\nu_{\oplus-} (L_{\oplus-}^{(1)} + L_{\oplus-}^{(3)}) \\
&\quad + R_{\ominus+}^{(n)}\nu_{\ominus+} (L_{\ominus+}^{(1)} + L_{\ominus+}^{(3)}) + R_{\oplus+}^{(n)}\nu_{\oplus+} (L_{\oplus+}^{(1)} + L_{\oplus+}^{(3)}) \big] \, \Psi^+(\lambda) \\
&= \phi^{(n)}\Psi^+(\lambda).
\end{aligned}
\tag{3.61}
$$

The homogeneous expectation value in real space is then (2.103)

$$c^{(n)} = \frac{1}{v_b} \int_{\text{BZ}} C^n(\mathbf{k}) \, d\mathbf{k} = \Phi^{(n)} \cdot \Psi^+(\lambda), \text{ with } \Phi^{(n)} = \frac{1}{v_b} \int_{\text{BZ}} \phi^{(n)}(\mathbf{k}) \, d\mathbf{k}. \quad (3.62)$$

This already confirms the functional form of Eq. (3.34) that we assumed in our analysis for higher spin values. We now still need to determine $\Phi^{(n)}$ through $\phi^{(n)}$.

Filling in the expressions for the right eigenvector components, $\phi^{(n)}$ becomes

$$\phi^{(n)} = \frac{MJ_{\text{tot}}}{4\sqrt{F}} \left\{ \frac{1}{\omega_+} [\nu_{\oplus+} P_{\oplus+}^{(n)} - \nu_{\ominus+} P_{\ominus+}^{(n)}] - \frac{1}{\omega_-} [\nu_{\oplus-} P_{\oplus-}^{(n)} - \nu_{\ominus-} P_{\ominus-}^{(n)}] \right\} \quad (3.63)$$

with

$$P_{\oplus\pm}^{(n)} = \kappa_{\oplus\pm} \overline{L_{\oplus\pm}^{(n)}} \left(L_{\oplus\pm}^{(1)} + L_{\oplus\pm}^{(3)} \right). \quad (3.64)$$

Now we can use $ax - by = (a + b)(x - y)/2 + (a - b)(x + y)/2$ in both terms and then the relations

$$\nu_{\oplus\pm} + \nu_{\ominus\pm} = -1 \quad (3.65a)$$

$$\nu_{\oplus\pm} - \nu_{\ominus\pm} = \coth\left(\frac{1}{2}\beta\omega_\pm\right) \quad (3.65b)$$

to subsequently obtain

$$\phi^{(n)} = \frac{MJ_{\text{tot}}}{8\sqrt{F}} \left\{ \frac{P_{\oplus+}^{(n)} + P_{\ominus+}^{(n)}}{\omega_+} \coth\left(\frac{1}{2}\beta\omega_+\right) - \frac{P_{\oplus-}^{(n)} + P_{\ominus-}^{(n)}}{\omega_-} \coth\left(\frac{1}{2}\beta\omega_-\right) \right.$$
$$\left. + \frac{P_{\ominus+}^{(n)} - P_{\oplus+}^{(n)}}{\omega_+} - \frac{P_{\ominus-}^{(n)} - P_{\oplus-}^{(n)}}{\omega_-} \right\}. \quad (3.66)$$

Now, let's first focus on $n = 1$, for which the terms $P_{\oplus\pm}^{(1)}$ simplify to

$$P_{\oplus\pm}^{(1)} = L_{\oplus\pm}^{(1)} + L_{\oplus\pm}^{(3)}, \quad (3.67)$$

as $\kappa_{\oplus\pm} \overline{L_{\oplus\pm}^{(n)}} = 1$. A straightforward calculation gives

$$\phi = \frac{A_+}{\omega_+} \coth\left(\frac{1}{2}\beta\omega_+\right) - \frac{A_-}{\omega_-} \coth\left(\frac{1}{2}\beta\omega_-\right) - \frac{1}{2} \quad (3.68)$$

with

$$A_\pm = \frac{MJ_{\text{tot}}}{4\sqrt{F}} \left\{ (g_R + g_I)(f_R g_I - f_I g_R) \right.$$
$$\left. + (a - f_R - f_I)\left(\pm\sqrt{F} - a(f_R + f_I) + h(g_R + g_I)\right) \right\}. \quad (3.69)$$

Notice that we wrote ϕ instead of $\phi^{(1)}$, where ϕ is equal to $\phi^{(1)}$ modulus the addition and removal of terms with an odd number of factors of f_{I} or g_{I}. The factors f_{I} and g_{I} are odd in $\mathbf{k}$, while a, h, f_{R} and g_{R} are all even in $\mathbf{k}$, as can be directly corroborated from the Fourier transform (3.18) and all $J_{\mathbf{lp}}^{\tau \upsilon}$ being real. Therefore, terms with an odd number of factors f_{I} or g_{I} do not change Φ, which corresponds to the average value of ϕ in the first Brillouin zone. The same result for ϕ can equivalently be obtained by calculating $\phi^{(3)}$, which confirms that under the applied conditions, the magnetisation is the same on both the A and B sublattice.

In summary, the magnetisation M in the extended Heisenberg model is given by the expression (3.39) for larger spin values, with

$$\Phi = \frac{1}{v_b} \int\limits_{\mathrm{BZ}} \phi(\mathbf{k}) \, \mathrm{d}\mathbf{k}, \quad \phi = \frac{A_+}{\omega_+} \coth\left(\tfrac{1}{2}\beta\omega_+\right) - \frac{A_-}{\omega_-} \coth\left(\tfrac{1}{2}\beta\omega_-\right) - \frac{1}{2} \quad (3.70)$$

and

$$\begin{aligned}
A_\pm = \frac{M J_{\mathrm{tot}}}{4\sqrt{F}} &\left\{ (g_{\mathrm{R}} + g_{\mathrm{I}}) \left(f_{\mathrm{R}} g_{\mathrm{I}} - f_{\mathrm{I}} g_{\mathrm{R}} \right) \right. \\
&\left. + (a - f_{\mathrm{R}} - f_{\mathrm{I}}) \left(\pm\sqrt{F} - a \left(f_{\mathrm{R}} + f_{\mathrm{I}} \right) + h \left(g_{\mathrm{R}} + g_{\mathrm{I}} \right) \right) \right\}.
\end{aligned} \quad (3.71)$$

The dispersion relations for the system's excitations are

$$\omega_\pm = M J_{\mathrm{tot}} \sqrt{a^2 + f_{\mathrm{R}}^2 + f_{\mathrm{I}}^2 - (h^2 + g_{\mathrm{R}}^2 + g_{\mathrm{I}}^2) \pm 2\sqrt{F}} \quad (3.72)$$

with

$$F = a^2 \left(f_{\mathrm{R}}^2 + f_{\mathrm{I}}^2 \right) - 2ah \left(f_{\mathrm{R}} g_{\mathrm{R}} + f_{\mathrm{I}} g_{\mathrm{I}} \right) + h^2 \left(g_{\mathrm{R}}^2 + g_{\mathrm{I}}^2 \right) - \left(f_{\mathrm{R}} g_{\mathrm{I}} - f_{\mathrm{I}} g_{\mathrm{R}} \right)^2. \quad (3.73)$$

The angle of the magnetisation is related to its magnitude through the angular condition

$$g_{\mathrm{e}} \mu_{\mathrm{B}} B^x = M \sin 2\theta \sum_{\mathrm{l}} J_{\mathbf{lp}} \Delta_{\mathbf{lp}}, \quad \mathbf{p} \in \alpha. \quad (3.74)$$

The other quantities in use are

$$a = \Gamma^{\mathrm{AA},++}(\mathbf{k})/(M J_{\mathrm{tot}}) = b^z + \left(J_{\mathrm{A}}^{zz}(0) - J_{\mathrm{AA}}^{+-}(\mathbf{k}) \right)/J_{\mathrm{tot}} \quad (3.75\mathrm{a})$$

$$h = \Gamma^{\mathrm{AA},-+}(\mathbf{k})/(M J_{\mathrm{tot}}) = 2 J_{\mathrm{AA}}^{++}(\mathbf{k})/J_{\mathrm{tot}} \quad (3.75\mathrm{b})$$

$$f_{\mathrm{R}} = \mathrm{Re}\,\Gamma^{\mathrm{AB},++}(\mathbf{k})/(M J_{\mathrm{tot}}) = -\,\mathrm{Re}\, J_{\mathrm{BA}}^{+-}(\mathbf{k})/J_{\mathrm{tot}} \quad (3.75\mathrm{c})$$

$$f_{\mathrm{I}} = \mathrm{Im}\,\Gamma^{\mathrm{AB},++}(\mathbf{k})/(M J_{\mathrm{tot}}) = -\,\mathrm{Im}\, J_{\mathrm{BA}}^{+-}(\mathbf{k})/J_{\mathrm{tot}} \quad (3.75\mathrm{d})$$

$$g_{\mathrm{R}} = \mathrm{Re}\,\Gamma^{\mathrm{AB},-+}(\mathbf{k})/(M J_{\mathrm{tot}}) = 2\,\mathrm{Re}\, J_{\mathrm{BA}}^{++}(\mathbf{k})/J_{\mathrm{tot}} \quad (3.75\mathrm{e})$$

$$g_{\mathrm{I}} = \mathrm{Im}\,\Gamma^{\mathrm{AB},-+}(\mathbf{k})/(M J_{\mathrm{tot}}) = 2\,\mathrm{Im}\, J_{\mathrm{BA}}^{++}(\mathbf{k})/J_{\mathrm{tot}}. \quad (3.75\mathrm{f})$$

For later convenience, we introduced the normalised magnetic field (components)

$$b = \frac{g_e \mu_B B}{M J_{\text{tot}}} \text{ and } b^x = b \sin(\theta_B - \theta), b^z = b \cos(\theta_B - \theta). \tag{3.76}$$

From these very general expressions for the magnetisation, it is possible to deduce expressions for the Curie temperature. In the absence of a magnetic field, the angular condition (3.74) only allows the solution $\theta = 0$ and $\theta = \pi/2$. Which solution to choose depends on the overall anisotropy of the system: the former should be chosen if the anisotropy is out-of-plane, while the latter holds when there is in-plane anisotropy. From Eq. (3.39), it can be seen that when the magnetisation M vanishes, the value of Φ becomes arbitrarily large. Expansion of that equation in this regime leads to the relation

$$M = \frac{S(S+1)}{3}\frac{1}{\Phi}. \tag{3.77}$$

The expression (3.70) for ϕ can also be reduced in the regime relevant for the Curie temperature. When no magnetic field is present, the system's characteristic frequencies $\omega_\pm$ are linear in the magnetisation M. The expansion

$$\coth x \overset{x \to 0}{\approx} \frac{1}{x} + \frac{x}{3} - \cdots = \frac{1}{x} + \mathcal{O}(x) \tag{3.78}$$

can thus be used in the region of small magnetisation to write ϕ as

$$\phi = \frac{2}{\beta}\left(\frac{A_+}{\omega_+^2} - \frac{A_-}{\omega_-^2}\right) - \frac{1}{2} = \frac{1}{M}\frac{2}{\beta}\left(\frac{A_+/M}{\omega_+^2/M^2} - \frac{A_-/M}{\omega_-^2/M^2}\right). \tag{3.79}$$

In the second equality, all magnetisation dependence is in the first factor and we noticed that the last constant term is negligible when M becomes small. We can plug this into Eq. (3.77), eliminate a factor M and find for the Curie temperature

$$k_B T_C = \frac{S(S+1)}{3}\frac{1}{\Phi_C}, \tag{3.80a}$$

with

$$\Phi_C = \frac{1}{v_b}\int\limits_{\text{BZ}} \phi_C(\mathbf{k})\,\mathrm{d}\mathbf{k}, \quad \phi_C(\mathbf{k}) = 2\left(\frac{A_+/M}{\omega_+^2/M^2} - \frac{A_-/M}{\omega_-^2/M^2}\right). \tag{3.80b}$$

This formula for the Curie temperature looks rather complex, especially considering the various substitutions that still need to be made. However, it is important to stress that its complexity is for a large part related to its generality. It is valid for any lattice type with one or two atoms in the atomic basis, with any spatial dimensionality and with a general exchange interaction. The latter can be anisotropic in spin-space and can be taken into account for as many nearest neighbours as desired. The interaction does not even need to be of exchange type, it just needs to satisfy a few conditions that we specified just below Eq. (3.45).

3.4   Cubic materials

In the previous section we ended up with complex-looking, but very generally applicable results. In this and the following section, we will demonstrate the usefulness of those formulas and analyse the results. This section specifically focuses on materials with cubic lattice structures and exchange interactions that act only on the nearest neighbours (NN). Focussing on NN-only interactions makes it possible to limit the size of the parameter space, while capturing the essential physics. The choice for studying cubic lattices is obvious: they can be described by a Bravais lattice, which considerably simplifies the formulae. Moreover, they allow for a direct comparison between different dimensions. Specifically, the magnetic properties of the two-dimensional square lattice will be compared extensively with the simple cubic lattice, its three-dimensional analogue. In 3D, we will also show results for the body- and face-centred cubic lattices, which describe common materials such as Ni, Co and Fe. We published most of these results in [120] and presented them at several conferences [121–128], but provide some additional analysis here.

3.4.1   Reduction of the formulae

Since each atom only interacts with its NN, the exchange interaction and its anisotropy have the functional form

$$J_{\mathbf{ld}} = J\zeta_{1,\mathbf{ld}} \text{ and } \Delta_{\mathbf{ld}} = \Delta\zeta_{1,\mathbf{ld}}, \tag{3.81}$$

where $\zeta_{1,\mathbf{ld}}$ is the nearest-neighbour function (see Sec. 2.1.3) for the considered lattice type. The spatial Fourier transforms of these functions are

$$J(\mathbf{k}) = J\zeta_1(\mathbf{k}) \text{ and } \Delta(\mathbf{k}) = \Delta\zeta_1(\mathbf{k}) \tag{3.82}$$

with $\zeta_1(\mathbf{k})$ given by $\zeta_1^{\mathrm{SC}}(\mathbf{k})$, $\zeta_1^{\mathrm{BCC}}(\mathbf{k})$, $\zeta_1^{\mathrm{FCC}}(\mathbf{k})$ or $\zeta_1^{\mathrm{SQ}}(\mathbf{k})$ as derived in Sec. 2.1.4. The relevant Fourier transformed exchange tensor components [cf. Eqs. (3.8b) and (3.18)] are

$$\begin{aligned}
J^{++}(\mathbf{k}) &= \frac{1}{2}\Delta \sin^2\theta J(\mathbf{k}) \\
J^{zz}(\mathbf{k}) &= [1 + \Delta\cos 2\theta]\, J(\mathbf{k}) \\
J^{+-}(\mathbf{k}) &= [1 - \Delta\cos^2\theta]\, J(\mathbf{k}),
\end{aligned} \tag{3.83}$$

where we denoted $J^{\tau\upsilon}(\mathbf{k}) = J_{\mathrm{AA}}^{\tau\upsilon}(\mathbf{k})$. There are no separate sublattices, so all quantities interlinking them vanish. Similar to the normalised magnetic field (3.76), we introduce the normalized exchange interaction

$$\eta(\mathbf{k}) = \frac{J(\mathbf{k})}{J_{\mathrm{tot}}} = \eta_1\zeta_1(\mathbf{k}), \text{ with } \eta_1 = \frac{J}{J_{\mathrm{tot}}} = \frac{1}{z}, \tag{3.84}$$

where the total exchange strength as felt by an atom is now $J_{\text{tot}} = J(0) = zJ$. The complete set of formulas to determine the magnetisation M reduces to substituting

$$\Phi = \frac{1}{v_b} \int\limits_{\text{BZ}} \phi(\mathbf{k}) \, d\mathbf{k}, \quad \phi = \frac{M J_{\text{tot}} a}{2\omega} \coth\left(\frac{1}{2}\beta\omega\right) - \frac{1}{2} \tag{3.85a}$$

in the expression (3.39) for larger spin values. Compared to Eq. (3.70), the terms related to ω_+ and ω_- contribute exactly the same, since $A_- = -A_+$ and $\omega_+ = \omega_-$. Indeed, since the crystals only have a single atom in their atomic basis, there is only a single dispersion relation

$$\omega = \omega_\pm = M J_{\text{tot}} \sqrt{a^2 - h^2}. \tag{3.85b}$$

The angle of the magnetisation can be determined from the angular condition

$$b^x = \Delta \sin 2\theta, \tag{3.85c}$$

where the magnetisation magnitude and exchange strength are hidden in the normalised magnetic field. The solution to this relation is visualised in Figure 3.3. The other quantities in use are

$$a = b^z + 1 + \Delta \cos 2\theta - \left[1 - \Delta \cos^2 \theta\right] \eta(\mathbf{k}) \tag{3.85d}$$

$$h = \Delta \sin^2 \theta \eta(\mathbf{k}). \tag{3.85e}$$

For an isotropic material with the magnetic field applied in the Z-direction and $S = 1/2$, this reduces further to the formulae obtained in section 2.3.3.

3.4.2 Curie temperature

Formula (3.80) to calculate the Curie temperature for cubic materials becomes

$$k_{\text{B}} T_{\text{C}} = \frac{S(S+1)}{3} \frac{1}{\Phi_{\text{C}}}, \tag{3.86a}$$

with

$$\Phi_{\text{C}} = \frac{1}{v_b} \int\limits_{\text{BZ}} \phi_{\text{C}}(\mathbf{k}) \, d\mathbf{k}, \quad \phi_{\text{C}}(\mathbf{k}) = \frac{1}{J_{\text{tot}}} \frac{a}{a^2 - h^2}. \tag{3.86b}$$

From these expressions, it is already possible to derive some properties of the Curie temperature. It scales with spin as $T_{\text{C}} \propto S(S+1)$, which is a general feature of quantum models and related to the fact that $\langle \hat{\mathbf{S}}^2 \rangle = S(S+1)$. This should be contrasted to classical models, where the T_{C} scales as S^2 (subsection 1.4.2). The
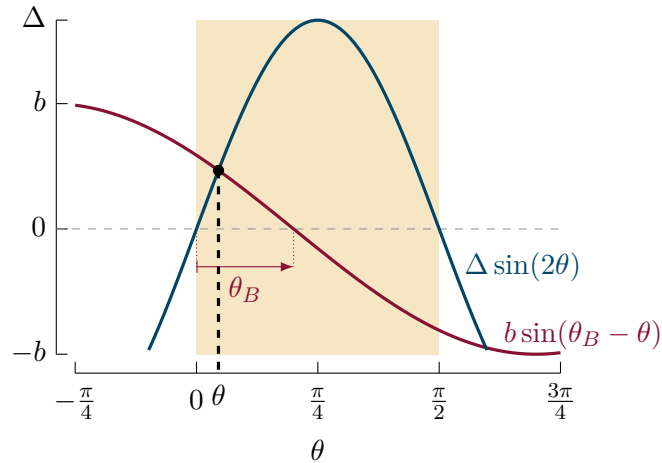
Figure 3.3 Graphical solution of the angular condition (3.85c), useful to get an intuition and to understand later results. The magnetisation angle θ is determined by the intersection of the two curves within the domain $[0, \pi/2]$ (yellow background). The normalised magnetic field b is always positive. When it is zero, either $M = 0$ and the magnetisation angle is not well-defined, or no external field is present and the correct solution ($\theta = 0$ or $\pi/2$) should be chosen in agreement with the anisotropy. This anisotropy Δ can be either positive or negative, which would turn the blue curve upside-down. There will always be a single intersection point in the given domain, except possibly when $\Delta > 0$ and $\theta_B = \pi/2$ or $\Delta < 0$ and $\theta_B = 0$. When there is a choice, $\theta = \theta_B$ is never the correct solution, as it leads to imaginary energies in the dispersion relation (3.85b). Note that the same solution for θ can be found by substituting $\Delta \to MzJ\Delta$ and $b \to g_\mathrm{e}\mu_\mathrm{B}B$. It is sometimes easier to reason using those substituted quantities.
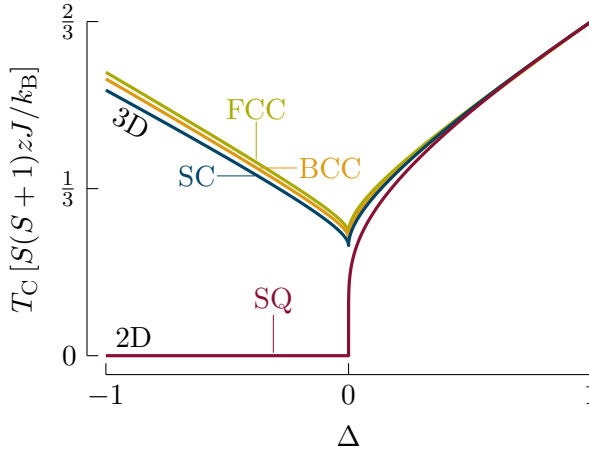
Figure 3.4 The Curie temperature as function of anisotropy for the different cubic lattice types. All three-dimensional lattices have the lowest T_C for the isotropic system, as all spins have the most freedom in this case. When the magnitude of the anisotropy increases, the spins have an inherent preference to align in one ($\Delta \geqslant 0$) or two ($\Delta < 0$) directions. The Curie temperature is relatively speaking larger for easy-axis materials as compared to easy-plane materials since the spins are already confined to a lower-dimensional space. While the curves for the SC, BCC and FCC lattice types are almost the same, their actual Curie temperatures vary due to their different coordination numbers z. The two-dimensional cubic, i.e. square, lattice type has a similar dependence as the three-dimensional types for positive anisotropies. However, as the anisotropy decreases and the material becomes isotropic, the Curie temperature vanishes. Also for negative anisotropies, no spontaneous magnetisation is possible in square lattices.

Curie temperature is also directly proportional to the total exchange strength J_{tot} and thus scales linearly with the strength of the exchange interaction J and the number of neighbours z that each atom interacts with.

Since an external field is absent, any spontaneous magnetisation must have an angle $\theta = 0$ or $\theta = \pi/2$ according to the angular condition (3.85c). The former is the solution for easy-axis anisotropic ($\Delta > 0$) materials, while the latter should be chosen for materials with easy-plane anisotropy ($\Delta < 0$). The corresponding integrands

$$\phi_C(\mathbf{k}) = \begin{cases} \dfrac{1}{J_{\text{tot}}} \dfrac{1}{1 + \Delta - (1 - \Delta)\,\eta(\mathbf{k})} & \Delta > 0 \\[4mm] \dfrac{1}{J_{\text{tot}}} \dfrac{1 - \Delta - \eta(\mathbf{k})}{(1 - \Delta - \eta(\mathbf{k}))^2 - (\Delta \eta(\mathbf{k}))^2} & \Delta < 0 \end{cases} \tag{3.87}$$

can be used to calculate the Curie temperature as function of the anisotropy for the different lattice structure (Figure 3.4). Apart from the dependencies of T_C

described above, it also strongly depends on the anisotropy—a larger magnitude of which leads to a higher Curie temperature—and dimensionality of the material. In contrast, it does not depend that much on the specific lattice type. Two dimensional materials need an easy-axis anisotropy to exhibit spontaneous magnetisation at non-zero temperatures. An easy-plane anisotropy is insufficient to get a non-zero Curie temperature. Such an anisotropy does not break the in-plane SO(2) symmetry, causing detrimental quantum fluctuations that destroy any in-plane spontaneous magnetisation at temperatures different from absolute zero. Our results are thus in agreement with the Mermin-Wagner theorem [4]. This can also be analysed analytically. Since each of the neighbour functions $\zeta_1(\mathbf{k})$ under consideration expands for small $\mathbf{k}$ as (where $\mathbf{k}$ is actually $a\mathbf{k}$)

$$\zeta_1(\mathbf{k}) \overset{\mathbf{k}\to 0}{\approx} z - \mathbf{k}^2 + \mathcal{O}(\mathbf{k}^4), \tag{3.88}$$

the behaviour of the integrand $\phi_\mathrm{C}(\mathbf{k})$ around the origin of the first Brillouin zone is

$$\phi_\mathrm{C}(\mathbf{k}) \overset{\mathbf{k}\to 0}{\approx} \begin{cases} \dfrac{1}{J_\mathrm{tot}} \dfrac{1}{2\Delta + (1-\Delta)\,\mathbf{k}^2/z} & \Delta > 0 \\[3mm] \dfrac{1}{J_\mathrm{tot}} \dfrac{z}{2\,(1-\Delta)\,\mathbf{k}^2} & \Delta < 0. \end{cases} \tag{3.89}$$

The integrand thus remains finite at $\mathbf{k} = 0$ for easy-axis anisotropies. On the other hand, the integrand is singular at the origin for easy-plane anisotropies. While this singularity is integrable in three-dimensions, it becomes a non-integrable singularity when the spatial dimensionality is reduced.

In the Ising limit ($\Delta = 1$), the Curie temperature can be calculated exactly from Eq. (3.86) to be $k_\mathrm{B}T_\mathrm{C} = 2S\,(S+1)\,zJ/3$, which agrees with the result for the quantum Ising model as obtained from molecular field theory (subsection 1.4.2, with exchange strength $(1+\Delta)\,J = 2J$). This is not entirely unexpected. The exchange Hamiltonian (3.8a) only contains the term with exchange tensor component J_ld^{zz} in this Ising limit. After performing the Tyablikov decoupling, this term only has a dispersionless contribution in the equation of motion (3.24). Most materials only have an anisotropy of the order of 0.01, where our theory outperforms the mean field approximation by including dispersive contributions. A more complicated decoupling scheme—either of first order, such as that of Callen [91], or of higher order, e.g., [129] or [130]—could lead to an improvement over the mean field approximation in these extreme cases.

3.4.3 Dispersion relation

The dispersion relation $\omega(\mathbf{k})$, Eq. (3.85b), gives the energy of a quasiparticle excitation with a given momentum $\mathbf{k}$. For the lattices with a single atomic basis

considered here, there is only a single branch to the dispersion relation. The energy spectra allow us to better understand the Curie temperature results.

Similar as for the Curie temperature, we consider a possible magnetisation that is out-of-plane ($\theta=0$) for easy-axis anisotropic systems and in-plane ($\theta=\pi/2$) for easy-plane anisotropic systems. To allow for a more extended discussion, we furthermore allow for a magnetic field applied parallel with that natural magnetisation direction (i.e. the applied field does not have an influence on the angle of magnetisation). The excitation spectrum then becomes

$$\omega(\mathbf{k}) = \begin{cases} MJ_{\text{tot}}\left|b^Z + 1 + \Delta - (1-\Delta)\,\eta(\mathbf{k})\right| & \Delta > 0 \\ MJ_{\text{tot}}\sqrt{\left(b^X + 1 - \Delta - \eta(\mathbf{k})\right)^2 - (\Delta\eta(\mathbf{k}))^2} & \Delta < 0. \end{cases} \tag{3.90}$$

Notice that the excitation spectrum gets renormalised by the magnetisation, which is itself temperature-dependent. This temperature dependence of the excitation spectrum is a distinguishing feature as compared to the mean field theory or results based on the Holstein-Primakoff approximation. The precise value of the magnetisation depends on the entire excitation spectrum, since all excited states are sampled with a certain temperature-dependent magnitude by the Bose distribution function. On the contrary, whether a non-zero magnetisation is possible at all depends only on the behaviour of the excitation spectrum around its minimum energy, that is around $\mathbf{k} = 0$. Around this centre of the first Brillouin zone (the $\mathbf{\Gamma}$ point), $\omega(\mathbf{k})$ can again be expanded using Eq. (3.88) to become

$$\omega(\mathbf{k}) \stackrel{\mathbf{k}\to 0}{\approx} \begin{cases} MJ_{\text{tot}}\left(b^Z + 2\Delta + (1-\Delta)\,\mathbf{k}^2/z\right) + \mathcal{O}(\mathbf{k}^4) & \Delta > 0 \\ MJ_{\text{tot}}\sqrt{b^X\left(b^X - 2\Delta\right) + 2\left(b^X - \Delta\left(1-\Delta\right)\right)\mathbf{k}^2/z} + \mathcal{O}(\mathbf{k}^4) & \Delta < 0. \end{cases} \tag{3.91}$$

The condition relevant to extract the Curie Temperature corresponds to zero magnetic field. The dispersion relation (3.90) for that case is shown along the high symmetry lines of the first Brillouin zone for the simple cubic and square lattices in Figure 3.5. A non-zero Curie temperature is only possible when the number of possible excitations is low, such that they do not destroy the magnetised ground state. For an easy-axis ferromagnet, the dispersion is parabolic around $\mathbf{\Gamma}$ with an excitation gap of size $2\Delta MJ_{\text{tot}}$. Due to the excitation gap, one may find a temperature low enough to suppress detrimental quantum fluctuations. The highest such temperature is the Curie temperature. For easy-plane ferromagnets, the situation is more complicated. The excitation spectrum in the absence of an external field around the $\mathbf{\Gamma}$ point is $\omega(\mathbf{k} \to 0) \approx 2\sqrt{|\Delta|\left(1 - |\Delta|\right)/z}|\mathbf{k}| + \mathcal{O}(\mathbf{k}^3)$, where the important feature is its linearity in $\mathbf{k}$. Since excitations with energies all the way down to zero are allowed, it is not always possible to find a non-zero temperature at which sufficient excitations are suppressed. The linearity
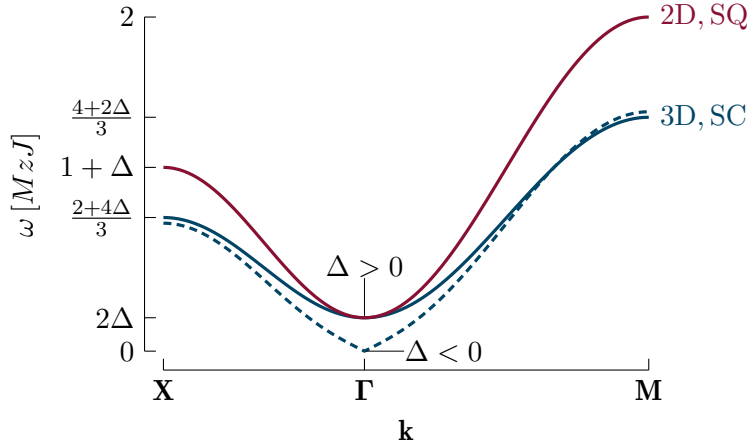
Figure 3.5 Dispersion relation $\omega(\mathbf{k})$ for the three-dimensional simple cubic (blue) and two-dimensional square (red) lattice types below their Curie temperature in the absence of an externally applied field. The dispersion is shown along the high symmetry lines in the $k^X k^Y$-plane of the first Brillouin zone. The centre of the first Brillouin zone is $\mathbf{\Gamma}$, while $\mathbf{X}$ and $\mathbf{M}$ are the middle of an edge and a corner in the $k^X k^Y$-plane, respectively. For easy-axis materials, the dispersion is parabolic around $\mathbf{\Gamma}$ with an energy gap. Easy-plane materials have a linear dispersion around their minimum. For this figure, $|\Delta| = 0.1$ was used.

of the dispersion relation makes it possible to find such a temperature in three dimensions, but not in two dimensions. This explains the distinct behaviour of two- and three-dimensional easy-plane Curie temperatures (Fig. 3.4).

When a magnetic field that assists the anisotropy is present, the situation changes. The energy gap of the easy-axis ferromagnet becomes $(b^Z + 2\Delta)\, M J_{\text{tot}}$. It grows linearly with the applied field. Notice that the energy gap never entirely vanishes when a field is applied. In contrast to the gap without applied field, this even holds when $M \to 0$ since $b^Z \propto 1/M$. The dispersion relation for easy-plane anisotropic materials with an in-plane magnetic field applied also becomes parabolic with an excitation gap of size $M J_{\text{tot}} \sqrt{b^X (b^X - 2\Delta)}$. It is thus sufficient to apply a small field to get a non-zero magnetisation in an in-plane anisotropic material.

3.4.4 Temperature and field dependence

The temperature dependence of the magnetisation is shown in Figure 3.6 in the absence of a magnetic field and in fields of varying strengths applied along the natural magnetisation direction. This natural magnetisation direction is the direction preferred by the anisotropy, i.e. out-of-plane when $\Delta \geqslant 0$ and in-plane when $\Delta < 0$. Such a field applied collinear with the natural magnetisation allows
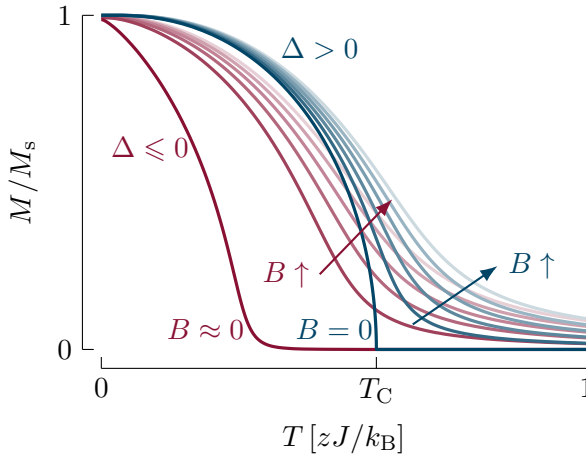
Figure 3.6 Normalised magnetisation as function of temperature for an easy-axis (blue) and easy-plane (red) two-dimensional material with square lattice structure and $S = 1/2$. The magnetisation behaviour of three-dimensional materials (either easy-axis or easy-plane) is qualitatively the same as the easy-axis curves that are shown here. All results were obtained for $|\Delta| = 0.1$, resulting in a Curie temperature of $0.57\, zJ/k_B$ for the easy-axis material (indicated T_C) and a vanishing Curie temperature for the easy-plane material. The magnetisation is calculated for several values (from light to dark: $g_e\mu_B B/zJ = 0.05, 0.04, 0.03, 0.02, 0.01$ and $B \simeq 0$) of a magnetic field that is applied parallel to the direction preferred by the anisotropy. The darkest curve for the easy-axis ferromagnet shows the spontaneous magnetisation curve ($B = 0$). Since spontaneous magnetisation is not possible in the easy-plane case, the darkest red curve corresponds to a very small magnetic field of $g_e\mu_B B/zJ = 10^{-5}$.

us to study the magnetisation magnitude separately, without the need to consider the magnetisation angle.

When a material's Curie temperature is zero (two-dimensional with no easy-axis anisotropy), the magnetisation vanishes by definition for all temperatures in the absence of an applied field. For all other situations with a Curie temperature that does not vanish, our results are qualitatively the same. In the absence of an external field, the magnetisation is reduced from its saturated value as soon as the temperature is raised above 0 K. This is the correct low-temperature behaviour, which includes magnons as predicted by Bloch [79] and Dyson [80]. As the temperature increases, the magnetisation drops further, vanishing exactly at the Curie temperature calculated before (Fig. 3.4). At temperatures above the T_C the magnetisation remains identically zero. When the collinear magnetic field is applied, there is a finite magnetisation at all temperatures. It only drops to zero in the limit of infinite temperature. The magnetic susceptibility is largest at the Curie temperature, as it should. The magnetisation increases further for

larger applied field strengths. For large magnetic fields, the magnetisation curve for two-dimensional easy-plane systems is very similar, although the magnetisation is typically lower (for a comparable anisotropy strength). The situation is different in the limit of a vanishing applied field. Since the Curie temperature vanishes, the steepest drop of magnetisation does not happen around T_C. Instead, it happens at a magnetic field-dependent temperature, which slowly decreases to zero as the magnetic field vanishes. This is similar to the observations of Gong et al. [9] in the nearly ideal bilayer isotropic Heisenberg ferromagnet $Cr_2Ge_2Te_6$.

It is insightful to look at the above results from a different perspective: Figure 3.7 shows the magnetisation as function of the applied collinear field for several temperatures. For all materials and temperatures, the magnetisation increases as the applied field increases, with the largest increase at $B = 0$. The precise behaviour in that low-field regime depends strongly on whether the temperature is above or below the Curie temperature. For $T < T_C$, the magnetisation increases gently with the applied field, starting from the spontaneous magnetisation at that specific temperature. At the Curie temperature, the magnetisation is zero to start with and the magnetic susceptibility is infinite, leading to a strong increase in magnetisation as soon as a field is applied. At even higher temperatures, the magnetisation becomes again less susceptible to the magnetic field, increasing more slowly with increasing field strength. Two-dimensional easy-plane materials are always in this last regime since they have a vanishing T_C.

A great benefit of the theoretical framework as presented in this thesis, is that it allows to calculate the direction of the magnetisation through the angle θ that it makes with the Z-axis. Indicative results of such calculations are shown in Figure 3.8. The magnetisation direction θ does not automatically coincide with the applied field angle θ_B because of the competition with the magnet's anisotropy Δ. For a given magnetisation magnitude M, this competition is fully described by the angular condition (3.85c), which was visualised in Figure 3.3. At the lowest temperatures, there is a competition between the relative strengths of the applied field B and the anisotropy $zJM\Delta$, which get weighted by the total exchange strength J_{tot} and the magnetisation M. The magnetisation decreases with increasing temperature. As the temperature raises, the influence of the applied field thus slowly takes the overhand, such that the (small) magnetisation approximately aligns with the applied field direction at high temperatures. This dynamics can also be understood in terms of fluctuations: within $\hat{H}_{\text{ex}}$, the thermal or quantum fluctuations of $\hat{S}$ grow quadratically and, thus, faster than the linear growth in $\hat{H}_B$. The magnetisation is always lower when the applied field angle deviates further from the natural magnetisation direction. It takes some effort from the applied field to turn the spins in its direction and there is less (or no) cooperation from the anisotropic exchange interaction.
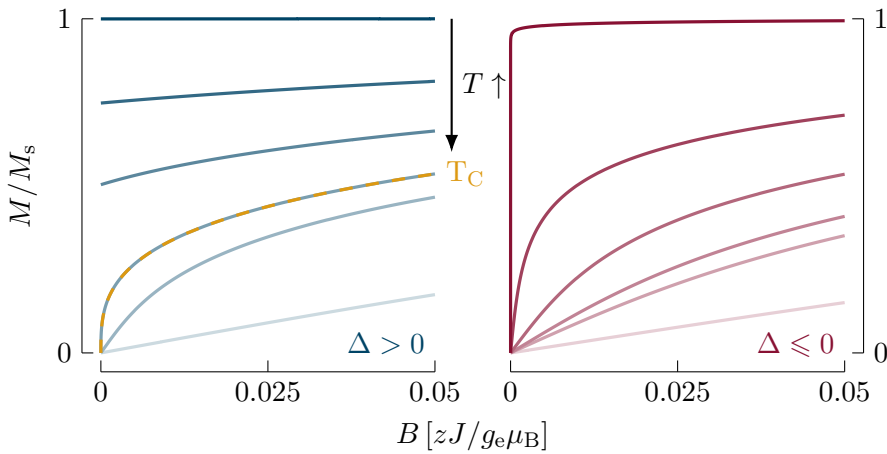
Figure 3.7 Normalised magnetisation as function of applied field for an easy-axis (blue, left panel) and easy-plane (red, right panel) two-dimensional material with square lattice structure, $|\Delta| = 0.1$ and $S = 1/2$. The two-dimensional easy-axis results are representative for three-dimensional materials regardless of their anisotropy. The results are shown for temperatures $k_{\mathrm{B}}T/zJ = 0.05, 0.4, 0.5, 0.57, 0.6, 0.8$ (top to bottom, dark to light), where $k_{\mathrm{B}}T/zJ = 0.57$ was chosen because it is the Curie temperature of the easy-axis material. There is a distinct behaviour in the low-field regime for temperatures above and below the Curie temperature. For the easy-axis material, all temperatures are above the vanishing Curie temperature.
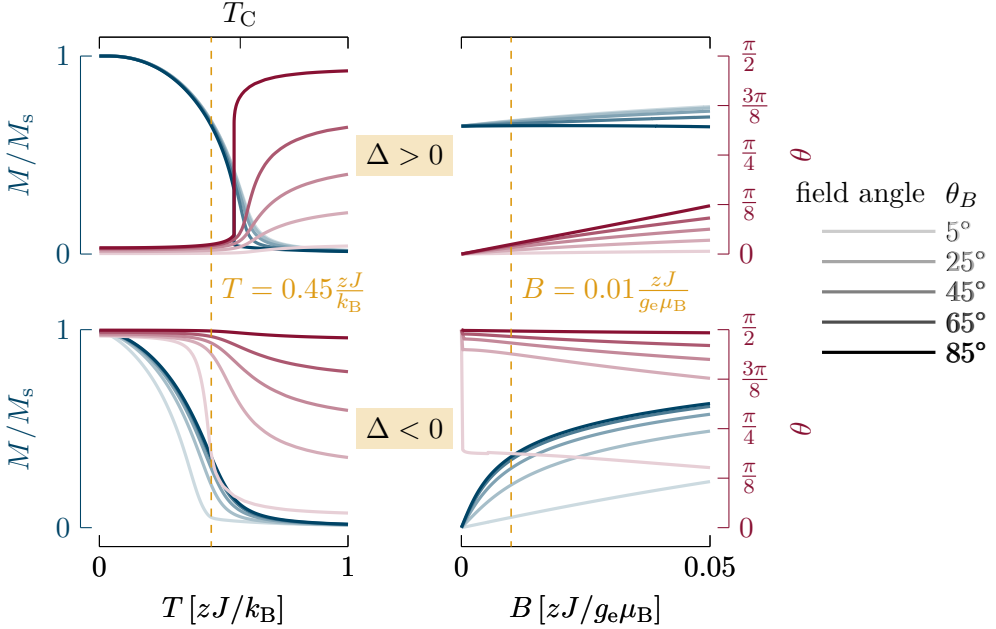
Figure 3.8 Magnetisation magnitude M (blue, left axis) and angle θ (red, right axis) as function of temperature (left panels) and applied field strength (right panels) at different angles θ_B. All results are for two-dimensional square-lattice materials. The panels at the top are for an easy-axis anisotropic material with $\Delta = 0.1$, while those at the bottom are for an easy-plane anisotropic material with $\Delta = -0.1$. Results for three-dimensional materials are in qualitative agreement with the top panels. The dashed yellow lines indicate the value at which the temperature and magnetic field were held constant when making the $M(B)$, respectively $M(T)$ plots. The same overall trends as for the collinear applied field can be seen. Notice that at low temperatures, the figures are in the regime $b \ll \Delta$, such that the magnetisation aligns predominantly along the direction preferred by the anisotropy as dictated by the angular condition (3.85c). As the temperature increases, the magnetisation reduces such that at high temperatures $b \gg \Delta$ and thus $\theta \approx \theta_B$. The magnetisation angle is slowly pulled in the direction of the applied field as this field becomes stronger. The susceptibility for the applied fields decreases as its angle with the natural magnetisation angle of the material increases. Some of the work done by the applied field goes into turning the magnetisation away from its preferred direction.
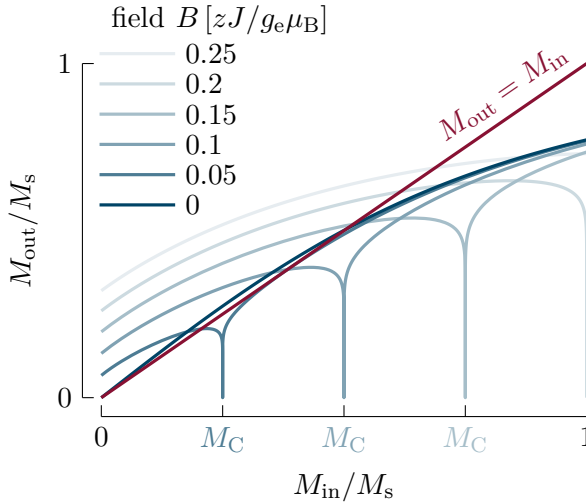
Figure 3.9 Visual representation of self-consistent solution to the set of equations (3.85) for an $S = 1$, easy-axis square (2D) material in a transverse field ($\theta_B = \pi/2$) at different strengths B. The temperature is $k_B T/zJ = 0.5$. The solution M_{out} to Eq. (3.39) when M_{in} is given as input, is shown by the blue lines. A self-consistent solution is achieved at the intersections of the red $M_{in} = M_{out}$ line with the blue lines. For some blue lines, there are multiple intersections due to the downward spike that occurs at $M_C = g_e \mu_B B/(2zJ\Delta)$. This situation is representative for other parameters, although the downward spike does not reach entirely to $M_{out} = 0$ in three dimensions.

3.4.5   Limitations of the theory

As shown above, the theory is applicable for anisotropic materials in magnetic fields applied at arbitrary angles. In this subsection, we demonstrate that accurate results cannot be guaranteed when the applied field is (almost) perpendicular to the natural magnetisation direction. We will call this direction, which is $\theta_B = 90°$ for $\Delta \geq 0$ and $\theta_B = 0°$ for $\Delta < 0$, the transverse direction. The attentive reader might have seen small signs of such inaccuracies in the $M(T)$ graphs at 5° deviation from the transverse direction in Figure 3.8.

To demonstrate the problem that occurs in the calculation, we evaluated Eq. (3.39) with M_{in} as the input magnetisation for the various substitutions (e.g., the angular condition (3.85c) and ϕ (3.85a)) and we call its result the output magnetisation M_{out}. The self-consistent solution M of the set of equations (3.85) should then be given by the point where the input and output magnetisation are the same $M_{in} = M_{out}$. It turns out that this condition can sometimes be satisfied by multiple magnetisations when the external field is applied transversely (Figure 3.9).

A natural question to ask is which of those multiple solutions is correct. However, the more pertinent question is whether any of those magnetisations is correct
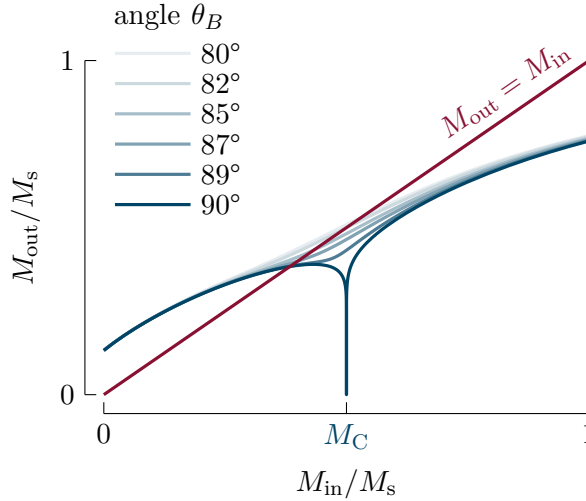
Figure 3.10 Visual representation of self-consistent solution for the same situation as in Figure 3.9. Now, however, the magnetic field strength is fixed at $B = 0.1zJ/g_e\mu_B$ while the applied field angle θ_B is changed such that it deviates slightly from the transverse $\theta_B = 90°$ direction. The downward spike quickly disappears with increasing deviations.

in this case. It turns out that the multiple solutions are caused by a downward spike around $M_{in} = M_C = g_e\mu_B B/(2zJ\Delta)$, where $M_{out}(M_C) = 0$. At this very point, the zero wave vector excitation energy $\omega(0) = 0$ vanishes. Moreover, it corresponds with the point where the solution to the angular condition (3.85c) switches between two regimes: $\theta = \arcsin\big(g_e\mu_B B/(2zJ\Delta M)\big)$ when $M > M_C$ and $\theta = \pi/2$ when $M \leq M_C$. The multiple solutions thus seem to be caused by a depression of $M_{out}(M_{in})$ in the cross-over regime of the dominating interaction— which changes from being the anisotropic exchange to being the Zeeman interaction. There is maximal frustration at this point in the system when the field is applied transversely. Together with the vanishing excitation energy, this might indicate that some other non-homogeneous excitations are present or a phase transition takes place. Some exotic type of ordering might even be present. The Tyablikov decoupling scheme, which neglects higher-order correlations between different spins, might not be suited well for such highly frustrated regimes. Moreover, a homogeneous magnetisation (direction) is not very plausible in those cases, either.

We emphasise that such a strong effect only occurs in a strictly transverse field. Figure 3.10 shows that the downward spike quickly disappears as soon as there is some deviation in the applied field angle θ_B. Even for transverse fields, good approximative solutions might still be obtained when magnetisations are far away from M_C.

This limitation was not yet observed at the time of publication of [120]. However, there we calculated $\langle \hat{S}_{\mathbf{p}}^{-} \hat{S}_{\mathbf{p}}^{-} \rangle$ concurrently with M from the Green function formalism for the spin $S = 1/2$ system under consideration. This quantity gave a good indication of the error in our calculations, since it should vanish in an exact solution. In agreement with the observations in this section, the error estimate could be seen to grow significantly in the region where $M = M_{\mathrm{C}}$, indicating less accurate results in that region.

3.5 Honeycomb and hexagonal materials

The cubic and square lattices studied in the previous section are ideal for comparing two- and three-dimensional systems. Considering only nearest-neighbour interactions further helped to reduce the parameter space. This allowed us to significantly reduce the complexity of the equations to solve and get some intuition for the various effects at play. However, many two-dimensional materials are not of square, but rather hexagonal or honeycomb lattice structure, the most famous one being graphene. Most two-dimensional ferromagnets, with the most famous group being the chromium trihalides such as CrI_3, $CrBr_3$ and $CrCl_3$, are also of hexagonal or honeycomb structure. Changing from square to hexagonal Bravais lattices will not impact the results qualitatively. This is similar to a change from simple cubic to body centred or face centred cubic. More significant is the change from the hexagonal lattice with a monoatomic basis to the honeycomb lattice with a multiatomic basis. Honeycomb materials have the additional feature that interactions with second and third nearest neighbours are still significant compared to the first-nearest-neighbour interaction. These further neighbours thus need to be accounted for, together with their exchange anisotropies. We will focus on the results that are qualitatively different from those for square lattices and on the comparison to available experimental data. First we write down the explicit equations for the honeycomb and hexagonal material, as we did in section 3.4.1 for cubic lattices.

3.5.1 Reduction of the formulae

We will first give the specific formulae for the honeycomb lattice structure. To find the equations for the hexagonal lattice structure, either use the expressions for square lattices from section 3.4.1 with Eq. (2.39) for the neighbour function $\zeta_1(\mathbf{k})$, or use the expressions that we derive below, with only second NN interaction.

In the honeycomb lattice structure, the exchange interaction is considered to be significant for all atoms that are in direct view of each other. This means that interactions up to third nearest neighbours are important (Figure 2.3). Due to symmetry, both the exchange strength and anisotropy are considered equal for

equally-distant spins. The exchange interactions and anisotropy are thus

$$J_{\mathbf{ld}} = J_1\zeta_{1,\mathbf{ld}} + J_2\zeta_{2,\mathbf{ld}} + J_3\zeta_{3,\mathbf{ld}} \text{ and } \Delta_{\mathbf{ld}} = \Delta_1\zeta_{1,\mathbf{ld}} + \Delta_2\zeta_{2,\mathbf{ld}} + \Delta_3\zeta_{3,\mathbf{ld}} \qquad (3.92)$$

with $\zeta_{n,\mathbf{ld}}$ the neighbour functions as defined in subsection 2.1.3 and where $\mathbf{l}$ and $\mathbf{p}$ can be either part of sublattice A or B. Since the anisotropy always appears in combination with the exchange strength, we also introduce the anisotropic exchange as

$$K_{\mathbf{ld}} = K_1\zeta_{1,\mathbf{ld}} + K_2\zeta_{2,\mathbf{ld}} + K_3\zeta_{3,\mathbf{ld}} \text{ with } K_n = \Delta_n J_n. \qquad (3.93)$$

For the equations that follow, it is more convenient to express the (anisotropic) exchange interaction in a normalised form with respect to the total exchange strength

$$J_{\text{tot}} = J(0) = z_1 J_1 + z_2 J_2 + z_3 J_3 = 3J_1 + 6J_2 + 3J_3, \qquad (3.94)$$

which is the Fourier transform $J(\mathbf{k})$ evaluated at $\mathbf{k} = 0$. The normalised (anisotropic) exchange strengths are then

$$\eta_n = \frac{J_n}{J_{\text{tot}}} \text{ and } \kappa_n = \frac{K_n}{J_{\text{tot}}} \qquad (3.95)$$

and the normalised (anisotropic) exchange functions

$$\eta_{\mathbf{ld}} = \eta_1\zeta_{1,\mathbf{ld}} + \eta_2\zeta_{2,\mathbf{ld}} + \eta_3\zeta_{3,\mathbf{ld}} \text{ and } \kappa_{\mathbf{ld}} = \kappa_1\zeta_{1,\mathbf{ld}} + \kappa_2\zeta_{2,\mathbf{ld}} + \kappa_3\zeta_{3,\mathbf{ld}}. \qquad (3.96)$$

Analogous to the total exchange strength, we also define the total weighted anisotropy

$$\delta = \kappa(0) = \frac{K(0)}{J_{\text{tot}}} = 3\eta_1\Delta_1 + 6\eta_2\Delta_2 + 3\eta_3\Delta_3. \qquad (3.97)$$

Notice that all (normalised) (anisotropic) exchange functions above are of the form

$$\mathcal{P}_{\mathbf{ld}} = \mathcal{P}_1\zeta_{1,\mathbf{ld}} + \mathcal{P}_2\zeta_{2,\mathbf{ld}} + \mathcal{P}_3\zeta_{3,\mathbf{ld}} \qquad (3.98)$$

where $\mathcal{P}$ can be either J, K, η or κ. The parts of these functions that act on the same (second NN) or different (first and third NN) sublattices appear distinctly in the equations that we derive. It is thus instructive to split the function in two parts: (i) the odd part $\mathcal{P}_{\text{O},\mathbf{ld}} = \mathcal{P}_1\zeta_{1,\mathbf{ld}} + \mathcal{P}_3\zeta_{3,\mathbf{ld}}$ contains only the contribution from interactions between distinct sublattices, and (ii) the even part $\mathcal{P}_{\text{E},\mathbf{ld}} = \mathcal{P}_2\zeta_{2,\mathbf{ld}}$ contains those interactions acting only on the same sublattice. The Fourier transform of this function with respect to an atom located in sublattice A is $\mathcal{P}(\mathbf{k}) = \mathcal{P}_{\text{E}}(\mathbf{k}) + \mathcal{P}_{\text{O}}(\mathbf{k})$, where

$$\mathcal{P}_{\text{E}}(\mathbf{k}) = \mathcal{P}_2\zeta_2(\mathbf{k}) \text{ and } \mathcal{P}_{\text{O}}(\mathbf{k}) = \mathcal{P}_1\zeta_1(\mathbf{k}) + \mathcal{P}_3\zeta_3(\mathbf{k}). \qquad (3.99)$$

We used the simplified notation $\zeta_n(\mathbf{k})$ to represent the Fourier transformed neighbour functions $\zeta_{n,\mathrm{A}}^{\mathrm{HON}}(\mathbf{k})$ of the honeycomb lattice, as given in section 2.1.4. The function $\mathcal{P}_{\mathrm{O}}(\mathbf{k})$ is complex-valued and taking its complex conjugate gives the Fourier transform with respect to an atom located in sublattice B. We introduce additional notation for the real and imaginary parts of $\mathcal{P}_{\mathrm{O}}(\mathbf{k})$:

$$
\begin{aligned}
\mathcal{P}_{\mathrm{R}}(\mathbf{k}) = \operatorname{Re} \mathcal{P}_{\mathrm{O}}(\mathbf{k}) = \mathcal{P}_1 \zeta_{1,\mathrm{R}}(\mathbf{k}) + \mathcal{P}_3 \zeta_{3,\mathrm{R}}(\mathbf{k}) \text{ and} \\
\mathcal{P}_{\mathrm{I}}(\mathbf{k}) = \operatorname{Im} \mathcal{P}_{\mathrm{O}}(\mathbf{k}) = \mathcal{P}_1 \zeta_{1,\mathrm{I}}(\mathbf{k}) + \mathcal{P}_3 \zeta_{3,\mathrm{I}}(\mathbf{k}),
\end{aligned}
\tag{3.100}
$$

where $\zeta_{n,\mathrm{R}}(\mathbf{k}) = \operatorname{Re} \zeta_n(\mathbf{k})$ and $\zeta_{n,\mathrm{I}}(\mathbf{k}) = \operatorname{Im} \zeta_n(\mathbf{k})$.

With all these definitions at hand, only some straightforward substitutions in the expressions derived in section 3.3 are left in obtaining our final solution. The Fourier transformed exchange tensor components [cf. Eqs. (3.8b) and (3.18)] that are necessary for Eq. (3.75) are

$$
J_{\mathrm{A}}^{zz}(0) = J_{\mathrm{tot}} + K(0) \cos 2\theta \tag{3.101a}
$$

$$
J_{\mathrm{AA}}^{+-}(\mathbf{k}) = J_{\mathrm{E}}(\mathbf{k}) - K_{\mathrm{E}}(\mathbf{k}) \cos^2 \theta \tag{3.101b}
$$

$$
J_{\mathrm{AA}}^{++}(\mathbf{k}) = \frac{1}{2} K_{\mathrm{E}}(\mathbf{k}) \sin^2 \theta \tag{3.101c}
$$

$$
\operatorname{Re} J_{\mathrm{BA}}^{+-}(\mathbf{k}) = J_{\mathrm{R}}(\mathbf{k}) - K_{\mathrm{R}}(\mathbf{k}) \cos^2 \theta \tag{3.101d}
$$

$$
\operatorname{Im} J_{\mathrm{BA}}^{+-}(\mathbf{k}) = J_{\mathrm{I}}(\mathbf{k}) - K_{\mathrm{I}}(\mathbf{k}) \cos^2 \theta \tag{3.101e}
$$

$$
\operatorname{Re} J_{\mathrm{BA}}^{++}(\mathbf{k}) = \frac{1}{2} K_{\mathrm{R}}(\mathbf{k}) \sin^2 \theta \tag{3.101f}
$$

$$
\operatorname{Im} J_{\mathrm{BA}}^{++}(\mathbf{k}) = \frac{1}{2} K_{\mathrm{I}}(\mathbf{k}) \sin^2 \theta. \tag{3.101g}
$$

Using the quantities

$$
f_\alpha = \eta_\alpha(\mathbf{k}) - \kappa_\alpha(\mathbf{k}) \cos^2 \theta, \quad \alpha \in \{\mathrm{R}, \mathrm{I}, \mathrm{E}\} \tag{3.102a}
$$

$$
g_\alpha = \kappa_\alpha(\mathbf{k}) \sin^2 \theta, \quad \alpha \in \{\mathrm{R}, \mathrm{I}, \mathrm{E}\} \tag{3.102b}
$$

$$
a = b^z + 1 + \delta \cos 2\theta - f_{\mathrm{E}}, \tag{3.102c}
$$

with the normalised magnetic field component b^z given by Eq. (3.76), the full solution can be written as follows. The magnetisation is still given by Eq. (3.39) for systems with spin $S \geqslant 1/2$, but now

$$
\Phi = \frac{1}{v_b} \int_{\mathrm{BZ}} \phi(\mathbf{k}) \, \mathrm{d}\mathbf{k}, \quad \phi = \frac{A_+}{\omega_+} \coth\left(\frac{1}{2} \beta \omega_+\right) - \frac{A_-}{\omega_-} \coth\left(\frac{1}{2} \beta \omega_-\right) - \frac{1}{2}. \tag{3.103}
$$

The amplitudes are

$$
\begin{aligned}
A_\pm = \frac{M J_{\mathrm{tot}}}{4\sqrt{F}} \Big\{ & (g_{\mathrm{R}} + g_{\mathrm{I}}) \left(f_{\mathrm{R}} g_{\mathrm{I}} - f_{\mathrm{I}} g_{\mathrm{R}}\right) \\
& + (a - f_{\mathrm{R}} - f_{\mathrm{I}}) \left(\pm\sqrt{F} - a \left(f_{\mathrm{R}} + f_{\mathrm{I}}\right) + h \left(g_{\mathrm{R}} + g_{\mathrm{I}}\right)\right) \Big\}
\end{aligned}
\tag{3.104}
$$

and

$$F = (af_\mathrm{R} - g_\mathrm{E}g_\mathrm{R})^2 + (af_\mathrm{I} - g_\mathrm{E}g_\mathrm{I})^2 - (f_\mathrm{R}g_\mathrm{I} - f_\mathrm{I}g_\mathrm{R})^2. \qquad (3.105)$$

The quasi-particle excitation energies are

$$\omega_\pm = MJ_\mathrm{tot}\sqrt{a^2 + f_\mathrm{R}^2 + f_\mathrm{I}^2 - (g_\mathrm{E}^2 + g_\mathrm{R}^2 + g_\mathrm{I}^2) \pm 2\sqrt{F}} \qquad (3.106)$$

and the angular condition is

$$b^x = \delta \sin 2\theta. \qquad (3.107)$$

The visual representation of this angular condition is the same as for the cubic material (Figure 3.3) after making the identification $\delta \to \Delta$.

3.5.2   Curie temperature

The equation (3.80) to calculate the Curie temperature of honeycomb materials becomes

$$k_\mathrm{B}T_\mathrm{C} = \frac{S(S+1)}{3}\frac{1}{\Phi_\mathrm{C}}, \ \text{ with } \Phi_\mathrm{C} = \frac{1}{v_b}\int\limits_\mathrm{BZ} \phi_\mathrm{C}(\mathbf{k})\,\mathrm{d}\mathbf{k}, \qquad (3.108a)$$

where now

$$\phi_\mathrm{C}(\mathbf{k}) = \frac{1}{J_\mathrm{tot}}\frac{a + \eta_\mathrm{R}(\mathbf{k}) - \kappa_\mathrm{R}(\mathbf{k})}{a^2 - (\eta_\mathrm{R}(\mathbf{k}) - \kappa_\mathrm{R}(\mathbf{k}))^2 - (\eta_\mathrm{I}(\mathbf{k}) - \kappa_\mathrm{I}(\mathbf{k}))^2}, \qquad (3.108b)$$

with $a = 1 + \delta - \eta_\mathrm{E}(\mathbf{k}) + \kappa_\mathrm{E}(\mathbf{k})$. This result was obtained by setting $\theta = 0$. The other possible choice, $\theta = \pi/2$, results in a vanishing Curie temperature due to the divergence of the two-dimensional integral in a similar fashion as for the square lattice types (see section 3.4.2). Equation (3.108) yields non-zero Curie temperatures for positive weighted anisotropies $\delta > 0$. The Curie temperature is zero when the weighted anisotropy is negative.

While there are too many parameters to show results for the entire parameter space, as we did in section 3.4.2, we can show results for some specific materials. Apart from being of experimental relevance, this also helps to understand the magnitude of the various quantities that are involved. Specifically, we will focus on CrI_3, $CrBr_3$ and $MnSe_2$ that we discussed thoroughly in [131]. We reproduce some of those results here. The parameters Δ_n and J_n for these materials were obtained through DFT by Cihan Bacaksiz (Table 3.1). Both CrI_3 and $CrBr_3$ have their magnetically active Cr atoms placed in a honeycomb structure (Figure 2.3), while $MnSe_2$ is represented by spins at the Mn atom positions arranged in a hexagonal lattice. The atomic spins of Cr and Mn are $S = 3/2$.

Table 3.1 Values for the parameters obtained from DFT [131]. The ab initio calculations to obtain these values were performed by Cihan Bacaksiz [132, 133]. Next to the calculated exchange strengths J_n and anisotropies Δ_n, also the total exchange strength J_{tot} and weighted anisotropy δ are given.

	exchange strength (meV)				anisotropy			
	J_1	J_2	J_3	J_{tot}	Δ_1	Δ_2	Δ_3	δ
CrI_3	3.06	0.92	-0.01	14.67	0.08	-0.05	-0.92	0.033
$CrBr_3$	2.72	0.41	-0.10	10.32	0.01	-0.02	0.05	0.0017
$MnSe_2$		5.34		32.04		0.01		0.01

The Curie temperatures obtained using the parameters of Table 3.1 are given in Table 3.2. Overall, the results agree well with the limited available experimental values and they are a significant improvement over the commonly used Ising models. The calculated Curie temperature for $CrBr_3$ is in quantitative agreement with experiment. Also, the high value of T_C for $MnSe_2$ is successfully reproduced after the report of room temperature (RT) spontaneous magnetisation by O'Hara et al. [17]. The small remaining deviation between the experiments and our theory might have several sources. There is only little experimental data available, making it difficult to judge the error in experimental results. For instance, an important source of deviations might be interactions between the two-dimensional sample and its substrate [134, 135]. For DFT results it is also well-known that they can vary significantly depending on the used method, which consequently also changes the predicted Curie temperatures. Additional terms in the Hamiltonian, such as a single-ion anisotropy term or dipolar interaction terms, might be needed to accurately describe the materials at hand. Finally, it is also known that finite-size effect might play a significant role. While only little information is available in this regard, a study by Imry [6] implies that finite-size effects might increase the predicted Curie temperature.

For materials with a honeycomb lattice structure it is important to account for interactions beyond first neighbours. To illustrate this, we show in Figure 3.11 the influence on the Curie temperature when scaling the second and third neighbour interaction strengths of $CrBr_3$ and CrI_3 relative to their values in Table 3.1. Turning those interactions on or off leads to significant changes in the predicted Curie temperatures. Particular combinations of farther neighbour interactions can even lead to a vanishing T_C if overall in-plane anisotropy or anti-ferromagnetic interactions take the overhand.

To allow other researchers to easily use our results, we released together with [131] a Python program, which can be found at reference [136]. This tool can be used to calculate Curie temperatures based on the formalism derived here, cf.

Table 3.2 Comparison of the Curie temperature T_C between our theoretical results (Green), the existing experimental data and other solution methods. The Monte Carlo Ising T_C results [131] are obtained by Cihan Bacaksiz with the exchange strengths J_n as given in Table 3.1 but with full anisotropy $\Delta_n = 1$. The Ising NN results are obtained with only nearest-neighbour interactions and Ising anisotropy, using the exact relations (1.36).

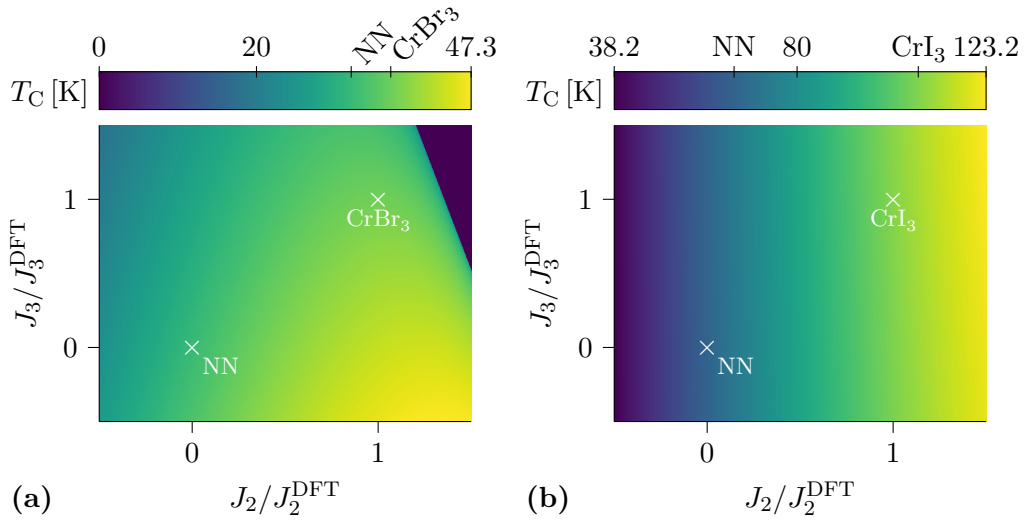|	T_C (K)			
	Green	Ising MC	Ising NN	experiment
CrI_3	108	241	118	45[8]
$CrBr_3$	37	157	108	34[15], 27[16]
$MnSe_2$	264	510	506	$\geqslant$RT[17]

Figure 3.11 The influence of farther neighbour interactions on the Curie temperature for **(a)** $CrBr_3$ and **(b)** CrI_3. The Curie temperature is shown for different combinations of the second (horizontal axis) and third (vertical axis) neighbour exchange strength. The results that correspond to having only nearest-neighbour interactions are indicated by NN. Those corresponding to the parameters of Table 3.1 are labeled by the chemical formula of the material. The apparent independence of T_C on J_3 in CrI_3 can be explained by its small value of J_3^{DFT} in absolute terms.

equation (3.108). It only requires the spin value S, the exchange strengths J_n and the corresponding anisotropies Δ_n up to third nearest neighbours. These parameters can be obtained through DFT calculations. The tool is very flexible in the sense that it only depends on these general parameters and not on their exact physical origin. Indeed, our results remain valid as long as the lattice keeps its honeycomb or hexagonal structure. We thus effectively reduced the problem of calculating Curie temperatures to the determination of DFT parameters. As such, the tool can be used for follow-up studies focusing on the engineering of materials with high T_C. One effect that could be studied is the influence of stress or strain on a sample, which can change the distance between the magnetically active atoms. On the one hand, this can alter the exchange strength, since the orbital overlap of these atoms changes. We expect that the exchange strength becomes stronger when the atoms are brought closer together, which would increase the Curie temperature. On the other hand, the modification of the interatomic spacing can lead to a deformation of the orbitals themselves, which can in turn influence both the exchange strengths and anisotropies. The latter effect might also take place when an external electric field is applied. We conclude that, together with DFT calculations, our tool can help both in the computational screening of new materials for potentially high Curie temperatures, and in the assessment of the optimal physical environment.

3.5.3 Excitation spectrum

The results for the Curie temperature can be understood to some the degree in terms of the quasi-particle excitation spectrum $\omega_\pm(\mathbf{k})$, Eq. (3.106), which is shown in Figure 3.12. As described in section 3.4.3, higher Curie temperatures are possible when less quasi-particles get excited. The non-zero Curie temperatures of the discussed materials can be explained by the fact that they all have a parabolic dispersion around their minimum with an excitation energy gap of $2M\delta J_{\text{tot}}$, for which the values can be found in Table 3.3. The gap for CrI_3 is larger than that for $CrBr_3$, resulting in its higher T_C. The lowest energy excitation of $MnSe_2$ is lower than that of CrI_3, so one would naively think that its Curie temperature would be larger. However, as we also discussed in section 3.4.3, the precise value of the T_C is not only determined by the excitation gap, but by the entire excitation spectrum. The steeper increasing dispersion of $MnSe_2$ can thus account for its higher Curie temperature.

Because the honeycomb lattice structure contains two atoms per Bravais lattice point, its quasi-particle dispersion has two branches. These Branches meet at the $\mathbf{K}$-points in Dirac cones—best known from the electronic band structure of graphene—that are typical for honeycomb lattice types [87]. It has been theorised that breaking the lattice inversion symmetry, for example when Dzyaloshinskii-
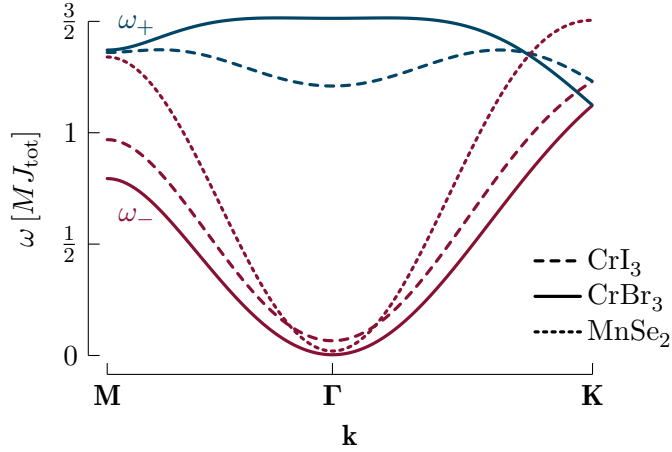
Figure 3.12 Quasi-particle excitation spectrum for CrI_3, $CrBr_3$ and $MnSe_2$ along the reciprocal cell's high symmetry lines (Figure 2.2) at a temperature below the Curie temperature in the absence of an external field. The spectrum is renormalised by temperature through the spontaneous magnetisation M. To compare the different materials, the excitation energies are shown in units of J_{tot}.

Table 3.3 Comparison of our theoretical results (Green) to the existing experimental data for excitation energies at the $\mathbf{\Gamma}$-point (assuming $M = M_s$). Both energies for the lower band $E_-(\mathbf{\Gamma})$ and higher band $E_+(\mathbf{\Gamma})$ are given when available.

	$E_-(\mathbf{\Gamma})$ (meV)		$E_+(\mathbf{\Gamma})$ (meV)	
	Green	experiment	Green	experiment
CrI_3	1.46	2.4[137]	26.6	19[137]
$CrBr_3$	0.052	0.1–0.2[2, 3]	23	15.5[3]
$MnSe_2$	0.96	-		

Moriya interactions are present, might allow for topological magnon edge states [137, 138] by opening up the Dirac cones.

For CrI_3 and $CrBr_3$ there are some experimental results available for the first and second excitation energy at the $\mathbf{\Gamma}$-point (Table 3.3). These are typically obtained from a bulk sample of the material with loosely coupled van der Waals layers [2, 3]. As such, they should only be considered to be approximations to the values of an atomically thin layer. Our results agree qualitatively with those experiments.

The results for these materials in the presence of a magnetic field (at arbitrary angle) are similar to those of the square materials studied in subsection 3.4.4. We refer to that section or the paper [131] for the details. To convert the dimensionless quantities into real physical units, one can use the Curie temperature T_C as reference point. For the applied field strengths, we note that $B = J_{\text{tot}}/g_e\mu_B$ corresponds to $127\,T$, $89\,T$ and $277\,T$ for CrI_3, $CrBr_3$ and $MnSe_2$, respectively. While these values might seem high, they are typically multiplied by a factor of the order 10^{-2} for the results shown in subsection 3.4.4, resulting in fields of the same order of magnitude as often found in experiments [9].

4 Dipolar interaction

In this chapter, we introduce the magnetic dipole-dipole interaction as an extension to the anisotropic Heisenberg Hamiltonian (3.1) that we discussed extensively in Chapter 3. The dipolar interaction is important with respect to the Mermin-Wagner theorem [4], since the corresponding spin-spin interactions are intrinsically anisotropic while having a longer range than exchange interactions. In view of the latter, a treatment with Monte Carlo is challenging. With our technique, this problem is circumvented since the long-range behaviour can be sufficiently described using a spatial Fourier transform. Nevertheless, the sums that arise are slowly converging and need to be treated by Ewald summations (see Section 4.2). Even more challenging, however, is the dipolar interaction's intrinsic anisotropy. The intuition and solution scheme that we built in Chapter 3 will be useful in this regard.

In contrast to exchange interactions, which give rise to a pure quantum mechanical and indirect spin-spin interaction of electrostatic nature, the dipole-dipole interaction is of direct magnetostatic nature and manifests itself even in a classical context. While it is always present in experiments, it is often completely neglected in literature related to spin systems. This is commonly justified by its pairwise energy contribution that is typically a factor 10 to 100 smaller compared to the exchange—or for that matter, Zeeman—interaction, while forgetting the fact that it is long-range and might change the system's anisotropy. When it is being taken into account, it is often replaced by its mean-field contribution. Only a few studies, generally using the Holstein-Primakoff approximation, account for the dipolar interaction to the same level of approximation as the other interactions [82, 139, 140]. All of those consider the magnetic field to be along a crystal direction. More crude approximations are sometimes justified because they allows calculating more properties or states of the system. De'Bell, MacIsaac and Whitehead [141] reviewed some of those considerations and results in more detail. Here, we will treat the dipolar interaction at the same level of approximation as the other terms in the Hamiltonian and again allow the magnetic field to be in arbitrary directions. While most of the calculations are valid for general lattice types, we limit ourselves here to simple cubic and square crystal structures. Parts of these results were presented in ref. [142].

4.1   Full Heisenberg model

The dipolar interaction is included by further extending the Hamiltonian (3.1) with the dipolar contribution $\hat{H}_D$. The full Hamiltonian is thus

$$\hat{H} = \hat{H}_B + \hat{H}_{ex} + \hat{H}_D, \tag{4.1}$$

with $\hat{H}_B$ and $\hat{H}_{ex}$ given by equation (3.3) respectively (3.2). Only nearest-neighbour interactions are considered and we write $J = J_1$ and $\Delta = \Delta_1$.

A magnetic moment $\mathbf{m}$ generates at a position $\mathbf{r}$ relative to itself a magnetic field [77]

$$\mathbf{B} = \frac{\mu_0}{4\pi} \left(3\frac{\mathbf{r}\left(\mathbf{m}\cdot\mathbf{r}\right)}{r^5} - \frac{\mathbf{m}}{r^3} \right), \tag{4.2}$$

where μ_0 is the vacuum permeability and $r = \|\mathbf{r}\|$. The magnetic moment of a spin $\mathbf{S}$ is $\mathbf{m} = g_e\mu_B\mathbf{S}$, such that it creates a field

$$\mathbf{B} = \frac{g_e\mu_B\mu_0}{4\pi} \left(3\frac{\mathbf{r}\left(\mathbf{S}\cdot\mathbf{r}\right)}{r^5} - \frac{\mathbf{S}}{r^3} \right). \tag{4.3}$$

The energy of a magnetic moment $\mathbf{m}$ in a field $\mathbf{B}$ is $-\mathbf{m}\cdot\mathbf{B}$. As such, the Hamiltonian of the newly added dipolar interaction is

$$\hat{H}_D = \frac{g}{2}\sum_{\mathbf{d},\mathbf{l}}\frac{1}{r_{\mathbf{dl}}^3}\hat{\mathbf{S}}_{\mathbf{d}}\cdot\hat{\mathbf{S}}_{\mathbf{l}} - \frac{3g}{2}\sum_{\mathbf{d},\mathbf{l}}\frac{1}{r_{\mathbf{dl}}^5}\left(\hat{\mathbf{S}}_{\mathbf{d}}\cdot\mathbf{r}_{\mathbf{dl}}\right)\left(\hat{\mathbf{S}}_{\mathbf{l}}\cdot\mathbf{r}_{\mathbf{dl}}\right), \tag{4.4}$$

with $\mathbf{r}_{\mathbf{dl}}$ the vector connecting lattice points $\mathbf{d}$ and $\mathbf{l}$, and $r_{\mathbf{dl}} = \|\mathbf{r}_{\mathbf{dl}}\|$ its length. The strength of the dipolar coupling is given by the parameter $g = (g_e\mu_B)^2\,\mu_0/4\pi = 2.147 \times 10^{-28}\,\text{meV}\cdot\text{m}^3 = 0.2147\,\text{meV}\cdot\text{nm}^3$, which should still be divided by a factor $r_{\mathbf{dl}}^3$ to get an actual energy. This is a small coupling constant as compared to exchange interactions, which can easily be several meV. Notice that the second term in Eq. (4.4) introduces an anisotropy by coupling the spin's direction in spin space to the lattice space direction connecting the two spins. The factors in this sum are explicitly given by $(\hat{\mathbf{S}}_{\mathbf{d}}\cdot\mathbf{r}_{\mathbf{dl}}) = \hat{S}_{\mathbf{d}}^X r_{\mathbf{dl}}^X + \hat{S}_{\mathbf{d}}^Y r_{\mathbf{dl}}^Y + \hat{S}_{\mathbf{d}}^Z r_{\mathbf{dl}}^Z$, where we used the components of $r_{\mathbf{dl}} = (r_{\mathbf{dl}}^X, r_{\mathbf{dl}}^Y, r_{\mathbf{dl}}^Z)$. It is implied that the sums do not include $\mathbf{d} = \mathbf{l}$.

To continue, the frame of reference is again changed from the crystallographic to the magnetisation coordinate system through transformation (3.4) (Figure 3.2). This assumes that the dipole-dipole interaction does not induce a rotation in the XY-plane. This turns out to be a reasonable assumption since we will find that it does not induce a rotation in the XZ-plane when there was none present yet due to the exchange anisotropy or the applied magnetic field in the absence of dipolar interaction. It is therefore reasonable to assume that the magnetic

dipole-dipole interaction does not induce a homogeneous magnetisation rotation in the XY-plane in the absence of other interactions inducing such a rotation. This, however, does not mean that such a rotation might not be introduced on the single-spin (inhomogeneous) level [141] that we do not intend to describe here. After the rotation to the magnetisation coordinate system, the Hamiltonian is

$$\hat{H}_D = -\frac{1}{2} \sum_{\mathbf{d},\mathbf{l}} \left[P_{\mathbf{ld}}^{++}\hat{S}_{\mathbf{d}}^{+}\hat{S}_{\mathbf{l}}^{+} + P_{\mathbf{ld}}^{--}\hat{S}_{\mathbf{d}}^{-}\hat{S}_{\mathbf{l}}^{-} + P_{\mathbf{ld}}^{zz}\hat{S}_{\mathbf{d}}^{z}\hat{S}_{\mathbf{l}}^{z} \right.$$
$$\left. + P_{\mathbf{ld}}^{+z}\hat{S}_{\mathbf{d}}^{+}\hat{S}_{\mathbf{l}}^{z} + P_{\mathbf{ld}}^{-z}\hat{S}_{\mathbf{d}}^{-}\hat{S}_{\mathbf{l}}^{z} + P_{\mathbf{ld}}^{+-}\hat{S}_{\mathbf{d}}^{+}\hat{S}_{\mathbf{l}}^{-} \right] , \tag{4.5a}$$

where

$$P_{\mathbf{ld}}^{++} = \overline{P_{\mathbf{ld}}^{--}} = +3g\frac{1}{r_{\mathbf{dl}}^{5}}P_{\mathbf{dl}}^{+}P_{\mathbf{dl}}^{+} \tag{4.5b}$$

$$P_{\mathbf{ld}}^{zz} = -g\frac{1}{r_{\mathbf{dl}}^{3}} + 3g\frac{1}{r_{\mathbf{dl}}^{5}}P_{\mathbf{dl}}^{z}P_{\mathbf{dl}}^{z} \tag{4.5c}$$

$$P_{\mathbf{ld}}^{+z} = \overline{P_{\mathbf{ld}}^{-z}} = +3g\frac{1}{r_{\mathbf{dl}}^{5}}2P_{\mathbf{dl}}^{+}P_{\mathbf{dl}}^{z} \tag{4.5d}$$

$$P_{\mathbf{ld}}^{+-} = -g\frac{1}{r_{\mathbf{dl}}^{3}} + 3g\frac{1}{r_{\mathbf{dl}}^{5}}2P_{\mathbf{dl}}^{+}P_{\mathbf{dl}}^{-} \tag{4.5e}$$

with

$$P_{\mathbf{dl}}^{+} = \overline{P_{\mathbf{dl}}^{-}} = \frac{1}{2}\left(r_{\mathbf{dl}}^{X}\cos\theta - \mathrm{i}r_{\mathbf{dl}}^{Y} - r_{\mathbf{dl}}^{Z}\sin\theta \right) \tag{4.5f}$$

$$P_{\mathbf{dl}}^{z} = \left(r_{\mathbf{dl}}^{X}\sin\theta + r_{\mathbf{dl}}^{Z}\cos\theta \right) . \tag{4.5g}$$

To obtain this result, we used the identity $P_{\mathbf{dl}}^{\alpha}P_{\mathbf{dl}}^{\beta} = P_{\mathbf{ld}}^{\alpha}P_{\mathbf{ld}}^{\beta}$. Notice that Eq. (4.5a) is identical in form to Eq. (3.8a) but now with dipolar tensor coefficients $P^{\alpha\beta}$ instead of the exchange tensor coefficients $J_{\mathbf{ld}}^{\alpha\beta}$. Since we did not use any specific properties of $J_{\mathbf{ld}}^{\alpha\beta}$ back in section 3.2 that do not apply here as well, we can directly reuse all the results from that section. Specifically, we use the same Green functions, commutator relations and Tyablikov decoupling approximation. Furthermore, we again perform a spatial Fourier transform, calculate the same inhomogeneity term and write the equation of motion in vectorised form. Since we are dealing only with simple cubic and square lattices here, it is sufficient to have a single atomic basis, such that the equation of motion consists of three coupled equations. The treatment of higher spin values is also identical. The Fourier-transformed dipolar tensor components are defined as

$$P^{\tau\upsilon}(\mathbf{k}) = \sum_{\mathbf{r_l}} \mathrm{e}^{\mathrm{i}\mathbf{k}\cdot\mathbf{r_{lp}}} P_{\mathbf{lp}}^{\tau\upsilon}, \quad \tau,\upsilon \in \{+,-,z\}. \tag{4.6}$$

Notice that the Fourier transforms of terms linear in r_{dl}^X, r_{dl}^Y or r_{dl}^Z vanish when evaluated at $\mathbf{k} = 0$ for two- and three-dimensional lattices with sufficient symmetry. Here, this implies that $\operatorname{Im} P^{++}(0) = 0$ and $\operatorname{Im} P^{+z}(0) = 0$. The coefficient matrix for the equation of motion is

$$\boldsymbol{\Gamma}(\mathbf{k}) = \begin{bmatrix} \Gamma^{++}(\mathbf{k}) & \Gamma^{+-}(\mathbf{k}) & \Gamma^{+z}(\mathbf{k}) \\ \Gamma^{-+}(\mathbf{k}) & \Gamma^{--}(\mathbf{k}) & \Gamma^{-z}(\mathbf{k}) \\ \Gamma^{z+}(\mathbf{k}) & \Gamma^{z-}(\mathbf{k}) & \Gamma^{zz}(\mathbf{k}) \end{bmatrix} = \begin{bmatrix} \Gamma^{++}(\mathbf{k}) & -\overline{\Gamma^{-+}(\mathbf{k})} & \Gamma^{+z}(\mathbf{k}) \\ \Gamma^{-+}(\mathbf{k}) & -\Gamma^{++}(\mathbf{k}) & -\overline{\Gamma^{+z}(\mathbf{k})} \\ \Gamma^{z+} & -\Gamma^{z+} & 0 \end{bmatrix}, \quad (4.7)$$

containing the elements

$$\Gamma^{++}(\mathbf{k}) = g_{\mathrm{e}}\mu_{\mathrm{B}}B^z + M\left[J^{zz}(0) - J^{+-}(\mathbf{k}) + P^{zz}(0) - P^{+-}(\mathbf{k}) \right] \tag{4.8a}$$

$$\Gamma^{+z}(\mathbf{k}) = -g_{\mathrm{e}}\mu_{\mathrm{B}}B^x - M\left[J^{-z}(0) + J^{-z}(\mathbf{k}) + P^{-z}(0) + P^{-z}(\mathbf{k}) \right] \tag{4.8b}$$

$$\Gamma^{-+}(\mathbf{k}) = 2M\left[J^{++}(\mathbf{k}) + P^{++}(\mathbf{k}) \right] \tag{4.8c}$$

$$\Gamma^{z+} = -\left(g_{\mathrm{e}}\mu_{\mathrm{B}}B^x + M\left[J^{+z}(0) + P^{+z}(0) \right] \right)/2. \tag{4.8d}$$

This resembles one of the diagonal block matrices in section 3.3, with the only structural difference being that $\Gamma^{+z}(\mathbf{k})$ and $\Gamma^{-+}(\mathbf{k})$ have an imaginary component for general $\mathbf{k}$ now. The determinant $\det(\boldsymbol{\Gamma}(\mathbf{k}))$ of the coefficient matrix is

$$-2\Gamma^{z+}\left[\operatorname{Im}\Gamma^{-+}(\mathbf{k})\operatorname{Re}\Gamma^{+z}(\mathbf{k}) + \left(\operatorname{Re}\Gamma^{-+}(\mathbf{k}) - \Gamma^{++}(\mathbf{k}) \right)\operatorname{Im}\Gamma^{+z}(\mathbf{k}) \right] \mathrm{i}. \tag{4.9}$$

Since proper excitation energies (eigenvalues of coefficient matrix) must be real, their product (i.e. the above determinant) must also be real. This can only be true for all $\mathbf{k}$ if $\Gamma^{z+} = 0$, which is the exact same condition as the regularity condition used in section 3.3. The angular condition is thus

$$g_{\mathrm{e}}\mu_{\mathrm{B}}B^x = -M\left[J^{+z}(0) + P^{+z}(0) \right], \tag{4.10a}$$

where

$$J^{+z}(0) = -\sin 2\theta \Delta J_{\mathrm{tot}} \tag{4.10b}$$

and

$$\begin{aligned} P^{+z}(0) &= 3g \sum_{\mathbf{r}_{\mathrm{l}}} \frac{1}{r_{\mathrm{dl}}^5}\left(r_{\mathrm{dl}}^X \cos\theta - \mathrm{i}r_{\mathrm{dl}}^Y - r_{\mathrm{dl}}^Z \sin\theta \right)\left(r_{\mathrm{dl}}^X \sin\theta + r_{\mathrm{dl}}^Z \cos\theta \right) \\ &= \frac{3g}{2} \sin 2\theta \sum_{\mathbf{r}_{\mathrm{l}}} \frac{r_{\mathrm{dl}}^X r_{\mathrm{dl}}^X - r_{\mathrm{dl}}^Z r_{\mathrm{dl}}^Z}{r_{\mathrm{dl}}^5}. \end{aligned} \tag{4.10c}$$

With the angular condition satisfied, the entire third row of the coefficient matrix $\boldsymbol{\Gamma}(\mathbf{k})$ vanishes. Therefore, $G^z(\mathbf{k}) = 0$ is a solution for the third component of the Green function vector $\mathbf{G}(\mathbf{k})$. For the remainder of the solution, this implies

that the third row and column of $\mathbf{\Gamma}(\mathbf{k})$, $\mathbf{G}(\mathbf{k})$ and $\mathbf{\Psi}(\mathbf{k})$ in the vector equation of motion (3.24) can be discarded. The remaining coefficient matrix is

$$\mathbf{\Gamma}(\mathbf{k}) = MJ_{\text{tot}} \begin{bmatrix} a & -h + \mathrm{i}p \\ h + \mathrm{i}p & -a \end{bmatrix}, \tag{4.11}$$

with the real-valued quantities

$$a = \Gamma^{++}(\mathbf{k})/(MJ_{\text{tot}}) \tag{4.12}$$
$$h = \operatorname{Re}\Gamma^{-+}(\mathbf{k})/(MJ_{\text{tot}}) \tag{4.13}$$
$$p = \operatorname{Im}\Gamma^{-+}(\mathbf{k})/(MJ_{\text{tot}}). \tag{4.14}$$

The eigenvalues are

$$\omega_{1,2}(\mathbf{k}) = \pm E, \text{ with } E = MJ_{\text{tot}}\sqrt{a^2 - h^2 - p^2} \tag{4.15}$$

and the corresponding left and right eigenvectors

$$\mathbf{L}_1 = MJ_{\text{tot}} \begin{bmatrix} a + E/(MJ_{\text{tot}}) & -h + \mathrm{i}p \end{bmatrix} \tag{4.16}$$
$$\mathbf{L}_2 = MJ_{\text{tot}} \begin{bmatrix} a - E/(MJ_{\text{tot}}) & -h + \mathrm{i}p \end{bmatrix} \tag{4.17}$$
$$\mathbf{R}_1 = \frac{1}{2\left(-h + p\mathrm{i}\right)E} \begin{bmatrix} -h + \mathrm{i}p \\ -a + E/(MJ_{\text{tot}}) \end{bmatrix} \tag{4.18}$$
$$\mathbf{R}_2 = \frac{1}{2\left(-h + p\mathrm{i}\right)E} \begin{bmatrix} h - \mathrm{i}p \\ a + E/(MJ_{\text{tot}}) \end{bmatrix}. \tag{4.19}$$

These eigenvectors can be combined into the matrices

$$\mathbf{L} = \begin{bmatrix} \mathbf{L}_1 \\ \mathbf{L}_2 \end{bmatrix} \text{ and } \mathbf{R} = \begin{bmatrix} \mathbf{R}_1 & \mathbf{R}_2 \end{bmatrix}, \tag{4.20}$$

which are orthonormal $\mathbf{L} \cdot \mathbf{R} = \mathbf{R} \cdot \mathbf{L} = \mathbb{1}$ and diagonalise the coefficient matrix as

$$\mathbf{L} \cdot \mathbf{\Gamma} \cdot \mathbf{R} = \mathbf{\Omega} = \begin{bmatrix} \omega_1 & 0 \\ 0 & \omega_2 \end{bmatrix}. \tag{4.21}$$

We define the diagonal matrix

$$\mathbf{\mathcal{E}} = \begin{bmatrix} \nu_1 & 0 \\ 0 & \nu_2 \end{bmatrix} \tag{4.22}$$

containing the Bose occupation numbers $\nu_{1,2} = (\mathrm{e}^{\beta\omega_{1,2}(\mathbf{k})} - 1)^{-1}$. We can now directly apply the solution presented in subsection 2.3.2 for the non-null space (the null space was eliminated through the angular condition). We find

$$\mathbf{C}(\mathbf{k}) = \mathbf{R}(\mathbf{k})\mathbf{\mathcal{E}}(\mathbf{k})\mathbf{L}(\mathbf{k})\mathbf{\Psi}(\mathbf{k}), \tag{4.23}$$

which has the first component

$$
\begin{aligned}
C^+(\mathbf{k}) &= \mathbf{R}^{(1)}(\mathbf{k})\boldsymbol{\mathcal{E}}(\mathbf{k})\mathbf{L}(\mathbf{k})\boldsymbol{\Psi}(\mathbf{k}) \\
&= \frac{1}{2E}\left[(\nu_1 - \nu_2)\,aMJ_{\text{tot}} + (\nu_1 + \nu_2)\,E\right]\Psi^+(\lambda) \\
&= \phi(\mathbf{k})\Psi^+(\lambda), \ \text{ with } \phi(\mathbf{k}) = \frac{MJ_{\text{tot}}a}{2E}\coth\!\left(\tfrac{1}{2}\beta E\right) - \frac{1}{2},
\end{aligned}
\tag{4.24}
$$

where we used relations similar to (3.65) to rewrite the sum and difference of the Bose occupation factors. Finally, using Eq. (2.103), the homogeneous expectation value in real space is

$$
c^+ = \frac{1}{v_b}\int_{\text{BZ}} C^+(\mathbf{k})\,\mathrm{d}\mathbf{k} = \Phi\Psi^+(\lambda), \ \text{ with } \Phi = \frac{1}{v_b}\int_{\text{BZ}} C^+(\mathbf{k})\,\mathrm{d}\mathbf{k}\,.
\tag{4.25}
$$

This equation is of the form of Eq. (3.34), such that we can use our solution for higher spin values as presented in subsection (3.2.4) to find the homogeneous magnetisation.

Altogether, the magnetisation in the presence of dipolar interaction is given by the expression (3.39) for larger spin values, where

$$
\Phi = \frac{1}{v_b}\int_{\text{BZ}}\phi(\mathbf{k})\,\mathrm{d}\mathbf{k}, \quad \phi = \frac{MJ_{\text{tot}}a}{2\omega}\coth\!\left(\tfrac{1}{2}\beta\omega\right) - \frac{1}{2}
\tag{4.26a}
$$

is to be substituted. So far, these equations are the same as those in the absence of dipolar interaction (3.85). However, the dispersion relation

$$
\omega = MJ_{\text{tot}}\sqrt{a^2 - h^2 - p^2}
\tag{4.26b}
$$

has an additional term under the square root and the constituents

$$
\begin{aligned}
a &= b^z + 1 + \Delta\cos 2\theta - (1 - \Delta\cos^2\theta)\,\eta(\mathbf{k}) \\
&\quad + \frac{g}{2J_{\text{tot}}}\Big[-2\sin^2\theta D^{XX}(0) - 2\cos^2\theta D^{ZZ}(0) \\
&\qquad\quad + \cos^2\theta D^{XX}(\mathbf{k}) + \sin^2\theta D^{ZZ}(\mathbf{k}) + D^{YY}(\mathbf{k}) - 2\cos\theta\sin\theta D^{XZ}(\mathbf{k})\Big]
\end{aligned}
\tag{4.26c}
$$

$$
\begin{aligned}
h &= \Delta\sin^2\theta\,\eta(\mathbf{k}) \\
&\quad + \frac{g}{2J_{\text{tot}}}\Big[D^{YY}(\mathbf{k}) - \cos^2\theta D^{XX}(\mathbf{k}) - \sin^2\theta D^{ZZ}(\mathbf{k}) + 2\cos\theta\sin\theta D^{XZ}(\mathbf{k})\Big]
\end{aligned}
\tag{4.26d}
$$

$$
p = \frac{g}{J_{\text{tot}}}\left[\cos\theta D^{XY}(\mathbf{k}) - \sin\theta D^{YZ}(\mathbf{k})\right]
\tag{4.26e}
$$

now contain terms related to the dipolar interaction. We again used the normalised exchange interaction $\eta(\mathbf{k})$ and applied field b components as introduced in respectively Eqs. (3.84) and (3.76). We also used the dipolar lattice sums

$$D^{\alpha\beta}(\mathbf{k}) = S_3(\mathbf{k})\delta_{\alpha\beta} - 3S_5^{\alpha\beta}(\mathbf{k}), \text{ where } \alpha, \beta \in \{X, Y, Z\}, \tag{4.26f}$$

defined in terms of the isotropic, respectively anisotropic, sums

$$S_n(\mathbf{k}) = \sum_{\mathbf{r_l}} \frac{\mathrm{e}^{\mathrm{i}\mathbf{k}\cdot\mathbf{r_{lp}}}}{r_{\mathbf{pl}}^n} \tag{4.26g}$$

$$S_n^{\alpha\beta}(\mathbf{k}) = \sum_{\mathbf{r_l}} \frac{\mathrm{e}^{\mathrm{i}\mathbf{k}\cdot\mathbf{r_{lp}}} r_{\mathbf{pl}}^\alpha r_{\mathbf{pl}}^\beta}{r_{\mathbf{pl}}^n}. \tag{4.26h}$$

The angular condition can similarly be written as

$$b^x = \sin 2\theta \left[\Delta - \frac{g}{2J_{\text{tot}}} \left(D^{ZZ}(0) - D^{XX}(0) \right) \right], \tag{4.26i}$$

It can immediately be seen that the dipolar interaction does not contribute anything to the angular condition for a three-dimensional material: the term $D^{ZZ}(0) - D^{XX}(0)$ cancels. The magnetisation angle can however still be influenced because the size of the magnetisation itself might change through the dipolar interaction. In two dimensions, $D^{ZZ}(0) = 0$ and the dipolar interaction has the same net effect as lowering the anisotropy in the angular condition. Further results require the evaluation of the dipolar lattice sums (4.26f).

4.2   Dipolar sums rewritten

The sums that need to be evaluated for the dipolar lattice sums (4.26f) are slowly converging. Since several of these sums need to be calculated for every $\mathbf{k}$-point evaluation in the integral (4.26a), it is important to speed up their calculation. An efficient way to compute such lattice sums is the Ewald summation technique [143]. The main idea of this technique is to split the slowly convergent series into two separate sums. One of those sums contains most of the short-range contributions and is easily summed in real space. The other sum mainly contains long-range contributions. This part is slow to compute in real space, but often converges fast in reciprocal space.

Since the available derivations and applications of the Ewald summation technique are often difficult to comprehend, we give a derivation in appendix C. The specific Ewald transformation formula that we will use, is given by

$$\sum_{\mathbf{l}} \mathrm{e}^{-r_{\mathbf{l}}^2 u/2 + \mathrm{i}\mathbf{r_l}\cdot\mathbf{k}} = \frac{v_b}{(2\pi u)^{d/2}} \sum_{\mathbf{l}} \mathrm{e}^{-(\mathbf{k}+\mathbf{G_l})^2/2u}, \tag{4.27}$$

where the real-valued u can be chosen freely.

In this section, we will rewrite the dipolar lattice sums (4.26f) using this Ewald transformation formula. We will do so in a few steps. First we transform the isotropic sums $S_n(\mathbf{k})$. While doing so, we will encounter the so-called Misra functions, for which we will list a few properties and relations. From the rewritten isotropic sum $S_5(\mathbf{k})$, expressions for the anisotropic sums $S_5^{\alpha\beta}(\mathbf{k})$ can be derived. Combining those results will give an expression for the dipolar lattice sums $D^{\alpha\beta}(\mathbf{k})$.

4.2.1   Isotropic sum

The isotropic lattice sum is

$$S_n(\mathbf{k}) = {\sum_{\mathbf{l}}}' \frac{e^{i\mathbf{k}\cdot\mathbf{r}_\mathbf{l}}}{\|\mathbf{r}_\mathbf{l}\|^n} = {\sum_{\mathbf{l}}}' \frac{e^{i\mathbf{k}\cdot\mathbf{r}_\mathbf{l}}}{(\mathbf{r}_\mathbf{l}^2)^{\frac{n}{2}}}, \tag{4.28}$$

as defined in Eq. (4.26g), with $\mathbf{l}$ a vector of integers, such that the entire lattice is covered by $\mathbf{r}_\mathbf{l}$. In this section, a prime next to the summation symbol explicitly indicates that the origin $\mathbf{l} = \mathbf{0}$ is left out of the sum.

Our derivation is strongly based on that of Born and Bradburn [144], with additional clarifications and a clearer notation. We start from equation (3.326.2) from Gradshteyn and Ryzhik [145]:

$$\int\limits_0^{+\infty} x^m e^{-\beta x^n}\, \mathrm{d}x = \frac{\Gamma(\gamma)}{n\beta^\gamma}, \qquad \gamma = \frac{m+1}{n}, \tag{4.29}$$

holding for $\mathrm{Re}(\beta) > 0$, $\mathrm{Re}(n) > 0$ and $\mathrm{Re}(m) > 0$. Next we make the substitutions

$$n \to 1, \quad \beta \to r^2, \quad m \to \frac{n}{2} - 1, \quad x \to \frac{u}{2}, \quad \text{and thus} \quad \gamma = \frac{n}{2}. \tag{4.30}$$

The conditions given before are satisfied as long as $n > 2$ and the relation becomes

$$2^{-n/2} \int\limits_0^{+\infty} u^{n/2-1} e^{-r^2 u/2}\, \mathrm{d}u = \frac{\Gamma(\frac{n}{2})}{(r^2)^{\frac{n}{2}}}. \tag{4.31}$$

The denominator of the isotropic sum (4.28) can thus be rewritten, such that

$$S_n(\mathbf{k}) = \frac{2^{-n/2}}{\Gamma(\frac{n}{2})} \int\limits_0^{+\infty} {\sum_{\mathbf{l}}}' u^{n/2-1} e^{-r_\mathbf{l}^2 u/2 + i\mathbf{k}\cdot\mathbf{r}_\mathbf{l}}\, \mathrm{d}u, \tag{4.32}$$

and splitting the integral in two parts at some $\tau \in [0, +\infty[$ yields

$$S_n(\mathbf{k}) = \frac{2^{-n/2}}{\Gamma(\frac{n}{2})} \left\{ \int_0^\tau u^{n/2-1} \sum_{\mathbf{l}} e^{-r_{\mathbf{l}}^2 u/2 + i\mathbf{k}\cdot\mathbf{r_l}} \, du - \frac{2\tau^{n/2}}{n} \right. \tag{4.33}$$
$$\left. + \int_\tau^{+\infty} u^{n/2-1} {\sum_{\mathbf{l}}}' e^{-r_{\mathbf{l}}^2 u/2 + i\mathbf{k}\cdot\mathbf{r_l}} \, du \right\} .$$

The prime in the first sum was removed and the corresponding term with $\mathbf{l} = \mathbf{0}$, $\int_0^\tau u^{n/2-1} \, du = 2\tau^{n/2}/n$, was subsequently subtracted again.

The first sum is now exactly of the form needed to apply the Ewald transformation formula (4.27), such that te first term in the curly brackets becomes

$$\int_0^\tau u^{n/2-1} \sum_{\mathbf{l}} e^{-r_{\mathbf{l}}^2 u/2 + i\mathbf{k}\cdot\mathbf{r_l}} \, du = \frac{v_b}{(2\pi)^{d/2}} \int_0^\tau u^{\frac{1}{2}(n-d)-1} \sum_{\mathbf{l}} e^{-\left(\mathbf{k}+\mathbf{G_l}\right)^2/2u} \, du . \tag{4.34}$$

Next, we substitute $u = \tau/\beta$ in this result and $u = \tau\beta$ in the primed sum, such that both integrals have the integration limits 1 to $+\infty$:

$$S_n(\mathbf{k}) = \left(\frac{\tau}{2}\right)^{\frac{n}{2}} \frac{1}{\Gamma(\frac{n}{2})} \left\{ \frac{v_b}{(2\pi\tau)^{d/2}} \int_1^{+\infty} \beta^{-\frac{1}{2}(n-d)-1} \sum_{\mathbf{l}} e^{-\beta\left(\mathbf{k}+\mathbf{G_l}\right)^2/2\tau} \, d\beta \right. \tag{4.35}$$
$$\left. - \frac{2}{n} + \int_1^{+\infty} (\beta)^{n/2-1} {\sum_{\mathbf{l}}}' e^{-r_{\mathbf{l}}^2 \tau\beta/2 + i\mathbf{k}\cdot\mathbf{r_l}} \, d\beta \right\} .$$

Using the Misra functions [146]

$$\phi_m(x) = \int_1^{+\infty} \beta^m e^{-\beta x} \, d\beta \tag{4.36}$$

the isotropic sum can be written as

$$S_n(\mathbf{k}) = \left(\frac{\tau}{2}\right)^{\frac{n}{2}} \frac{1}{\Gamma(\frac{n}{2})} \left\{ \frac{v_b}{(2\pi\tau)^{d/2}} \sum_{\mathbf{l}} \phi_{-\frac{1}{2}(n-d)-1}\left(\frac{(\mathbf{k}+\mathbf{G_l})^2}{2\tau}\right) \right. \tag{4.37}$$
$$\left. - \frac{2}{n} + {\sum_{\mathbf{l}}}' e^{i\mathbf{k}\cdot\mathbf{r_l}} \phi_{n/2-1}(r_{\mathbf{l}}^2\tau/2) \right\} .$$

Finally, this result can be specialised for simple cubic or square lattices. Such lattices with lattice constant a have reciprocal primitive cell volume $v_b = (2\pi/a)^d$,

Bravais lattice vectors $\mathbf{r_l} = a\mathbf{l}$ and reciprocal lattice vectors $\mathbf{G_l} = 2\pi\mathbf{l}/a$. The parameter τ can be chosen freely as to balance convergence speed of both sums. We choose it as $\tau = \pi/(2a^2)$. The isotropic lattice sum is then

$$S_n(\mathbf{k}) = a^{-n}\frac{(\pi/4)^{\frac{n}{2}}}{\Gamma(\frac{n}{2})}\left\{ {\sum_{\mathbf{l}}}' \mathrm{e}^{i a\mathbf{k}\cdot\mathbf{l}}\phi_{n/2-1}\left(\frac{\pi l^2}{4}\right) - \frac{2}{n}\right.$$

$$\left. +2^d \sum_{\mathbf{l}} \phi_{-\frac{1}{2}(n-d)-1}\left(\frac{(a\mathbf{k}+2\pi\mathbf{l})^2}{\pi}\right)\right\}. \tag{4.38}$$

from which both the expression for $S_3(\mathbf{k})$ and $S_5(\mathbf{k})$ can be deduced.

4.2.2 Misra functions

The Misra functions, as defined in Eq. (4.36), are related to the upper incomplete Gamma function (see Gradshteyn and Ryzhik [145], Eq. (3.351.2)) by

$$\phi_m(x) = x^{-m-1}\Gamma(m+1, x) \tag{4.39}$$

and to the generalised exponential integral (see Abramowitz and Stegun [147] Eqs. (6.5.9) and (6.5.10)) by

$$\phi_m(x) = E_{-m}(x) = \alpha_m(x). \tag{4.40}$$

A few special orders of the Misra functions are [148]

$$\phi_0(x) = \frac{\mathrm{e}^{-x}}{x} \tag{4.41a}$$

$$\phi_{-1}(x) = -\mathrm{Ei}(-x) \tag{4.41b}$$

$$\phi_{-\frac{1}{2}}(x) = \left(\frac{\pi}{x}\right)^{\frac{1}{2}}\left[1 - \Phi\left(x^{\frac{1}{2}}\right)\right], \tag{4.41c}$$

with $\mathrm{Ei}(x)$ an exponential integral and $\Phi(x)$ Gauss' error function. Other orders m can be related through the recursion relation

$$\phi_m(x) = \phi_0(x) + \frac{m}{x}\phi_{m-1}(x)$$

$$= \frac{1}{x}\left[\mathrm{e}^{-x} + m\phi_{m-1}(x)\right]. \tag{4.42}$$

From the definition (4.36) it is also easy to find the relation

$$\frac{\mathrm{d}}{\mathrm{d}x}\phi_m(x) = -\phi_{m+1}(x). \tag{4.43}$$

for taking the derivative of a Misra function. When studying limiting behaviour, it is also useful to have the series expansions around $x \approx 0$ and $x \to \infty$ at hand:

$$\phi_m(x) \overset{x \approx 0}{=} \Gamma(m+1)x^{-m-1} + \left[-\frac{1}{m+1} + \frac{x}{m+2} - \frac{x^2}{2m+6} + \mathcal{O}(x^3) \right] \quad (4.44\text{a})$$

$$\phi_m(x) \overset{x \to \infty}{=} \mathrm{e}^{-x} \left\{ \frac{1}{x} + \frac{m}{x^2} + \frac{m(m-1)}{x^3} + \mathcal{O}\!\left(\frac{1}{x^4}\right) \right\} \quad (4.44\text{b})$$

4.2.3 Anisotropic sum

From the expression (4.38) for isotropic sums $S_n(\mathbf{k})$, a similar expression for the anisotropic sums

$$S_n^{\alpha\beta}(\mathbf{k}) = {\sum_{\mathbf{l}}}' \frac{\mathrm{e}^{\mathrm{i}\mathbf{k}\cdot\mathbf{r}_{\mathbf{l}}} r_{\mathbf{l}}^{\alpha} r_{\mathbf{l}}^{\beta}}{\|\mathbf{r}_{\mathbf{l}}\|^n} = -\frac{\partial}{\partial k^{\alpha}} \frac{\partial}{\partial k^{\beta}} S_n(\mathbf{k}) \quad (4.45)$$

can be found through direct differentiation. A first derivative of $S_n(\mathbf{k})$ with respect to k^{β} gives

$$\frac{\partial}{\partial k^{\beta}} S_n(\mathbf{k}) = a^{1-n} \frac{(\pi/4)^{\frac{n}{2}}}{\Gamma(\frac{n}{2})} \left\{ {\sum_{\mathbf{l}}}' \left[\mathrm{i}l^{\beta} \mathrm{e}^{\mathrm{i}a\mathbf{k}\cdot\mathbf{l}} \phi_{n/2-1}\!\left(\frac{\pi l^2}{4}\right) \right] \right.$$
$$\left. + 2^d \sum_{\mathbf{l}} \left[-\frac{2}{\pi} \left(ak^{\beta} + 2\pi l^{\beta} \right) \phi_{-\frac{1}{2}(n-d)}\!\left(\frac{(a\mathbf{k}+2\pi\mathbf{l})^2}{\pi}\right) \right] \right\}. \quad (4.46)$$

Taking the derivative with respect to k^{α} and negating yields the final result for the anisotropic sum

$$S_n^{\alpha\beta}(\mathbf{k}) = a^{2-n} \frac{(\pi/4)^{\frac{n}{2}}}{\Gamma(\frac{n}{2})} \left\{ {\sum_{\mathbf{l}}}' \left[l^{\alpha} l^{\beta} \mathrm{e}^{\mathrm{i}a\mathbf{k}\cdot\mathbf{l}} \phi_{n/2-1}\!\left(\frac{\pi l^2}{4}\right) \right] \right. \quad (4.47)$$
$$- 2^d \sum_{\mathbf{l}} \left[\frac{4}{\pi^2} \left(ak^{\alpha} + 2\pi l^{\alpha} \right) \left(ak^{\beta} + 2\pi l^{\beta} \right) \phi_{-\frac{1}{2}(n-d)+1}\!\left(\frac{(a\mathbf{k}+2\pi\mathbf{l})^2}{\pi}\right) \right]$$
$$\left. + \delta_{\alpha\beta} 2^d \sum_{\mathbf{l}} \left[\frac{2}{\pi} \phi_{-\frac{1}{2}(n-d)}\!\left(\frac{(a\mathbf{k}+2\pi\mathbf{l})^2}{\pi}\right) \right] \right\}.$$

4.2.4 Dipolar lattice sum

The dipolar lattice sum (4.26f) is obtained by combining the isotropic sum (4.38) with $n = 3$ and the anisotropic sum (4.38) with $n = 5$. To rewrite the final expression, we use the Gamma function evaluations $\Gamma(3/2) = \sqrt{\pi}/2$ and $\Gamma(5/2) =$

$3\sqrt{\pi}/4$, and notice that the last term of $S_5^{\alpha\beta}(\mathbf{k})$ cancels with the last term of $S_3(\mathbf{k})$ in the dipolar lattice sum (4.26f). The result is

$$
D^{\alpha\beta}(\mathbf{k}) = \frac{\pi}{4a^3} \left\{ \delta_{\alpha\beta} \left[\sideset{}{'}\sum_{\mathbf{l}} e^{ia\mathbf{k}\cdot\mathbf{l}} \phi_{1/2}\left(\frac{\pi l^2}{4}\right) - \frac{2}{3} \right] \right.
$$
$$
- \frac{\pi}{2} \left[\sideset{}{'}\sum_{\mathbf{l}} l^\alpha l^\beta e^{ia\mathbf{k}\cdot\mathbf{l}} \phi_{3/2}\left(\frac{\pi l^2}{4}\right) \right. \tag{4.48}
$$
$$
\left. \left. - 2^d \frac{4}{\pi^2} \sum_{\mathbf{l}} (ak^\alpha + 2\pi l^\alpha)(ak^\beta + 2\pi l^\beta) \, \phi_{\frac{1}{2}(d-3)}\left(\frac{(a\mathbf{k}+2\pi\mathbf{l})^2}{\pi}\right) \right] \right\}.
$$

4.3   Dipolar sums for small k

In this section we will find the low-k behaviour of the dipolar lattice sums. As we have seen in chapter 3, the behaviour around the Brillouin zone's $\mathbf{\Gamma}$-point crucially determines the occurrence of a non-zero Curie temperature. We will discuss the two- and three-dimensional dipolar lattice sums separately as they behave very differently around $\mathbf{k} = \mathbf{0}$.

4.3.1   Two-dimensional lattice

The first term in the expansion of $D^{\alpha\beta}(\mathbf{k})$ for $d = 2$ is the zeroth order term, i.e. $D^{\alpha\beta}(0)$. Direct evaluation of Eq. (4.48) gives

$$
D^{\alpha\beta}(0) = \frac{\pi}{4a^3} \left\{ \delta_{\alpha\beta} \left[\sideset{}{'}\sum_{\mathbf{l}} \phi_{1/2}\left(\frac{\pi l^2}{4}\right) - \frac{2}{3} \right] \right.
$$
$$
\left. - \frac{\pi}{2} \left[\sideset{}{'}\sum_{\mathbf{l}} l^\alpha l^\beta \phi_{3/2}\left(\frac{\pi l^2}{4}\right) - 64 \sum_{\mathbf{l}} l^\alpha l^\beta \phi_{-1/2}(4\pi l^2) \right] \right\}. \tag{4.49}
$$

This quantity vanishes when $\alpha \neq \beta$ because the summands are odd in l^α. For equal $\beta = \alpha$ on the other hand, the result is

$$
D^{\alpha\alpha}(0) = -\frac{1}{2a^3}\xi_0, \ \text{ with } \xi_0 = 9.03362168, \tag{4.50}
$$

where the numerical factor ξ_0 is defined by the fast converging series

$$
-\frac{\pi}{2} \sideset{}{'}\sum_{\mathbf{l}} \left[\phi_{1/2}\left(\frac{\pi l^2}{4}\right) - \frac{\pi}{2}(l^\alpha)^2 \phi_{3/2}\left(\frac{\pi l^2}{4}\right) + 32\pi(l^\alpha)^2 \phi_{-1/2}(4\pi l^2) \right] + \frac{\pi}{3} \tag{4.51}
$$

Other techniques for obtaining this value are discussed by Topping [149], and Hoff and Benson [150].

We can now consider the lowest non-constant and non-vanishing term of Eq. (4.48) in $\mathbf{k}$. For the first two lines, the lowest contributing non-zero order in $\mathbf{k}$ is quadratic due to the lattice symmetries. With the help of expansion (4.44a) for the Misra function $\phi_{-1/2}(x)$, the sum in the last line of Eq. (4.48) is

$$\sideset{}{'}\sum_{\mathbf{l}} \left(4\pi^2 l^\alpha l^\beta + 2\pi a \left(l^\beta k_\alpha + l^\alpha k_\beta \right) + a^2 k^\alpha k^\beta \right)$$
$$\times \left(\frac{\pi}{|a\mathbf{k} + 2\pi\mathbf{l}|} - 2 + \frac{2}{3\pi} \left(a\mathbf{k} + 2\pi\mathbf{l} \right)^2 \right) \tag{4.52}$$

for small $\mathbf{k}$. The lowest order contribution of the factor on the last line is $\pi/|a\mathbf{k}|$ and happens in the term for which $\mathbf{l} = \mathbf{0}$. Together with the factor on the first line in that term, this leads to a linear dependence on $\mathbf{k}$. All other terms can be checked to either vanish or to be of higher order in $\mathbf{k}$. The linear term in $\mathbf{k}$ is thus the most important one for $\mathbf{k} \to 0$. Combining this linear term with the constant term found before yields

$$D^{\alpha\beta}(\mathbf{k}) \overset{\mathbf{k}\to 0}{\approx} -\frac{\xi_0}{2a^3} \delta_{\alpha\beta} + \frac{2\pi}{a^3} \frac{a k^\alpha a k^\beta}{a|\mathbf{k}|}. \tag{4.53}$$

This result was derived in a similar manner by Lee and Begchi [151] in the context of Frenkel excitons.

4.3.2   Three-dimensional lattice

The constant term in the small-k expansion of $D^{\alpha\beta}(\mathbf{k})$ for $d = 3$ is best calculated directly from the definition (4.26f). The isotropic and anisotropic sums are

$$S_3(0) = \sideset{}{'}\sum_{\mathbf{r_l}} \frac{1}{r_{\mathbf{pl}}^3} = \frac{1}{a^3} \sideset{}{'}\sum_{m,n,j=-\infty}^{+\infty} \frac{1}{(m^2 + n^2 + j^2)^{\frac{3}{2}}} = \frac{1}{a^3}\xi_3 \tag{4.54}$$

$$S_5^{\alpha\beta}(0) = \sideset{}{'}\sum_{\mathbf{r_l}} \frac{r_{\mathbf{pl}}^\alpha r_{\mathbf{pl}}^\beta}{r_{\mathbf{pl}}^5} = \frac{\delta_{\alpha,\beta}}{a^3} \sideset{}{'}\sum_{m,n,j=-\infty}^{+\infty} \frac{m^2}{(m^2 + n^2 + j^2)^{\frac{5}{2}}} = \frac{\delta_{\alpha,\beta}}{3a^3}\xi_3. \tag{4.55}$$

The sum defining ξ_3 does not converge, but it cancels out in the dipolar lattice sum. The constant term in the low-k expansion is thus

$$D^{\alpha\beta}(0) = S_3(0)\delta_{\alpha\beta} - 3S_5^{\alpha\beta}(0) = 0. \tag{4.56}$$

The lowest order contribution in $\mathbf{k}$ of $D^{\alpha\beta}(\mathbf{k})$ can be found by expanding Eq. (4.48) and eliminating some terms by using the lattice symmetries:

$$
2a^3 D^{\alpha\beta}(\mathbf{k}) \overset{\mathbf{k}\to 0}{\approx} {\sum_{\mathbf{l}}}' \left[\delta_{\alpha\beta} \frac{\pi}{2} \left(1 - \frac{a^2 (\mathbf{k}\cdot\mathbf{l})^2}{2} \right) \left[\phi_{1/2}\Big(\frac{\pi l^2}{4}\Big) - \frac{\pi}{2} (l^\alpha)^2 \phi_{3/2}\Big(\frac{\pi l^2}{4}\Big) \right] \right.
$$
$$
+ 8 \left(4\pi^2 l^\alpha l^\beta + 2\pi a (l^\beta k^\alpha + l^\alpha k^\beta) + a^2 k^\alpha k^\beta \right)
$$
$$
\left. \times \phi_0\Big(\frac{(a\mathbf{k} + 2\pi\mathbf{l})^2}{\pi} \Big) \right] \tag{4.57}
$$
$$
+ 8a^2 k^\alpha k^\beta \phi_0\Big(\frac{a^2 k^2}{\pi}\Big) - \delta_{\alpha\beta}\frac{\pi}{3}.
$$

The recursive relation (4.42) allows us to rewrite the combination

$$
\phi_{1/2}\Big(\frac{\pi l^2}{4}\Big) - \frac{\pi}{2} (l^\alpha)^2 \phi_{3/2}\Big(\frac{\pi l^2}{4}\Big) = \frac{l^2 - 3(l^\alpha)^2}{l^2} \phi_{1/2}\Big(\frac{\pi l^2}{4}\Big) - \frac{\pi}{2} (l^\alpha)^2 \phi_0\Big(\frac{\pi l^2}{4}\Big),
$$
$$
\tag{4.58}
$$

the first term of which vanishes when summed with constant factors over the three-dimensional cubic lattice. The expansion is then

$$
2a^3 D^{\alpha\beta}(\mathbf{k}) \overset{\mathbf{k}\to 0}{\approx} {\sum_{\mathbf{l}}}' \left[-\delta_{\alpha\beta}\frac{\pi^2}{4} (l^\alpha)^2 \phi_0\Big(\frac{\pi l^2}{4}\Big) \right.
$$
$$
- \delta_{\alpha\beta}\frac{\pi}{2}\frac{a^2 (\mathbf{k}\cdot\mathbf{l})^2}{2} \left[\frac{l^2 - 3(l^\alpha)^2}{l^2}\phi_{1/2}\Big(\frac{\pi l^2}{4}\Big) - \frac{\pi}{2} (l^\alpha)^2 \phi_0\Big(\frac{\pi l^2}{4}\Big) \right]
$$
$$
+ 8 \left(4\pi^2 l^\alpha l^\beta + 2\pi a (l^\beta k^\alpha + l^\alpha k^\beta) + a^2 k^\alpha k^\beta \right) \tag{4.59}
$$
$$
\left. \times \phi_0\Big(\frac{(a\mathbf{k} + 2\pi\mathbf{l})^2}{\pi} \Big) \right]
$$
$$
+ 8a^2 k^\alpha k^\beta \phi_0\Big(\frac{a^2 k^2}{\pi}\Big) - \delta_{\alpha\beta}\frac{\pi}{3}.
$$

It remains to find expansions for the $\mathbf{k}$ dependence in the Misra functions of order zero. The general expansion relation (4.44a) directly yields

$$
\phi_0\Big(\frac{a^2 k^2}{\pi}\Big) \overset{\mathbf{k}\to 0}{\approx} \frac{\pi}{a^2 k^2} - 1 + \frac{a^2 k^2}{2\pi}. \tag{4.60}
$$

A more extensive expansion effort also makes it possible to expand the other Misra function with $\mathbf{k}$-dependent argument as

$$
\phi_0\Big(\frac{(a\mathbf{k} + 2\pi\mathbf{l})^2}{\pi} \Big) \overset{\mathbf{k}\to 0}{\approx} \phi_0(4\pi l^2) \left\{ 1 - \frac{4\pi l^2 + 1}{\pi l^2} a\mathbf{k}\cdot\mathbf{l} \right.
$$
$$
\left. + \frac{8\pi^2 l^4 + 4\pi l^2 + 1}{\pi^2 l^4} (a\mathbf{k}\cdot\mathbf{l})^2 - \frac{4\pi l^2 + 1}{4\pi^2 l^2} (a\mathbf{k})^2 \right\}. \tag{4.61}
$$

Grouping terms of different order in $\mathbf{k}$ and eliminating third order contributions yields for the dipolar lattice sum

$$2a^3 D^{\alpha\beta}(\mathbf{k}) \stackrel{\mathbf{k}\to 0}{\approx} \frac{8\pi}{3}\left(3\frac{k^\alpha k^\beta}{k^2} - \delta_{\alpha\beta}\right) - 8a^2 k^\alpha k^\beta \tag{4.62}$$

$$+ a^2 \sideset{}{'}\sum_{\mathbf{l}}\left[8k^\alpha k^\beta \phi_0(4\pi l^2)\right.$$

$$- 8\phi_0(4\pi l^2)\frac{4\pi l^2 + 1}{l^2}\left(2\left((l^\beta)^2 + (l^\alpha)^2\right)k^\alpha k^\beta + \delta_{\alpha\beta}(l^\alpha)^2 k^2\right)$$

$$+ 32 l^\alpha l^\beta \phi_0(4\pi l^2)\frac{8\pi^2 l^4 + 4\pi l^2 + 1}{l^4}\sum_{j=1}^{3}\sum_{i=1}^{3} l^i l^j k^i k^j$$

$$\left.- \delta_{\alpha\beta}\frac{\pi}{4}l^2 k^2\left(\frac{1}{l^2}\left(l^2 - 3(l^\alpha)^2\right)\phi_{1/2}\left(\frac{\pi l^2}{4}\right) - \frac{\pi}{2}(l^\alpha)^2 \phi_0\left(\frac{\pi l^2}{4}\right)\right)\right]$$

where, once again, some terms have been eliminated due to the symmetry of the lattice, and we used the fact that

$$\sideset{}{'}\sum_{\mathbf{l}}\left[8\mathrm{e}^{-4\pi l^2} - \mathrm{e}^{-\pi l^2/4}\right] = -7. \tag{4.63}$$

Now, we use

$$l^\alpha l^\beta \sum_{j=1}^{3}\sum_{i=1}^{3} l^i l^j k^i k^j = \begin{cases} 2(l^\alpha)^2\left(l^1 l^2 k^1 k^2 + l^1 l^3 k^1 k^3 + l^2 l^3 k^2 k^3\right) & \alpha = \beta \\ l^\alpha l^\beta\left(2l^\alpha l^\beta k^\alpha k^\beta + (l)^2 (k)^2\right) & \alpha \neq \beta \end{cases} \tag{4.64}$$

and

$$\sideset{}{'}\sum_{\mathbf{l}}\left((l)^2 - 3(l^\alpha)^2\right) = 0 \tag{4.65}$$

on a simple cubic lattice, such that we finally find the result

$$
\begin{aligned}
D^{\alpha\beta}(\mathbf{k}) \overset{\mathbf{k}\to 0}{\approx} & \frac{4\pi}{3a^3}\left(3\frac{k^\alpha k^\beta}{k^2} - \delta_{\alpha\beta}\right) \\
& + \frac{4k^\alpha k^\beta}{a}\bigg\{ -1 + {\sum_{\mathbf{l}}}' \frac{\phi_0(4\pi l^2)}{l^4} \\
& \qquad \times \Big[\big((1 - 8\pi\,(l^\alpha)^2)\,(1 - 8\pi\,(l^\beta)^2) - 64\pi^2\delta_{\alpha\beta}\,(l^\alpha)^2\,(l^\beta)^2\big)\,l^4 \\
& \qquad\quad + \big(-2\,(l^\beta)^2 - 2\,(l^\alpha)^2 + 32\pi\,(1 - \delta_{\alpha\beta})\,(l^\alpha)^2\,(l^\beta)^2\big)\,l^2 \\
& \qquad\quad + 8\,(1 - \delta_{\alpha\beta})\,(l^\alpha)^2\,(l^\beta)^2\Big]\bigg\} \\
& + \frac{k^2\delta_{\alpha\beta}}{2a}{\sum_{\mathbf{l}}}' \frac{(l^\alpha)^2}{l^2}\left[-8\phi_0(4\pi l^2)\,(4\pi l^2 + 1) + \frac{\pi^2}{8}l^4\phi_0\Big(\frac{\pi l^2}{4}\Big)\right] \\
& + \frac{32\delta_{\alpha\beta}}{a}{\sum_{\mathbf{l}}}' \frac{(l^\alpha)^2}{l^4}A(\mathbf{k},\mathbf{l})
\end{aligned}
\tag{4.66}
$$

where

$$
A(\mathbf{k},\mathbf{l}) = \phi_0(4\pi l^2)\left(8\pi^2\,(l)^4 + 4\pi\,(l)^2 + 1\right)\left(l^1 l^2 k^1 k^2 + l^1 l^3 k^1 k^3 + l^2 l^3 k^2 k^3\right) \tag{4.67}
$$

This type of expansion was first found by Cohen and Keffer [148]. The second order terms are however difficult to compare due to the different notation and because their results are more generally applicable (they are also valid for BCC and FCC lattices). For a more elaborate discussion of the behaviour at and around $\mathbf{k} = 0$ and in finite lattices, we also refer to their paper.

Having found fast-converging expressions for the dipolar sums, and their low-$\mathbf{k}$ expansions, we collected all necessary ingredients for obtaining numerical results from the set of equation (4.26). This should allow the calculation of magnetisation and Curie temperature in the presence of dipolar interactions.

4.4   Discussion

Up to this point, the effect of the dipolar interaction was discussed in samples with infinite size, allowing for a direct extension of the methodology from previous chapters. In this context, we found that the dipole-dipole interaction contributes dispersive terms to both the integral (4.26a) that calculates Φ, and the excitation spectrum (4.26b). Moreover, it has by large the same effect as lowering the anisotropy Δ in the angular condition (4.26i) for 2D materials, the decrease being inversely proportional to the total exchange strength J_{tot}. For easy-axis anisotropic materials, the lowered effective anisotropy will lead to a smaller excitation energy

gap which will probably slightly lower the Curie temperature and magnetisation. For easy-plane anisotropic materials, the stronger in-plane anisotropy will not open an energy gap. However, the in-plane magnetisation is expected to be stabilised by the additional dispersive contributions [139, 140]. These expectations are in line with the work of Bruno [84], where he studies a similar system—containing an anisotropy term with a different form—within the Holstein-Primakoff framework. Moreover, Bruno finds a narrow regime where the original anisotropy Δ is positive, but the effective anisotropy is lowered to become negative. He indicates that, in this case, the original anisotropy is not strong enough to pull a homogeneous magnetisation out of the plane, and he finds a ripple-like fluctuation of the magnetisation direction.

Apart from these universal effects that are present, regardless of the exact size or shape of the sample, the dipolar interaction has additional impact on samples with finite sizes. The long-range magnetostatic interaction is more strongly affected by the exact size and shape of samples than the exchange interaction, because it has a direct influence on all spins. Indeed, as known from classical theory, one needs to consider the presence of a demagnetisation field in finite-sized samples, associated with the fact that the ferromagnetic sample generates its own magnetic field throughout space. However, we avoid going into the details here, as the corresponding macroscopic description of magnetism may look confusing when it comes to embed it in the microscopic quantum theory. Moreover, the corresponding notation could be hardly reconciled with the one we decided to use, cf. subsection 1.4.1. It suffices to know that the energy associated with the demagnetisation field is large when the entire ferromagnet is homogeneously magnetised, i.e. consists of a single domain. This energy can be lowered by splitting the magnet into several domains, each having a uniform magnetisation within the domain, but possibly in different directions with respect to each other. Such a lowering of the demagnetization energy is accompanied by an increase of the exchange energy at the domain boundaries. The balance of these effects determines the final domain structure in the ferromagnet [45, 77].

These finite-size effects, including inhomogeneous magnetisations and domain wall formation, are difficult—if not impossible—to describe in full detail using the Green function method presented in this thesis, judging by the lack of literature. Therefore, we would recommend to use better suited techniques, such as micromagnetic simulations [75], for calculations that fundamentally depend on the system's shape. Those techniques can still use results, such as the excitation spectra, that were extensively discussed in this thesis. Nonetheless, we would like to suggest a few pathways—ordered from high-risk and very novel to low-risk and less novel—that could give some estimates for the effects of the dipolar interactions in finite-sized samples:

- In the Green function formalism as discussed in this thesis, we fundamentally exploited the system's translational invariance by taking the spatial Fourier transform. This invariance is lost in finite-sized systems. As an alternative, the Fourier transform might be replaced by a Fourier cosine or sine expansion when supplementing the system with Neumann, Dirichlet, or other boundary conditions. This choice should be assessed based on its physical implications on the magnetisation behaviour at the boundaries, which is expected to be reduced compared to the interior of the sample.

- The calculation of the magnetisation involves an integration over the first Brillouin zone in the reciprocal space. A first estimation of finite-size effects could involve ignoring excitations with wavelengths longer than the sample size. Practically, this can be implemented by neglecting—or partially damping through a weight function—contributions to the integral of wave vectors smaller than those limiting wavelengths. It is, however, not a priori clear whether the excitation spectrum renormalisation is still valid in this case.

- Some of the finite-size effects can be described by including the demagnetisation field as an additional effective magnetic field. This could be particularly effective if the sample can be approximated by an ellipsoid, for which the demagnetisation field is uniform throughout the entire sample [152].

5 Conclusion

5.1 Conclusion

We solved the quantum mechanical Heisenberg model at non-zero temperatures for $S \geqslant 1/2$ with anisotropic exchange interactions that can reach beyond nearest neighbours. The anisotropy is allowed to be of either easy-axis or easy-plane type and the model can describe both two- and three-dimensional materials. Furthermore, we allow for a homogeneous magnetic field in arbitrary directions. Our presented solution method is based on Zubarev's Green functions, supplemented with a necessary regularity condition, all applied after a suitable coordinate rotation. We showed that the method can further be extended to incorporate dipolar interactions.

We demonstrated our general solution technique in three ways: (i) studying the difference between ferromagnets in two- and three-dimensional cubic materials and the effect of anisotropy on them, (ii) investigating a few recently discovered single-layer materials with hexagonal and honeycomb lattices, and (iii) working out the relations for taking into account dipolar interactions at the same level of approximation as the other magnetic effect.

In accordance with the Mermin-Wagner theorem, we found that an easy-axis anisotropy is necessary for spontaneous magnetisation to be possible in two-dimensional materials. This can be understood from the opening of an excitation gap by the easy-axis anisotropy. In contrast, the easy-plane anisotropy leaves the excitation spectrum linear and gapless around its minimum, such that magnons—detrimental for the spontaneous magnetisation—get too easily excited at finite temperatures. At very small magnetic fields, easy-plane materials have a substantial magnetisation up to some non-zero temperature. This temperature is strongly field-dependent and is in experiments sometimes considered as a Curie temperature. For bulk materials, the Curie temperature was found to be non-zero for any anisotropy, but with lower values for easy-plane than easy-axis anisotropies of comparable size. In general, bulk materials are found to have similar properties as monolayers with easy-axis anisotropy. When a magnetic field is applied at an angle, the anisotropy is mostly decisive for the magnetisation direction at low temperatures and small fields. On the contrary, at high temperatures or large fields the magnetisation is mostly parallel to the applied field.

Most recently discovered two-dimensional ferromagnets are of hexagonal or honeycomb lattice type, the latter being more challenging to study because it has a multiatomic basis and exchange interactions beyond nearest-neighbours become important. Using parameters obtained from ab initio calculations, we found that or model is well-suited to describe CrI_3, $CrBr_3$ and $MnSe_2$, which all have a total weighted easy-axis anisotropy and thus non-vanishing Curie temperature. Overall, our calculated Curie temperatures and excitation gaps agree well—and better than other methods, such as Monte Carlo simulations and the Ising model—with available experiments. For honeycomb materials in particular, we found that farther neighbours can have a large effect on the predicted Curie temperature. To enable further computational discoveries of new two-dimensional ferromagnets and predict their Curie temperatures—with or without additional strain, stress or electric fields—we made a computer program publicly available to calculate T_C just from DFT parameters, all based on the solutions presented here. In general, we expect the highest Curie temperatures for materials with both a large total exchange strength J_{tot}—which can also be achieved through the interaction with further neighbours—and a large total weighted easy-axis anisotropy $\delta > 0$.

Finally, we also worked out the formulas to account for dipolar interaction, at the same level of approximation as the other interactions, using our formalism. The computational challenge of slow-converging dipolar lattice sums was alleviated by converting them into fast-converging ones applying Ewald summation techniques. For two-dimensional materials specifically, we expect the dipolar interaction to have a stabilising effect and turn materials with a small easy-axis anisotropy into materials with an effective easy-plane anisotropy.

5.2   Future work

Clearly, we made a lot of progress in understanding and computing properties of magnetism in two-dimensional materials. On the other hand, it is also clear that there is still room for improvements and extensions of the applicability. For instance, within the framework presented in this thesis, it should be possible to treat multiatomic lattices with less symmetry, such that each sublattice can have a different magnetisation (angle). Similarly, an extension to multilayer materials should be possible. The model to be solved could also be extended to incorporate different types of interactions and anisotropies. Finally, this thesis focused on static properties, while also the dynamics of quantum Heisenberg systems are not well understood. Below, we give a brief description of possible continuations for the presented work.

5.2.1   Multilayers

Although it is nowadays possible to create single layers of given materials, most integrated circuit devices will use multilayers rather than monolayer. Our method should be extensible to such cases. However, one should take into account that the different layers might—and probably will—have distinct magnetisation magnitudes and angles [102, 116, 153, 154]. Due to their exposed surfaces, the outermost layers might moreover have different interactions than the inner layers [134, 135].

So far, there is consensus in the available literature that the Curie temperature rises with the number of layers N, approaching the 3D limit as the number of layers becomes very large. As a side note, this increasing Curie temperature is observed when using fixed interaction parameters. Those parameters might however also be different for the 2D and 3D versions of a given material [134]. In the ferromagnetic state, the magnetisation in the inner layers is generally larger than that of the outer layers, but the difference is still fairly small for very thin films of a few layers [116, 154]. There is no clear consensus on the exact variation of the Curie temperature T_{C}^{N} for N layers, relative to that for fully 2D ($T_{\mathrm{C}}^{\mathrm{2D}}$) or 3D ($T_{\mathrm{C}}^{\mathrm{3D}}$) systems. For example, Fisher and Barber [155] claim that $T_{\mathrm{C}}^{N}/T_{\mathrm{C}}^{\mathrm{3D}} = 1 - (C/N)^{1/\nu}$ for large N, with C a material-dependent constant and ν the 3D critical exponent. For a small number of layers, Zhang and Willis [156] claim a linear dependence of the Curie temperature on the number of layers. Some other results are available, but do not give a functional relation for T_{C}^{N}. The general trend in those results is that the Curie temperature increases fairly rapidly for small N, flattening as the number of layers increases [102, 154, 157].

5.2.2   Other interactions

Other interactions than those discussed in this thesis, could be included as effective spin interactions or lattice distortions. For example, one could include the effect of an external electric field as a combination of shifted sublattices and distorted atomic orbitals that lead to different DFT parameters.

The Dzyaloshinskii-Moriya interaction (DMI) [158–160]—also called anti-symmetric exchange interaction—originates from a combination of superexchange and strong spin-orbit interactions. It adds a term

$$\hat{\mathrm{H}}_{\mathrm{DMI}} = \sum_{\langle i,j \rangle} \mathbf{D}_{ij} \cdot \left(\hat{\mathbf{S}}_i \times \hat{\mathbf{S}}_j \right) \tag{5.1}$$

to the spin Hamiltonian, where the sum is over all pairs of spins $\langle i, j \rangle$. It favours spin configurations that make a clockwise or counter-clockwise rotation from spin $\hat{\mathbf{S}}_i$ to spin $\hat{\mathbf{S}}_j$, depending on the direction of the DMI vector $\mathbf{D}_{ij}$. In principle, it can be accounted for through the same formalism as we used in this thesis. However, for

general DMI vectors and spin configurations, its anti-symmetric nature prohibits a conversion into the form of the general spin Hamiltonian (3.8a), as we did for the dipolar interaction. This means that the results from section 3.7 cannot be reused and must be derived again to include DMI. In turn, this might lead to a decoupling matrix $\mathbf{\Gamma}$ with different symmetry properties, which can result in additional technical difficulties and heavier computational burden. Furthermore, we note that DMI is often studied in the context of magnetic skyrmions—topologically protected, vortex-like excitations [161]. However, the excitations characterising skyrmions and also spin profiles arising from DMI are topologically distinct from those related to single or multiple spin flips acting on the ferromagnetic ground state[1]. In particular, the quantum mechanical operator equivalent of a skyrmionic or DMI magnetisation profile—the eigenvalues of which correspond to measurable values of the vorticity or any relevant observable—has, to the best of our knowledge, not yet been constructed so far. Hence, a meaningful quantum mechanical treatment is not attainable yet, regardless whether it would invoke the present Green function formalism or any other approach.

A single-ion anisotropy

$$\hat{H}_{\text{single-ion}} = -K \sum_i \left(\hat{S}_i^Z \right)^2 \tag{5.2}$$

is often considered instead of an anisotropic exchange interaction. One should, however, be very careful with its treatment as it is a localised interaction. Many studies use a Tyablikov decoupling to handle it [162], while it is known that such a decoupling is not well-suited. A few other decoupling schemes have been proposed, which give more satisfying results [88, 102, 113, 114, 154, 163]. Qualitatively, it is generally agreed upon that the single-ion anisotropy has the same effect on ferromagnets as the exchange anisotropy that we considered in this work [73], except for $S = 1/2$, in which case it merely leads to a shift in the zero-point energy. Apart from DFT studies, Bander and Mills [164] found that the 3D and 2D Curie temperatures when including single-ion anisotropy are related by

$$T_{\text{C}}^{\text{2D}} = \frac{T_{\text{C}}^{\text{3D}}}{\ln\left(\frac{3\pi k_{\text{B}} T_{\text{C}}^{\text{3D}}}{4K} \right)} \tag{5.3}$$

using renormalization group theory. This is indeed a similar behaviour as we observed as function of Δ, with non-zero T_{C}^{2D} for positive K.

5.2.3   Dynamics

There have not been many studies on spin wave-like dynamics in quantum Heisenberg systems, most of them having limited results or being restricted to one

---

[1]Adding DMI may even lower the ground-state energy below that of the ferromagnetic state.

spatial dimension [165–170]. On the contrary, in classical spin systems, a lot of results are available through the use of micromagnetic simulations. To tackle the quantum mechanical problem, our technique using Zubarev's Green functions is not directly applicable because it does not, for instance, give any insight in the specific excitations leading to the dispersion relations. For known excitations, such as the Bloch magnons, the derived dispersion relations might be a starting point for further investigations. Furthermore, the presented theory assumes in, for instance, Eq. (2.50) that the Hamiltonian generating the time-evolution of the Heisenberg operators is the same as that appearing in the initial density matrix.

Related to the present research, we propose to directly solve the Heisenberg equation of motion for the relevant spin operators, making use of a Tyablikov-like decoupling along the way to make the resulting set of equations solvable. The Heisenberg equation of motion for a spin $\hat{\mathbf{S}}_j$ evolving in time according to interactions given by a Hamiltonian $\hat{\mathrm{H}}$ is

$$i\frac{d\hat{\mathbf{S}}_j}{dt} = [\hat{\mathbf{S}}_j, \hat{\mathrm{H}}].$$
(5.4)

When the Hamiltonian is the isotropic Heisenberg exchange Hamiltonian, this can further be worked out to be

$$\frac{d\hat{\mathbf{S}}_j}{dt} = \frac{\partial\hat{\mathrm{H}}}{\partial\hat{\mathbf{S}}_j} \times \hat{\mathbf{S}}_j, \text{ where } \frac{\partial\hat{\mathrm{H}}}{\partial\hat{\mathbf{S}}_j} = \frac{\partial\hat{\mathrm{H}}}{\partial\hat{\mathrm{S}}_j^x}\mathbf{x} + \frac{\partial\hat{\mathrm{H}}}{\partial\hat{\mathrm{S}}_j^y}\mathbf{y} + \frac{\partial\hat{\mathrm{H}}}{\partial\hat{\mathrm{S}}_j^z}\mathbf{z}.$$
(5.5)

In the classical analogue, this last quantity can be seen as an effective magnetic field and the derived equation of motion is equivalent to the Landau–Lifshitz–Gilbert (LLG) equation [76]. The right-hand side of the equation of motion already contains products of spin operators that can be decoupled at this stage using a Tyablikov-like decoupling scheme. Doing so would, however, neglect all quantum mechanical correlations and results in essentially classical spin waves. Instead, one should write similar Heisenberg equations of motion for the different spin combinations and close the spin algebra at that level. From the equation of motion, it should then be possible to calculate time-dependent expectation values, such as the time evolution of the local magnetisation. In order to average the operator equations, one has to choose appropriate initial density matrices. Initial studies could focus on localised spin inversions in an otherwise uniformly magnetised lattice, as could be achieved by applying a large, localised field in a low-temperature environment. If this should fail, one could try to do the same thing after applying the Holstein-Primakoff approximation, up to first or second order.

Appendices

A ∣ Tanh-sinh quadrature

In this appendix, we exactly repdroduce the contents of the manuscript *Tanh-sinh quadrature for single and multiple integration using floating-point arithmetic* by Vanherck, Sorée and Magnus [112] (except for a few layout changes) that has been submitted for publication.

Abstract

The problem of estimating single- and multi-dimensional integrals, with or without end-point singularities, is prevalent in all fields of scientific research, and in particular in physics. Although tanh-sinh quadrature is known to handle most of these cases excellently, its use is not widely spread among physicists. Moreover, while most calculations are limited by the use of finite-precision floating-point arithmetic, similar considerations for tanh-sinh quadrature are mostly lacking in literature, where infinite-precision floating-point numbers are often assumed. Also, little information is available on the application of tanh-sinh quadrature to multiple integration. We have investigated the risks and limitations associated with limited-precision floating-point numbers when using tanh-sinh quadrature for both single and multiple integration, while obtaining excellent convergence rates. In addition, this paper provides recommendations for a straightforward implementation using limited-precision floating-point numbers and for avoiding numerical instabilities.

A.1   Introduction

While many automatic integration routines yield excellent results in general, they often fail in specific circumstances, such as the occurrence of end-point singularities. In these situations, it is paramount to account for the limitations of a specific routine in order to exploit its full potential. Tanh-sinh quadrature for numerical integration already exists about half a century [107], but is not well-known in the physics community, though being adopted in some recent publications [120, 171, 172]. The corresponding scheme can be invoked as an almost general purpose quadrature, which is especially efficient for divergent integrands. Due to its exponential convergence rate and its good behaviour in general, tanh-sinh quadrature has become rather popular in the field of experimental mathematics. It even has been

coined to be the best scheme for integrands typically encountered in that field, which focuses on high-precision integral calculations [110, 111, 173].

We describe the quadrature in an accessible manner in Sec. A.2 while elaborating on its implementation with limited-precision floating-point numbers in Sec. A.3. Specifically, we explain how numerical instabilities can be avoided, while showing how to extend the quadrature to multiple integration, which is indispensable in computational physics. Examples of integrals calculated with the tanh-sinh rule are given in Sec. A.4, whereas the conclusions and final remarks are presented in Section A.5.

A.2   Tanh-sinh quadrature

Tanh-sinh quadrature computes integrals of the form[1]

$$\mathcal{I} = \int_{-1}^{1} f(x)\,\mathrm{d}x\,. \tag{A.1}$$

The quadrature is based on a variable substitution $x = \Psi(t)$, mapping the original, finite domain $x \in\,]-1,\, 1[$ onto the entire real axis $t \in\,]-\infty,\, +\infty[$:

$$\mathcal{I} = \int_{-\infty}^{\infty} g(t)\,\mathrm{d}t, \quad g(t) \coloneqq f\big(\Psi(t)\big)\Psi'(t). \tag{A.2}$$

For integration over the entire real axis of exponentially decaying integrands as $|t| \to \infty$, the trapezoidal rule (also known as Sinc quadrature [171]) is the most efficient [108, 109, 174–176] among quadratures with equidistant abscissae. Applying this rule with a step size h between the evaluation points yields the approximate integral

$$\mathcal{I}_h = \lim_{m\to\infty} \sum_{i=-m}^{+m} h\Psi'(t_i)f\big(\Psi(t_i)\big), \tag{A.3}$$

the transformed evaluation points being

$$t_i \coloneqq ih, \quad i = 0, \pm 1, \pm 2, \ldots \tag{A.4}$$

while introducing a discretization error $\Delta\mathcal{I}_h$. Keeping only $N \coloneqq 2n + 1$ function evaluations, we are left with

$$Q_h^n = \sum_{i=-n}^{+n} h\Psi'(t_i)f\big(\Psi(t_i)\big), \tag{A.5}$$

---

[1]Any integral $\int_a^b f(y)\,\mathrm{d}y$ with a and b finite can be cast in this form by the linear substitution $2y = (b - a)\,x + (b + a)$.

thereby introducing a truncation error ϵ_t, since the transformed integration domain is now limited to the window $[t_{-n}, t_n]$. The total error of the resulting approximation as compared to the original integral is limited by $\left|\mathcal{I} - Q_h^n\right| \leqslant \Delta Q_h^n :=$ $|\Delta\mathcal{I}_h| + |\epsilon_t|$.

As to the mapping $\Psi(t)$, Takahasi and Mori [107] proposed a *tanh-sinh* transformation

$$\Psi(t) = \tanh\big(\lambda \sinh(t)\big) \tag{A.6a}$$

$$\Psi'(t) = \frac{\lambda \cosh(t)}{\cosh^2\big(\lambda \sinh(t)\big)}, \tag{A.6b}$$

where $\lambda = \pi/2$. With this choice, which is illustrated in Fig. A.1, the behaviour of $g(t)$ as $|t| \to \infty$ is optimal in the sense that a faster decay leads to a higher discretization error for a given h, while a slower decay causes a larger truncation error because $\Psi'(t)f\big(\Psi(t)\big)$ remains significant for large values of $|t|$. An extended error analysis in the complex plane indeed shows that, for a large number of evaluation points, the above transformation often yields an optimal error [107, 108] as compared to other quadratures based on a variable transformation. This error is of the order [107–109, 176]

$$|\Delta Q_h^n| = \mathcal{O}\bigg(\exp\Big(-\frac{\pi dN}{\ln(2dN)}\Big)\bigg), \quad \text{with } N = 2n + 1 \tag{A.7}$$

when h is chosen optimally. The parameter d has to be chosen such that the analytical continuation of the integrand $g(z) = \Psi'(z)f\big(\Psi(z)\big)$ in the complex plane is regular in the strip around the real axis defined by $|\mathrm{Im}\, z| < d$, meaning that the integrand lies within the Hardy space [108, 177]. The choice of d and h will be detailed in Sec. A.3.3, the latter being of particular importance in avoiding numerical instabilities.

The tanh-sinh quadrature scheme has several advantages worth pointing out explicitly. (i) The error estimate (A.7) shows that doubling the number of evaluation points also roughly doubles the number of significant digits, which makes the quadrature especially suited for high precision calculations [110, 111]. (ii) Even when not all conditions for the error estimate (A.7) are strictly fulfilled by the integrand, convergence is still rather fast. (iii) For integrands with end-point singularities tanh-sinh quadrature converges especially fast as compared to other schemes, thanks to its double-exponential suppression of these divergences (Fig. A.1). (iv) The abscissae and weights can be directly extracted from the transformation formulas (A.6a) and (A.6b), in contrast to some other quadrature schemes leaning on iterative processes. (v) Finally, the transformed integral has equidistant abscissae (trapezoidal rule, Fig. A.1), which can straightforwardly be reused together with
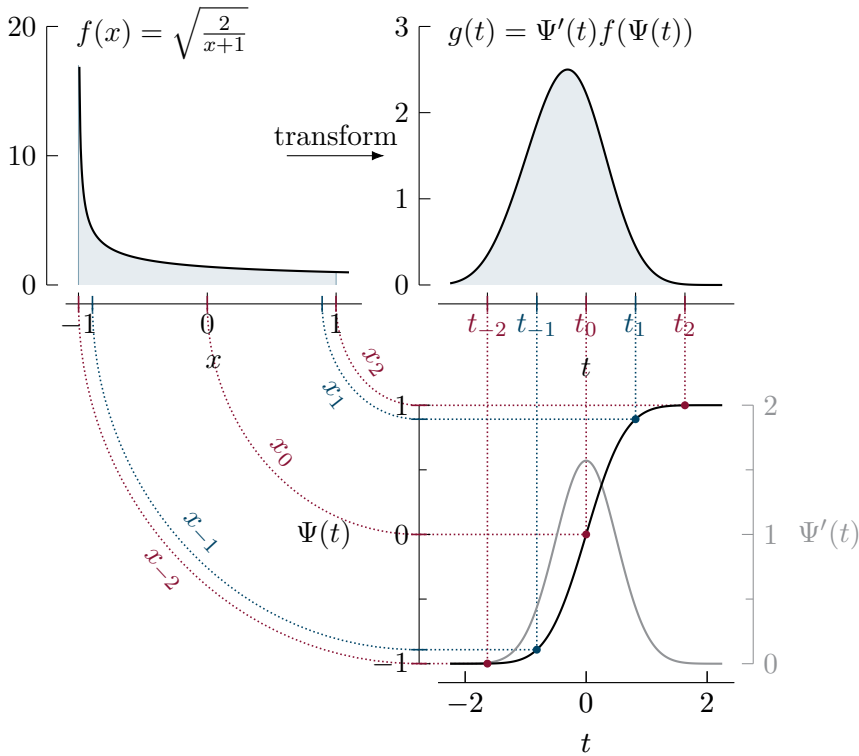
Figure A.1 Tanh-sinh transformation applied to the integral $\int_0^1 \frac{1}{\sqrt{x}}\, \mathrm{d}x$, brought to the standard domain $]-1, 1[$ (top left). The tanh-sinh transformation transforms the integration domain from $x \in]-1, 1[$ to $t \in]-\infty, \infty[$, while the integrands magnitude is strongly suppressed as $t \to \infty$ (e.g., $g(t)|_{t=-2.5} \approx 10^{-7}$ and $g(t)|_{t=-4.5} \approx 10^{-59}$). The trapezoidal rule is then applied to this transformed integrand within the window $t \in [-t_n, t_n]$, for $n = 2$ (5 evaluation points) as an illustration (top right). The abscissa x_i of the original integration domain to which the equidistant points t_i in the transformed domain correspond, can be recovered as $x_i = \Psi(t_i)$ (bottom right and dotted connection lines). Notice that most of the abscissae x_i end up very close to the domain boundaries. At those points, the effect of the original integrand is strongly suppressed because it is multiplied by $\Psi'(t)$ (bottom right, grey). This results in the excellent convergence properties of the tanh-sinh quadrature, especially for integrands with singularities near the end-points.

the weights and the function evaluations when doubling the quadrature order is required.

In the present paper we focus on the quadrature scheme as presented above and its generalization to multiple integration, although several extensions are possible. In general, the transformation function $\Psi(t)$ should be chosen such that the transformed integrand $g(t)$ behaves like

$$|g(t)| \propto \exp\left(-\frac{\pi}{2}\exp(|t|)\right) \quad \text{as} \quad t \to \pm\infty \tag{A.8}$$

for the quadrature to be optimal [107]. This observation underlies various transformations involving (semi-)infinite domains and integrands with peculiar behavior near the integration boundaries [107]. Quadratures based on such transformations are called double exponential (DE) quadratures for obvious reasons. A second extension is possible when the function $g(t)$ has very different decay-rates for $t \to +\infty$ and $t \to -\infty$. In that case, it can be beneficial to use an unequal number of evaluation points for $t > 0$ and $t < 0$ when truncating the series of the trapezoid rule (A.3). The details, including error estimates with explicit constants, have been worked out by Okayama et al. [171] and more information on asymmetric ranges can be found in Chapter 2 of the book on Sinc methods by Lund and Bowers [178]. Finally, specific modifications for handling oscillatory [179, 180] or indefinite integrals are discussed in refs. [181, 182].

A.3 Discussion

The above mentioned favorable properties of tanh-sinh quadrature can only be achieved if numerical instabilities are avoided, especially when dealing with finite-precision floating-point numbers. Related caveats will be treated and resolved in the following subsection, together with the extension of tanh-sinh quadrature to multi-dimensional integration domains.

A.3.1 Avoiding numerical instabilities

The above presented N-point quadrature scheme can be summarized as

$$Q_h^n = h(n)\sum_{i=-n}^{+n} w_i f(x_i), \tag{A.9}$$

the weights and abscissae respectively being $w_i = \Psi'(t_i)$ and $x_i = \Psi(t_i)$. It depends crucially on evaluations very close to the end-points of the integration domain, where the density of abscissae x_i is very high (Fig. A.1). Correspondingly, one

should be careful not to lose significant figures and therefore it is a good practice to store the array [107]

$$y_i = 1 \pm x_i = \frac{\exp\left(\pm \frac{\pi}{2} \sinh t_i\right)}{\cosh\left(\frac{\pi}{2} \sinh t_i\right)} \quad \text{for} \quad i \lessgtr 0, \tag{A.10}$$

containing the distances from the respective abscissae x_i to the closest interval bound.

In the context of tanh-sinh quadrature, the most important cause of numerical instability is numerical underflow, occurring when numerical values become smaller than the underflow level (UFL). This smallest positive normalized floating-point number is $F_{\min} = 2^L$, where L is the smallest exponent representable in a given floating-point model. Specifically, we need to pay attention to the weights, the abscissae, and the function evaluations at these abscissae. Both the smallest weight $w_n = \min\{w_i\}$ and the smallest stored abscissa value $y_n = \min\{y_i\}$ are determined by window size t_n, which bounds the transformed integration window $t_i \in [-t_n, t_n]$. We will determine a window limit $t_{\max}$ and choose $t_n \leqslant t_{\max}$ to avoid numerical underflow in a given floating-point model.

For the weights, numerical underflow is avoided if $w_n = \Psi'(t_n) \geqslant F_{\min}$, such that the corresponding window limit is

$$t_{\max}^w = \max\{t \mid \Psi'(t) \geqslant F_{\min}\} \tag{A.11}$$

Similarly, the smallest stored abscissa should exceed the UFL, $y_n = 1 - x_n = 1 - \Psi(t_n) \geqslant F_{\min}$, such that we can define

$$t_{\max}^x = \max\{t \mid t \leqslant \Psi^{-1}(1 - F_{\min})\} \tag{A.12}$$

as the window limit, where

$$\Psi^{-1}(1 - F_{\min}) = \sinh^{-1}\left(\frac{\ln\left(\frac{2}{F_{\min}} - 1\right)}{\pi}\right). \tag{A.13}$$

Both window limits $t_{\max}^w$ and $t_{\max}^x$ are *intrinsic* to the used floating-point model as well as to the dimensionality of the integral, as will be discussed in subsection A.3.2. Since both conditions always apply simultaneously, it is convenient to introduce the intrinsic window limit $t_{\max}^{xw} = \min\{t_{\max}^x, t_{\max}^w\}$. All above mentioned intrinsic quantities are listed in Table A.1 for a few common floating-point models.

Besides the calculation of the abscissae and weights, also the integrand evaluations need to be carefully inspected in view of the numerical stability, which can be accomplished by a proper choice of another window limit $t_{\max}^{\text{eval}}$. Examples will be discussed in section Sec. A.4.

Finally, we take $t_{\max} = \min\{t_{\max}^{xw}, t_{\max}^{\text{eval}}\}$ as the window limit, imposing the maximum on the transformed abscissae values t_i as to avoid numerical instabilities.

Table A.1 This table shows the smallest representable exponent L, the corresponding underflow level $F_{\min}$, the window limits $t_{\max}^x$, $t_{\max}^w$ and $t_{\max}^{xw}$, and the corresponding intrinsic maximal optimal order $n_{\max}^{xw}$ for various floating-point (fp) models (IEEE 754–2008).

fp model	L	$F_{\min}$	D	$t_{\max}^x$	$t_{\max}^w$	$t_{\max}^{xw}$	$n_{\max}^{xw}$
single	-126	$1.175 \cdot 10^{-38}$	1,2	4.026	4.076	4.026	37
			3	4.026	3.425	3.425	18
double	-1022	$2.225 \cdot 10^{-308}$	1,2	6.112	6.121	6.112	442
			3	6.112	5.437	5.437	201
extended	-16382	$3.362 \cdot 10^{-4932}$	1,2	8.885	8.886	8.885	10228
			3	8.885	8.194	8.194	4725

A.3.2   Multiple integration

Whereas higher dimensional integrals ($D > 1$) are commonplace in physics [111, 173], we restrict ourselves to integration domains that are Cartesian products of lower dimensional domains, or that can be transformed to such a region by variable substitutions or coordinate transformations. In these cases, it is possible to apply the one-dimensional quadrature rules repeatedly in each dimension, but, once again, caution is in order to avoid numerical underflow. Slightly more complex multiple integrals, having boundaries that are integration variables in an exterior loop, are accessible through the use of indefinite integration [183].

As an example in two dimensions, consider the integration of a function $f(x, y)$ over the domain $-1 \leqslant x, y \leqslant 1$, which is typically approximated as

$$\int\limits_{-1}^{1} \int\limits_{-1}^{1} f(x, y) \, \mathrm{d}y \, \mathrm{d}x \approx Q_{h_1, h_2}^{n_1, n_2} = h_1 h_2 \sum_{i=-n_1}^{+n_1} \sum_{j=-n_2}^{+n_2} w_i w_j f(x_i, x_j), \qquad \text{(A.14)}$$

where $n_1 \neq n_2$ in general, although $n_1 = n_2$ is often a very convenient choice. While it is clear from Eq. (A.14) how to extend the quadrature rule to even higher dimensions, it is recommended to calculate the weights $w_i = \Psi'(t_i)$ in each dimension separately, and multiply them with the function evaluation on the fly, as underflow problems may quickly arise otherwise. It is reasonable to limit the weight-specific window limit $t_{\max}^w$, for which we take the same value in each direction, even more in higher dimensions (multiplying many very small weight quickly renders all the weights effectively zero). A good value for $t_{\max}^w$ was found to be such that

$$t_{\max}^w = \max\{t \mid (\Psi'(t))^{\mathcal{D}} \geqslant F_{\min}\}, \text{ where } \mathcal{D} = \max\{1, D - 1\}, \qquad \text{(A.15)}$$

since then $w_n^{\mathcal{D}} \geqslant F_{\min}$. This ensures that each weight separately exceeds the UFL. For higher dimensions, the product of all but one weight should also be higher than the UFL in order that the corresponding term contribute to the sum. In the latter case, one weight can be disregarded, because it can be compensated by a large value from the function evaluation. Examples for one, two and three dimensions are given in Table A.1.

A.3.3   Abscissae spacing

For most quadrature schemes, the choice of the quadrature order n, together with a window size that is fixed by the integration bounds, determines the abscissae spacing h. In the tanh-sinh quadrature schemes, the window size $[-t_n, t_n]$ is not fixed a priori, with bounds $t_n = n \cdot h$ that depend themselves on the abscissae spacing. A smart choice for $h(n)$ is indispensable. We will discuss two alternatives: (i) the optimal $h_{\mathrm{opt}}(n)$ and (ii) the *maximal* $h_{\max}(n)$.

The optimal spacing

$$h(n) = h_{\mathrm{opt}}(n) := \frac{2}{N} \, \mathrm{W}(2dN), \quad \text{with } N = 2n + 1 \tag{A.16}$$

leads to the optimal error bounds (A.7) by making the discretization error $\Delta \mathcal{I}_h$ and the truncation error ϵ_{t} contribute equally [107–109, 176]. The Lambert W-function $\mathrm{W}(z)$ is implicitly defined as the solution of $z = w e^w$ for w. One should note here that, in most of literature, the optimal width is given by $h = 2/N \ln(2dN)$, which is only correct in the limit of large N [176]. The optimal abscissae spacing (A.16) depends on the strip width d of regularity of the transformed integrand around the real axis. Strictly speaking, this strip width needs to be specifically determined for each integral to achieve optimal convergence. However, when the integrand is the result of a complex numerical routine, such a determination of d is not always possible, let alone desirable when a large range of integrals needs to be calculated. In practice, $d = \pi/2$ often leads to reasonable convergence rates. The optimal transformed abscissae spacing then becomes

$$h_{\mathrm{opt}}(n) = \frac{2}{N} \, \mathrm{W}(\pi N), \quad \text{with } N = 2n + 1. \tag{A.17}$$

While $h_{\mathrm{opt}}(n)$ is theoretically optimal in an infinite-precision context, its outstanding results cannot always be achieved due to the limitations of floating-point types. The main problem is the window size $t_n = n h_{\mathrm{opt}}(n)$ that can quickly reach beyond the window limit $t_{\max}$, sometimes before full convergence is reached. In order to avoid numerical instabilities, the optimal spacing should never be used for orders higher than $n_{\max} = \max\{n \mid n h_{\mathrm{opt}}(n) \leqslant t_{\max}\}$ at which this happens. This maximal order can depend on numerical difficulties in the integrand evaluation

through $t_{\max}$ and must therefore be determined on a per-case basis. The maximal order itself is always limited by the intrinsic maximal order $n_{\max}^{xw}$ which is fully determined by the floating-point type and dimension (Table A.1).

As an alternative to the optimal spacing, we propose to use the maximal spacing

$$h(n) = h_{\max}(n) := \frac{t_{\max}}{n} \tag{A.18}$$

instead. Here, the window size t_n is fixed, independent of the order n, to $t_{\max}$ so as to avoid numerical underflow. Besides the obvious simplicity of the $h_{\max}(n)$, also the reusability of function evaluations obtained from lower order estimates, is an advantage when it comes to doubling the order index n.

A.4 Worked examples

In this section, we demonstrate the use of the tanh-sinh quadrature as described above, specifically comparing results using optimal and maximal spacing for different floating-point types. For each example integral, possible pitfalls and noteworthy features are discussed, while showing the relative error as a function of the quadrature order. This relative error is intrinsically limited from below by the machine precision ϵ_{m}, which is indicated by dashed lines for each floating-point models. The results for optimal spacing can only be obtained up to the maximum quadrature order $n_{\max}$, which is shown as a larger data point if it falls within the shown domain. Results obtained using double-precision Gauss-Legendre quadrature with the same number of evaluation points are always shown for comparison. We focus on integrands with a singularity near the origin of the original integration domain, as may be relevant to solve numerous problems in physics. For benchmarking purposes, it is not the intent to evaluate the specific integral, but rather to demonstrate how the quadrature behaves for different types of limiting behavior.

A.4.1 Integrands with a non-integrable singularity

Sometimes, one needs to integrate a function with a non-integrable singularity located close to one of the integration limits. A straightforward example of this type is the integral

$$\mathcal{I}_\delta = \int\limits_\delta^1 \frac{1}{x}\,\mathrm{d}x = -\ln\delta, \tag{A.19}$$

where δ is an arbitrarily small positive number. In spite of $\ln\delta$ quickly diverging when δ tends to zero, tanh-sinh quadrature quickly yields remarkably high precision
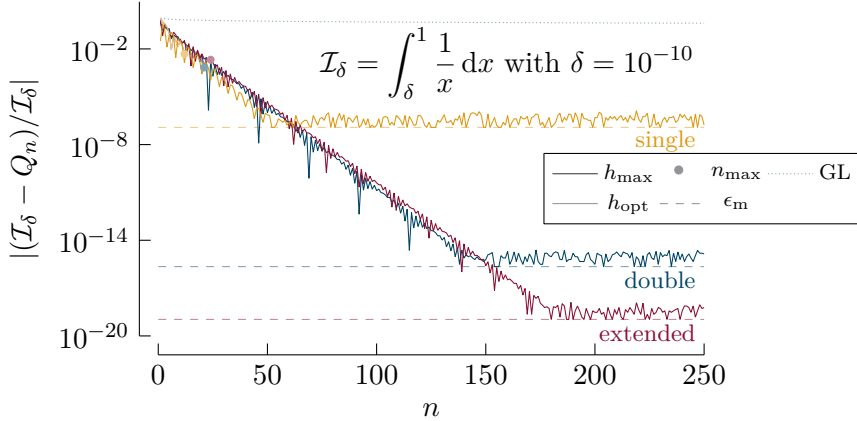
Figure A.2 The relative error decreases exponentially with quadrature order n. Both optimal and maximal spacing yield similar convergence rates. However, whereas the maximal spacing reaches full precision for all floating-point types, the optimal spacing can barely converge because n_{max} is very small. The fluctuations as a function of n decrease upon increasing a. No convergence can be distinguished when using Gauss-Legendre quadrature.

integrals when the integrand is sampled with many points near $x = \delta$ (Fig. A.2). This can, however, also be a source of errors: if the sampling points are closer to $x = \delta$ than machine precision permits, the function evaluations will be inaccurate. To prevent this, t_{max}^{eval} should be chosen such that the abscissae $x = x_{-n}$ remains distinguishable from $x = \delta$. For the errors shown in Fig. A.2, we chose t_{max}^{eval} such that $(x_{-n} - \delta)/\delta > a \cdot \epsilon_m$, with $a = 100$. Increasing the value of a diminishes the fluctuations of the resulting error, but increases the achieved minimal relative error.

Notice in Fig. A.2 that n_{max} is very small and the corresponding error using optimal spacing is still far above the achievable error. The use of the proposed maximal spacing does allow for a steady and fast decrease of the relative error up to full precision. Gauss-Legendre quadrature fails completely in this test. It lacks the fine-grained sampling around $x = \delta$.

A.4.2 Multiple integration with singular integrands

Next, we consider D-dimensional integrals

$$\mathcal{I}_D = \int_{]0,1]^D} \mathrm{d}^D\mathbf{r}\, f_D(\mathbf{r}), \tag{A.20}$$

where the integrands are chosen to be

$$f_1(x) = \frac{1}{\sqrt{x}}$$

$$f_2(x,y) = \frac{1}{\sqrt{x^2 + y^2}}$$

$$f_3(x,y,z) = \frac{1}{x^2 + y^2 + z^2},$$

all containing a integrable singularity at $\mathbf{r} = 0$. Integrals of the type $\mathcal{I}_D$ are typically encountered in solid state physics, where integration over the first Brillouin zone is very common. For example, in a recent study of anisotropic quantum Heisenberg ferromagnets [120], one of the integrands that determines the Curie temperature falls of in the same way as $f_3(\mathbf{r})$. The results[2] for each of these integrals are shown in Fig. A.3. The convergence rate is especially large for the one-dimensional integral, but also for higher dimensions the convergence is fast and steady up to maximum precision. While no special numerical concerns apply to f_1, numerical underflow in the calculation of the denominator of f_2 and f_3 needs to be avoided by choosing t_{eval} such that $x_{-n} \geqslant \sqrt{F_{\text{min}}}$.

In the latter two cases, the maximal order n_{max} was reached in the single precision optimal scheme before convergence up to full precision was achieved. In the double-precision equivalent, full precision is reached at an order just below n_{max}. All convergence rates seem to become lower when the dimensionality of the integral is increased. This might be due to the fact that the choice of $d = \pi/2$ in Eq. (A.16) is not optimal for the outer integrals. The scheme using maximal spacing always reaches full precision. Even though its convergence rate is somewhat slower than the optimal (especially for the extended-precision calculation), it still has a decent performance. In every case, Gauss-Legendre quadrature converges, be it at a much lower rate than the tanh-sinh quadratures.

A.5   Conclusion

We have reviewed tanh-sinh quadrature, which is very efficient for integrands with end-point singularities, that are often encountered in physics. We demonstrated that even limited-precision floating-point arithmetic facilitates fast convergence at machine precision levels. Extending the scheme to higher dimensions turns out to be straightforward, although the convergence rate is typically lower as a function of the quadrature order.

---

[2]Elementary integration of the function class $f_D(\mathbf{r})$ leads to $\mathcal{I}_1 = 2$, $\mathcal{I}_2 = 2\ln(1 + \sqrt{2})$ and $\mathcal{I}_3 = 3\left(\text{Ti}_2(3 - 2\sqrt{2}) - C\right) + \frac{3\pi}{4}\tanh^{-1}\left(\frac{2\sqrt{2}}{3}\right)$, where $\text{Ti}_2(x)$ and C are respectively the inverse tangent integral and the Catalan constant.
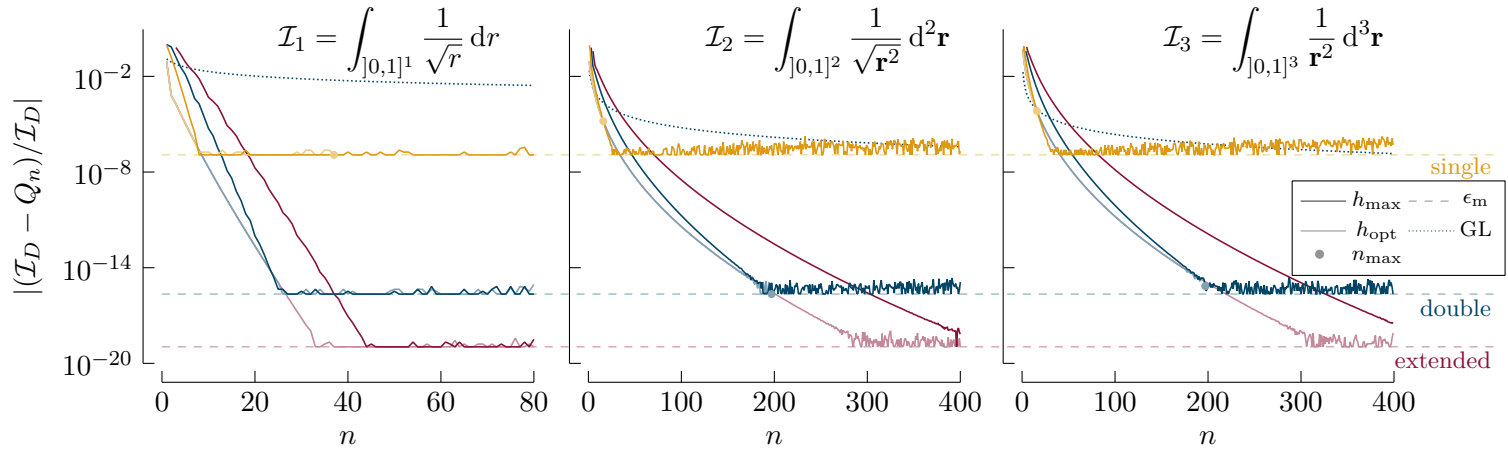
Figure A.3 The relative error as compared to the exact result for one-dimensional quadrature order n for functions with an integrable singularity at the origin in one, two and three dimensions. The total number of sampling points in D dimensions is $(2n+1)^D$. The quadrature with optimal spacing always converges slightly faster than the maximal spacing variant. However, it does not reach full precision for the single-precision floating-point type in the two- and three-dimensional examples, whereas the quadrature with $h_{\max}(n)$ does. While still being fast, the convergence is more slow in higher dimensions. Gauss-Legendre quadrature converges, but only very slowly.

We showed that care has to be taken to avoid numerical underflow in the abscissae and the weights, as well as to avoid other numerical instabilities related to integrand evaluations. These problems can typically be resolved straightaway by choosing a suitable window limit $t_{\max}$. For the optimal spacing $h_{\mathrm{opt}}(n)$, this implies a maximum usable quadrature order $n_{\max}$, sometimes hampering convergence. The proposed maximal spacing rule $h_{\max}(n)$ alleviates this limitation. Despite having slightly slower convergence rates, this rule achieves full machine precision accuracy more consistently. Moreover, its implementation is even more straightforward and it allows for the reuse of abscissae, weights, and function evaluations when it comes to recompute a particular integral for increasing quadrature orders, as is often convenient to monitor convergence.

B Solution differential equation for larger spin values

In this appendix, we give a step-by-step solution of the differential equation (3.36)

$$\Omega''(\lambda) + \frac{(1+\Phi)\,\mathrm{e}^\lambda + \Phi}{(1+\Phi)\,\mathrm{e}^\lambda - \Phi}\Omega'(\lambda) - S\,(S+1)\,\Omega(\lambda) = 0, \tag{B.1}$$

with the boundary conditions

$$\Omega(0) = 1 \tag{B.2a}$$

$$\mathrm{D}\Omega(0) = \prod_{r=-S}^{+S}\left(\frac{\mathrm{d}}{\mathrm{d}\lambda} - r\right)\Omega(\lambda)\Big|_{\lambda=0} = 0. \tag{B.2b}$$

Finding a solution to this differential equation is not trivial and the original work by Callen omits many steps.

We assume that the solution consist of functions of the form of the ansatz

$$\omega(x,\lambda) = \frac{\mathrm{e}^{x\lambda}}{\zeta}, \text{ with the shorthand } \zeta = (1+\Phi)\,\mathrm{e}^\lambda - \Phi. \tag{B.3}$$

The first two derivatives of this function with respect to λ are

$$\zeta^2\frac{\mathrm{d}\omega}{\mathrm{d}\lambda} = \zeta x\mathrm{e}^{x\lambda} - (1+\Phi)\,\mathrm{e}^{(1+x)\lambda} \tag{B.4}$$

and

$$\begin{aligned}
\zeta^3\frac{\mathrm{d}^2\,\omega}{\mathrm{d}\lambda^2} &= \zeta\mathrm{e}^{x\lambda}\left\{(1+\Phi)\,\mathrm{e}^\lambda x + \zeta x^2 - (x+1)\,(1+\Phi)\,\mathrm{e}^\lambda\right\} \\
&\quad - \left\{\zeta x - (1+\Phi)\,\mathrm{e}^\lambda\right\}\mathrm{e}^{(x+1)\lambda}2\,(1+\Phi).
\end{aligned} \tag{B.5}$$

Substituting the ansatz and its derivatives into the differential equation, multiplying by $\zeta\mathrm{e}^{-x\lambda}$ and grouping the terms by their power of x quickly reduces to the characteristic equation

$$x^2 - x - S\,(S+1) = 0 \tag{B.6}$$

which determines the values

$$x = S + 1 \text{ and } x = -S \tag{B.7}$$

for which the ansatz is a valid solution. The functions $\omega(-S, \lambda)$ and $\omega(S + 1, \lambda)$ are thus particular solutions of the differential equation.

The general solution of the differential equation is then

$$\Omega(\lambda) = K_1 \omega(-S, \lambda) + K_2 \omega(S + 1, \lambda). \tag{B.8}$$

To find a particular solution, we use the boundary conditions

$$\Omega(0) = 1, \text{ so } K_1 + K_2 = 1 \tag{B.9}$$

and

$$D\Omega(0) = 0, \quad \text{so} \quad K_1 D\omega(-S, 0) + K_2 D\omega(S + 1, 0) = 0 \tag{B.10}$$

to fix K_1 and K_2. The solution is thus given by

$$\Omega(\lambda) = \frac{[D\omega(S + 1, 0)]\, \omega(-S, \lambda) - [D\omega(-S, 0)]\, \omega(S + 1, \lambda)}{D\omega(S + 1, 0) - D\omega(-S, 0)}. \tag{B.11}$$

The task that remains is to calculate the quantities $D\omega(S + 1, 0)$ and $D\omega(-S, 0)$. To do so, first we use the substitution $y = e^\lambda$:

$$
\begin{aligned}
D\omega(x, 0) &= \prod_{r=-S}^{S} \left(\frac{d}{d\lambda} - r \right) \frac{e^{x\lambda}}{(1 + \Phi)\, e^\lambda - \Phi}\Big|_{\lambda=0} \\
&= \prod_{r=-S}^{S} \left(\frac{dy}{d\lambda} \frac{d}{dy} - r \right) \frac{y^x}{(1 + \Phi)\, y - \Phi}\Big|_{y=1} \\
&= -\frac{1}{\Phi} \prod_{r=-S}^{S} \left(y \frac{d}{dy} - r \right) \frac{y^x}{1 - \frac{1+\Phi}{\Phi} y}\Big|_{y=1}.
\end{aligned}
\tag{B.12}
$$

Now we use a series expansion for the fraction. Note that, since in general $y(1 + \Phi)/\Phi$ lies in the range $[1, +\infty[$, we cannot use the typical Taylor series expansion of $1/(1 - x)$ around $x = 0$. Instead, we need the Laurent series around $1/x \to 0$: $1/(1 - x) = -\sum_{n=1}^{\infty} 1/x^n$. In the specific case here, we have

$$\frac{1}{1 - \frac{1+\Phi}{\Phi} y} = -\sum_{n=1}^{\infty} \left(\frac{\Phi}{1 + \Phi} \right)^n y^{-n}. \tag{B.13}$$

As such, we calculate further:

$$
\begin{aligned}
\mathrm{D}\omega(x,0) &= \frac{1}{\Phi} \prod_{r=-S}^{S} \left(y\frac{\mathrm{d}}{\mathrm{d}y} - r\right) \sum_{n=1}^{\infty} \left(\frac{\Phi}{1+\Phi}\right)^n y^{x-n}\bigg|_{y=1} \\
&= \frac{1}{\Phi} \sum_{n=1}^{\infty} \left(\frac{\Phi}{1+\Phi}\right)^n \prod_{r=-S}^{S} (x - n - r)\, y^{x-n}\bigg|_{y=1} \\
&= -\frac{1}{\Phi} \sum_{n=1}^{\infty} \left(\frac{\Phi}{1+\Phi}\right)^n \prod_{r=-S}^{S} (n - x + r) \\
&= -\frac{1}{\Phi} \left(\frac{1+\Phi}{\Phi}\right)^{-x} \sum_{n=1-x}^{\infty} \left(\frac{\Phi}{1+\Phi}\right)^n \prod_{r=-S}^{S} (n + r)\,.
\end{aligned}
\tag{B.14}
$$

Now, for $x = S + 1$, the first $2S + 1$ terms vanish because r takes all values in $[-S, S]$, such that one of the factors in the product vanishes:

$$
\mathrm{D}\omega(S+1,0) = -\frac{1}{\Phi} \left(\frac{1+\Phi}{\Phi}\right)^{-S+1} \sum_{n=S+1}^{\infty} \left(\frac{\Phi}{1+\Phi}\right)^n \prod_{r=-S}^{S} (n + r)\,.
\tag{B.15}
$$

On the other hand, for $x = -S$, we have

$$
\mathrm{D}\omega(-S,0) = -\frac{1}{\Phi} \left(\frac{1+\Phi}{\Phi}\right)^{S} \sum_{n=S+1}^{\infty} \left(\frac{\Phi}{1+\Phi}\right)^n \prod_{r=-S}^{S} (n + r)\,.
\tag{B.16}
$$

Combining the two results gives

$$
\mathrm{D}\omega(-S,0) = \left(\frac{1+\Phi}{\Phi}\right)^{2S+1} \mathrm{D}\omega(S+1,0).
\tag{B.17}
$$

The final solution for the differential equation with boundary conditions is thus

$$
\begin{aligned}
\Omega(\lambda) &= \frac{\omega(-S,\lambda)\Phi^{2S+1} - \omega(S+1,\lambda)\,(1+\Phi)^{2S+1}}{\Phi^{2S+1} - (1+\Phi)^{2S+1}} \\
&= \frac{(1+\Phi)^{2S+1}\,\mathrm{e}^{(S+1)\lambda} - \Phi^{2S+1}\mathrm{e}^{-S\lambda}}{\left[(1+\Phi)^{2S+1} - \Phi^{2S+1}\right] \cdot \left[(1+\Phi)\,\mathrm{e}^{\lambda} - \Phi\right]}\,,
\end{aligned}
\tag{B.18}
$$

which immediately leads to the expression (3.39).

C Ewald transformation formula

We give a derivation of the Ewald transformation formula here, as the available derivations are often difficult to comprehend. We start with a derivation of the formula in one dimension, following the derivation in *A brief introduction to θ functions* by Bellman [184], and extend the result to higher dimensions afterwards.

During the derivation of the Ewald summation formula, we define a Fourier expansion of a periodic function $g(y)$ with period L as

$$g(y) = \sum_{j=-\infty}^{+\infty} a_j \mathrm{e}^{2\pi \mathrm{i} jy/L}, \tag{C.1}$$

with a_j determined by

$$a_j = \frac{1}{L} \int_0^L g(y) \mathrm{e}^{-2\pi \mathrm{i} jy/L} \, \mathrm{d}y. \tag{C.2}$$

Given a continuous function $f(y)$ with $y \in \mathbb{R}$, a periodic function $g(y)$ with period L can be constructed as

$$g(y) = \sum_{n=-\infty}^{+\infty} f(y + nL), \tag{C.3}$$

assuming the series converges uniformly in every non-zero interval of y. This newly constructed function clearly has the property

$$g(y + L) = g(y). \tag{C.4}$$

Since $g(y)$ is periodic, it is useful to expand it in a Fourier series. The Fourier coefficients can be calculated by direct substitution of the definition (C.3) in

Eq. (C.2). By using the property (C.4), the coefficients become

$$a_j = \frac{1}{L} \sum_{n=-\infty}^{+\infty} \int_0^L f(y + nL)e^{-2\pi i j y/L} \, dy$$

$$= \frac{1}{L} \sum_{n=-\infty}^{+\infty} \int_{nL}^{(n+1)L} f(y)e^{-2\pi i j y/L} \, dy \qquad (\text{C.5})$$

$$= \frac{1}{L} \int_{-\infty}^{+\infty} f(y)e^{-2\pi i j y/L} \, dy,$$

where $\int_{-\infty}^{+\infty} |f(y)| \, dy$ is assumed to converge. Substituting these coefficients in the definition of the Fourier transform (C.1) and using the definition (C.3) of $g(y)$ results in the important identity

$$\sum_{n=-\infty}^{+\infty} f(y + nL) = \frac{1}{L} \sum_{j=-\infty}^{+\infty} e^{2\pi i j y/L} \int_{-\infty}^{+\infty} f(y_1)e^{-2\pi i j y_1/L} \, dy_1, \qquad (\text{C.6})$$

provided that $\sum_{j=-\infty}^{+\infty} |a_j|$ converges. When using $y = 0$ in this general relation, the Poisson summation formula

$$\sum_{n=-\infty}^{+\infty} f(nL) = \frac{1}{L} \sum_{j=-\infty}^{+\infty} \int_{-\infty}^{+\infty} f(y_1)e^{-2\pi i j y_1/L} \, dy_1 \qquad (\text{C.7})$$

is obtained, which is more commonly known.

Next to the extended form of the Poisson summation formula (C.6), we also need the integral relation

$$\int_{-\infty}^{+\infty} e^{-ty^2 + 2\pi i j y/L} \, dy = \sqrt{\frac{\pi}{t}} e^{-(\pi j)^2/(tL^2)} \qquad (\text{C.8})$$

that holds for all j and $\mathrm{Re}(t) > 0$ to derive the Ewald transformation formula. The Ewald transformation formula is now obtained by using the function $f(y) = e^{-ty^2}$ (with $\mathrm{Re}(t) > 0$) in the general Poisson summation formula (C.6) and applying the integral identity (C.8):

$$\sum_{n=-\infty}^{\infty} e^{-t(y+nL)^2} = \frac{1}{L} \sum_{j=-\infty}^{+\infty} e^{2\pi i j y/L} \int_{-\infty}^{+\infty} e^{-ty_1^2 - 2\pi i j y_1/L} \, dy_1$$

$$= \frac{1}{L} \sqrt{\frac{\pi}{t}} \sum_{j=-\infty}^{+\infty} e^{2\pi i j y/L - (\pi j)^2/(tL^2)}. \qquad (\text{C.9})$$

This powerful identity is also known as the Poisson-Jacobi formula or Ewald theta transformation. Moreover, it can be shown to be equivalent to the transformation formula

$$\vartheta_3(j, t) = (-\mathrm{i}t)^{-1/2}\, \mathrm{e}^{j^2/(\pi \mathrm{i}t)} \vartheta_3\left(\frac{j}{t}, -\frac{1}{t}\right), \tag{C.10}$$

where

$$\vartheta_3(j, t) := \sum_{n=-\infty}^{+\infty} q^{n^2}\eta^n, \text{ with } q = \mathrm{e}^{\pi \mathrm{i}t},\ \eta = \mathrm{e}^{2\pi \mathrm{i}j} \tag{C.11}$$

for the theta-function $\vartheta_3(j, t)$.

To demonstrate the strength of the Ewald transformation formula (C.9), consider the relation with $y = 0$ and $L = 1$:

$$\sum_{n=-\infty}^{\infty} \mathrm{e}^{-tn^2} = \sqrt{\frac{\pi}{t}} \sum_{n=-\infty}^{+\infty} \mathrm{e}^{-\pi^2 n^2/t}, \tag{C.12}$$

which can be written with one final substitution as

$$g(t) = \sum_{n=-\infty}^{\infty} \mathrm{e}^{-\pi n^2 t} = \sqrt{\frac{1}{t}} \sum_{n=-\infty}^{+\infty} \mathrm{e}^{-\pi n^2/t} = \sqrt{\frac{1}{t}} g\left(\frac{1}{t}\right). \tag{C.13}$$

We can estimate the achieved accuracy and convergence behaviour at $t = 0.01$ by looking the magnitude of the nth term. In the sum $g(t)$, the term $n = 25$ is 3.0×10^{-9}, such that achieved accuracy after summing about fifty terms is approximately 10^{-10}. This should be contrasted to a value of 3.7×10^{-136} for the $n = 1$ term when using the right-hand side sum $\sqrt{1/t}g(1/t)$. Since the next term is as small as 1.8×10^{-545}, summing just a few terms suffices to achieve an extraordinary accuracy. The Ewald summation formula can thus significantly speed up the calculation of slowly converging sums.

The Ewald theta transformation formula (C.9) can be extended to higher dimensions. The terms in the summation are then typically interpreted as (reciprocal) lattice points. As indicated at the beginning of this chapter, we limit ourselves to the simple cubic and square lattice types. Substituting $L = 2\pi/a$ in Eq. (C.9) gives

$$\sum_{n=-\infty}^{\infty} \mathrm{e}^{-t\left(y+n\frac{2\pi}{a}\right)^2} = \frac{a}{2\pi}\sqrt{\frac{\pi}{t}} \sum_{j=-\infty}^{+\infty} \mathrm{e}^{\mathrm{i}jay-(ja)^2/(4t)}. \tag{C.14}$$

If a is the lattice constant, $n\frac{2\pi}{a}$ can be identified as one component of the reciprocal lattice vector $\mathbf{G_n}$ (see subsection 2.1.4). Similarly, ja can be interpreted as a

component of the direct lattice vector $\mathbf{r_j}$ and y as the corresponding component of $\mathbf{k}$. Applying the above formula to all d components of the d-dimensional cubic lattice and multiplying those results gives

$$\sum_{\mathbf{n}} e^{-t\left(\mathbf{k}+\mathbf{G_n}\right)^2} = \frac{\pi^{d/2}}{v_b t^{d/2}} \sum_{\mathbf{j}} e^{i\mathbf{r_j}\cdot\mathbf{k}-r_j^2/(4t)}. \tag{C.15}$$

Finally, we substitute $t = 1/(2u)$, rename both summation indices to be $\mathbf{l}$ and rearrange the equation. The multidimensional Ewald transformation formula then becomes

$$\sum_{\mathbf{l}} e^{-r_l^2 u/2+i\mathbf{r_l}\cdot\mathbf{k}} = \frac{v_b}{(2\pi)^{d/2} u^{d/2}} \sum_{\mathbf{l}} e^{-\left(\mathbf{k}+\mathbf{G_l}\right)^2/2u}. \tag{C.16}$$

Publications

Articles

J. Vanherck, J. Schulenborg, R. B. Saptsov, J. Splettstoesser and M. R. Wegewijs, 'Relaxation of quantum dots in a magnetic field at finite bias – Charge, spin, and heat currents', Phys. Status Solidi B **254**, 1600614 (2017)

J. Schulenborg, A. Di Marco, J. Vanherck, M. R. Wegewijs and J. Splettstoesser, 'Thermoelectrics of Interacting Nanosystems—Exploiting Superselection Instead of Time-Reversal Symmetry', Entropy **19**, 668 (2017)

J. Vanherck, B. Sorée and W. Magnus, 'Anisotropic bulk and planar heisenberg ferromagnets in uniform, arbitrarily oriented magnetic fields', J. Phys.: Condens. Matter **30**, 275801 (2018)

J. Vanherck, C. Bacaksiz, B. Sorée, M. V. Milošević and W. Magnus, '2D ferromagnetism at finite temperatures under quantum scrutiny', Appl. Phys. Lett. **117**, 052401 (2020)

J. Vanherck, B. Sorée and W. Magnus, 'Tanh-sinh quadrature for single and multiple integration using floating-point arithmetic', arXiv:2007.15057 (2020)

Conference contributions

J. Vanherck, J. Schulenborg and J. Splettstoesser, 'Heat currents through quantum dots subject to high-frequency driving', Fourth quantum thermodynamics conference, 7th course of the international school of statistical physics, COST action MP1209, Erice, Italy, poster presentation (May 2016)

J. Vanherck, B. Sorée and W. Magnus, 'Spin wave-like excitations in low-dimensional ferromagnets', Theory at sea, Oostduinkerke, oral presentation (June 2017)

J. Vanherck, B. Sorée and W. Magnus, 'Ferromagnetism from a different angle: magnetic reorientation transition', Faculty of science - research day, Campus Groenenborger, UAntwerpen, poster presentation (Jan. 2018)

J. Vanherck, B. Sorée and W. Magnus, 'Ferromagnetism from a different angle: magnetic reorientation transition', Belgian physical society - general meeting 2018, Campus Drie Eiken, UAntwerpen, poster presentation (Apr. 2018)

J. Vanherck, B. Sorée and W. Magnus, 'Ferromagnetism from a different angle:

magnetic reorientation transition', Theory at sea, Oostduinkerke, poster presentation (June 2018)

J. Vanherck, B. Sorée and W. Magnus, 'Ferromagnetism from a different angle: magnetic reorientation transition', 23rd international colloquium on magnetic films and surfaces (ICMFS-2018), UC Santa Cruz CA, USA, poster presentation (July 2018)

J. Vanherck, B. Sorée and W. Magnus, 'Magnetic reorientation in anisotropic heisenberg ferromagnets', 9th joint european magnetic symposia (JEMS) conference, Mainz, Germany, oral presentation (Sept. 2018)

J. Vanherck, B. Sorée and W. Magnus, 'Dipolar interaction and exchange anisotropy in two-dimensional ferromagnetic quantum heisenberg spin lattices', APS march meeting 2019, Boston, Massachusetts, USA, oral presentation (Mar. 2019)

J. Vanherck, B. Sorée and W. Magnus, 'Ferromagnetism from a different angle: magnetic reorientation transition', 44th conference of the Middle European Cooperation in Statistical Physics (MECO44), Kloster Seeon, Germany, poster presentation (May 2019)

J. Vanherck, B. Sorée and W. Magnus, 'Two-dimensional ferromagnetism', Theory at sea, Oostende, oral presentation (June 2019)

J. Vanherck, B. Sorée and W. Magnus, 'The honeycomb quantum heisenberg ferromagnet model with anisotropic exchange interactions', APS march meeting 2020, Denver, Colorado, USA, oral presentation (cancelled due to COVID-19) (Mar. 2020)

Other

Scholarship of EMM Nanoscience and Nanotechnology Consortium. Leuven, Belgium and Göteborg, Sweden (2015-2016)

J. Vanherck, J. Schulenborg and J. Splettstoesser, *Time-dependent particle and energy currents through interacting quantum dots (master thesis)* (Technical report MC2 - Department of Microtechnology and Nanoscience, Chalmers University of Technology, Göteborg, 2016)

J. Vanherck, B. Sorée and W. Magnus, *Finalist in best student presentation award at ICMFS-2018*, UC Santa Cruz CA, USA, July 2018

J. Vanherck, C. Bacaksiz, B. Sorée, M. V. Milošević and W. Magnus, 'Calculate_curie', `https://sourceforge.net/projects/calculate-curie/`, Software (2020)

Bibliography

[1] A. K. Geim and K. S. Novoselov, 'The rise of graphene', Nat. Mater. **6**, 183–191 (2007).

[2] E. J. Samuelsen, R. Silberglitt, G. Shirane and J. P. Remeika, 'Spin waves in ferromagnetic CrBr3 studied by inelastic neutron scattering', Phys. Rev. B **3**, 157–166 (1971).

[3] W. B. Yelon and R. Silberglitt, 'Renormalization of large-wave-vector magnons in ferromagnetic CrBr3 studied by inelastic neutron scattering: spin-wave correlation effects', Phys. Rev. B **4**, 2280–2286 (1971).

[4] N. D. Mermin and H. Wagner, 'Absence of ferromagnetism or antiferromagnetism in one- or two-dimensional isotropic heisenberg models', Phys. Rev. Lett. **17**, 1133–1136 (1966).

[5] H. Nakano and M. Takahashi, 'Magnetic properties of quantum heisenberg ferromagnets with long-range interactions', Phys. Rev. B **52**, 6606–6610 (1995).

[6] Y. Imry, 'Effective long range order and phase transitions in finite, macroscopic one and two dimensional systems', Ann. Phys. **51**, 1–27 (1969).

[7] C. A. F. Vaz, J. A. C. Bland and G. Lauhoff, 'Magnetism in ultrathin film structures', Rep. Prog. Phys. **71**, 056501 (2008).

[8] B. Huang et al., 'Layer-dependent ferromagnetism in a van der waals crystal down to the monolayer limit', Nature **546**, 270–273 (2017).

[9] C. Gong et al., 'Discovery of intrinsic ferromagnetism in two-dimensional van der waals crystals', Nature **546**, 265–269 (2017).

[10] N. Samarth, 'Condensed-matter physics: magnetism in flatland', Nature **546**, News & Views, 216–218 (2017).

[11] S. Jiang, J. Shan and K. F. Mak, 'Electric-field switching of two-dimensional van der Waals magnets', Nat. Mater. **17**, 406–410 (2018).

[12] B. Huang et al., 'Electrical control of 2D magnetism in bilayer CrI3', Nat. Nanotechnol. **13**, 544–548 (2018).

[13] M. Gibertini, M. Koperski, A. F. Morpurgo and K. S. Novoselov, 'Magnetic 2d materials and heterostructures', Nat. Nanotechnol. **14**, 408–419 (2019).

[14] K. S. Burch, D. Mandrus and J.-G. Park, 'Magnetism in two-dimensional van der Waals materials', Nature **563**, 47–52 (2018).

[15]Z. Zhang et al., 'Direct photoluminescence probing of ferromagnetism in monolayer two-dimensional CrBr3', Nano Lett. **19**, 3138–3142 (2019).

[16]M. Kim et al., 'Micromagnetometry of two-dimensional ferromagnets', Nature Electronics **2**, 457–463 (2019).

[17]D. J. O'Hara et al., 'Room temperature intrinsic ferromagnetism in epitaxial manganese selenide films in the monolayer limit', Nano Lett. **18**, 3125–3131 (2018).

[18]M. Bonilla et al., 'Strong room-temperature ferromagnetism in VSe2 monolayers on van der waals substrates', Nat. Nanotechnol. **13**, 289–293 (2018).

[19]A. Fert, 'Nobel lecture: origin, development, and future of spintronics', Rev. Mod. Phys. **80**, 1517–1530 (2008).

[20]M. N. Baibich et al., 'Giant Magnetoresistance of (001)Fe/(001)Cr Magnetic Superlattices', Phys. Rev. Lett. **61**, 2472–2475 (1988).

[21]G. Binasch, P. Grünberg, F. Saurenbach and W. Zinn, 'Enhanced magnetoresistance in layered magnetic structures with antiferromagnetic interlayer exchange', Phys. Rev. B **39**, 4828–4830(R) (1989).

[22]T. Jungwirth, X. Marti, P. Wadley and J. Wunderlich, 'Antiferromagnetic spintronics', Nat. Nanotechnol. **11**, 231–241 (2016).

[23]V. Baltz et al., 'Antiferromagnetic spintronics', Rev. Mod. Phys. **90**, 015005 (2018).

[24]L.-D. Yuan, Z. Wang, J.-W. Luo, E. I. Rashba and A. Zunger, 'Giant momentum-dependent spin splitting in centrosymmetric low-Z antiferromagnets', Phys. Rev. B **102**, 014422 (2020).

[25]A. Manchon and J. Železný, 'Spin Polarization Without Net Magnetization', Physics **13** (2020).

[26]J. Sinova, S. O. Valenzuela, J. Wunderlich, C. H. Back and T. Jungwirth, 'Spin Hall effects', Rev. Mod. Phys. **87**, 1213–1260 (2015).

[27]A. D. Kent and D. C. Worledge, 'A new spin on magnetic memories', Nat. Nanotechnol. **10**, 187–191 (2015).

[28]S. Cherepov et al., 'Electric-field-induced spin wave generation using multiferroic magnetoelectric cells', Appl. Phys. Lett. **104**, 082403 (2014).

[29]W. Eerenstein, N. D. Mathur and J. F. Scott, 'Multiferroic and magnetoelectric materials', Nature **442**, 759–765 (2006).

[30]T. Maruyama et al., 'Large voltage-induced magnetic anisotropy change in a few atomic layers of iron', Nat. Nanotechnol. **4**, 158–161 (2009).

[31]A. Srivastava, 'At the flick of a switch', Nat. Mater. **17**, 391–392 (2018).

[32] C. Gong and X. Zhang, 'Two-dimensional magnetic crystals and emergent heterostructure devices', Science **363**, eaav4450 (2019).

[33] S. S. P. Parkin et al., 'Giant tunnelling magnetoresistance at room temperature with MgO (100) tunnel barriers', Nat. Mater. **3**, 862–867 (2004).

[34] A. Khitun, M. Bao and K. L. Wang, 'Magnonic logic circuits', J. Phys. D: Appl. Phys. **43**, 264005 (2010).

[35] S.-K. Kim, 'Micromagnetic computer simulations of spin waves in nanometre-scale patterned magnetic elements', J. Phys. D: Appl. Phys. **43**, 264004 (2010).

[36] A. Khitun, 'Multi-frequency magnonic logic circuits for parallel data processing', J. Appl. Phys. **111**, 054307 (2012).

[37] S. Klingler et al., 'Design of a spin-wave majority gate employing mode selection', Appl. Phys. Lett. **105**, 152410 (2014).

[38] A. V. Chumak, V. I. Vasyuchka, A. A. Serga and B. Hillebrands, 'Magnon spintronics', Nat. Phys. **11**, 453–461 (2015).

[39] G. Csaba, Á. Papp and W. Porod, 'Perspectives of using spin waves for computing and signal processing', Phys. Lett. A **381**, 1471–1476 (2017).

[40] Q. Wang et al., 'Reconfigurable nanoscale spin-wave directional coupler', Sci. Adv. **4**, e1701517 (2018).

[41] O. Zografos et al., 'Non-volatile spin wave majority gate at the nanoscale', AIP Advances **7**, 056020 (2017).

[42] B. Rana, Y. Fukuma, K. Miura, H. Takahashi and Y. Otani, 'Excitation of coherent propagating spin waves in ultrathin CoFeB film by voltage-controlled magnetic anisotropy', Appl. Phys. Lett. **111**, 052404 (2017).

[43] I. P. Radu et al., 'Spintronic majority gates', 2015 IEEE international electron devices meeting (IEDM) (Dec. 2015).

[44] T. Fischer et al., 'Experimental prototype of a spin-wave majority gate', Appl. Phys. Lett. **110**, 152401 (2017).

[45] N. W. Ashcroft and N. Mermin, *Solid state physics* (Cengage Learning, Inc, 2nd Jan. 1976), 848 pp.

[46] J. J. Sakurai and J. J. Napolitano, *Modern quantum mechanics* (Addison Wesley Pub Co Inc, 2010), 550 pp.

[47] W. Heitler and F. London, 'Wechselwirkung neutraler Atome und homöopolare Bindung nach der Quantenmechanik', Zeitschrift für Physik **44**, 455–472 (1927).

[48] W. Heisenberg, 'Zur theorie des ferromagnetismus', Zeitschrift für Physik **49**, 619–636 (1928).

[49]P. A. M. Dirac, 'Quantum mechanics of many-electron systems', Proceedings of the Royal Society A: Mathematical, Physical and Engineering Sciences **123**, 714–733 (1929).

[50]C. Kittel, *Introduction to solid state physics* (John Wiley and Sons Ltd, 11th Nov. 2004), 704 pp.

[51]J. A. Blanco and V. M. P. Pidal, 'On a general heisenberg exchange effective hamiltonian', Eur. J. Phys. **16**, 195–198 (1995).

[52]H. Bethe, 'Zur theorie der metalle', Zeitschrift für Physik **71**, 205–226 (1931).

[53]W. Lenz, 'Beitrag zum verständnis der magnetischen erscheinungen in festen körpern', Z. Phys. **21**, 613–615 (1920).

[54]E. Ising, 'Beitrag zur theorie des ferromagnetismus', Zeitschrift für Physik **31**, 253–258 (1925).

[55]S. G. Brush, 'History of the Lenz-Ising Model', Rev. Mod. Phys. **39**, 883–893 (1967).

[56]K. Huang, *Statistical mechanics* (John Wiley & Sons, 29th Apr. 1987), 508 pp.

[57]W. Greiner, L. Neise and H. Stöcker, *Thermodynamics and statistical mechanics* (Springer-Verlag New York, 1995).

[58]T. D. Lee and C. N. Yang, 'Statistical Theory of Equations of State and Phase Transitions. II. Lattice Gas and Ising Model', Phys. Rev. **87**, 410–419 (1952).

[59]W. L. Bragg and E. J. Williams, 'The effect of thermal agitation on atomic arrangement in alloys', Proc. R. Soc. London A **145**, 699–730 (1934).

[60]D. J. Amit, H. Gutfreund and H. Sompolinsky, 'Spin-glass models of neural networks', Phys. Rev. A **32**, 1007–1018 (1985).

[61]L. Onsager, 'Crystal statistics. i. a two-dimensional model with an order-disorder transition', Phys. Rev. **65**, 117–149 (1944).

[62]W. Schoenmaker and W. Magnus, 'Non-Abelian Random Polygons: A New Model in Statistical Physics', J. Stat. Phys. **94**, 389–413 (1999).

[63]N. Metropolis, A. W. Rosenbluth, M. N. Rosenbluth, A. H. Teller and E. Teller, 'Equation of state calculations by fast computing machines', The Journal of Chemical Physics **21**, 1087–1092 (1953).

[64]W. K. Hastings, 'Monte carlo sampling methods using markov chains and their applications', Biometrika **57**, 97–109 (1970).

[65]V. Berezinskii, 'Destruction of long-range order in one-dimensional and two-dimensional systems having a continuous symmetry group i. classical systems', Sov. Phys. JETP **32**, 493–500 (1971).

[66] J. M. Kosterlitz and D. J. Thouless, 'Ordering, metastability and phase transitions in two-dimensional systems', J. Phys. C: Solid State Phys. **6**, 1181–1203 (1973).

[67] F. Bonechi, E. Celeghini, R. Giachetti, E. Sorace and M. Tarlini, 'Heisenberg XXZ model and quantum galilei group', J. Phys. A: Math. Gen. **25**, L939–L943 (1992).

[68] P. Jordan and E. Wigner, 'Über das Paulische Äquivalenzverbot', Z. Angew. Phys. **47**, 631–651 (1928).

[69] E. Lieb, T. Schultz and D. Mattis, 'Two soluble models of an antiferromagnetic chain', Ann. Phys. **16**, 407–466 (1961).

[70] S. Katsura, 'Statistical mechanics of the anisotropic linear heisenberg model', Phys. Rev. **127**, 1508–1518 (1962).

[71] T. Matsubara and H. Matsuda, 'A lattice model of liquid helium, i', Progress of Theoretical Physics **16**, 569–582 (1956).

[72] J. E. Hirsch and D. J. Scalapino, 'Excitonic mechanism for superconductivity in a quasi-one-dimensional system', Phys. Rev. B **32**, 117–134 (1985).

[73] P. Fröbrich and P. Kuntz, 'Many-body green's function theory for thin ferromagnetic anisotropic heisenberg films: treatment of the exchange anisotropy', The European Physical Journal B - Condensed Matter **32**, 445–455 (2003).

[74] M. d'Aquino, C. Serpico, G. Miano and C. Forestiere, 'A novel formulation for the numerical computation of magnetization modes in complex micromagnetic systems', J. Comput. Phys. **228**, 6130–6149 (2009).

[75] G. P. Müller et al., 'Spirit: Multifunctional framework for atomistic spin simulations', Phys. Rev. B **99**, 224414 (2019).

[76] M. Lakshmanan, 'The fascinating world of the landau-lifshitz-gilbert equation: an overview', Philosophical Transactions of the Royal Society A: Mathematical, Physical and Engineering Sciences **369**, 1280–1300 (2011).

[77] D. J. Griffiths, *Introduction to Electrodynamics* (Cambridge University Press, June 2017).

[78] R. M. F. Houtappel, 'Order-disorder in hexagonal lattices', Physica **16**, 425–455 (1950).

[79] F. Bloch, 'Zur theorie des ferromagnetismus', Zeitschrift für Physik **61**, 206–219 (1930).

[80] F. J. Dyson, 'General theory of spin-wave interactions', Phys. Rev. **102**, 1217–1230 (1956).

[81] F. J. Dyson, 'Thermodynamic behavior of an ideal ferromagnet', Phys. Rev. **102**, 1230–1244 (1956).

[82] T. Holstein and H. Primakoff, 'Field dependence of the intrinsic domain magnetization of a ferromagnet', Phys. Rev. **58**, 1098–1113 (1940).

[83] P. Bruno, 'Theory of the curie temperature of cobalt-based ferromagnetic ultrathin films and multilayers', Journal of the Magnetics Society of Japan **15**, S1_15–20 (1991).

[84] P. Bruno, 'Spin-wave theory of two-dimensional ferromagnets in the presence of dipolar interactions and magnetocrystalline anisotropy', Phys. Rev. B **43**, 6015–6021 (1991).

[85] S. Kar, K. Wierschem and P. Sengupta, 'Magnons in a two-dimensional transverse-field XXZ model', Phys. Rev. B **96**, 045126 (2017).

[86] A. J. Princep et al., 'The full magnon spectrum of yttrium iron garnet', npj Quantum Materials **2**, 1–5 (2017).

[87] S. S. Pershoguba et al., 'Dirac magnons in honeycomb ferromagnets', Phys. Rev. X **8**, 011010 (2018).

[88] Z. Li, T. Cao and S. G. Louie, 'Two-dimensional ferromagnetism in few-layer van der waals crystals: renormalized spin-wave theory and calculations', J. Magn. Magn. Mater. **463**, 28–35 (2018).

[89] D. Wallace, *Thermodynamics of crystals* (Dover Publications, Mineola, N.Y, 1998).

[90] D. N. Zubarev, 'Double-time green functions in statistical physics', Soviet Physics Uspekhi **3**, 320–345 (1960).

[91] H. B. Callen, 'Green function theory of ferromagnetism', Phys. Rev. **130**, 890–898 (1963).

[92] K. W. H. Stevens and G. A. Toombs, 'Green functions in solid state physics', Proceedings of the Physical Society **85**, 1307–1308 (1965).

[93] J. G. Ramos and A. A. Gomes, 'Remarks on the retarded, advanced and thermodynamic green's functions', Il Nuovo Cimento A **3**, 441–455 (1971).

[94] P. E. Bloomfield and N. Nafari, 'Commutator and anticommutator green's functions, zero-frequency poles, and long-time correlations', Phys. Rev. A **5**, 806–813 (1972).

[95] J. F. Fernandez and H. A. Gersch, 'Note on the zero-frequency pole in green's functions', Proceedings of the Physical Society **91**, 505–506 (1967).

[96] H. Callen, R. Swendsen and R. Tahir-Kheli, 'Zero-frequency behavior of thermodynamic green's functions', Phys. Lett. A **25**, 505–506 (1967).

[97] S. Katsura and T. Horiguchi, 'First order green function theory of ferromagnetism II', Phys. Lett. A **28**, 342–343 (1968).

154

[98]G. L. Lucas and G. Horwitz, 'Correlation functions and green functions: zero-frequency anomalies', J. Phys. A: Gen. Phys. **2**, 503–508 (1969).

[99]M. F. Sarry, 'Internal consistency of the method of two-time thermal green's functions', Soviet Physics Journal **23**, 621–624 (1980).

[100]J. D. Patterson and W. H. Southwell, 'Green's Function Theory of Ferromagnetism', Am. J. Phys. **36**, 343 (1968).

[101]G. L. Lucas, 'Green Function Theory of the Two-Spin System', Am. J. Phys. **36**, 942 (1968).

[102]P. Fröbrich and P. Knutz, 'Many-body green's function theory of heisenberg films', Phys. Rep. **432**, 223–304 (2006).

[103]S. Tyablikov, 'Retarded and advanced green functions in the theory of ferromagnetism', Ukrainskyi Matematychnyi Zhurnal **11**, 287 (1959).

[104]S. V. Tyablikov, *Methods in the quantum theory of magnetism* (Springer US, 1967).

[105]F. Englert, 'Theory of a heisenberg ferromagnet in the random phase approximation', Phys. Rev. Lett. **5**, 102–103 (1960).

[106]H. B. Callen, 'Statistical Mechanics of Ferromagnetism', J. Appl. Phys. **33**, 1172 (1962).

[107]H. Takahasi and M. Mori, 'Double exponential formulas for numerical integration', Publications of the Research Institute for Mathematical Sciences **9**, 721–741 (1973).

[108]M. Sugihara, 'Optimality of the double exponential formula - functional analysis approach -', Numerische Mathematik **75**, 379–395 (1997).

[109]M. Mori, 'Discovery of the double exponential transformation and its developments', Publications of the Research Institute for Mathematical Sciences **41**, 897–935 (2005).

[110]D. H. Bailey, K. Jeyabalan and X. S. Li, 'A comparison of three high-precision quadrature schemes', Experimental Mathematics **14**, 317–329 (2005).

[111]D. Bailey and J. Borwein, 'High-precision numerical integration: progress and challenges', Journal of Symbolic Computation **46**, 741–754 (2011).

[112]J. Vanherck, B. Sorée and W. Magnus, 'Tanh-sinh quadrature for single and multiple integration using floating-point arithmetic', arXiv:2007.15057 (2020).

[113]S. Schwieger, J. Kienert and W. Nolting, 'Theory of field-induced spin reorientation transition in thin heisenberg films', Phys. Rev. B **71**, 024428 (2005).

[114]M. G. Pini, P. Politi and R. L. Stamps, 'Anisotropy effects on the magnetic excitations of a ferromagnetic monolayer below and above the curie temperature', Phys. Rev. B **72**, 014454 (2005).

[115]P. J. Jensen, K. H. Bennemann, D. K. Morr and H. Dreyssé, 'Two-dimensional heisenberg antiferromagnet in a transverse field', Phys. Rev. B **73**, 144405 (2006).

[116]P. Bruno, 'Magnetization and curie temperature of ferromagnetic ultrathin films: the influence of magnetic anisotropy and dipolar interactions (invited)', MRS Proceedings **231**, 299 (1991).

[117]L. Janssen and M. Vojta, 'Heisenberg–kitaev physics in magnetic fields', J. Phys.: Condens. Matter **31**, 423002 (2019).

[118]R. A. Tahir-Kheli and D. ter Haar, 'Use of green functions in the theory of ferromagnetism. i. general discussion of the spin- s case', Phys. Rev. **127**, 88–94 (1962).

[119]W. Nolting and A. Ramakanth, *Quantum theory of magnetism* (Springer Berlin Heidelberg, 2009).

[120]J. Vanherck, B. Sorée and W. Magnus, 'Anisotropic bulk and planar heisenberg ferromagnets in uniform, arbitrarily oriented magnetic fields', J. Phys.: Condens. Matter **30**, 275801 (2018).

[121]J. Vanherck, B. Sorée and W. Magnus, 'Spin wave-like excitations in low-dimensional ferromagnets', Theory at sea, Oostduinkerke, oral presentation (June 2017).

[122]J. Vanherck, B. Sorée and W. Magnus, 'Ferromagnetism from a different angle: magnetic reorientation transition', Faculty of science - research day, Campus Groenenborger, UAntwerpen, poster presentation (Jan. 2018).

[123]J. Vanherck, B. Sorée and W. Magnus, 'Ferromagnetism from a different angle: magnetic reorientation transition', Belgian physical society - general meeting 2018, Campus Drie Eiken, UAntwerpen, poster presentation (Apr. 2018).

[124]J. Vanherck, B. Sorée and W. Magnus, 'Magnetic reorientation in anisotropic heisenberg ferromagnets', 9th joint european magnetic symposia (JEMS) conference, Mainz, Germany, oral presentation (Sept. 2018).

[125]J. Vanherck, B. Sorée and W. Magnus, 'Ferromagnetism from a different angle: magnetic reorientation transition', 23rd international colloquium on magnetic films and surfaces (ICMFS-2018), UC Santa Cruz CA, USA, poster presentation (July 2018).

[126]J. Vanherck, B. Sorée and W. Magnus, 'Ferromagnetism from a different angle: magnetic reorientation transition', Theory at sea, Oostduinkerke, poster presentation (June 2018).

[127]J. Vanherck, B. Sorée and W. Magnus, 'Two-dimensional ferromagnetism', Theory at sea, Oostende, oral presentation (June 2019).

[128]J. Vanherck, B. Sorée and W. Magnus, 'Ferromagnetism from a different angle: magnetic reorientation transition', 44th conference of the Middle European Cooperation in Statistical Physics (MECO44), Kloster Seeon, Germany, poster presentation (May 2019).

[129]J. F. Cooke and H. A. Gersch, 'Second-order green's-function theory of the heisenberg ferromagnet', Phys. Rev. **153**, 641–653 (1967).

[130]W. Marshall and G. Murray, 'Spin-wave interactions in a heisenberg ferromagnet', J. Appl. Phys. **39**, 380–382 (1968).

[131]J. Vanherck, C. Bacaksiz, B. Sorée, M. V. Milošević and W. Magnus, '2D ferromagnetism at finite temperatures under quantum scrutiny', Appl. Phys. Lett. **117**, 052401 (2020).

[132]H. Xiang, C. Lee, H.-J. Koo, X. Gong and M.-H. Whangbo, 'Magnetic properties and energy-mapping analysis', Dalton Trans. **42**, 823–853 (2013).

[133]D. Šabani, C. Bacaksiz and M. V. Milošević, 'Ab initio methodology for magnetic exchange parameters: Generic four-state energy mapping onto a Heisenberg spin Hamiltonian', Phys. Rev. B **102**, 014457 (2020).

[134]K. Baberschke, 'The magnetism of nickel monolayers', Appl. Phys. A **62**, 417–427 (1996).

[135]M. Pajda, J. Kudrnovský, I. Turek, V. Drchal and P. Bruno, 'Oscillatory curie temperature of two-dimensional ferromagnets', Phys. Rev. Lett. **85**, 5424–5427 (2000).

[136]J. Vanherck, C. Bacaksiz, B. Sorée, M. V. Milošević and W. Magnus, 'Calculate_curie', `https://sourceforge.net/projects/calculate-curie/`, Software (2020).

[137]L. Chen et al., 'Topological spin excitations in honeycomb ferromagnet CrI3', Phys. Rev. X **8**, 041028 (2018).

[138]S. A. Owerre, 'A first theoretical realization of honeycomb topological magnon insulator', J. Phys.: Condens. Matter **28**, 386001 (2016).

[139]S. Maleev, 'Dipole forces in two-dimensional and layered ferromagnets', JETP **43**, 1240 (1976).

[140]Y. Yafet, J. Kwo and E. M. Gyorgy, 'Dipole-dipole interactions and two-dimensional magnetism', Phys. Rev. B **33**, 6519–6522 (1986).

[141]K. De'Bell, A. B. MacIsaac and J. P. Whitehead, 'Dipolar effects in magnetic thin films and quasi-two-dimensional systems', Rev. Mod. Phys. **72**, 225–257 (2000).

[142] J. Vanherck, B. Sorée and W. Magnus, 'Dipolar interaction and exchange anisotropy in two-dimensional ferromagnetic quantum heisenberg spin lattices', APS march meeting 2019, Boston, Massachusetts, USA, oral presentation (Mar. 2019).

[143] P. P. Ewald, 'Die berechnung optischer und elektrostatischer gitterpotentiale', Ann. Phys. **369**, 253–287 (1921).

[144] M. Born and M. Bradburn, 'The thermodynamics of crystal lattices', Math. Proc. Cambridge Philos. Soc. **39**, 104 (1943).

[145] A. Jeffrey and D. Zwillinger, *Table of integrals, series, and products* (Elsevier Science, 2007).

[146] R. D. Misra and M. Born, 'On the stability of crystal lattices. II', Math. Proc. Cambridge Philos. Soc. **36**, 173 (1940).

[147] M. Abramowitz and I. Stegun, *Handbook of mathematical functions: with formulas, graphs, and mathematical tables*, Applied mathematics series (Dover Publications, 1964).

[148] M. H. Cohen and F. Keffer, 'Dipolar sums in the primitive cubic lattices', Phys. Rev. **99**, 1128–1134 (1955).

[149] J. Topping, 'On the mutual potential energy of a plane network of doublets', Proceedings of the Royal Society A: Mathematical, Physical and Engineering Sciences **114**, 67–72 (1927).

[150] B. M. E. van der Hoff and G. C. Benson, 'A method for the evaluation of some lattice sums occurring in calculations of physical properties of crystals', Can. J. Phys. **31**, 1087–1094 (1953).

[151] M. H. Lee and A. Begchi, 'Two-dimensional lattice sums and the dispersion relation of frenkel excitons', Phys. Rev. B **22**, 2645–2648 (1980).

[152] J. A. Osborn, 'Demagnetizing Factors of the General Ellipsoid', Phys. Rev. **67**, 351–357 (1945).

[153] P. Fröbrich, P. Jensen, P. Kuntz and A. Ecker, 'Many-body green's function theory for the magnetic reorientation of thin ferromagnetic films', The European Physical Journal B **18**, 579–594 (2000).

[154] R. Schiller and W. Nolting, 'Thickness dependent Curie temperatures of ferromagnetic Heisenberg films', Solid State Commun. **110**, 121–125 (1999).

[155] M. E. Fisher and M. N. Barber, 'Scaling theory for finite-size effects in the critical region', Phys. Rev. Lett. **28**, 1516–1519 (1972).

[156] R. Zhang and R. F. Willis, 'Thickness-dependent curie temperatures of ultrathin magnetic films: effect of the range of spin-spin interactions', Phys. Rev. Lett. **86**, 2665–2668 (2001).

[157]W. Jin et al., 'Raman fingerprint of two terahertz spin wave branches in a two-dimensional honeycomb ising ferromagnet', Nat. Commun. **9**, 1–7 (2018).

[158]I. Dzyaloshinsky, 'A thermodynamic theory of "weak" ferromagnetism of anti-ferromagnetics', J. Phys. Chem. Solids **4**, 241–255 (1958).

[159]P. W. Anderson, 'New Approach to the Theory of Superexchange Interactions', Phys. Rev. **115**, 2–13 (1959).

[160]T. Moriya, 'New Mechanism of Anisotropic Superexchange Interaction', Phys. Rev. Lett. **4**, 228–230 (1960).

[161]A. Fert, N. Reyren and V. Cros, 'Magnetic skyrmions: advances in physics and potential applications', Nat. Rev. Mater. **2**, 1–15 (2017).

[162]D. Torelli and T. Olsen, 'Calculating critical temperatures for ferromagnetic order in two-dimensional materials', 2D Mater. **6**, 015028 (2018).

[163]P. Fröbrich, P. J. Jensen and P. J. Kuntz, 'Field-induced magnetic reorientation and effective anisotropy of a ferromagnetic monolayer within spin wave theory', European Physical Journal B - Condensed Matter and Complex Systems **13**, 477–489 (2000).

[164]M. Bander and D. L. Mills, 'Ferromagnetism of ultrathin films', Phys. Rev. B **38**, 12015–12018(R) (1988).

[165]K. Tomita and M. Tanaka, 'Green's Function Theory of Magnetic Relaxation. IGeneral Formulation', Prog. Theor. Phys. **29**, 528–549 (1963).

[166]Y. Murayama, 'Decoupling a retarded green function defined in a non-equilibrium state', Phys. Lett. A **31**, 537–538 (1970).

[167]R. Balakrishnan and A. R. Bishop, 'Nonlinear dynamics of a quantum ferro-magnetic chain: Spin-coherent-state approach', Phys. Rev. B **40**, 9194–9203 (1989).

[168]F. Yan, L. Yang and B. Li, 'Formal exact solution for the Heisenberg spin system in a time-dependent magnetic field and Aharonov-Anandan phase', Phys. Lett. A **251**, 289–293 (1999).

[169]V. Mukherjee, U. Divakaran, A. Dutta and D. Sen, 'Quenching dynamics of a quantum XY spin-$\frac{1}{2}$ chain in a transverse field', Phys. Rev. B **76**, 174303 (2007).

[170]F. Iglói and H. Rieger, 'Quantum relaxation after a quench in systems with boundaries', Phys. Rev. Lett. **106**, 035701 (2011).

[171]T. Okayama, T. Matsuo and M. Sugihara, 'Error estimates with explicit constants for sinc approximation, sinc quadrature and sinc indefinite integration', Numerische Mathematik **124**, 361–394 (2013).

[172]P. J. Gaudreau, R. M. Slevinsky and H. Safouhi, 'Computing energy eigenvalues of anharmonic oscillators using the double exponential sinc collocation method', Ann. Phys. **360**, 520–538 (2015).

[173]R. M. Slevinsky and S. Olver, 'On the use of conformal maps for the acceleration of convergence of the trapezoidal rule and sinc numerical methods', SIAM Journal on Scientific Computing **37**, A676–A700 (2015).

[174]E. T. Goodwin, 'The evaluation of integrals of the form $\int_{-\infty}^{\infty} f(x)e^{-x^2}\mathrm{d}x$', Math. Proc. Cambridge Philos. Soc. **45**, 241–245 (1949).

[175]C. Schwartz, 'Numerical integration of analytic functions', J. Comput. Phys. **4**, 19–29 (1969).

[176]L. N. Trefethen and J. A. C. Weideman, 'The exponentially convergent trapezoidal rule', SIAM Review **56**, 385–458 (2014).

[177]G. H. Hardy, 'The mean value of the modulus of an analytic function', Proceedings of the London Mathematical Society **s2_14**, 269–277 (1915).

[178]J. Lund and K. Bowers, *Sinc methods for quadrature and differential equations*, Other Titles in Applied Mathematics (Society for Industrial and Applied Mathematics, 1992).

[179]T. Ooura and M. Mori, 'The double exponential formula for oscillatory functions over the half infinite interval', J. Comput. Appl. Math. **38**, 353–360 (1991).

[180]T. Ooura and M. Mori, 'A robust double exponential formula for fourier-type integrals', J. Comput. Appl. Math. **112**, 229–241 (1999).

[181]F. Stenger, 'Numerical methods based on whittaker cardinal, or sinc functions', SIAM Review **23**, 165–224 (1981).

[182]M. Muhammad and M. Mori, 'Double exponential formulas for numerical indefinite integration', J. Comput. Appl. Math. **161**, 431–448 (2003).

[183]M. Muhammad and M. Mori, 'Numerical iterated integration based on the double exponential transformation', Jpn. J. Ind. Appl. Math. **22**, 77–86 (2005).

[184]R. Bellman, *A brief introduction to theta functions*, Dover Books on Mathematics (Dover Publications, 2013).